Network of European Research Infrastructures for Earthquake Risk Assessment and Mitigation

Report

Structural fragility assessment using field monitoring data

Activity:	*Vulnerability Assessment from Field Monitoring*
Activity number:	*WP15*
Deliverable:	*Structural fragility assessment using field monitoring data*
Deliverable number:	*15.4*
Responsible activity leader:	*VCE*
Responsible participant:	*VCE*
Author:	

Seventh Framework Programme
EC project number: 262330

Summary

High protection measures should be taken to increase the resilience of our society and minimize the effects of seismic events. One of the crucial steps for the mitigation of the seismic risk is indeed the capacity of assessing the risk and its correlated uncertainties. A unified methodology and tools for the Earthquake Engineering Community should be developed for seismic vulnerability assessment, accounting for different typologies of building and building aggregates. Within this methodology, field monitoring data will help to reduce the epistemic as well as aleatory uncertainties associated with the risk assessment procedure, allowing the creation of real time assessment tools.

Fragility curves, as damage intensity predictors of various structures and life lines under different demand levels, have to be derived in a way to reflect the most realistic view of the performance of the structure.

This report treats the derivation of fragility curves of structures of which the finite element model has been calibrated by comparison between calculated and measured dynamic properties.

Table of Contents

Summary 2
Table of Contents 3
1. Introduction 6
2. Developing fragility curves 7
3. Field Monitoring 9
4. Calibration (updating) of Finite Element Models 10
5. Test cases 11
5.1 Secondary School Building at Comune di Val di Sotto 11
5.2 Spittelbreitengasse 11
5.3 The AHEPA hospital in Thessaloniki 11
5.4 Bossigasse 12
6. Reference list 13
Appendix A: 14
7. Table of Contents 15
8. List of Figures 17
9. List of Tables 21
10. Introduction 23
11. Description of the updating procedure 24
11.1 Numerical simulations 24
11.2 Modal analysis 26
11.3 Time history analysis 30
12. Preliminary analyses 32
12.1 Analysis with Complete Measured Data 34
12.1.1 Geometry 34
12.1.2 Simulation of the Field Monitoring Data 36
12.1.3 Calibration of the Mechanical Characteristics Simulation 40
12.1.4 Results TEST 1 41
12.1.5 Results TEST 2 45
12.1.6 Conclusions 51
12.2 Analysis with Incomplete Measured Data 51
12.2.1 Results TEST 1 53
12.2.2 Results TEST 2 57
12.2.3 Conclusions 63
13. Case study – secondary school building at comune di val di sotto (so), italy 65

13.1 General description of the building 67
13.2 Dynamic identification measurements 69
13.3 Mode shape expansion 81
13.4 Modeling 83
13.5 Results 98
13.5.1 Simulation type 1 (μ_{fck}=18 N/mm^2, σ_{fck}=6 N/mm^2) 98
13.5.2 A.4.5.2 Simulation type 2 (μ_{fck}=18 N/mm^2, σ_{fck}=6 N/mm^2) 104
13.5.3 A.4.5 3 Simulation type 3 (μ_{fck}=18 N/mm^2, σ_{fck}=6 N/mm^2) 109
13.5.4 A.4.5.4 Simulation type 1 - Calibration of the mechanical characteristic generation 114
13.6 Conclusions 120
14. Closing remarks and further developments 122
15. Reference List 123
Appendix B: 124
16. Introduction 125
16.1 Fragility Curves Derivation 125
16.2 Structural Response Evaluation 126
16.3 Eigen Angular Frequencies ωi 127
16.4 Mode Shapes 132
16.5 Modal Damping Coefficients 134
16.6 Ground Motion Hazard Level Selection 135
16.7 Numerical Evaluations and Arithmetic Statistics 137
17. Curve Fitting and Fragility Functions 141
18. Example: Spittelbreitengasse 148
18.1 Introduction 148
18.2 System Identification 148
18.2.1 Eigenfrequencies and Eigenvectors 149
18.2.2 Modal Damping 150
18.3 Numerical Finite Element Modeling 150
18.3.1 Finite Element Model Calibration 150
18.3.2 Material Properties 151
18.3.3 Time History Analysis 152
18.4 Numerical Evaluations and Arithmetic Statistics 152
18.5 Summary and Future Work 156
19. Conclusion 156
20. Reference list 159

Appendix C: 162
21. Introduction 163
22. Optimal sensor location 168
22.1 Algorithm 168
22.2 Measurement design of the hospital building 169
Appendix D: 173
23. Introduction 174
24. Fragility functions 175
24.1 From the field test data to the updated FE model of the structure 175
24.1.1 Field testing data 176
24.1.2 From the initial model of the structure to the updated one 177
24.2 Assessment of the structural capacity: the nonlinear static analysis 179
24.3 Ground Motion Hazard Level Selection 183
24.4 Nonlinear dynamic analysis 188
24.5 Fragility function estimation and curve fitting 193
24.6 Analysis of the fragility functions 196
25. Conclusion and remarks 199
26. Reference list 201

1. Introduction

In the last decade, several earthquakes produced severe damage and casualties around the world and in the European-Mediterranean region. Recent events like L'Aquila (Italy), 2009, Athens (Greece), 1999 and Izmit (Turkey), 1999, remind us that the vulnerability and exposure of our built environment are high and the seismic risk cannot be underestimated. Therefore higher protection measures should be taken to increase the resilience of our society and minimize the effects of seismic events. One of the crucial steps for the mitigation of the seismic risk is indeed the capacity of assessing the risk and its correlated uncertainties. A unified methodology and tools for the Earthquake Engineering Community should be developed for seismic vulnerability assessment, accounting for different typologies of building and building aggregates. Within this methodology, field monitoring data will help to reduce the epistemic as well as aleatory uncertainties associated with the risk assessment procedure, allowing the creation of real time assessment tools.

The uncertainty behind any attempt to represent reality by a mathematical model is mainly caused by lack of knowledge and may exist in all aspects of the modeling procedure. Physical structural features, i.e. material, mass and geometry, are likely to be selected as updating parameters in order to improve accuracy. This process will quantify the difference between experimental and numerical results and it will subsequently modify the numerical values of the input parameters to increase the correlation between the observed dynamic response of the structure and the prediction from the numerical model.

Natural phenomena such as fatigue, creep and degradation of material properties during the life time of the structures as well as the plausible damages due to the occurrence of the external hazards including but not limited to the ground motions, may result into a notable deviation in the global characteristics and dynamic performance of the buildings at real-time from the initial, theoretically assumed, design values. So not only in a seismic context updating of numerical models based on experimental in situ results is mandatory.

Fragility curves, as damage intensity predictors of various structures and life lines under different demand levels, have to be derived in a way to reflect the most realistic view of the performance of the structure. Fragility curves are to represent the probability of the occurrence of a specific damage state to a structure, under a certain level of ground motion shaking [1][2][3][4][5]. As a result, any phenomena, such as degrading of the structural material properties due to aging or probable damages by various events during the lifetime of the structure could inherently influence the extent of response of the building to any arbitrary excitations in comparison to the original intact state. This is to imply that the fragility curves of a specific structure might not potentially hold their initial configuration and could need an upgrade to the "real time" condition.

This report treats the derivation of fragility curves of structures of which the finite element model has been calibrated by comparison between calculated and measured dynamic properties.

2. Developing fragility curves

The vulnerable conditions of a building can be described using fragility functions that describe the probability of exceeding different limit states (such as damage or injury levels) given a level of ground shaking.

Different methods can be used to estimate a fragility function. It is possible to classify them into four generic groups:

- *Empirical fragility curves* are constructed based on statistics of observed damage from past earthquakes, such as from data collected by post-earthquake surveys.
- *Expert opinion-based fragility curves* depend on judgment and information of experts. These experts are asked to provide an estimate of the mean loss or probability of damage for different types of structures and several levels of ground shaking.
- *Analytical fragility curves* are constructed starting from the statistical elaboration of damage distributions that are simulated from analyses of structural models under increasing earthquake intensity. It is worth noting that the application of the analytical methods might be limited by the computational effort of the analyses.
- *Hybrid fragility curves* are based on the combination of different methods for damage prediction. Often, the aim is to compensate for the lack of observational data, the deficiencies of the structural models and the subjectivity in expert opinion data [10][11]

Referring to the definitions of the fragility functions (analytically determined fragility functions) as the probability of the occurrence or exceedance of a specific damage state by the structure under a certain level of ground motion, the methodology of developing fragility curves includes the following steps:

1. Define scenario earthquake(s) and derive the corresponding demand (response) spectra (for weak, medium, strong … shaking / for different damping values) : spectral acceleration versus spectral spectral displacement (ADRS format).
2. Build capacity curves (with control points: yield capacity, ultimate capacity) (also: pushover curves): calculated base shear versus top roof displacement curves can be rescaled (converted) to spectral acceleration versus spectral spectral displacement capacity curves.
3. Building response points (performance points, demand points) are given by the intersection of demand spectra and building capacity curves.
4. Finally fragility curves are built: lognormal functions that describe the probability of reaching, or exceeding, structural and nonstructural damage states, given median estimates of spectral response, for example spectral displacement. These curves take into account the variability and uncertainty associated with capacity curve properties, damage states and ground shaking.

Development of a damage-state medians (e.g. of spectral displacment) involves three basic steps (which will be significantly different for structural and nonstructural systems):

a. Develop a detailed understanding of damage to elements and components as a continuous function of building response. For example, average inter-story drift (i.e., roof displacement divided by building height) or floor acceleration can be used. In developing fragility functions, the pushover analysis can be used: it must appropriately capture the damage patterns of elements and components of the building. This requires more detailed and complex analysis than that required simply for evaluation of building response (step 2).

b. Select specific values of building response that best represent the threshold of each discrete damage state.

c. Convert damage-state threshold values (e.g., average inter-story drift) to spectral response coordinates (i.e., same coordinates as those of the capacity curve).

- An example of ground motion hazard level selection (step 1) is given in Appendix B (section 2.5).

When evaluating the exact response of the structure, the accuracy of the eigen frequencies and mode shapes of the building as well as the modal participation factors and damping coefficients are of undeniable importance [6]. Consequently, application of the measured "real time" modal parameters can be the best way to reflect the "as-of-the-date" dynamic performance of the structure (see Appendix B, section 2.1 and reference [4]).

3. Field Monitoring

Field monitoring can help in the following ways:

- By the modal results from forced or ambient vibration measurements (initial) finite element models can be calibrated that are used for pushover (response) analysis (steps 2 and 4a.).
- A simple model based on frequencies, mode shapes and damping, taken from ambient vibrations, can allow direct computation of the response of the structures and comparison of inter-storey drifts with the limits found in the literature for the slight damage grade, considered here as the limit of elastic behaviour [4].
- Extensive guidelines are available in deliverable D6.2 "Guidelines for designing optimal dynamic monitoring strategies", deliverable D6.3 "Guidelines for optimal design of forced vibration method", deliverable D15.1 "Developed integrated field monitoring technologies".

For the instrumentation of field monitoring several questions have to be answered:

1. How many sensors are needed for a good identification of all modes which are relevant for assessment of seismic vulnerability?
2. What are the optimum positions, depending on the number of available sensors.

In Appendix C a method [9] is proposed to choose the sensor locations so that the uncertainty of the identified modal coordinates, as measured by their information entropy, is minimized.

Appendix C presents also the application of this method to the AHEPA hospital in Thessaloniki which is instrumented with a limited number of triaxial accelerometers.

4. Calibration (updating) of Finite Element Models

Extensive overviews of recent literature about FE-updating can be found in [7] and [8].

Basic principle is minimizing the differences ("errors") between measured and calculated modal properties (natural frequencies, mode shapes, modal strains or combinations of these values).

This is done in an optimization context defining uncertain (updating) parameters (like stifnesses, boundary conditions etc.) and an objective function. The updating parameters can be constrained to "reasonable" values. The objective function ("error function") can be built upon differences in natural frequencies, mode shapes, modal strains etc.

In Appendix A, another error criterion called "Generalized Modal Error" is evaluated combining the MAC index (Modal Assurance Criterion), based in the difference between the eigenvectors $\mathbf{\Phi}_j$ of the numerical model and the eigenvectors $\mathbf{\Phi}_{Ei}$ obtained from dynamic identification, and the error between the numerically evaluated eigenfrequencies ω_j and the experimental ones ω_{Ei}.

5. Test cases

5.1 *Secondary School Building at Comune di Val di Sotto*

In Appendix A, a case study (Secondary School Building At Comune Di Val Di Sotto (So), Italy) is presented.

The measured data obtained from the field monitoring of the school are used to test the updating methodology. The analyses are performed considering the three different type of simulations:

1. simulated numerical models with one value of Young's Modulus for the entire structure;
2. simulated numerical models with one value of Young's Modulus for all the elements of the storey;
3. simulated numerical models with a different value of Young's Modulus for each different element.

For each of the three different types of simulation, an increasing value of generated models is considered for the different tests. The results in terms of generalized modal error are compared in order to understand where the stabilization of the values starts, which means the minimum number of samples which should be generated to obtain satisfactory error index values.

Ones, the type of simulation which exhibits the lowest range of generalized modal error has been identified, the same simulation is used to investigate the results by changing the mean and the standard deviation values for the characteristic compressive strength of the concrete.

5.2 *Spittelbreitengasse*

This case is treated in section 4 of Appendix B. The building under consideration is an old three-story unreinforced masonry structure, located at Spittelbreitengasse, Vienna, Austria. The linear dynamic properties of the structure, namely the natural frequencies belonging to the linear mode shapes and the modal damping values of the building, required for the estimation of the linear structural response under any arbitrary excitations have been derived based on the data processing of the on-site measurement records by Vienna Consulting Engineers.

5.3 *The AHEPA hospital in Thessaloniki*

The AHEPA hospital in Thessaloniki, Greece is a seven-story reinforced concrete structure with basement. The building is instrumented with the purpose of an early earthquake warning system and structural health monitoring.

There are 13 triaxial accelerometers available. For the time being they are installed as follows: one at the basement, one at the 1st floor, 4 at the middle and 7 at the top floor.

In Appendix C, an Optimal Sensor Location (OSL) algorithm is applied to see if relevant modes could be identified with the available set of accelerometers and to investigate other (better) sensor distributions.

5.4 ***Bossigasse***

The unreinforced clay brick masonry building analyzed in the appendix D is located in the thirteenth district of Vienna, Austria. This is a typical Wilhelminian style building with raised ground floor and garret used as storing area. The building was tested with forced vibration method and the structural response was recorded through 7 mono-axial velocity sensors in 4 different layouts. The field testing data were used to estimate the linear dynamic characteristics of the buildings. For this study only the first 5 natural frequency of the building were identified. These linear dynamic characteristics of the structure were used to update an initial Finite Element Model.

A hybrid method mainly based on the indications of the Eurocode 8 was developed to estimate the seismic vulnerability assessment of this building. The capacity of the structure was estimated with a nonlinear static analysis and it was supposed to be deterministic, while the seismic demand was considered to be stochastic. The structural capacity and seismic demand were combined through a dynamic method.

The results of the comparison between the seismic vulnerability estimated using the initial FEM and the updated one show that the use of field testing method is recommendable to improve the vulnerability assessment of existing buildings.

6. Reference list

[1] Boroumand, P. *Real-Time Fragility Curves: Outlines of the plausibility considerations*, Vienna Consulting Engineers Internal Report

[2] Burningham, C., Mosqueda, G., and Saavedra, R.R. *Comparison of Seismic fragility of free standing equipment using current testing protocols and recorded building floor motions*, Retrieved online from http://mceer.buffalo.edu/education/reu/2007/content/20Burningham.pdf on 16/3/2012

[3] Chon, Y-S., and Elnashai, A.S. *A simplified framework for probabilistic earthquake loss estimation*, *J. Prob. Eng. Mech.,* 25 (2010) 355-364

[4] Michel, C., Guéguen, P. and Causse, M. *Seismic vulnerability assessment to slight damage based on experimental modal parameters*. Earthquake Engng. Struct. Dyn., 41: 81–98. doi: 10.1002/eqe.1119.

[5] *FEMA. HAZUS-MH MR3 Technical Manual*. Federal Emergency Management Agency, Washington, DC, U.S.A., 2003

[6] Chopra, A.K. *Dynamics of Structures - Theory and applications to Earthquake Engineering*, Pearson Education Asia Limited and Tsinghua University Press, Beijing, 2001

[7] Teughels A. and De Roeck, G.. *Damage detection and parameter identification by finite element model updating*, Archives of Computational Methods in Engineering, 12(2):123-164, 2005.

[8] Teughels, A. *Inverse modelling of civil engineering structures based on operational modal data*, PhD thesis, Department of Civil Engineering, KU Leuven, 2003.

[9] Papadimitriou C., Lombaert, G. *The effect of prediction error correlation on optimal sensor placement in structural dynamics*, Mechanical Systems and Signal Processing 28 (2012) 105-127.

[10] *SYNER-G Deliverable D3.1. Fragility functions for common RC building types in Europe*, UPAV, UPAT, JRC, METU. 2011

[11] Pinho, R., Magenes, G., Bommer, J.J., Restrepo-Vélez, L.F., Crowley, H., *Development of seismic vulnerability assessment methodologies over the past 30 years*, 3, 2006, ISET Journal of Earthquake Technology, Bd. 43, S. 75-104.

Appendix A:

Secondary school building at Comune di Val di Sotto

EUCentre

7. Table of Contents

Summary 2
Table of Contents 3
1. Introduction 6
2. Developing fragility curves 7
3. Field Monitoring 9
4. Calibration (updating) of Finite Element Models 10
5. Test cases 11
5.1 Secondary School Building at Comune di Val di Sotto 11
5.2 Spittelbreitengasse 11
5.3 The AHEPA hospital in Thessaloniki 11
5.4 Bossigasse 12
6. Reference list 13
Appendix A: 14
7. Table of Contents 15
8. List of Figures 17
9. List of Tables 21
10. Introduction 23
11. Description of the updating procedure 24
11.1 Numerical simulations 24
11.2 Modal analysis 26
11.3 Time history analysis 30
12. Preliminary analyses 32
12.1 Analysis with Complete Measured Data 34
12.1.1 Geometry 34
12.1.2 Simulation of the Field Monitoring Data 36
12.1.3 Calibration of the Mechanical Characteristics Simulation 40
12.1.4 Results TEST 1 41
12.1.5 Results TEST 2 45
12.1.6 Conclusions 51
12.2 Analysis with Incomplete Measured Data 51
12.2.1 Results TEST 1 53
12.2.2 Results TEST 2 57
12.2.3 Conclusions 63
13. Case study – secondary school building at comune di val di sotto (so), italy 65
13.1 General description of the building 67
13.2 Dynamic identification measurements 69
13.3 Mode shape expansion 81
13.4 Modeling 83
13.5 Results 98
13.5.1 Simulation type 1 (μ_{fck}=18 N/mm^2, σ_{fck}=6 N/mm^2) 98
13.5.2 A.4.5.2 Simulation type 2 (μ_{fck}=18 N/mm^2, σ_{fck}=6 N/mm^2) 104
13.5.3 A.4.5 3 Simulation type 3 (μ_{fck}=18 N/mm^2, σ_{fck}=6 N/mm^2) 109
13.5.4 A.4.5.4 Simulation type 1 - Calibration of the mechanical characteristic generation 114

13.6 Conclusions 120
14. Closing remarks and further developments 122
15. Reference List 123
Appendix B: 124
16. Introduction 125
16.1 Fragility Curves Derivation 125
16.2 Structural Response Evaluation 126
16.3 Eigen Angular Frequencies ωi 127
16.4 Mode Shapes 132
16.5 Modal Damping Coefficients 134
16.6 Ground Motion Hazard Level Selection 135
16.7 Numerical Evaluations and Arithmetic Statistics 137
17. Curve Fitting and Fragility Functions 141
18. Example: Spittelbreitengasse 148
18.1 Introduction 148
18.2 System Identification 148
18.2.1 Eigenfrequencies and Eigenvectors 149
18.2.2 Modal Damping 150
18.3 Numerical Finite Element Modeling 150
18.3.1 Finite Element Model Calibration 150
18.3.2 Material Properties 151
18.3.3 Time History Analysis 152
18.4 Numerical Evaluations and Arithmetic Statistics 152
18.5 Summary and Future Work 156
19. Conclusion 156
20. Reference list 159
Appendix C: 162
21. Introduction 163
22. Optimal sensor location 168
22.1 Algorithm 168
22.2 Measurement design of the hospital building 169
Appendix D: 173
23. Introduction 174
24. Fragility functions 175
24.1 From the field test data to the updated FE model of the structure 175
24.1.1 Field testing data 176
24.1.2 From the initial model of the structure to the updated one 177
24.2 Assessment of the structural capacity: the nonlinear static analysis 179
24.3 Ground Motion Hazard Level Selection 183
24.4 Nonlinear dynamic analysis 188
24.5 Fragility function estimation and curve fitting 193
24.6 Analysis of the fragility functions 196
25. Conclusion and remarks 199
26. Reference list 201

8. List of Figures

Figure 1 - TEST 1 - Geometry 32
Figure 2 - TEST 2 – Geometry 32
Figure 3 - TEST 1 - Perspective, plan, front and side views 34
Figure 4 - TEST 2 - Perspective, plan, front and side views 35
Figure 5 - Generalized Modal Errors (set 4.6 - Analysis 1 _ TEST 1) 41
Figure 6 - Mode shape 1 - Comparison between updated model and experimental results - Analysis 1 _ TEST 1 43
Figure 7 - Mode shape 2 - Comparison between updated model and experimental results - Analysis 1 _ TEST 1 43
Figure 8 - Mode shape 3 - Comparison between updated model and experimental results - Analysis 1 _ TEST 1 44
Figure 9 - Generalized Modal Errors (set 5.2 - Analysis 2 _ TEST 2) 45
Figure 10 - Mode shape 1 - Comparison between updated model and experimental results - Analysis 2 _ TEST 2 49
Figure 11 - Mode shape 2 - Comparison between updated model and experimental results - Analysis 2 _ TEST 2 49
Figure 12 - Mode shape 3 - Comparison between updated model and experimental results - Analysis 2 _ TEST 2 50
Figure 13 - TEST 1 - Geometry 52
Figure 14 - TEST 2 - Geometry 52
Figure 15 - Generalized Modal Errors (set 4.6 - Analysis 3 _ TEST 1) 53
Figure 16 - Mode shape 1 - Comparison between updated model and experimental results - Analysis 3 _ TEST 1 55
Figure 17 - Mode shape 2 - Comparison between updated model and experimental results - Analysis 3 _ TEST 1 55
Figure 18 - Mode shape 3 - Comparison between updated model and experimental results - Analysis 3 _ TEST 1 56
Figure 19 - Generalized Modal Errors (set 5.2 - Analysis 4 _ TEST 2) 57
Figure 20 - Mode shape 1 - Comparison between updated model and experimental results - Analysis 4 _ TEST 2 61
Figure 21 - Mode shape 2 - Comparison between updated model and experimental results - Analysis 4 _ TEST 2 61
Figure 22 - Mode shape 3 - Comparison between updated model and experimental results - Analysis 4 _ TEST 2 62
Figure 23 - Mode 1 - Analysis 1 63
Figure 24 - Mode 1 - Analysis 2 63
Figure 25 - Mode 2 - Analysis 1 63
Figure 26 - Mode 2 - Analysis 2 63
Figure 27 - Mode 3 - Analysis 1 64
Figure 28 - Mode 3 - Analysis 2 64
Figure 29 - Building of the Elementary and Secondary School at *Comune di Val di Sotto* (SO), Italy 65
Figure 30 - Tri-axial seismometer (geophone) 65
Figure 31 - Installallation of the apparatus for the excitation of the structure and the recording of the displacements 65
Figure 32 - Analysis of the signals 65

Figure 33 - Plan view of the school's structure (3rd level) 67
Figure 34 - Secondary School's structure - Plan view 1st level 68
Figure 35 - Secondary School's structure - Plan view 2nd and 3rd level 68
Figure 36 - Position of the tri-axial seismometers - 1st storey 69
Figure 37 - Position of the tri-axial seismometers - 2nd and 3rd storey 69
Figure 38 - FFT channels X direction - 6 Hz - Flexural mode shape X and Y direction 70
Figure 39 - FFT channels Y direction - 6 Hz - Flexural mode shape X and Y direction 70
Figure 40 - FFT channels X direction - 7.375 Hz - Flexural mode shape X direction 71
Figure 41 - FFT channels Y direction - 8.125 Hz - Flexural mode shape Y direction 71
Figure 42 - Harmonic excitation 5-10Hz X direction - Channel 0 72
Figure 43 - Harmonic excitation 5-10Hz X direction - Channel 3 72
Figure 44 - Harmonic excitation 5-10Hz X direction - Channel 6 73
Figure 45 - Harmonic excitation 5-10Hz X direction - Channel 9 73
Figure 46 - Harmonic excitation 5-10Hz X direction - Channel 12 74
Figure 47 - Harmonic excitation 5-10Hz X direction - Channel 15 74
Figure 48 - Harmonic excitation 5-10Hz X direction - Channel 18 75
Figure 49 - Harmonic excitation 5-10Hz Y direction - Channel 1 76
Figure 50 - Harmonic excitation 5-10Hz Y direction - Channel 4 76
Figure 51 - Harmonic excitation 5-10Hz Y direction - Channel 7 77
Figure 52 - Harmonic excitation 5-10Hz Y direction - Channel 10 77
Figure 53 - Harmonic excitation 5-10Hz Y direction - Channel 13 78
Figure 54 - Harmonic excitation 5-10Hz Y direction - Channel 16 78
Figure 55 - Harmonic excitation 5-10Hz Y direction - Channel 19 79
Figure 56 - Harmonic excitation 5-10Hz Y direction - Channel 22 79
Figure 57 - Mode shape 1 - 6 Hz 80
Figure 58 - Mode shape 2 - 7.375 Hz 80
Figure 59 - Mode shape 3 - 8.125 Hz 80
Figure 60 - Normalized modal displacements - Mode 1 - 1st floor 81
Figure 61 - Normalized modal displacements - Mode 1 - 2nd floor 81
Figure 62 - Normalized modal displacements - Mode 1 - 3rd floor 81
Figure 63 - Normalized modal displacements - Mode 2 - 1st floor 82
Figure 64 - Normalized modal displacements - Mode 2 - 2nd floor 82
Figure 65 - Normalized modal displacements - Mode 2 - 3rd floor 82
Figure 66 - Normalized modal displacements - Mode 3 - 1st floor 82
Figure 67 - Normalized modal displacements - Mode 3 - 2nd floor 82
Figure 68 - Normalized modal displacements - Mode 3 - 3rd floor 82
Figure 69 - Initial numerical model (SAP) 84
Figure 70 - Initial numerical model - 3D and side views (SAP) 84
Figure 71 - Initial numerical model - Deformed shape mode 1 (SAP) 86
Figure 72 - Initial numerical model - Deformed shape mode 2 (SAP) 86
Figure 73 - Initial numerical model - Deformed shape mode 3 (SAP) 87
Figure 74 - Initial numerical model (OpenSees) 87
Figure 75 - Initial numerical model - Deformed shape mode 1 (OpenSees) 96
Figure 76 - Initial numerical model - Deformed shape mode 2 (OpenSees) 96
Figure 77 - Initial numerical model - Deformed shape mode 3 (OpenSees) 97
Figure 78 - Result of the simulations (type 1) - Generalized modal errors 98
Figure 79 - Result of the simulations (type 1) - Young's Modulus 99

Figure 80 - Deformed shape mode 1 (normalized according to node 117) - Initial model 99
Figure 81 - Generation of the mechanical properties f_{cm} and E_{cm} for the 4000 samples simulation (type 1) 100
Figure 82 - Generalized modal errors for the 4000 samples simulation (type 1) - Updated model n°2355 100
Figure 83 - Comparison between numerical updated (model n°2355) and measured modal displacements - Deformed shape mode 1 101
Figure 84 - Elastic THA - Comparison between initial and updated model - X direction (longitudinal) ... 102
Figure 85 - Elastic THA - Comparison between initial and updated model - Y direction (vertical) 102
Figure 86 - Elastic THA - Comparison between initial and updated model - Z direction (transversal).... 103
Figure 87 - Absolute value of the displacement responses between initial and updated numerical models for each of the 3 directions 103
Figure 88 - Result of the simulations (type 2) - Generalized modal errors 104
Figure 89 - Deformed shape mode 1 (normalized according to node 117) - Initial model 105
Figure 90 - Generalized modal errors for the 8000 samples simulation (type 2) - Updated model n°997 105
Figure 91 - Comparison between numerical updated (model n°977) and measured modal displacements - Deformed shape mode 1 106
Figure 92 - Elastic THA - Comparison between initial and updated model - X direction (longitudinal) ... 107
Figure 93 - Elastic THA - Comparison between initial and updated model - Y direction (vertical) 107
Figure 94 - Elastic THA - Comparison between initial and updated model - Z direction (transversal).... 108
Figure 95 - Absolute value of the displacement responses between initial and updated numerical models for each of the 3 directions 108
Figure 96 - Result of the simulations (type 3) - Generalized modal errors 109
Figure 97 - Deformed shape mode 1 (normalized according to node 117) - Initial model 110
Figure 98 - Generalized modal errors for the 8000 samples simulation (type 3) - Updated model n°7784 110
Figure 99 - Comparison between numerical updated (model n°7784) and measured modal displacements - Deformed shape mode 1 111
Figure 100 - Elastic THA - Comparison between initial and updated model - X direction (longitudinal) . 112
Figure 101 - Elastic THA - Comparison between initial and updated model - Y direction (vertical) 112
Figure 102 - Elastic THA - Comparison between initial and updated model - Z direction (transversal) .. 113
Figure 103 - Absolute value of the displacement responses between initial and updated numerical models for each of the 3 directions 113
Figure 104 - Calibration of the mechanical characteristic generation (Sim. type 1) - Generalized modal errors 114
Figure 105 - Calibration of the mechanical characteristic generation (Sim. type 1) - Young's Modulus . 114
Figure 106 - Calibration of the mechanical characteristic generation 1 - f_{cm} and E_{cm} (Sim 1) 115
Figure 107 - Calibration of the mechanical characteristic generation 1 - Generalized modal errors (Sim. 1) - Updated model n°1781 115
Figure 108 - Calibration of the mechanical characteristic generation 2 - f_{cm} and E_{cm} (Sim. 1) 115
Figure 109 - Calibration of the mechanical characteristic generation 2 - Generalized modal errors (Sim. 1) - Updated model n°852 115
Figure 110 - Calibration of the mechanical characteristic generation 3 - f_{cm} and E_{cm} (Sim. 1) 115
Figure 111 - Calibration of the mechanical characteristic generation 3 - Generalized modal errors (Sim. 1) - Updated model n°759 115

Figure 112 - Calibration of the mechanical characteristic generation 1 - Comparison between numerical updated (model n°1781) and measured modal displacements - Deformed shape mode 1 116
Figure 113 - Calibration of the mechanical characteristic generation 2 - Comparison between numerical updated (model n°852) and measured modal displacements - Deformed shape mode 1..... 116
Figure 114 - Calibration of the mechanical characteristic generation 3 - Comparison between numerical updated (model n°759) and measured modal displacements - Deformed shape mode 1..... 117
Figure 115 - Elastic THA - Comparison between initial and updated model 1781- X direction (long) 118
Figure 116 - Elastic THA - Comparison between initial and updated model 852- X direction (long) 118
Figure 117 - Elastic THA - Comparison between initial and updated model 759- X direction (long) 118
Figure 118 - Elastic THA - Comparison between initial and updated model 1781- Y direction (vert)..... 118
Figure 119 - Elastic THA - Comparison between initial and updated model 852- Y direction (vert)..... 118
Figure 120 - Elastic THA - Comparison between initial and updated model 759- Y direction (vert)..... 118
Figure 121 - Elastic THA - Comparison between initial and updated model 1781- Z direction (transv) . 119
Figure 122 - Elastic THA - Comparison between initial and updated model 852- Z direction (transv) ... 119
Figure 123 - Elastic THA - Comparison between initial and updated model 759- Z direction (transv) ... 119
Figure 124 - Absolute value of the displacement responses between initial and updated numerical model 1781 119
Figure 125 - Absolute value of the displacement responses between initial and updated numerical model 852 119
Figure 126 - Absolute value of the displacement responses between initial and updated numerical model 759 119
Figure 127 - Comparison between the results of Simulation 1, 2 and 3 - Generalized modal error..... 120

9. List of Tables

Table 1 - Data entry for the modal analysis routine 28
Table 2 - Data entry for the time history analysis routine 30
Table 3 - List of the performed tests for the preliminary analyses 33
Table 4 - Mechanical characteristics of the structural elements - Analysis 1 _ TEST 1 36
Table 5 - Mechanical characteristics of the structural elements - Analysis 2 _ TEST 2 36
Table 6 - Comparison between initial and measured eigenvalues - Analysis 1 _ TEST 1 39
Table 7 - Comparison between initial and measured eigenvalues - Analysis 2 _ TEST 2 39
Table 8 - Mean and standard deviation for f_{ck} [N/mm^2] 40
Table 9 - Upper part of the simulation of E_{cm} [N/mm^2] 40
Table 10 - Lower part of the simulation of E_{cm} [N/mm^2] 40
Table 11 - Calibration of the methodology for Analysis 1 - TEST 1 40
Table 12 - Calibration of the methodology for Analysis 2 - TEST 2 40
Table 13 - Results of all the set of simulations - Analysis 1 _ TEST 1 41
Table 14 - Comparison of measured eigenfrequencies, initial updated models - Analysis 1 _ TEST 1 42
Table 15 - Comparison for the Young's Modulus between the model that simulate the field monitoring data, initial and updated models - Analysis 1 _ TEST 1 42
Table 16 - Results of all the set of simulations - Analysis 2_TEST 2 45
Table 17 - Comparison of measured eigenfrequencies, initial updated models - Analysis 2 _ TEST 2 46
Table 18 - Comparison for the Young's Modulus between the model that simulate the field monitoring data, initial and updated models - Analysis 2 _ TEST 2 46
Table 19 - Simulated dynamic identification measurements - Analysis 3 _TEST 1 52
Table 20 - Simulated dynamic identification measurements - Analysis 4 _ TEST 2 52
Table 21 - Results of all the set of simulations - Analysis 3 _ TEST 1 53
Table 22 - Comparison of measured eigenfrequencies, initial updated models - Analysis 3 _ TEST 1 54
Table 23 - Comparison for the Young's Modulus between the model that simulate the field monitoring data, initial and updated models - Analysis 3 _ TEST 1 54
Table 24 - Results of all the set of simulations - Analysis 4 _ TEST 2 57
Table 25 - Comparison of measured eigenfrequencies, initial updated models - Analysis 4 _ TEST 2 57
Table 26 - Comparison for the Young's Modulus between the model that simulate the field monitoring data, initial and updated models - Analysis 4 _ TEST 2 58
Table 27 - Secondary School - Dynamic identification measurements 69
Table 28 - Slab masses 83
Table 29 - Results modal analysis (SAP) and comparison with the measured values from dynami identification 85
Table 30 - Modal partecipating mass ratios (SAP) 85
Table 31 - Script of the initial numerical model (OpenSees) 88
Table 32 - Results modal analysis (OpenSees) and comparison with the results obtained from SAP2000 and with the measured values from dynami identification 95
Table 33 - Result of the simulations (type 1) - Generalized modal errors 98
Table 34 - Comparison between numerical results from the initial and updated model and measured values - Updated model n° 2355 101
Table 35 - Result of the simulations (type 2) - Generalized modal errors 104
Table 36 - Comparison between numerical results from the initial and updated model and measured values - Updated model n° 977 106
Table 37 - Result of the simulations (type 3) - Generalized modal errors 109

Table 38 - Comparison between numerical results from the initial and updated model and measured values - Updated model n° 7784 111
Table 39 - Calibration of the mechanical characteristic generation (Sim. type 1) - Generalized modal errors 114
Table 40 - Calibration of the mechanical characteristic generations - Comparison between numerical results from the initial and updated model and measured values 117

10. Introduction

In Work Package 15 the contribution of the EUCENTRE team focused the development of a methodology for the numerical model updating of buildings using field monitoring data. The aim of the procedure presented herein is to find the best suitable model within a class of simulated structural models, based on incomplete modal data, as well as the most probable value of the system natural frequencies and the full system mode shapes.

The method is based on a Montecarlo simulation scheme of the structural parameters selected for the updating procedure thus it requires matching of the measured modal deformed shapes with the eigenmodes obtained from the simulated models. For the purpose of updating a numerical model according to the data obtained from a dynamic identification, the parameter Young's Modulus has been selected for the sensitivity analysis. Changes of geometry, masses, boundary conditions and other structural characteristics have not considered at this stage. To estimate the most probable value for the sensitivity parameter, the Modal Assurance Criterion (MAC) is used for the evaluation of the generalized modal error, involving both frequency values and modal displacements. Finally, elastic time history analysis is performed in order to better assess the difference in the response between the initial structural model and the updated model. A two-storey and a three-storey frame models are used for the initial considerations.

A routine has been created using Matlab, for the numerical simulations and the post-processing calculations, and OpenSees, for the structural analyses.

The methodology was then finally tested using a real three-storey frame building (school building), which has been characterized through a dynamic identification performed by EUCENTRE in the Comune di Val di Sotto (SO), Italy, and fully described in Deliverables 15.1 and 15.2 of Work Package 15.

Once an updated structural model is characterized using the developed procedure the updated fragility is obtained by applying the methodology presented by the EUCENTRE team in Deliverable 14.2 of Work Package 14.

11. Description of the updating procedure

A general description of the developed methodology is provided herein. The procedure has been split into three parts: *generation of the numerical models*, *modal analysis* and *time history analysis*.

11.1 *Numerical simulations*

The first part, regarding the numerical simulations, requires the following specifications.

1. *Type of Young's Modulus simulation for the generated numerical models*.

   Three different types of numerical simulation can be selected. The first (*type 1*) considers one value of Young's Modulus for the overall structure, the second (*type 2*) considers one value of Young's Modulus for all the elements at each storey and the third (*type 3*) considers one value of Young's Modulus for each structural element. Between the simplest option of having one value for all the elements and the more sophisticated one in which every single element has its own elastic modulus, the second type of simulation seems to represent theoretically the closest solution thinking about what is the common practice when the building is being constructed. For normal RC buildings, in fact, each slab is commonly cast-in-place together with the columns of the lower level, having in this way a possible different distribution of the concrete characteristics along the height of the structure, storey-by-storey.

2. *Number of samples for the class of simulated numerical models*.

3. *Number of floors* (needed for Young's Modulus simulation type 2 only).

4. *Mechanical characteristics of the material (concrete)***.**

   The definition of the mean value for the *characteristic compressive cylinder strength* of the concrete $\mathbf{f_{ck}}$ and its standard deviation is fundamental for a good matching between simulated numerical models and field monitoring data. These two parameters are used for the generation of random values of $\mathbf{f_{ck}}$ following a normal distribution, according to the aforementioned type of Young's Modulus simulation and the number of samples selected for the analysis. Hence, the number of samples is used to set, also, the number of randomly generated $\mathbf{f_{ck}}$.
   Subsequently, the evaluation of the mean value for the characteristic compressive cylinder strength of the concrete $\mathbf{f_{cm}}$ and the Young's Modulus $\mathbf{E_{cm}}$, for each of the simulated $\mathbf{f_{ck}}$, are done using the formulas of the Italian Code (*NTC 2008*) (Decreto Ministeriale 2008) as follow:

$$f_{cm} = f_{ck} + 8 \qquad \text{[MPa]}$$
$$E_{cm} = 22000 * \left(\frac{f_{cm}}{10}\right)^{0.3} \qquad \text{[MPa]}$$

Once the previous specifications has been set, the simulated numerical models are generated following few passages. In case of Young's Modulus simulation *type 1* and *type 2*, the

procedure is straightforward. The values of $\mathbf{f_{cm}}$ and $\mathbf{E_{cm}}$ are evaluated starting from $\mathbf{f_{ck}}$, previously defined through its mean and standard deviation. Hence each numerical model is created considering directly a different value of $\mathbf{E_{cm}}$. Instead, in case of Young's Modulus simulation *type 3*, the values of $\mathbf{f_{cm}}$ and $\mathbf{E_{cm}}$ are still evaluated starting from $\mathbf{f_{ck}}$, but then the values of mean and standard deviation of the $\mathbf{E_{cm}}$ distribution are needed. These two values are used to perform a further random generation, regarding, in this case, the Young's Modulus, according to the number of numerical simulations and structural elements. More clearly, each element has a total number of elastic modulus equal to the number of samples selected to perform the updating procedure, with the same mean and standard deviation of the $\mathbf{E_{cm}}$ distribution. Finally, the numerical models can be created.

Kolmogorov-Smirnov test is performed in order to check the distribution of the elastic modulus in all the elements, to be compared with a standard normal distribution.

11.2 *Modal analysis*

The second part of the procedure, creates the numerical models (*scripts*) for OpenSees (McKenna et al., 2000), according to the previously simulated elastic characteristics of the elements. Furthermore, some features concerning the modeling of the building have to be selected. Below, in Table 1, the initial part of the routine for the data entries of the program is indicated.

```
%%%%%%%%%%%%%%%%%%%%%%%%%%%%%%%%%%%%%%%%%%%%%%%%%%%%%%%%%%%%%%%%%%%%%%%%%%%%%
%INPUT DATA%%%%%%%%%%%%%%%%%%%%%%%%%%%%%%%%%%%%%%%%%%%%%%%%%%%%%%%%%%%%%%%%%%%
%%%%%%%%%%%%%%%%%%%%%%%%%%%%%%%%%%%%%%%%%%%%%%%%%%%%%%%%%%%%%%%%%%%%%%%%%%%%%

%UNITS
%Force   ->   kN
%Mass    ->   ton
%Length  ->   m
%Time    ->   sec

close all

%OUTPUT OF THE ANALYSIS & MEASUREMENTS
%set the name of the model (script file) to be run in OpenSees before the
%field measurements
nameScript='TEST.txt';
nameScriptModel='TEST';
%set the name of the output folder
nameFolderOut='Results_Modal_Analysis';
%set the name of the measured eigenfrequencies and mode shapes
nameFieldEigenfrequencies='eigenfrequenciesDI.txt';
nameFieldMode shapes='eigenvectorsDI.txt';


%DIMENSION OF THE ANALYSIS AND DOFs --> __DON'T CHANGE__
%http://opensees.berkeley.edu/wiki/index.php/Model_command
ndm=3; %dimension of the analysis
ndf=6; %number of DOFs for each node (used to build the script for OpenSees)


%MODEL GEOMETRY & MASSES

%   NODES
%-> http://opensees.berkeley.edu/wiki/index.php/Node_command
%   Note: write the node tag in ascending order
node=importdata('node.txt'); %[m]

%   BOUNDARY CONDITIONS
%   http://opensees.berkeley.edu/wiki/index.php/Fix_command
fix=importdata('fix.txt');

%   MP CONSTRAINTS (EQUAL DOFs)
%   http://opensees.berkeley.edu/wiki/index.php/EqualDOF_command
%   set the possibility of loading the constraints of the model (if any)
%   set -> 1 YES there are constraints
%   set -> 0 NO there are no constraints
mpconstraints_equalDOF=0; %set the constraints
mpconstraint_equalDOF=importdata('mpconstraint_equalDOF.txt');
```

```
%   MP CONSTRAINTS (RIGID DIAPHRAGMs)
%   http://opensees.berkeley.edu/wiki/index.php/RigidDiaphragm_command
%   set the possibility of considering rigid diaphragms in the model (if
%   any)
%   set -> 1 YES there are rigid diaphragms
%   set -> 0 NO there are no rigid diaphragms
mpconstraints_rigidDiaphragm=1; %set the rigid diaphragms
mpconstraint_rigidDiaphragm=importdata('mpconstraint_rigidDiaphragm.txt');

%   MASSES (nodal masses for the lumped mass model - 6 values to implement)
%   http://opensees.berkeley.edu/wiki/index.php/Mass_Command
%   Note: write the mass tag in ascending order
mass=importdata('mass.txt'); %[tons]

%   ELEMENTS (type of element used for the analysis)
%   http://opensees.berkeley.edu/wiki/index.php/Element_Command
%   Note: write the element tag in ascending order
eleType='elasticBeamColumn'; %string -> type of element used
element=importdata('element_elasticBeamColumn.txt');

%   GEOMETRIC TRANSFORMATION (The geometric-transformation command is used
%   to construct a coordinate-transformation (CrdTransf) object, which
%   transforms beam element stiffness and resisting force from the basic
%   system to the global-coordinate system. The command has at least one
%   argument, the transformation type.
%   http://opensees.berkeley.edu/wiki/index.php/Geometric_Transformation_Co
%   mmand
transfType_beam='Linear 1 0 0 1'; %string -> type of transformation used
transfType_column='Linear 2 0 1 0'; %string -> type of transformation used

%   LINKS
%   http://opensees.berkeley.edu/wiki/index.php/RigidLink_command
%   or
%   http://opensees.berkeley.edu/wiki/index.php/Two_Node_Link_Element
%   http://opensees.berkeley.edu/wiki/index.php/UniaxialMaterial_Command
%   set ->  0 no LINK
%   set ->  1 for RIGID LINK
%           the type of rigid link can be:
%           'beam'  ->  both the translational and rotational degrees of
%                       freedom are constrained
%           'bar'   ->  only the translational degree-of-freedom will be
%                       constrained to be exactly the same as those at
%                       the master node
%   set ->  2 for TWO NODE LINK ELEMENT
linkType=0; %set the type of link

rigidLinkType='beam'; %string -> type of RIGID LINK used
rigidLink=importdata('rigidLink_beam.txt');

nodeLinkType='twoNodeLink'; %string -> type of NODE LINK TYPE used
%set the tag for the uniaxialMaterial considered for the link's dofs
nodeLinkUniaxialMaterialType='Elastic'; %string -> type of uniaxialMaterial
%set the tag for each of the material objects associated to the dofs
%considered for the link element
nodeLinkMat='1 2 3 4 5 6'; %string -> material objects used
%set the material directions:
%1,2,3 - translation along local x,y,z axes, respectively
%4,5,6 - rotation about local x,y,z axes, respectively
nodeLinkDir='1 2 3 4 5 6'; %string -> material directions considered
nodeLinkUniaxialMaterial=importdata('uniaxialMaterial_NodeLink_Elastic.txt');
nodeLink=importdata('element_twoNodeLink.txt');
```

```
%Analysis Type: MODAL ANALYSIS
%set the number of modes (if a modal analysis is carried out)
%maximum number of modes -> 20
numModes=1;

%set the dof provided in the output of the modal analysis for the
%evaluation of the mode shape [x y z rx ry rz]
%indicate -> dof=[1 2 3]        <modal displacements provided>
%or
%indicate -> dof=[1 2 3 4 5 6]  <modal displacements and rotations provided>
dof=[1 2 3];

%set the amplification factor for the plot of the mode shape
ampFactor=1;
ampFactorModalDisplacement=1;

%NORMALIZE the eigenvectors
%   set ->  0 keep the normalize eigenvectors from OpenSees
%   set ->  1 normalize the eigenvectors according to another criteria
normalize=0; %set the normalized eigenvectors

%set the specification to normalize the eigenvectors
%   set ->  1 normalize according to a scaling factor for modal
%           displacements and rotations
%   set ->  2 normalize according to a modal displacement and
%           rotation. Select node tag and relative dof to perform the
%           normalize eigenvectors
%
%           indicate   ->   1 normalization according to the modal
%                           displacement along X direction & rotation about
%                           X axis
%           indicate   ->   2 normalization according to the modal
%                           displacement along Y direction & rotation about
%                           Y axis
%           indicate   ->   3 normalization according to the modal
%                           displacement along Z direction & rotation about
%                           Z axis
%
typeNorm=2; %set the type of normalization

nodeNorm=12; %node tag to normalize the modal displacements
dirNorm=3; %node dof tag to normalize the modal displacements

dispFactorNorm=0.5; %displacement factor to normalize the modal displacements
rotFactorNorm=0.2; %rotation factor to normalize the modal rotations

%NUMBER OF GENERATED MODELS (different Young's Modulus combinations among
%the elements)
%this value is coming from the previous matlab routine regarding the
%Montecarlo simulation test
nms=nsample;

%%%%%%%%%%%%%%%%%%%%%%%%%%%%%%%%%%%%%%%%%%%%%%%%%%%%%%%%%%%%%%%%%%%%%%%%%%%%%%%%%END OF THE INPUT%
```

Table 1 - Data entry for the modal analysis routine

After performing the modal analysis of the initial model, the same analysis is repeated for all the simulated numerical models. In order to select, among all the samples, the one that more

closely fits the results from the dynamic identification measurements, the following criteria is introduced. Among all the generated simulations, only one is judged as superior comparing to the initial model, according the error index described as follow.

A *Generalized Modal Error* is evaluated combining the *MAC* index (*Modal Assurance Criterion*), (e.g. Alvin, 1997; Farhat and Hemez, 1993; Lekidis et al., 2004; Papadimitriou et al., 1997), based in the difference between the eigenvectors $\boldsymbol{\Phi_j}$ of the numerical model and the eigenvectors $\boldsymbol{\Phi_{Ei}}$ obtained from dynamic identification, and the error between the numerically evaluated eigenfrequencies $\boldsymbol{\omega_j}$ and the experimental ones $\boldsymbol{\omega_{Ei}}$. The formula used for the evaluation of the *Generalized Modal Error* are showed below:

$$MAC_{ij} = \frac{\left(\Phi_j^T M \Phi_{Ei}\right)^2}{\left(\Phi_j^T M \Phi_j\right)\left(\Phi_{Ei}^T M \Phi_{Ei}\right)}$$

$$\alpha_i = \left(\Phi_{Ei}^T M \Phi_{Ei}\right)$$

$$Generalized\ Modal\ Error = \alpha_i \sum_j \left(\frac{\omega_j^2 - \omega_{Ei}^2}{\omega_j^2}\right)^2 \left(MAC_{ij}\right)$$

where:

$\boldsymbol{\Phi_j}$ eigenvector j from the numerical model;

$\boldsymbol{\Phi_{Ei}}$ eigenvector i from the dynamic identification;

M mass matrix;

$\boldsymbol{\omega_j}$ eigenfrequency j from the numerical model;

$\boldsymbol{\omega_{Ei}}$ eigenfrequency i from the dynamic identification;

The model that performed the lowest error index is then identified, and its mode shapes are plotted together with the mode shapes obtained from the dynamic identification measurements. A first qualitative comparison can be done through the plots, together with the numerical results.

11.3 *Time history analysis*

In the third and last part of the procedure, a time history analysis of both initial and updated models is performed. In Table 2, the final specifications needed to start the analysis are indicated, as they appear in the data input of the program. The purpose of this last part is to compare the displacements response of the two models, in order to have an additional criterion for the evaluation of the results coming from the updating procedure.

Table 2 - Data entry for the time history analysis routine

```
%   DEFINE RECORDERS
%   http://opensees.berkeley.edu/wiki/index.php/Recorder_Command
%   http://opensees.berkeley.edu/wiki/index.php/Node_Recorder
%   http://opensees.berkeley.edu/wiki/index.php/Node_Envelope_Recorder
%   http://opensees.berkeley.edu/wiki/index.php/Drift_Recorder
%   http://opensees.berkeley.edu/wiki/index.php/Element_Recorder
%   http://opensees.berkeley.edu/wiki/index.php/ElementEnvelopeRecorder
%   http://opensees.berkeley.edu/wiki/index.php/Plot_Recorder
%
%   Note: MODIFY THE SCRIPT generation according to the number of monitored
%   displacements and drifts

nodeRecorderDisp=109; %monitored free node displacements
nodeRecorderDispDof=[1 2 3]; %dofs of the displacements

%%%MODIFY%%%%%%%%%%%%%%%%%%%%%%%%%%%%%%%%%%%%%%
nodeRecorderDrift1iNode=1; %lateral drift iNode
nodeRecorderDrift1jNode=21; %lateral drift jNode
nodeRecorderDrift2iNode=21; %lateral drift iNode
nodeRecorderDrift2jNode=61; %lateral drift jNode
%%%%%%%%%%%%%%%%%%%%%%%%%%%%%%%%%%%%%%%%%%%MODIFY%%%
nodeRecorderDriftDofX=1; %dof of the monitored drift
nodeRecorderDriftDofZ=3; %dof of the monitored drift

%set of the perpendicular global directions (1=X, 2=Y (vert), 3=Z)-> this
%input is needed to calculate the length between the nodes whose drift is
%calculated
nodeRecorderDriftDofPerpDirnColumn=2; %for the columns
nodeRecorderDriftDofPerpDirnBeamX=2; %for the beams along X direction
nodeRecorderDriftDofPerpDirnBeamZ=2; %for the beams along Z direction

%   DEFINE DYNAMIC GROUND-MOTION ANALYSIS
%   http://opensees.berkeley.edu/wiki/index.php/Path_TimeSeries
%   http://opensees.berkeley.edu/wiki/index.php/Uniform_Exciatation_Pattern
%
%   http://opensees.berkeley.edu/wiki/index.php/Time_Series_Command
%   http://opensees.berkeley.edu/wiki/index.php/Analysis_Commands
%   http://opensees.berkeley.edu/wiki/index.php/Examples_Manual#3D_Structur
%   al_Modeling_.26_Analysis_Examples
%
%   Note: MODIFY THE SCRIPT according to the number of earthquake records
%   to be considered for the analysis. One record in one of the two
%   horizontal direction is set as default

record='LOMAP-CLS.txt'; %set the name of the earthquake record
G=9.81; %[g] set the scale factor for the acceleration
```

```
dt=0.005; %[sec] set the time step of the acceleration record
directionEQ=1; %set the direction of the analysis
dampRatio=0.02; %set the damping ratio
tolerance=1e-12; %tolerance for the convergence of the algorithm
maxIterations=100; %max number of iterations for the convergence of the
algorithm
recordValues=7989; %set the steps of the analysis
timeStep=0.005; %set the time step of the analysis

%%%%%%%%%%%%%%%%%%%%%%%%%%%%%%%%%%%%%%%%%%%%%%%%%%%%%%%%%%%%%%%%%%%%%END OF THE INPUT%
```

12. Preliminary analyses

For an initial verification of the aforementioned procedure, several tests have been performed considering two different buildings, showed in Figure 1 and Figure 2. The models were created with the idea of testing first (*TEST 1*), a very simple and small structure, with regularity in plan and in elevation, and then going through some tests of a more complex structure (*TEST 2*), much bigger in dimension and with a modest plan irregularity.

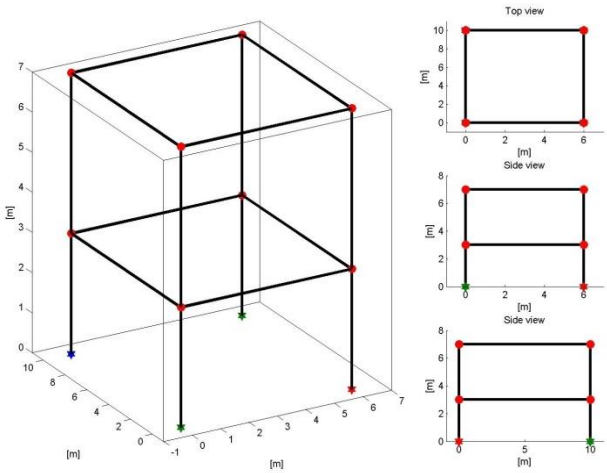

Figure 1 - TEST 1 - Geometry

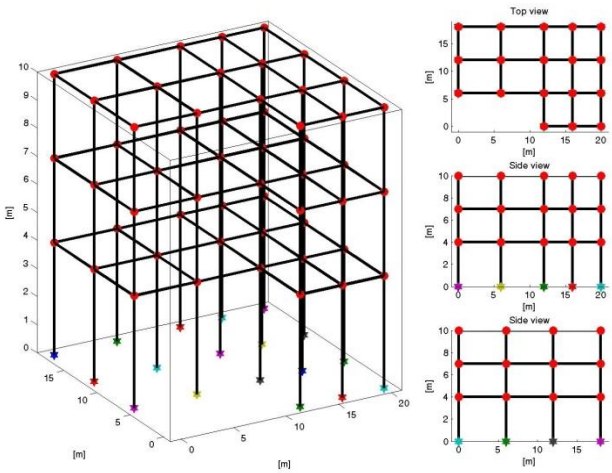

Figure 2 - TEST 2 – Geometry

Starting with an initial model in which all the Young's Modulus are equal to E=30000000 kN/m^2, the field monitoring data were all numerically simulated by arbitrarily changing the distribution of the elastic modulus among the structural elements. Appreciable changing in the modal response was obtained, although the deformed shape of all the considered modes, due to the simplicity of the structure, remained practically unchanged.

It has to be pointed out that at the time of these initial tests, only the possibility of generating numerical models with a non-uniform distribution of elastic modulus between the elements could be investigated (see simulation type 3). The other two options, related to the type of mechanical characteristics simulation, have been added later.

As a total, four analyses were done with the two buildings, two for the first and two for the second. Some data regarding the simulations are indicated in Table 3.

Considering ***TEST 1***, the finite element model updating was done, initially, considering 20 simulated measured modes with 6 dofs per node. Each run consisted in 10000 numerical simulations, repeated 10 times, for a total of 100000 numerical simulations. The need of performing several time the same amount of simulations comes from the fact that the methodology have to be calibrated in terms of both mean and standard deviation values of the *characteristic compressive strength of the concrete*. The procedure was done manually but the idea of adding to the methodology the possibility for a self-calibration of the concrete's mechanical characteristics simulation, will be discussed and implemented in the following tests. Finally, reasonable values for **μ** and **σ** of $\mathbf{f_{ck}}$ were obtained and the identified quantities were $\boldsymbol{\mu_{fck}}$**=16 N/mm**^{2} and $\boldsymbol{\sigma_{fck}}$**=5 N/mm**^{2}. The second part of the analysis concerning the same structure, were done performing the updating procedure considering only the first 3 simulated measured modes and excluding the modal rotations from the matching of the mode shapes. This reflects a more common situation, taking into account that, in reality, only the first modes are identified during dynamic identification and only the modal displacements are recorded from the instruments. The difficulty in exciting the structure in order to identify higher modes and the impossibility of having a tri-axial instrument (geophone) for each of the structural node so as to record the modal displacement in all the structure, represent the two major limits for the problem of finite element model updating of building using dynamic identification measurements.

Considering, instead, ***TEST 2***, the two analysis executed have the same specifications as in the first two analysis of *TEST 1*. Like mentioned before, the field monitoring data are simulated considering a non-uniform distribution of Young's Modulus among the members. The first analysis (n° 4) takes into account 20 simulated measured modes with 6 dofs per node while the second analysis (n° 5) considers the same field monitoring data. However, in this case, only 3 simulated measured modes, with 3 dofs per node (translations), contribute to the updating process.

Analysis	Structure	Total Simulations	(Simulated) Measured Modes n°
1	TEST 1	100000	20
2	TEST 2	12000	20
3	TEST 1	10000	3 (no rotations)
4	TEST 2	2000	3 (no rotations)

Table 3 - List of the performed tests for the preliminary analyses

12.1 *Analysis with Complete Measured Data*

12.1.1 Geometry

The structures considered for the test of the methodology are showed in Figure 3 and Figure 4. The one presented initially has a very simple and regular geometry. Some features are indicated as follow, together with Figure 3, showing the geometry of the building:

- *bay length X direction* 6 m;
- *bay length Z direction* 10 m;
- *interstorey height - level 1* 3 m;
- *interstorey height - level 2* 4 m;
- *beam section* 0.20x0.20 m;
- column section 0.30x0.30 m.

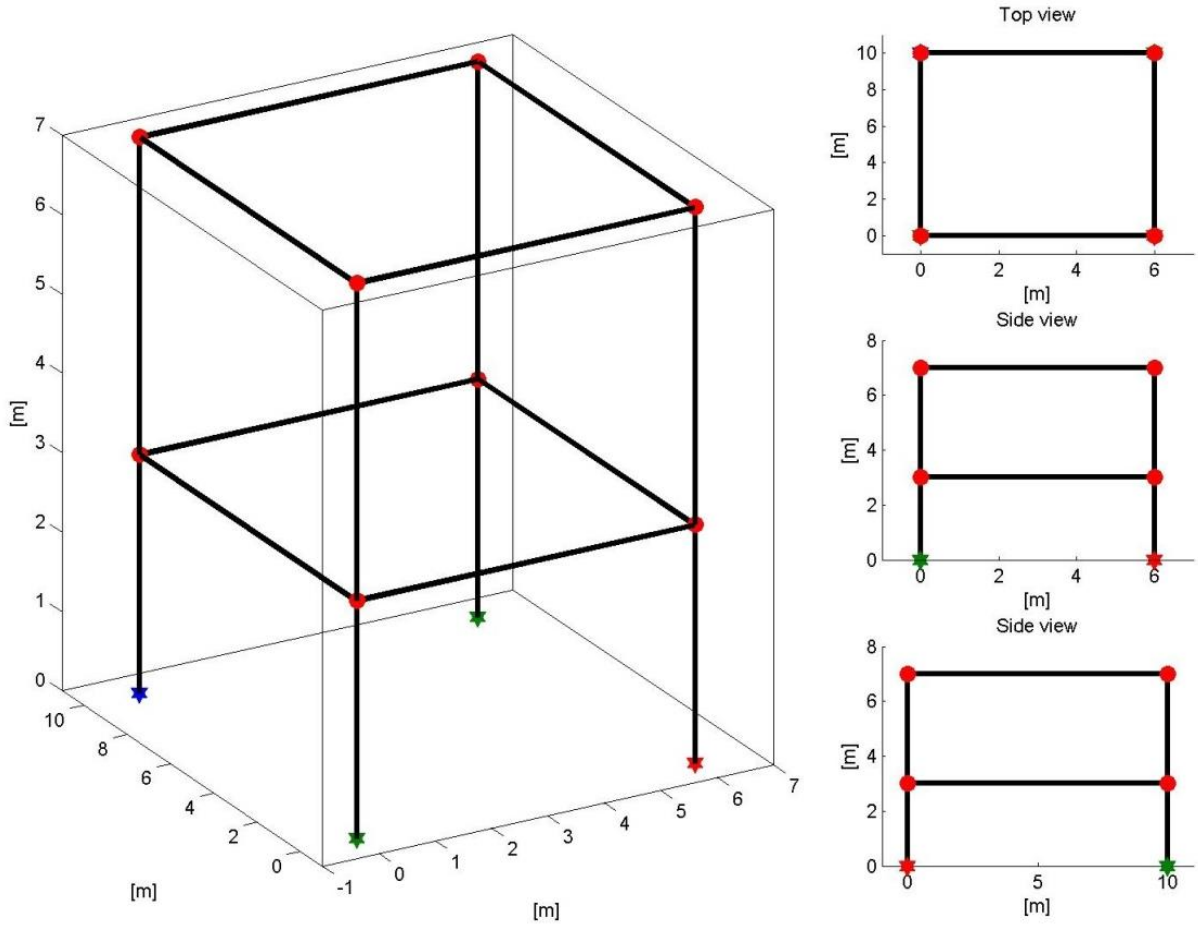

Figure 3 - TEST 1 - Perspective, plan, front and side views

The test is further repeated considering a second structure, showed in Figure 4. The geometrical characteristics of the building are indicated below:

- *bay length X direction* 6 m and 4 m;
- *bay length Z direction* 6 m and 4 m;
- *interstorey height - level 1* 4 m;
- *interstorey height - level 2* 3 m;
- *interstorey height - level 3* 3 m;
- *beam's section* 0.30x0.30 m;
- *column's section* 0.30x0.30 m.

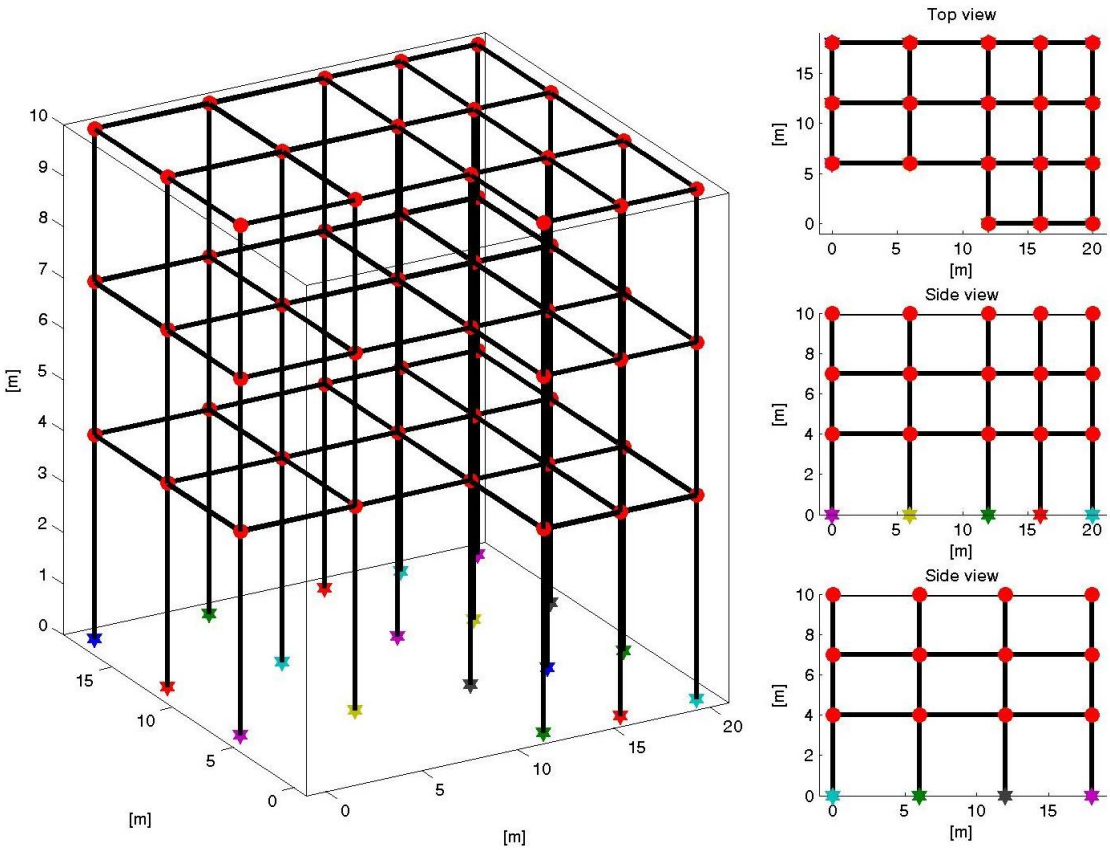

Figure 4 - TEST 2 - Perspective, plan, front and side views

12.1.2 Simulation of the Field Monitoring Data

Regarding the field monitoring data, those were simulated by arbitrarily assigning different elastic modulus to the elements. In Table 4 and Table 5, the mechanical characteristics of the elements for the simulation of the measured eigenfrequencies and eigenvectors are showed, for both structures.

Table 4 - Mechanical characteristics of the structural elements - Analysis 1 _ TEST 1

eleType	eleTag	iNode	jNode	A [m^2]	**E [kN/m^2]**	G [kN/m^2]	J [m^4]	I_y [m^4]	I_z [m^4]	trans Tag
elasticBeamColumn	1	1	3	0.09	**28000000**	11666666	0.001142	0.000675	0.000675	1
elasticBeamColumn	2	2	4	0.09	**31000000**	12916666	0.001142	0.000675	0.000675	1
elasticBeamColumn	3	3	5	0.09	**27000000**	11250000	0.001142	0.000675	0.000675	1
elasticBeamColumn	4	4	6	0.09	**32000000**	13333333	0.001142	0.000675	0.000675	1
elasticBeamColumn	5	7	9	0.09	**27000000**	11250000	0.001142	0.000675	0.000675	1
elasticBeamColumn	6	8	10	0.09	**27000000**	11250000	0.001142	0.000675	0.000675	1
elasticBeamColumn	7	9	11	0.09	**30000000**	12500000	0.001142	0.000675	0.000675	1
elasticBeamColumn	8	10	12	0.09	**26000000**	10833333	0.001142	0.000675	0.000675	1
elasticBeamColumn	9	3	4	0.04	**30000000**	12500000	0.000226	0.000133	0.000133	2
elasticBeamColumn	10	3	9	0.04	**30000000**	12500000	0.000226	0.000133	0.000133	2
elasticBeamColumn	11	9	10	0.04	**29000000**	12083333	0.000226	0.000133	0.000133	2
elasticBeamColumn	12	4	10	0.04	**29000000**	12083333	0.000226	0.000133	0.000133	2
elasticBeamColumn	13	5	6	0.04	**30000000**	12500000	0.000226	0.000133	0.000133	2
elasticBeamColumn	14	5	11	0.04	**30000000**	12500000	0.000226	0.000133	0.000133	2
elasticBeamColumn	15	11	12	0.04	**31000000**	12916666	0.000226	0.000133	0.000133	2
elasticBeamColumn	16	6	12	0.04	**30000000**	12500000	0.000226	0.000133	0.000133	2

Table 5 - Mechanical characteristics of the structural elements - Analysis 2 _ TEST 2

eleType	eleTag	iNode	jNode	A [m^2]	**E [kN/m^2]**	G [kN/m^2]	J [m^4]	I_y [m^4]	I_z [m^4]	trans Tag
elasticBeamColumn	1	19	20	0.09	**30000000**	12500000	0.001142	0.000675	0.000675	2
elasticBeamColumn	2	20	21	0.09	**29000000**	12083333	0.001142	0.000675	0.000675	2
elasticBeamColumn	3	22	23	0.09	**27000000**	11250000	0.001142	0.000675	0.000675	2
elasticBeamColumn	4	23	24	0.09	**31000000**	12916666	0.001142	0.000675	0.000675	2
elasticBeamColumn	5	24	25	0.09	**32000000**	13333333	0.001142	0.000675	0.000675	2
elasticBeamColumn	6	25	26	0.09	**26000000**	10833333	0.001142	0.000675	0.000675	2
elasticBeamColumn	7	27	28	0.09	**33000000**	13750000	0.001142	0.000675	0.000675	2
elasticBeamColumn	8	28	29	0.09	**30000000**	12500000	0.001142	0.000675	0.000675	2
elasticBeamColumn	9	29	30	0.09	**29000000**	12083333	0.001142	0.000675	0.000675	2
elasticBeamColumn	10	30	31	0.09	**28000000**	11666666	0.001142	0.000675	0.000675	2
elasticBeamColumn	11	32	33	0.09	**30000000**	12500000	0.001142	0.000675	0.000675	2
elasticBeamColumn	12	33	34	0.09	**30000000**	12500000	0.001142	0.000675	0.000675	2
elasticBeamColumn	13	34	35	0.09	**26000000**	10833333	0.001142	0.000675	0.000675	2
elasticBeamColumn	14	35	36	0.09	**27000000**	11250000	0.001142	0.000675	0.000675	2
elasticBeamColumn	15	37	38	0.09	**31000000**	12916666	0.001142	0.000675	0.000675	2
elasticBeamColumn	16	38	39	0.09	**32000000**	13333333	0.001142	0.000675	0.000675	2
elasticBeamColumn	17	40	41	0.09	**30000000**	12500000	0.001142	0.000675	0.000675	2
elasticBeamColumn	18	41	42	0.09	**30000000**	12500000	0.001142	0.000675	0.000675	2
elasticBeamColumn	19	42	43	0.09	**30000000**	12500000	0.001142	0.000675	0.000675	2
elasticBeamColumn	20	43	44	0.09	**30000000**	12500000	0.001142	0.000675	0.000675	2
elasticBeamColumn	21	45	46	0.09	**27000000**	11250000	0.001142	0.000675	0.000675	2
elasticBeamColumn	22	46	47	0.09	**33000000**	13750000	0.001142	0.000675	0.000675	2
elasticBeamColumn	23	47	48	0.09	**32000000**	13333333	0.001142	0.000675	0.000675	2

elasticBeamColumn	24	48	49	0.09	**26000000**	10833333	0.001142	0.000675	0.000675	2
elasticBeamColumn	25	50	51	0.09	**30000000**	12500000	0.001142	0.000675	0.000675	2
elasticBeamColumn	26	51	52	0.09	**29000000**	12083333	0.001142	0.000675	0.000675	2
elasticBeamColumn	27	52	53	0.09	**28000000**	11666666	0.001142	0.000675	0.000675	2
elasticBeamColumn	28	53	54	0.09	**30000000**	12500000	0.001142	0.000675	0.000675	2
elasticBeamColumn	29	55	56	0.09	**30000000**	12500000	0.001142	0.000675	0.000675	2
elasticBeamColumn	30	56	57	0.09	**30000000**	12500000	0.001142	0.000675	0.000675	2
elasticBeamColumn	31	58	59	0.09	**30000000**	12500000	0.001142	0.000675	0.000675	2
elasticBeamColumn	32	59	60	0.09	**30000000**	12500000	0.001142	0.000675	0.000675	2
elasticBeamColumn	33	60	61	0.09	**33000000**	13750000	0.001142	0.000675	0.000675	2
elasticBeamColumn	34	61	62	0.09	**27000000**	11250000	0.001142	0.000675	0.000675	2
elasticBeamColumn	35	63	64	0.09	**31000000**	12916666	0.001142	0.000675	0.000675	2
elasticBeamColumn	36	64	65	0.09	**32000000**	13333333	0.001142	0.000675	0.000675	2
elasticBeamColumn	37	65	66	0.09	**30000000**	12500000	0.001142	0.000675	0.000675	2
elasticBeamColumn	38	66	67	0.09	**26000000**	10833333	0.001142	0.000675	0.000675	2
elasticBeamColumn	39	68	69	0.09	**30000000**	12500000	0.001142	0.000675	0.000675	2
elasticBeamColumn	40	69	70	0.09	**26000000**	10833333	0.001142	0.000675	0.000675	2
elasticBeamColumn	41	70	71	0.09	**29000000**	12083333	0.001142	0.000675	0.000675	2
elasticBeamColumn	42	71	72	0.09	**28000000**	11666666	0.001142	0.000675	0.000675	2
elasticBeamColumn	43	21	26	0.09	**30000000**	12500000	0.001142	0.000675	0.000675	2
elasticBeamColumn	44	26	31	0.09	**30000000**	12500000	0.001142	0.000675	0.000675	2
elasticBeamColumn	45	31	36	0.09	**33000000**	13750000	0.001142	0.000675	0.000675	2
elasticBeamColumn	46	20	25	0.09	**30000000**	12500000	0.001142	0.000675	0.000675	2
elasticBeamColumn	47	25	30	0.09	**30000000**	12500000	0.001142	0.000675	0.000675	2
elasticBeamColumn	48	30	35	0.09	**26000000**	10833333	0.001142	0.000675	0.000675	2
elasticBeamColumn	49	19	24	0.09	**27000000**	11250000	0.001142	0.000675	0.000675	2
elasticBeamColumn	50	24	29	0.09	**31000000**	12916666	0.001142	0.000675	0.000675	2
elasticBeamColumn	51	29	34	0.09	**32000000**	13333333	0.001142	0.000675	0.000675	2
elasticBeamColumn	52	23	28	0.09	**30000000**	12500000	0.001142	0.000675	0.000675	2
elasticBeamColumn	53	28	33	0.09	**30000000**	12500000	0.001142	0.000675	0.000675	2
elasticBeamColumn	54	22	27	0.09	**33000000**	13750000	0.001142	0.000675	0.000675	2
elasticBeamColumn	55	27	32	0.09	**30000000**	12500000	0.001142	0.000675	0.000675	2
elasticBeamColumn	56	39	44	0.09	**30000000**	12500000	0.001142	0.000675	0.000675	2
elasticBeamColumn	57	44	49	0.09	**26000000**	10833333	0.001142	0.000675	0.000675	2
elasticBeamColumn	58	49	54	0.09	**28000000**	11666666	0.001142	0.000675	0.000675	2
elasticBeamColumn	59	38	43	0.09	**30000000**	12500000	0.001142	0.000675	0.000675	2
elasticBeamColumn	60	43	48	0.09	**27000000**	11250000	0.001142	0.000675	0.000675	2
elasticBeamColumn	61	48	53	0.09	**31000000**	12916666	0.001142	0.000675	0.000675	2
elasticBeamColumn	62	37	42	0.09	**32000000**	13333333	0.001142	0.000675	0.000675	2
elasticBeamColumn	63	42	47	0.09	**30000000**	12500000	0.001142	0.000675	0.000675	2
elasticBeamColumn	64	47	52	0.09	**30000000**	12500000	0.001142	0.000675	0.000675	2
elasticBeamColumn	65	41	46	0.09	**30000000**	12500000	0.001142	0.000675	0.000675	2
elasticBeamColumn	66	46	51	0.09	**26000000**	10833333	0.001142	0.000675	0.000675	2
elasticBeamColumn	67	40	45	0.09	**31000000**	12916666	0.001142	0.000675	0.000675	2
elasticBeamColumn	68	45	50	0.09	**32000000**	13333333	0.001142	0.000675	0.000675	2
elasticBeamColumn	69	57	62	0.09	**30000000**	12500000	0.001142	0.000675	0.000675	2
elasticBeamColumn	70	62	67	0.09	**30000000**	12500000	0.001142	0.000675	0.000675	2
elasticBeamColumn	71	67	72	0.09	**29000000**	12083333	0.001142	0.000675	0.000675	2
elasticBeamColumn	72	56	61	0.09	**28000000**	11666666	0.001142	0.000675	0.000675	2
elasticBeamColumn	73	61	66	0.09	**30000000**	12500000	0.001142	0.000675	0.000675	2
elasticBeamColumn	74	66	71	0.09	**30000000**	12500000	0.001142	0.000675	0.000675	2
elasticBeamColumn	75	55	60	0.09	**26000000**	10833333	0.001142	0.000675	0.000675	2
elasticBeamColumn	76	60	65	0.09	**30000000**	12500000	0.001142	0.000675	0.000675	2
elasticBeamColumn	77	65	70	0.09	**30000000**	12500000	0.001142	0.000675	0.000675	2
elasticBeamColumn	78	59	64	0.09	**30000000**	12500000	0.001142	0.000675	0.000675	2
elasticBeamColumn	79	64	69	0.09	**30000000**	12500000	0.001142	0.000675	0.000675	2
elasticBeamColumn	80	58	63	0.09	**26000000**	10833333	0.001142	0.000675	0.000675	2
elasticBeamColumn	81	63	68	0.09	**26000000**	10833333	0.001142	0.000675	0.000675	2

elasticBeamColumn	82	1	19	0.09	**27000000**	11250000	0.001142	0.000675	0.000675	1
elasticBeamColumn	83	19	37	0.09	**31000000**	12916666	0.001142	0.000675	0.000675	1
elasticBeamColumn	84	37	55	0.09	**33000000**	13750000	0.001142	0.000675	0.000675	1
elasticBeamColumn	85	2	20	0.09	**30000000**	12500000	0.001142	0.000675	0.000675	1
elasticBeamColumn	86	20	38	0.09	**29000000**	12083333	0.001142	0.000675	0.000675	1
elasticBeamColumn	87	38	56	0.09	**28000000**	11666666	0.001142	0.000675	0.000675	1
elasticBeamColumn	88	3	21	0.09	**30000000**	12500000	0.001142	0.000675	0.000675	1
elasticBeamColumn	89	21	39	0.09	**26000000**	10833333	0.001142	0.000675	0.000675	1
elasticBeamColumn	90	39	57	0.09	**30000000**	12500000	0.001142	0.000675	0.000675	1
elasticBeamColumn	91	8	26	0.09	**27000000**	11250000	0.001142	0.000675	0.000675	1
elasticBeamColumn	92	26	44	0.09	**30000000**	12500000	0.001142	0.000675	0.000675	1
elasticBeamColumn	93	44	62	0.09	**33000000**	13750000	0.001142	0.000675	0.000675	1
elasticBeamColumn	94	7	25	0.09	**27000000**	11250000	0.001142	0.000675	0.000675	1
elasticBeamColumn	95	25	43	0.09	**31000000**	12916666	0.001142	0.000675	0.000675	1
elasticBeamColumn	96	43	61	0.09	**32000000**	13333333	0.001142	0.000675	0.000675	1
elasticBeamColumn	97	6	24	0.09	**27000000**	11250000	0.001142	0.000675	0.000675	1
elasticBeamColumn	98	24	42	0.09	**30000000**	12500000	0.001142	0.000675	0.000675	1
elasticBeamColumn	99	42	60	0.09	**30000000**	12500000	0.001142	0.000675	0.000675	1
elasticBeamColumn	100	5	23	0.09	**29000000**	12083333	0.001142	0.000675	0.000675	1
elasticBeamColumn	101	23	41	0.09	**28000000**	11666666	0.001142	0.000675	0.000675	1
elasticBeamColumn	102	41	59	0.09	**33000000**	13750000	0.001142	0.000675	0.000675	1
elasticBeamColumn	103	4	22	0.09	**27000000**	11250000	0.001142	0.000675	0.000675	1
elasticBeamColumn	104	22	40	0.09	**30000000**	12500000	0.001142	0.000675	0.000675	1
elasticBeamColumn	105	40	58	0.09	**30000000**	12500000	0.001142	0.000675	0.000675	1
elasticBeamColumn	106	13	31	0.09	**27000000**	11250000	0.001142	0.000675	0.000675	1
elasticBeamColumn	107	31	49	0.09	**31000000**	12916666	0.001142	0.000675	0.000675	1
elasticBeamColumn	108	49	67	0.09	**32000000**	13333333	0.001142	0.000675	0.000675	1
elasticBeamColumn	109	12	30	0.09	**27000000**	11250000	0.001142	0.000675	0.000675	1
elasticBeamColumn	110	30	48	0.09	**30000000**	12500000	0.001142	0.000675	0.000675	1
elasticBeamColumn	111	48	66	0.09	**30000000**	12500000	0.001142	0.000675	0.000675	1
elasticBeamColumn	112	11	29	0.09	**27000000**	11250000	0.001142	0.000675	0.000675	1
elasticBeamColumn	113	29	47	0.09	**31000000**	12916666	0.001142	0.000675	0.000675	1
elasticBeamColumn	114	47	65	0.09	**32000000**	13333333	0.001142	0.000675	0.000675	1
elasticBeamColumn	115	10	28	0.09	**29000000**	12083333	0.001142	0.000675	0.000675	1
elasticBeamColumn	116	28	46	0.09	**28000000**	11666666	0.001142	0.000675	0.000675	1
elasticBeamColumn	117	46	64	0.09	**30000000**	12500000	0.001142	0.000675	0.000675	1
elasticBeamColumn	118	9	27	0.09	**27000000**	11250000	0.001142	0.000675	0.000675	1
elasticBeamColumn	119	27	45	0.09	**32000000**	13333333	0.001142	0.000675	0.000675	1
elasticBeamColumn	120	45	63	0.09	**30000000**	12500000	0.001142	0.000675	0.000675	1
elasticBeamColumn	121	18	36	0.09	**32000000**	13333333	0.001142	0.000675	0.000675	1
elasticBeamColumn	122	36	54	0.09	**27000000**	11250000	0.001142	0.000675	0.000675	1
elasticBeamColumn	123	54	72	0.09	**30000000**	12500000	0.001142	0.000675	0.000675	1
elasticBeamColumn	124	17	35	0.09	**27000000**	11250000	0.001142	0.000675	0.000675	1
elasticBeamColumn	125	35	53	0.09	**33000000**	13750000	0.001142	0.000675	0.000675	1
elasticBeamColumn	126	53	71	0.09	**32000000**	13333333	0.001142	0.000675	0.000675	1
elasticBeamColumn	127	16	34	0.09	**29000000**	12083333	0.001142	0.000675	0.000675	1
elasticBeamColumn	128	34	52	0.09	**28000000**	11666666	0.001142	0.000675	0.000675	1
elasticBeamColumn	129	52	70	0.09	**30000000**	12500000	0.001142	0.000675	0.000675	1
elasticBeamColumn	130	15	33	0.09	**33000000**	13750000	0.001142	0.000675	0.000675	1
elasticBeamColumn	131	33	51	0.09	**27000000**	11250000	0.001142	0.000675	0.000675	1
elasticBeamColumn	132	51	69	0.09	**27000000**	11250000	0.001142	0.000675	0.000675	1
elasticBeamColumn	133	14	32	0.09	**27000000**	11250000	0.001142	0.000675	0.000675	1
elasticBeamColumn	134	32	50	0.09	**33000000**	13750000	0.001142	0.000675	0.000675	1
elasticBeamColumn	135	50	68	0.09	**32000000**	13333333	0.001142	0.000675	0.000675	1

Table 6 - Comparison between initial and measured eigenvalues - Analysis 1 _ TEST 1

Mode	ω_I [rad/sec]	$\boldsymbol{\omega_E}$ **[rad/sec]**	**Δ [%]**
1	16.95	**16.64**	1.82%
2	19.03	**18.74**	1.53%
3	20.15	**19.87**	1.40%
4	24.14	**23.93**	0.87%
5	61.54	**60.87**	1.08%
6	73.36	**72.76**	0.83%
7	79.85	**78.00**	2.31%
8	80.25	**79.92**	0.41%
9	82.50	**80.83**	2.02%
10	83.25	**81.19**	2.47%
11	84.67	**83.57**	1.29%
12	91.45	**91.08**	0.41%
13	111.20	**108.28**	2.62%
14	118.15	**114.95**	2.71%
15	122.54	**121.08**	1.19%
16	129.17	**127.36**	1.40%
17	131.25	**128.20**	2.33%
18	133.94	**129.94**	2.98%
19	134.79	**131.47**	2.47%
20	136.03	**133.53**	1.84%

Table 7 - Comparison between initial and measured eigenvalues - Analysis 2 _ TEST 2

Mode	ω_I [rad/sec]	$\boldsymbol{\omega_E}$ **[rad/sec]**	**Δ [%]**
1	21.00	**21.28**	1.29%
2	21.96	**22.24**	1.25%
3	22.47	**22.89**	1.83%
4	30.89	**31.18**	0.93%
5	39.26	**39.78**	1.30%
6	45.94	**46.52**	1.25%
7	55.61	**56.35**	1.31%
8	59.96	**60.58**	1.03%
9	69.40	**70.47**	1.52%
10	71.51	**72.41**	1.24%
11	74.69	**75.44**	0.99%
12	77.03	**77.69**	0.85%
13	80.30	**81.12**	1.01%
14	84.50	**85.33**	0.97%
15	88.87	**89.79**	1.02%
16	90.38	**91.49**	1.22%
17	93.93	**94.92**	1.04%
18	113.97	**115.43**	1.26%
19	130.25	**131.71**	1.11%
20	133.06	**133.96**	0.67%

In Table 6 and Table 7, the comparison between the eigenfrequencies of the initial model and the eigenfrequencies obtained simulating the results of a dynamic identification are indicated for *TEST 1* and *TEST 2*. Although among the elements of *TEST 1*, the Young's Modulus range from E=26000000 kN/m^2 up to E=32000000 kN/m^2 (Δ_E=18.75%), the difference in the results of the eigenvalue analysis are not higher than the 2 % for the first 3 modes, and not more than 3% considering all the considered modes. For *TEST 2*, instead, the range of variability of the elastic modulus goes from E=26000000 kN/m^2 up to E=33000000 kN/m^2 (Δ_E=21.21%) and the difference in the results of the modal analysis are below the 2% for all the considered modes.

A number of **20 simulated measured eigenvectors**, considering **6 dofs per node**, are taken into account for the updating of the initial numerical models.

12.1.3 Calibration of the Mechanical Characteristics Simulation

In this preliminary analysis, a necessary step, as it can be observed in Table 11 and Table 12, was the calibration of the Young's Modulus generation for the two tested structures. In each test, fixed the number of generated numerical models, different values of mean and standard deviation for the characteristic compressive strength are investigated in order to see the variability of the generalized modal error.

Concrete	μ_{fck} [N/mm^2]	σ_{fck} [N/mm^2]
C28/35	28	8
C25/30	25	5
C20/25	22	5
C20/25	19	5
C16/20	16	5

Table 8 - Mean and standard deviation for f_{ck} [N/mm^2]

$f_{ck} + \sigma_{fck}$	f_{cm} [N/mm^2]	E_{cm} [N/mm^2]
36	44	34313
30	38	32837
27	35	32036
24	32	31187
21	29	30279

Table 9 - Upper part of the simulation of E_{cm} [N/mm^2]

$f_{ck} - \sigma_{fck}$	f_{cm} [N/mm^2]	E_{cm} [N/mm^2]
20	28	29962
20	28	29962
17	25	28960
14	22	27871
11	19	26672

Table 10 - Lower part of the simulation of E_{cm} [N/mm^2]

Test	N. Models	μ_{fck} [N/mm^2]	σ_{fck} [N/mm^2]
3.7	10000	28	8
3.8	10000	28	8
4.0	10000	25	5
4.1	10000	25	5
4.2	10000	22	5
4.3	10000	22	5
4.4	10000	19	5
4.5	10000	19	5
4.6	10000	16	5
4.7	10000	16	5

Table 11 - Calibration of the methodology for Analysis 1 - TEST 1

Test	N. Models	μ_{fck} [N/mm^2]	σ_{fck} [N/mm^2]
5.0	2000	25	5
5.1	2000	22	5
5.2	2000	19	5
5.3	2000	16	5
5.4	2000	19	8
5.5	2000	19	6

Table 12 - Calibration of the methodology for Analysis 2 - TEST 2

12.1.4 Results TEST 1

Among the set of simulations for *TEST 1*, the one that exhibited the lowest generalized modal error is the *model n°1332* from simulation 4.6. In Figure 5, all the numerical models, generated for test 4.6 are compared on the basis of the generalize modal error. A detailed comparison in terms of eigenfrequencies and distribution of Young's Modulus is subsequently done in Table 14 and Table 15, between the model that simulated the dynamic identification measurements, the initial model and the updated model. Finally, the first 3 mode shapes regarding updated model and field monitoring data are showed.

Table 13 - Results of all the set of simulations - Analysis 1 _ TEST 1

Test	N. Models	μ_{fck} [N/mm^2]	σ_{fck} [N/mm^2]	Best Fit Model n°	Gen. Modal Error
3.7	10000	28	8	3203	0.06065
3.8	10000	28	8	9439	0.07782
4.0	10000	25	5	3203	0.00335
4.1	10000	25	5	3203	0.00335
4.2	10000	22	5	5448	0.00480
4.3	10000	22	5	5612	0.00649
4.4	10000	19	5	5081	0.00214
4.5	10000	19	5	5081	0.00214
4.6	10000	16	5	1332	0.00172
4.7	10000	16	5	1332	0.00172

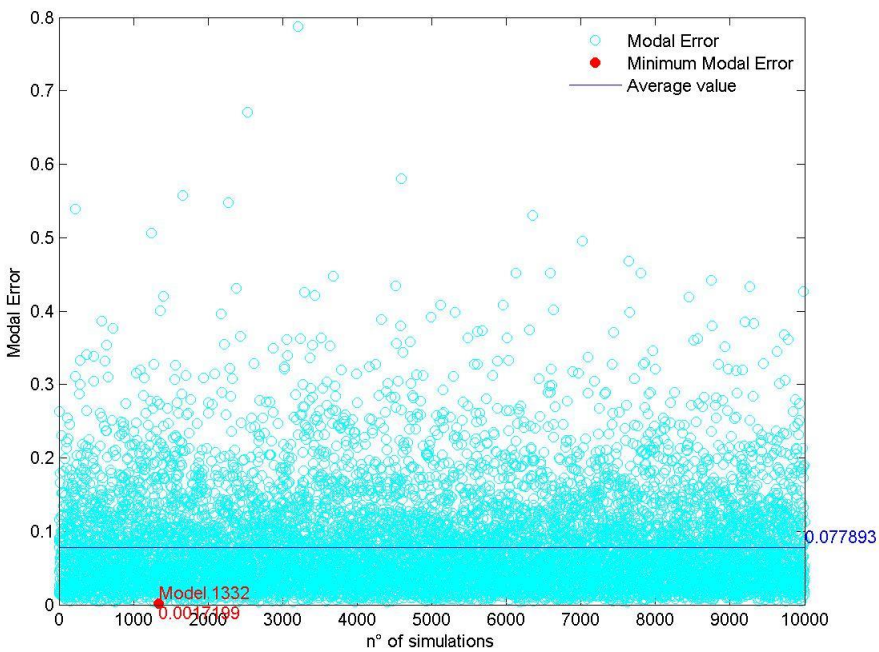

Figure 5 - Generalized Modal Errors (set 4.6 - Analysis 1 _ TEST 1)

Table 14 - Comparison of measured eigenfrequencies, initial updated models - Analysis 1 _ TEST 1

Mode	Measured data	Initial model	$\omega_{Ei}/\ \omega_{Ii}$	Model 1332	$\omega_{Ei}/\ \omega_{Ui}$
	ω_{Ei} [rad/sec]	ω_{Ii} [rad/sec]		ω_{Ui} [rad/sec]	
1	16.64	16.95	0.982	16.64	1.000
2	18.74	19.03	0.985	18.81	0.996
3	19.87	20.15	0.986	19.88	0.999
4	23.93	24.14	0.991	23.91	1.001
5	60.87	61.54	0.989	60.83	1.001
6	72.76	73.36	0.992	72.73	1.000
7	78.00	79.85	0.977	77.76	1.003
8	79.92	80.25	0.996	79.88	1.001
9	80.83	82.50	0.980	80.57	1.003
10	81.19	83.25	0.975	80.98	1.003
11	83.57	84.67	0.987	83.18	1.005
12	91.08	91.45	0.996	91.07	1.000
13	108.28	111.20	0.974	108.34	0.999
14	114.95	118.15	0.973	115.84	0.992
15	121.08	122.54	0.988	120.48	1.005
16	127.36	129.17	0.986	127.04	1.003
17	128.20	131.25	0.977	127.52	1.005
18	129.94	133.94	0.970	129.23	1.005
19	131.47	134.79	0.975	131.58	0.999
20	133.53	136.03	0.982	133.64	0.999

Table 15 - Comparison for the Young's Modulus between the model that simulate the field monitoring data, initial and updated models - Analysis 1 _ TEST 1

Element	Measured model	Initial model	$E_{Ej}/\ E_{Ij}$	Model 1332	$E_{Ej}/\ E_{Uj}$
	E_{Ej} [kN/m^2]	E_{Ij} [kN/m^2]		E_{Uj} [kN/m^2]	
1	28000000	30000000	0.933	27643000	1.013
2	31000000	30000000	1.033	27368000	1.133
3	27000000	30000000	0.900	28543000	0.946
4	32000000	30000000	1.067	26131000	1.225
5	27000000	30000000	0.900	28338000	0.953
6	27000000	30000000	0.900	29639000	0.911
7	30000000	30000000	1.000	29303000	1.024
8	26000000	30000000	0.867	29214000	0.890
9	30000000	30000000	1.000	31028000	0.967
10	30000000	30000000	1.000	30260000	0.991
11	29000000	30000000	0.967	30770000	0.942
12	29000000	30000000	0.967	29429000	0.985
13	30000000	30000000	1.000	30558000	0.982
14	30000000	30000000	1.000	30335000	0.989
15	31000000	30000000	1.033	29710000	1.043
16	30000000	30000000	1.000	29469000	1.018

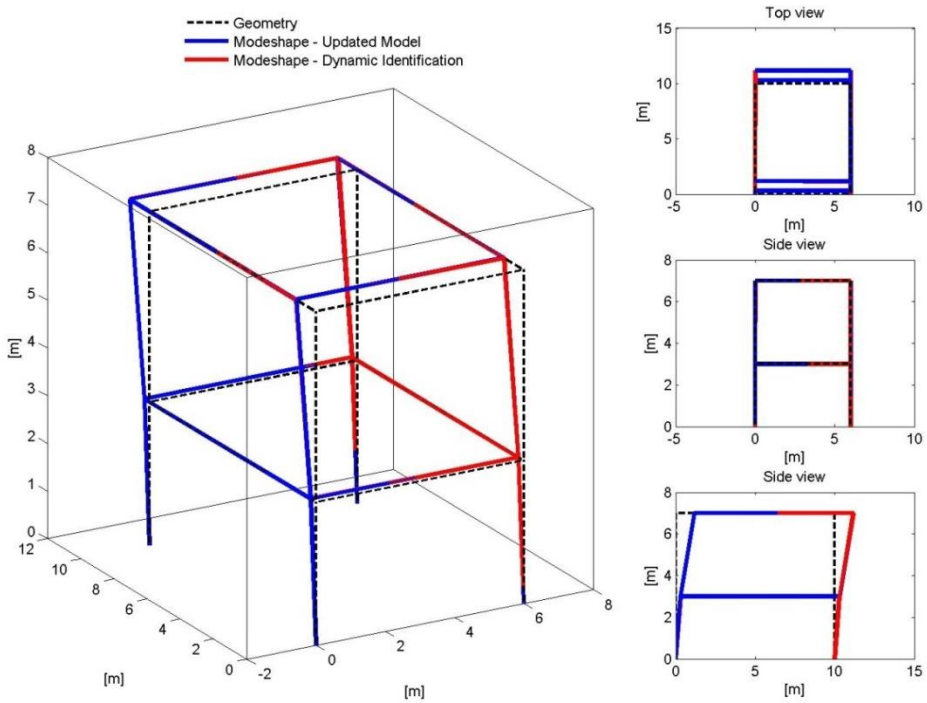

Figure 6 - Mode shape 1 - Comparison between updated model and experimental results - Analysis 1 _ TEST 1

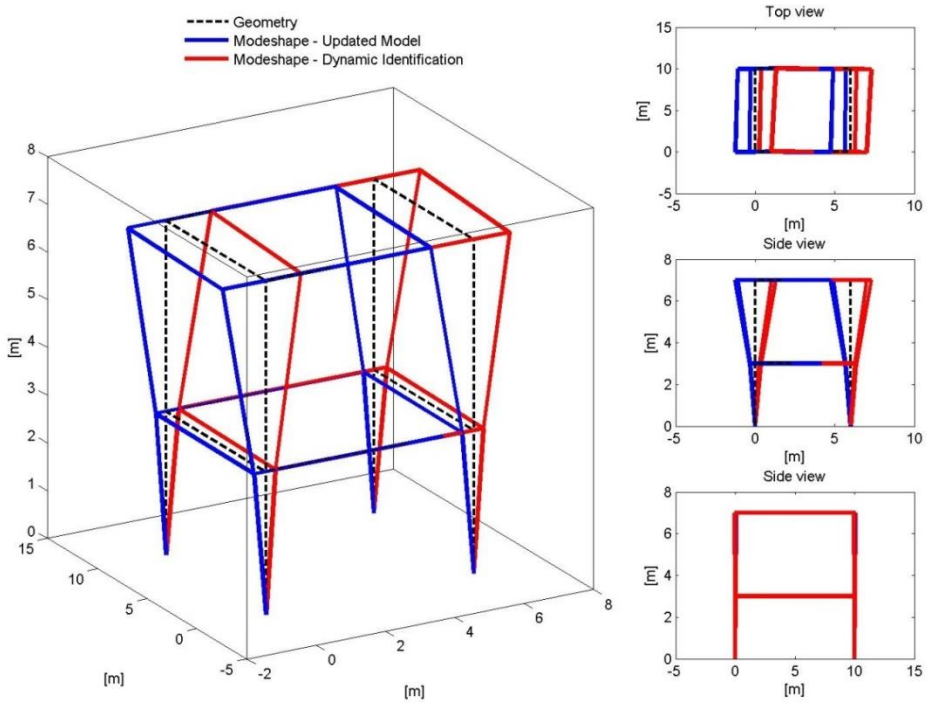

Figure 7 - Mode shape 2 - Comparison between updated model and experimental results - Analysis 1 _ TEST 1

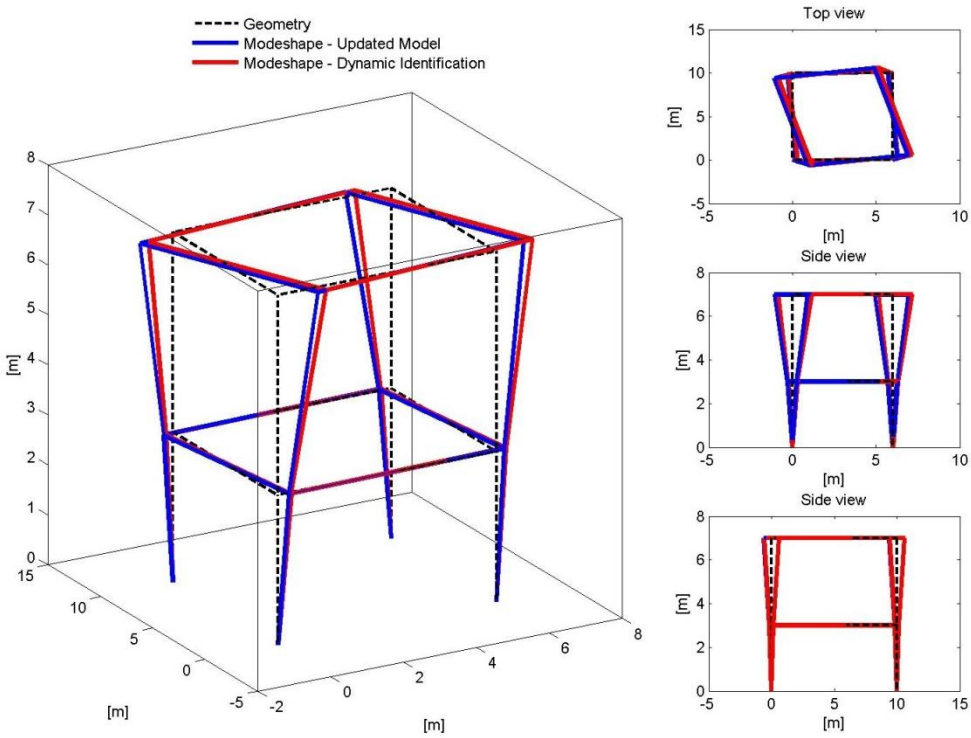

Figure 8 - Mode shape 3 - Comparison between updated model and experimental results - Analysis 1 _ TEST 1

12.1.5 Results TEST 2

Among the set of simulations for *TEST 2*, the one that exhibited the lowest generalized modal error is the *model n°165* from simulation 5.2. In Figure 9, all the numerical models, generated for test 5.2 are compared on the basis of the generalize modal error. A detailed comparison in terms of eigenfrequencies and distribution of Young's Modulus is subsequently done in Table 17 and Table 18, between the model that simulated the dynamic identification measurements, the initial model and the updated model. Finally, the first 3 mode shapes regarding updated model and field monitoring data are showed.

Table 16 - Results of all the set of simulations - Analysis 2_TEST 2

Test	N. Models	μ_{fck} [N/mm^2]	σ_{fck} [N/mm^2]	Best Fit Model	Modal Error
5.0	2000	25	5	247	0.23995
5.1	2000	22	5	247	0.04642
5.2	2000	19	5	165	0.00171
5.3	2000	16	5	1332	0.02016
5.4	2000	19	8	543	0.00220
5.5	2000	19	6	1822	0.00184

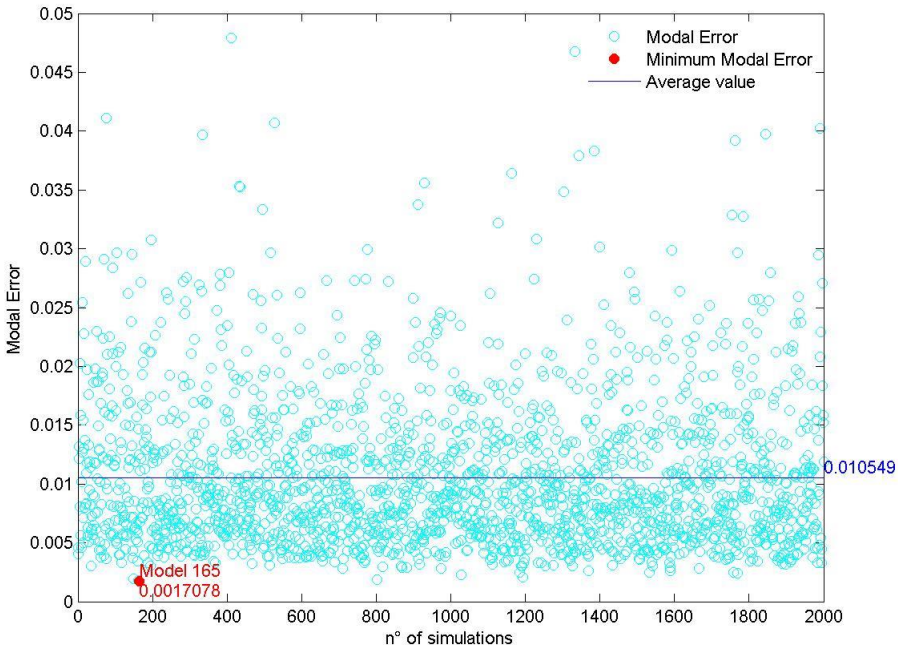

Figure 9 - Generalized Modal Errors (set 5.2 - Analysis 2 _ TEST 2)

Table 17 - Comparison of measured eigenfrequencies, initial updated models - Analysis 2 _ TEST 2

Mode	Measured data	Initial model	$\omega_{Ei}/\ \omega_{Ii}$	Model 165	$\omega_{Ei}/\ \omega_{Ui}$
	ω_{Ei} [rad/sec]	ω_{Ii} [rad/sec]		ω_{Ui} [rad/sec]	
1	21.00	21.28	0.987	20.96	1.002
2	21.96	22.24	0.987	21.93	1.001
3	22.47	22.89	0.982	22.55	0.996
4	30.89	31.18	0.991	30.73	1.005
5	39.26	39.78	0.987	39.21	1.001
6	45.94	46.52	0.987	46.07	0.997
7	55.61	56.35	0.987	55.61	1.000
8	59.96	60.58	0.990	59.91	1.001
9	69.40	70.47	0.985	69.34	1.001
10	71.51	72.41	0.988	71.66	0.998
11	74.69	75.44	0.990	74.81	0.998
12	77.03	77.69	0.992	77.05	1.000
13	80.30	81.12	0.990	80.24	1.001
14	84.50	85.33	0.990	84.43	1.001
15	88.87	89.79	0.990	88.74	1.001
16	90.38	91.49	0.988	90.70	0.996
17	93.93	94.92	0.990	93.88	1.001
18	113.97	115.43	0.987	113.84	1.001
19	130.25	131.71	0.989	130.46	0.998
20	133.06	133.96	0.993	133.53	0.996

Table 18 - Comparison for the Young's Modulus between the model that simulate the field monitoring data, initial and updated models - Analysis 2 _ TEST 2

Mode	Measured model	Initial model	$E_{Ej}/\ E_{Ij}$	Model 165	$E_{Ej}/\ E_{Uj}$
	E_{Ej} [kN/m2]	E_{Ij} [kN/m2]		E_{Uj} [kN/m2]	
1	30000000	30000000	1.000	29533000	1.016
2	29000000	30000000	0.967	29217000	0.993
3	27000000	30000000	0.900	29733000	0.908
4	31000000	30000000	1.033	29394000	1.055
5	32000000	30000000	1.067	27535000	1.162
6	26000000	30000000	0.867	28400000	0.915
7	33000000	30000000	1.100	30025000	1.099
8	30000000	30000000	1.000	33110000	0.906
9	29000000	30000000	0.967	27450000	1.056
10	28000000	30000000	0.933	28321000	0.989
11	30000000	30000000	1.000	27095000	1.107
12	30000000	30000000	1.000	26695000	1.124
13	26000000	30000000	0.867	28091000	0.926
14	27000000	30000000	0.900	28795000	0.938
15	31000000	30000000	1.033	28289000	1.096
16	32000000	30000000	1.067	29658000	1.079
17	30000000	30000000	1.000	27804000	1.079
18	30000000	30000000	1.000	27520000	1.090
19	30000000	30000000	1.000	31355000	0.957
20	30000000	30000000	1.000	30112000	0.996
21	27000000	30000000	0.900	27662000	0.976
22	33000000	30000000	1.100	26714000	1.235

23	32000000	30000000	1.067	27970000	1.144
24	26000000	30000000	0.867	31461000	0.826
25	30000000	30000000	1.000	29819000	1.006
26	29000000	30000000	0.967	31132000	0.932
27	28000000	30000000	0.933	30062000	0.931
28	30000000	30000000	1.000	29579000	1.014
29	30000000	30000000	1.000	29270000	1.025
30	30000000	30000000	1.000	30200000	0.993
31	30000000	30000000	1.000	29224000	1.027
32	30000000	30000000	1.000	27159000	1.105
33	33000000	30000000	1.100	29307000	1.126
34	27000000	30000000	0.900	31881000	0.847
35	31000000	30000000	1.033	30861000	1.005
36	32000000	30000000	1.067	29450000	1.087
37	30000000	30000000	1.000	27989000	1.072
38	26000000	30000000	0.867	30085000	0.864
39	30000000	30000000	1.000	30063000	0.998
40	26000000	30000000	0.867	30500000	0.852
41	29000000	30000000	0.967	30764000	0.943
42	28000000	30000000	0.933	30049000	0.932
43	30000000	30000000	1.000	27033000	1.110
44	30000000	30000000	1.000	30654000	0.979
45	33000000	30000000	1.100	28013000	1.178
46	30000000	30000000	1.000	28317000	1.059
47	30000000	30000000	1.000	31454000	0.954
48	26000000	30000000	0.867	28099000	0.925
49	27000000	30000000	0.900	28256000	0.956
50	31000000	30000000	1.033	30797000	1.007
51	32000000	30000000	1.067	28449000	1.125
52	30000000	30000000	1.000	27722000	1.082
53	30000000	30000000	1.000	27982000	1.072
54	33000000	30000000	1.100	30152000	1.094
55	30000000	30000000	1.000	29892000	1.004
56	30000000	30000000	1.000	30224000	0.993
57	26000000	30000000	0.867	33548000	0.775
58	28000000	30000000	0.933	24912000	1.124
59	30000000	30000000	1.000	29413000	1.020
60	27000000	30000000	0.900	26294000	1.027
61	31000000	30000000	1.033	30638000	1.012
62	32000000	30000000	1.067	30906000	1.035
63	30000000	30000000	1.000	31924000	0.940
64	30000000	30000000	1.000	29340000	1.022
65	30000000	30000000	1.000	31735000	0.945
66	26000000	30000000	0.867	25166000	1.033
67	31000000	30000000	1.033	28713000	1.080
68	32000000	30000000	1.067	27332000	1.171
69	30000000	30000000	1.000	29472000	1.018
70	30000000	30000000	1.000	30035000	0.999
71	29000000	30000000	0.967	31142000	0.931
72	28000000	30000000	0.933	31179000	0.898
73	30000000	30000000	1.000	29591000	1.014
74	30000000	30000000	1.000	28607000	1.049
75	26000000	30000000	0.867	29485000	0.882
76	30000000	30000000	1.000	28979000	1.035
77	30000000	30000000	1.000	28006000	1.071
78	30000000	30000000	1.000	29263000	1.025
79	30000000	30000000	1.000	29101000	1.031
80	26000000	30000000	0.867	26359000	0.986

81	26000000	30000000	0.867	30791000	0.844
82	27000000	30000000	0.900	25947000	1.041
83	31000000	30000000	1.033	27073000	1.145
84	33000000	30000000	1.100	31353000	1.053
85	30000000	30000000	1.000	30978000	0.968
86	29000000	30000000	0.967	29835000	0.972
87	28000000	30000000	0.933	29749000	0.941
88	30000000	30000000	1.000	29852000	1.005
89	26000000	30000000	0.867	31752000	0.819
90	30000000	30000000	1.000	30712000	0.977
91	27000000	30000000	0.900	28085000	0.961
92	30000000	30000000	1.000	30662000	0.978
93	33000000	30000000	1.100	28001000	1.179
94	27000000	30000000	0.900	25021000	1.079
95	31000000	30000000	1.033	32922000	0.942
96	32000000	30000000	1.067	30932000	1.035
97	27000000	30000000	0.900	27218000	0.992
98	30000000	30000000	1.000	31449000	0.954
99	30000000	30000000	1.000	30453000	0.985
100	29000000	30000000	0.967	28730000	1.009
101	28000000	30000000	0.933	29051000	0.964
102	33000000	30000000	1.100	30423000	1.085
103	27000000	30000000	0.900	29267000	0.923
104	30000000	30000000	1.000	30649000	0.979
105	30000000	30000000	1.000	33201000	0.904
106	27000000	30000000	0.900	29578000	0.913
107	31000000	30000000	1.033	32533000	0.953
108	32000000	30000000	1.067	30063000	1.064
109	27000000	30000000	0.900	29462000	0.916
110	30000000	30000000	1.000	29695000	1.010
111	30000000	30000000	1.000	28411000	1.056
112	27000000	30000000	0.900	31441000	0.859
113	31000000	30000000	1.033	29842000	1.039
114	32000000	30000000	1.067	29283000	1.093
115	29000000	30000000	0.967	28851000	1.005
116	28000000	30000000	0.933	30412000	0.921
117	30000000	30000000	1.000	28310000	1.060
118	27000000	30000000	0.900	30774000	0.877
119	32000000	30000000	1.067	29861000	1.072
120	30000000	30000000	1.000	28198000	1.064
121	32000000	30000000	1.067	30851000	1.037
122	27000000	30000000	0.900	29324000	0.921
123	30000000	30000000	1.000	29084000	1.031
124	27000000	30000000	0.900	28146000	0.959
125	33000000	30000000	1.100	29207000	1.130
126	32000000	30000000	1.067	33040000	0.969
127	29000000	30000000	0.967	30090000	0.964
128	28000000	30000000	0.933	28128000	0.995
129	30000000	30000000	1.000	30294000	0.990
130	33000000	30000000	1.100	29154000	1.132
131	27000000	30000000	0.900	30649000	0.881
132	27000000	30000000	0.900	29172000	0.926
133	27000000	30000000	0.900	27487000	0.982
134	33000000	30000000	1.100	28359000	1.164
135	32000000	30000000	1.067	29793000	1.074

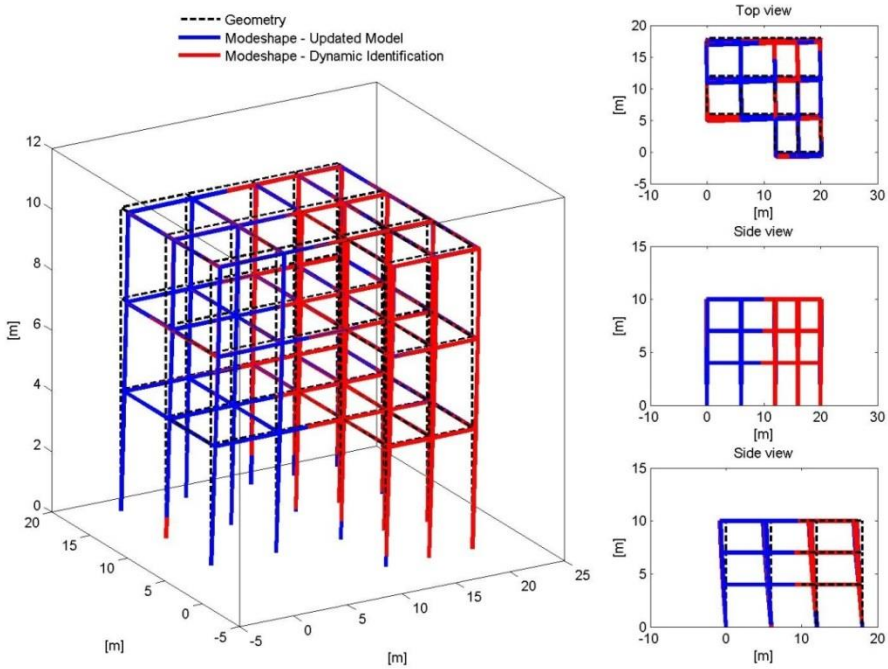

Figure 10 - Mode shape 1 - Comparison between updated model and experimental results - Analysis 2 _ TEST 2

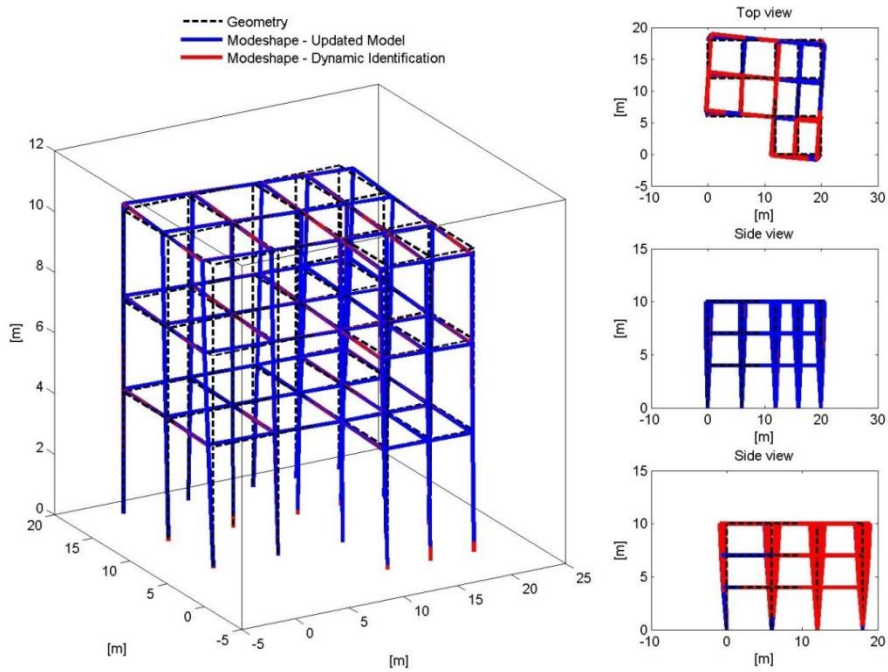

Figure 11 - Mode shape 2 - Comparison between updated model and experimental results - Analysis 2 _ TEST 2

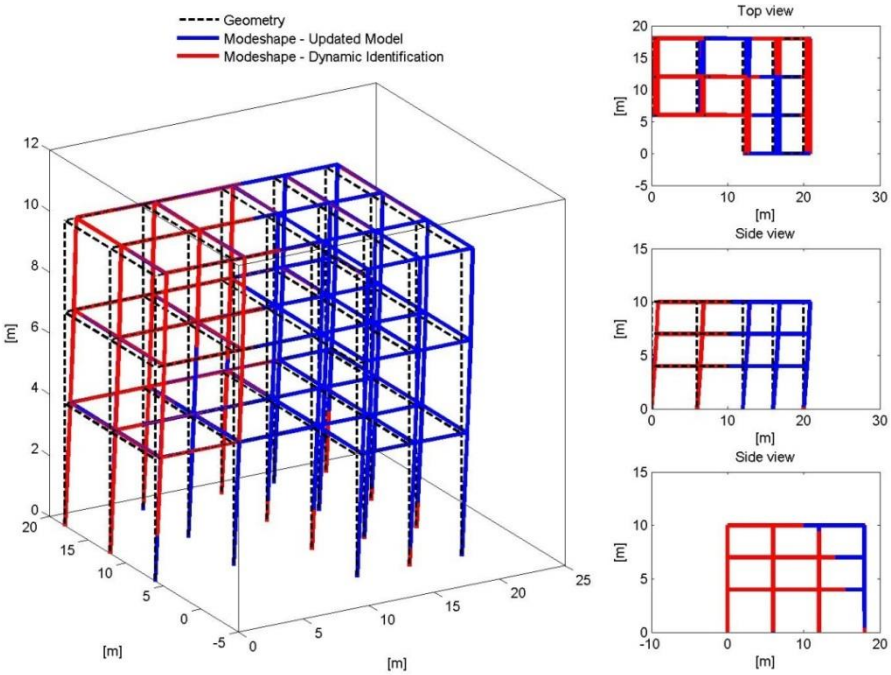

Figure 12 - Mode shape 3 - Comparison between updated model and experimental results - Analysis 2 _ TEST 2

12.1.6 Conclusions

TEST 1

The analysis performed well and the updated model n°1332, indentified among set of simulations 4.6, showed a very good matching with the simulated experimental results, in terms of eigenfrequencies. For all the considered modes, the corresponding numerical eigenfrequency improved its value towards the experimental simulated one. It has to be pointed out, however, that the experimental results were already close enough to the modal results of the initial model. Due to the simple geometry of the structure, it's not possible to generate a considerable different modal response by changing only the distribution of the Young's Modulus among the structural members, for the simulation of the experimental modal quantities.

It can be noticed, also, that some of the set of simulations exhibited the same modal error. This is explained by the fact that, in Matlab (MathWorks, Inc., 2009), the implemented function which does the simulation of random numbers, following a standard normal distribution, repeated the same simulation of elastic modulus. Hence tests 4.6 and 4.7 (same 4.0 and 4.1, 4.4 and 4.5) deals practically with the same simulated numerical models.

Concerning the comparisons of the mode shapes, it's clear the perfect matching of the first translational mode. The second mode shape, also translational as the first one but in the other horizontal direction, has a good matching, although the two mode shapes, experimental and numerical, are opposite between each other. Finally, in the third torsional mode shape, small differences can be appreciate for the modal displacements.

TEST 2

For the calibration of the procedure in *TEST 2*, only tests with a number of 2000 simulations each were performed, while for the analyses with *TEST 1*, 10000 simulations were considered per time. Although this difference in terms of simulations, the updated model n°165, identified among the set of simulations 5.2, exhibited the lowest generalized modal error with an order of magnitude comparable with the errors obtained for the same type of test, but using the smaller structure.

For all the considered modes, the corresponding numerical eigenfrequency improved its value towards the measured ones, and the ratio between measured and numerical eigenfrequencies are practically equal to 1 for each of the 20 modes.

Concerning the comparisons of the deformed shapes, the numerical mode shapes qualitatively match the experimental results for all the first three eigenmodes.

12.2 *Analysis with Incomplete Measured Data*

In this second analysis the simulated field monitoring data are kept equal as in the previous analysis. However, for this specific case, only the first **3 simulated eigenfrequencies** and eigenvectors are considered for the updating procedure and the **modal rotations** are **not included** in the process.

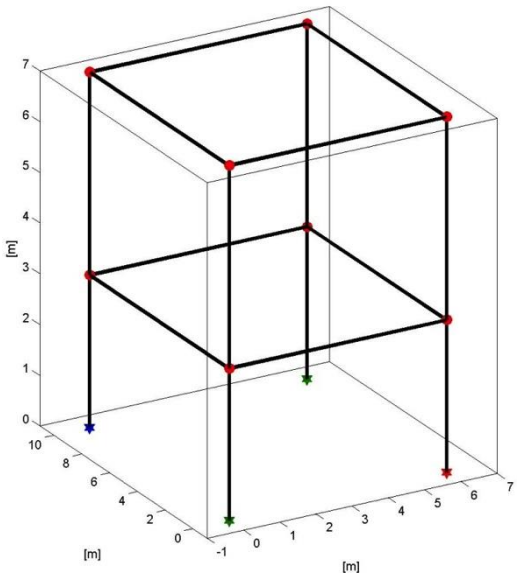

Figure 13 - TEST 1 - Geometry

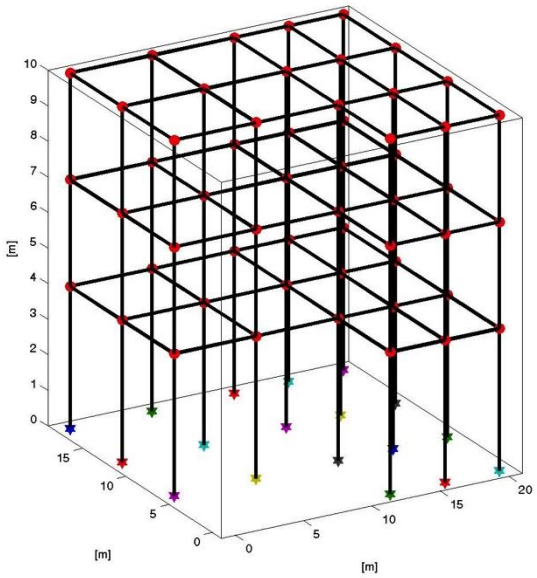

Figure 14 - TEST 2 - Geometry

Mode	ω_I [rad/sec]	ω_E **[rad/sec]**	**Δ [%]**
1	16.95	**16.64**	1.82%
2	19.03	**18.74**	1.53%
3	20.15	**19.87**	1.40%

Table 19 - Simulated dynamic identification measurements - Analysis 3 _TEST 1

Mode	ω_I [rad/sec]	ω_E **[rad/sec]**	**Δ [%]**
1	21.00	**21.28**	1.29%
2	21.96	**22.24**	1.25%
3	22.47	**22.89**	1.83%

Table 20 - Simulated dynamic identification measurements - Analysis 4 _ TEST 2

The simulations have been performed to verify the difference in the results of the updating procedure when the specifications regarding the values of mean and standard deviation of the concrete characteristic compressive strength concrete remain the same, and only the experimental measured data change. The simulation run with $\boldsymbol{\mu_{fck}=16\ N/mm^2}$ and $\boldsymbol{\sigma_{fck}=5\ N/mm^2}$ for *TEST 1* and $\boldsymbol{\mu_{fck}=19\ N/mm^2}$ and $\boldsymbol{\sigma_{fck}=5\ N/mm^2}$ for *TEST 2*, like in the previous analyses.

12.2.1 Results TEST 1

The lowest modal error has been calculated for *model 2133*, as indicated in Table 21 and Figure 15. A detailed comparison in terms of eigenfrequencies and distribution of Young's Modulus is subsequently done in Table 22 and Table 23, between the model that simulated the dynamic identification measurements, the initial model and the updated model. Finally, the first 3 mode shapes regarding updated model and field monitoring data are showed.

Table 21 - Results of all the set of simulations - Analysis 3 _ TEST 1

Test	N. Models	μ_{fck} [N/mm^2]	σ_{fck} [N/mm^2]	Best Fit Model	Modal Error
4.6	10000	16	5	2133	1.40550E-06

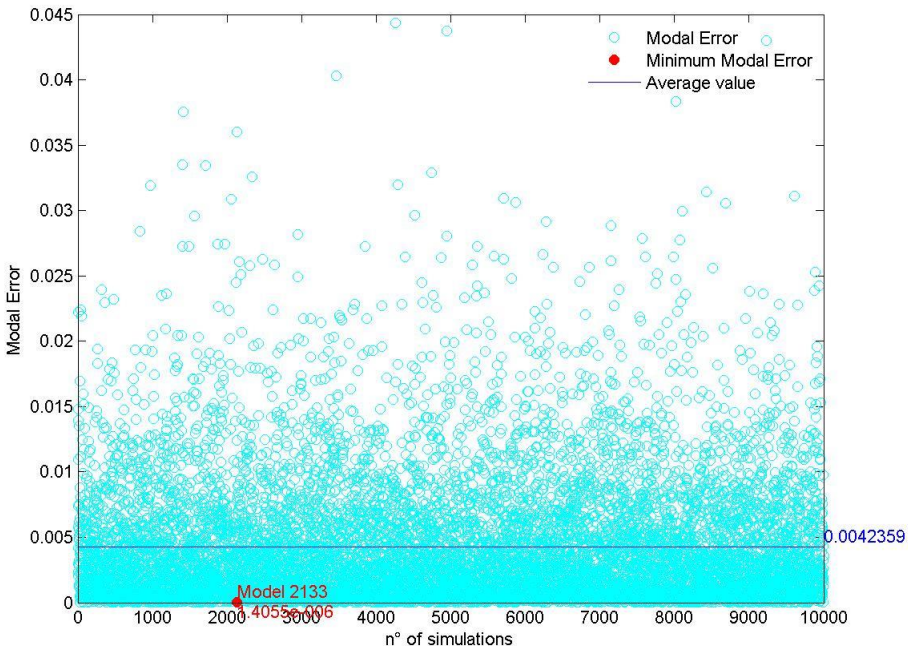

Figure 15 - Generalized Modal Errors (set 4.6 - Analysis 3 _ TEST 1)

Table 22 - Comparison of measured eigenfrequencies, initial updated models - Analysis 3 _ TEST 1

Mode	**Measured data**	**Initial model**	$\omega_{Ei}/\ \omega_{Ii}$	**Model 2133**	$\omega_{Ei}/\ \omega_{Ui}$
	ω_{Ei} [rad/sec]	ω_{Ii} [rad/sec]		ω_{Ui} [rad/sec]	
1	16.64	16.95	0.982	16.64	1.000
2	18.74	19.03	0.985	18.74	1.000
3	19.87	20.15	0.986	19.87	1.000

Table 23 - Comparison for the Young's Modulus between the model that simulate the field monitoring data, initial and updated models - Analysis 3 _ TEST 1

Element	**Measured model**	**Initial model**	$E_{Ej}/\ E_{Ij}$	**Model 2133**	$E_{Ej}/\ E_{Uj}$
	E_{Ej} [kN/m^2]	E_{Ij} [kN/m^2]		E_{Uj} [kN/m^2]	
1	28000000	30000000	0.933	29017000	0.965
2	31000000	30000000	1.033	27563000	1.125
3	27000000	30000000	0.900	27038000	0.999
4	32000000	30000000	1.067	26973000	1.186
5	27000000	30000000	0.900	28008000	0.964
6	27000000	30000000	0.900	32931000	0.820
7	30000000	30000000	1.000	30522000	0.983
8	26000000	30000000	0.867	27726000	0.938
9	30000000	30000000	1.000	27780000	1.080
10	30000000	30000000	1.000	30593000	0.981
11	29000000	30000000	0.967	31299000	0.927
12	29000000	30000000	0.967	32113000	0.903
\13	30000000	30000000	1.000	29715000	1.010
14	30000000	30000000	1.000	28391000	1.057
15	31000000	30000000	1.033	28390000	1.092
16	30000000	30000000	1.000	25471000	1.178

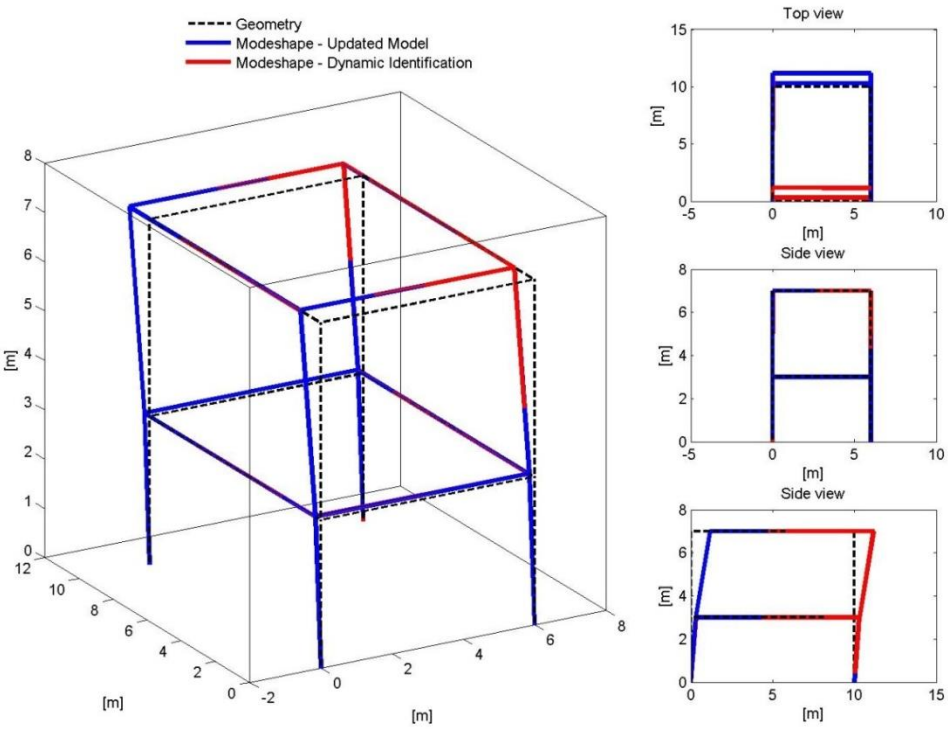

Figure 16 - Mode shape 1 - Comparison between updated model and experimental results - Analysis 3 _ TEST 1

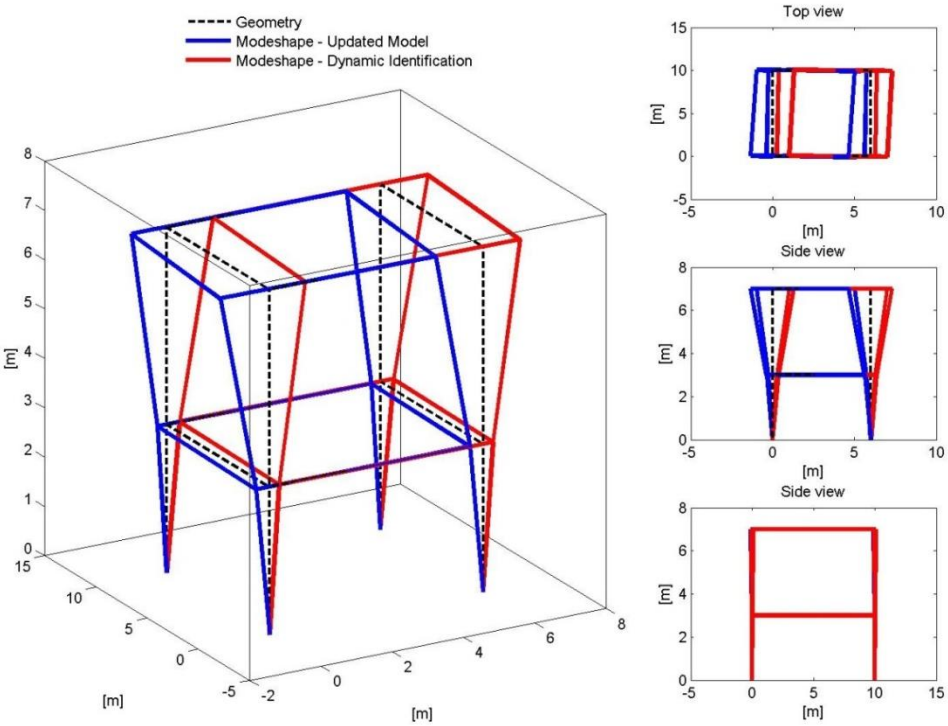

Figure 17 - Mode shape 2 - Comparison between updated model and experimental results - Analysis 3 _ TEST 1

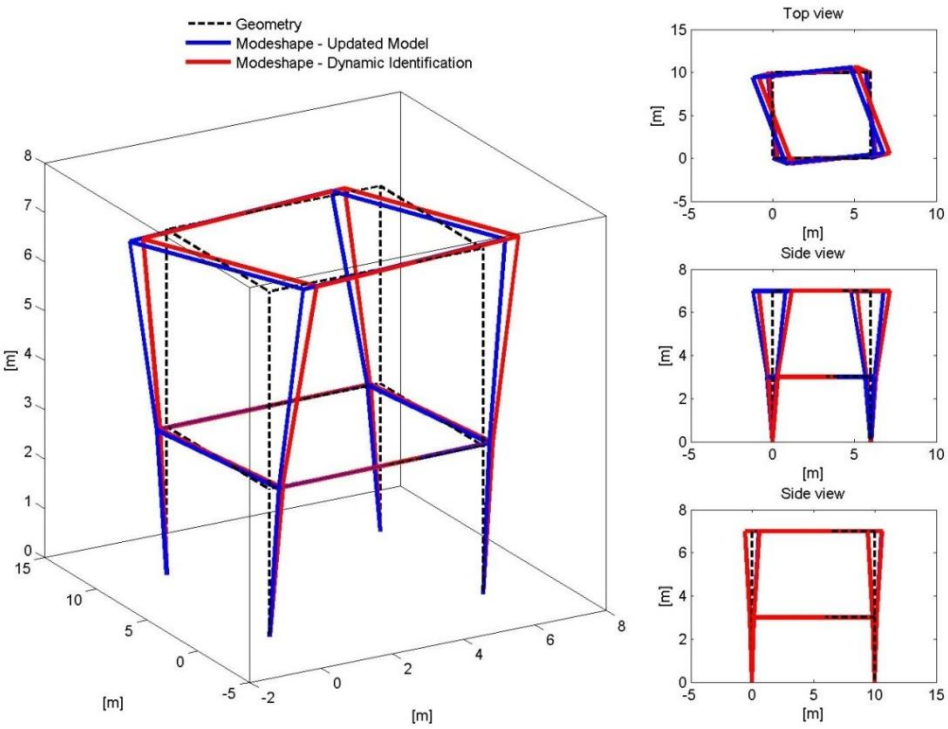

Figure 18 - Mode shape 3 - Comparison between updated model and experimental results - Analysis 3 _ TEST 1

12.2.2 Results TEST 2

The lowest modal error has been calculated for *model 615*, as indicated in Table 24 and Figure 19. A detailed comparison in terms of eigenfrequencies and distribution of Young's Modulus is subsequently done in Table 25 and Table 26, between the model that simulated the dynamic identification measurements, the initial model and the updated model. Finally, the first 3 mode shapes regarding updated model and field monitoring data are illustrated.

Table 24 - Results of all the set of simulations - Analysis 4 _ TEST 2

Test	N. Models	μ_{fck} [N/mm^2]	σ_{fck} [N/mm^2]	Best Fit Model	Modal Error
5.2	2000	19	5	615	6.37730E-06

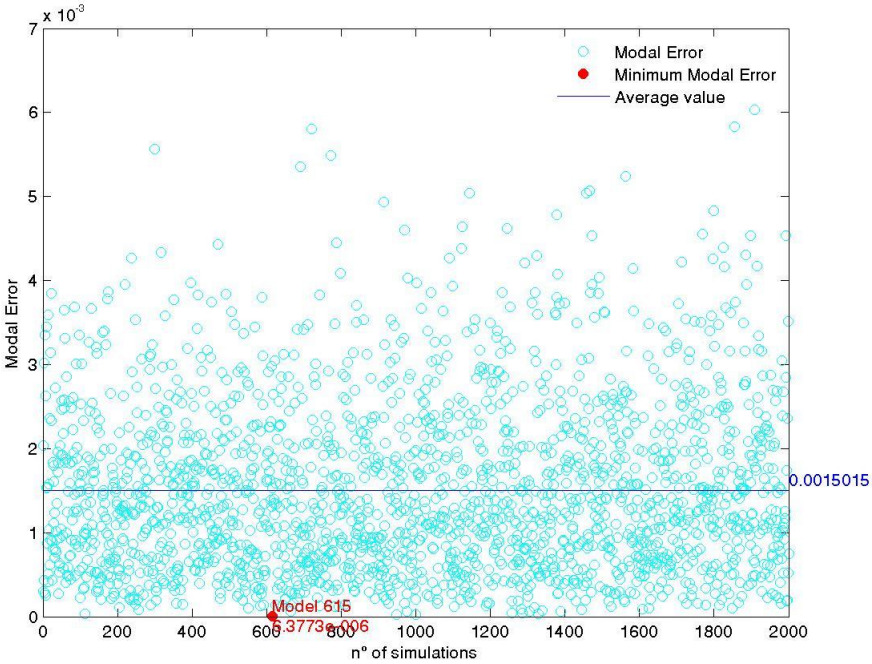

Figure 19 - Generalized Modal Errors (set 5.2 - Analysis 4 _ TEST 2)

Table 25 - Comparison of measured eigenfrequencies, initial updated models - Analysis 4 _ TEST 2

Mode	Measured data	Initial model	$\omega_{Ei}/\ \omega_{Ii}$	Model 615	$\omega_{Ei}/\ \omega_{Ui}$
	ω_{Ei} [rad/sec]	ω_{Ii} [rad/sec]		ω_{Ui} [rad/sec]	
1	21.00	21.28	0.987	20.98	1.001
2	21.96	22.24	0.987	21.96	1.000
3	22.47	22.89	0.982	22.46	1.000

Table 26 - Comparison for the Young's Modulus between the model that simulate the field monitoring data, initial and updated models - Analysis 4 _ TEST 2

Mode	**Measured model**	**Initial model**	E_{Ej}/ E_{Ij}	**Model 615**	E_{Ej}/ E_{Uj}
	E_{Ej} [kN/m2]	E_{Ij} [kN/m2]		E_{Uj} [kN/m2]	
1	30000000	30000000	1.000	28901000	1.038
2	29000000	30000000	0.967	27029000	1.073
3	27000000	30000000	0.900	30152000	0.895
4	31000000	30000000	1.033	29338000	1.057
5	32000000	30000000	1.067	29231000	1.095
6	26000000	30000000	0.867	28090000	0.926
7	33000000	30000000	1.100	29809000	1.107
8	30000000	30000000	1.000	26614000	1.127
9	29000000	30000000	0.967	29172000	0.994
10	28000000	30000000	0.933	30000000	0.933
11	30000000	30000000	1.000	28475000	1.054
12	30000000	30000000	1.000	30668000	0.978
13	26000000	30000000	0.867	29412000	0.884
14	27000000	30000000	0.900	27083000	0.997
15	31000000	30000000	1.033	29895000	1.037
16	32000000	30000000	1.067	31137000	1.028
17	30000000	30000000	1.000	33918000	0.884
18	30000000	30000000	1.000	27297000	1.099
19	30000000	30000000	1.000	30314000	0.990
20	30000000	30000000	1.000	28738000	1.044
21	27000000	30000000	0.900	28566000	0.945
22	33000000	30000000	1.100	28284000	1.167
23	32000000	30000000	1.067	31809000	1.006
24	26000000	30000000	0.867	28263000	0.920
25	30000000	30000000	1.000	28369000	1.057
26	29000000	30000000	0.967	31992000	0.906
27	28000000	30000000	0.933	29232000	0.958
28	30000000	30000000	1.000	26794000	1.120
29	30000000	30000000	1.000	29708000	1.010
30	30000000	30000000	1.000	28280000	1.061
31	30000000	30000000	1.000	29286000	1.024
32	30000000	30000000	1.000	28836000	1.040
33	33000000	30000000	1.100	27147000	1.216
34	27000000	30000000	0.900	31457000	0.858
35	31000000	30000000	1.033	31001000	1.000
36	32000000	30000000	1.067	25533000	1.253
37	30000000	30000000	1.000	31800000	0.943
38	26000000	30000000	0.867	28618000	0.909
39	30000000	30000000	1.000	30438000	0.986
40	26000000	30000000	0.867	28778000	0.903
41	29000000	30000000	0.967	30673000	0.945
42	28000000	30000000	0.933	28377000	0.987
43	30000000	30000000	1.000	28593000	1.049
44	30000000	30000000	1.000	34852000	0.861
45	33000000	30000000	1.100	30387000	1.086
46	30000000	30000000	1.000	26590000	1.128
47	30000000	30000000	1.000	31773000	0.944
48	26000000	30000000	0.867	29496000	0.881
49	27000000	30000000	0.900	31285000	0.863
50	31000000	30000000	1.033	31032000	0.999
51	32000000	30000000	1.067	28484000	1.123

52	30000000	30000000	1.000	32091000	0.935
53	30000000	30000000	1.000	28637000	1.048
54	33000000	30000000	1.100	27701000	1.191
55	30000000	30000000	1.000	30117000	0.996
56	30000000	30000000	1.000	29482000	1.018
57	26000000	30000000	0.867	28477000	0.913
58	28000000	30000000	0.933	30716000	0.912
59	30000000	30000000	1.000	31063000	0.966
60	27000000	30000000	0.900	30956000	0.872
61	31000000	30000000	1.033	30077000	1.031
62	32000000	30000000	1.067	27445000	1.166
63	30000000	30000000	1.000	31658000	0.948
64	30000000	30000000	1.000	29166000	1.029
65	30000000	30000000	1.000	26344000	1.139
66	26000000	30000000	0.867	28729000	0.905
67	31000000	30000000	1.033	30542000	1.015
68	32000000	30000000	1.067	31877000	1.004
69	30000000	30000000	1.000	27820000	1.078
70	30000000	30000000	1.000	28678000	1.046
71	29000000	30000000	0.967	31324000	0.926
72	28000000	30000000	0.933	29598000	0.946
73	30000000	30000000	1.000	29949000	1.002
74	30000000	30000000	1.000	27286000	1.099
75	26000000	30000000	0.867	30214000	0.861
76	30000000	30000000	1.000	27968000	1.073
77	30000000	30000000	1.000	27542000	1.089
78	30000000	30000000	1.000	29279000	1.025
79	30000000	30000000	1.000	28626000	1.048
80	26000000	30000000	0.867	28055000	0.927
81	26000000	30000000	0.867	32978000	0.788
82	27000000	30000000	0.900	26991000	1.000
83	31000000	30000000	1.033	29732000	1.043
84	33000000	30000000	1.100	29941000	1.102
85	30000000	30000000	1.000	27125000	1.106
86	29000000	30000000	0.967	30309000	0.957
87	28000000	30000000	0.933	30845000	0.908
88	30000000	30000000	1.000	31740000	0.945
89	26000000	30000000	0.867	31910000	0.815
90	30000000	30000000	1.000	31080000	0.965
91	27000000	30000000	0.900	29500000	0.915
92	30000000	30000000	1.000	29476000	1.018
93	33000000	30000000	1.100	31247000	1.056
94	27000000	30000000	0.900	26277000	1.028
95	31000000	30000000	1.033	25400000	1.220
96	32000000	30000000	1.067	30413000	1.052
97	27000000	30000000	0.900	28094000	0.961
98	30000000	30000000	1.000	29501000	1.017
99	30000000	30000000	1.000	27503000	1.091
100	29000000	30000000	0.967	28537000	1.016
101	28000000	30000000	0.933	30414000	0.921
102	33000000	30000000	1.100	30129000	1.095
103	27000000	30000000	0.900	25998000	1.039
104	30000000	30000000	1.000	28285000	1.061
105	30000000	30000000	1.000	32325000	0.928
106	27000000	30000000	0.900	28324000	0.953
107	31000000	30000000	1.033	27805000	1.115
108	32000000	30000000	1.067	30606000	1.046
109	27000000	30000000	0.900	28423000	0.950

110	30000000	30000000	1.000	31335000	0.957
111	30000000	30000000	1.000	27881000	1.076
112	27000000	30000000	0.900	29746000	0.908
113	31000000	30000000	1.033	27906000	1.111
114	32000000	30000000	1.067	25359000	1.262
115	29000000	30000000	0.967	29481000	0.984
116	28000000	30000000	0.933	30769000	0.910
117	30000000	30000000	1.000	28606000	1.049
118	27000000	30000000	0.900	29782000	0.907
119	32000000	30000000	1.067	30481000	1.050
120	30000000	30000000	1.000	30340000	0.989
121	32000000	30000000	1.067	32335000	0.990
122	27000000	30000000	0.900	31562000	0.855
123	30000000	30000000	1.000	28801000	1.042
124	27000000	30000000	0.900	28511000	0.947
125	33000000	30000000	1.100	29245000	1.128
126	32000000	30000000	1.067	28637000	1.117
127	29000000	30000000	0.967	28914000	1.003
128	28000000	30000000	0.933	30154000	0.929
129	30000000	30000000	1.000	26724000	1.123
130	33000000	30000000	1.100	27280000	1.210
131	27000000	30000000	0.900	28984000	0.932
132	27000000	30000000	0.900	30315000	0.891
133	27000000	30000000	0.900	29245000	0.923
134	33000000	30000000	1.100	24821000	1.330
135	32000000	30000000	1.067	28326000	1.130

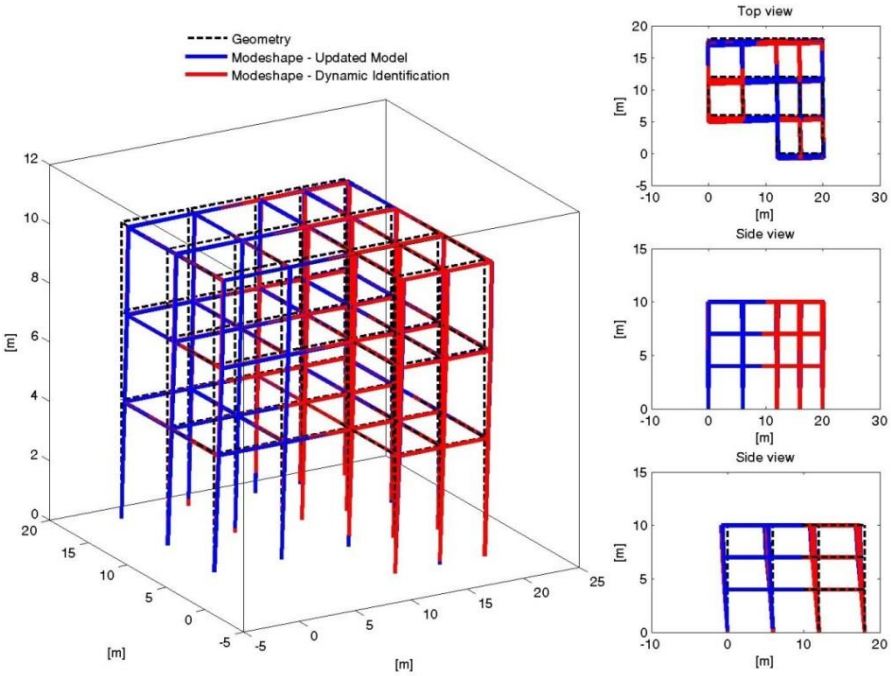

Figure 20 - Mode shape 1 - Comparison between updated model and experimental results - Analysis 4 _ TEST 2

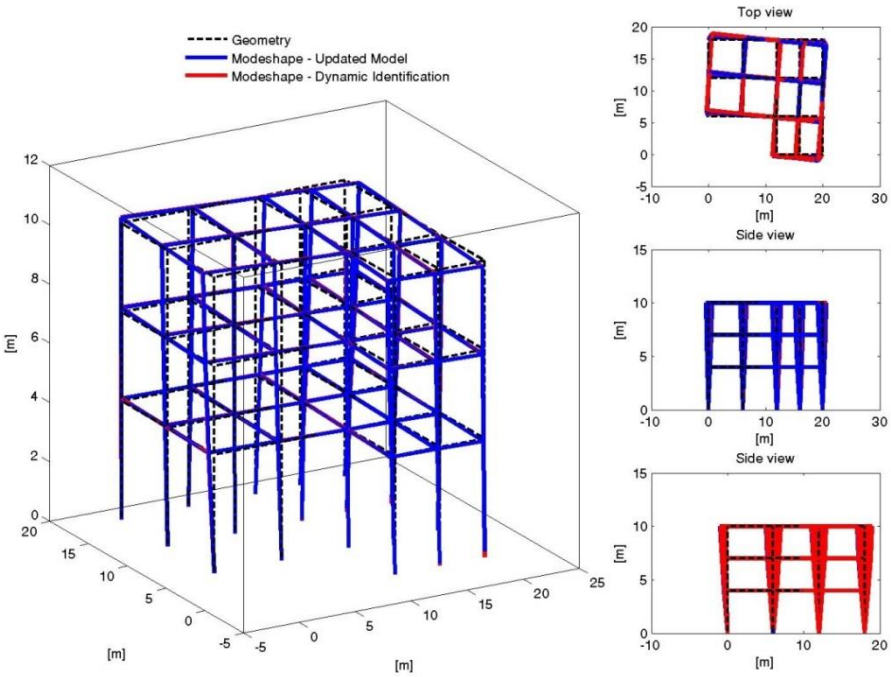

Figure 21 - Mode shape 2 - Comparison between updated model and experimental results - Analysis 4 _ TEST 2

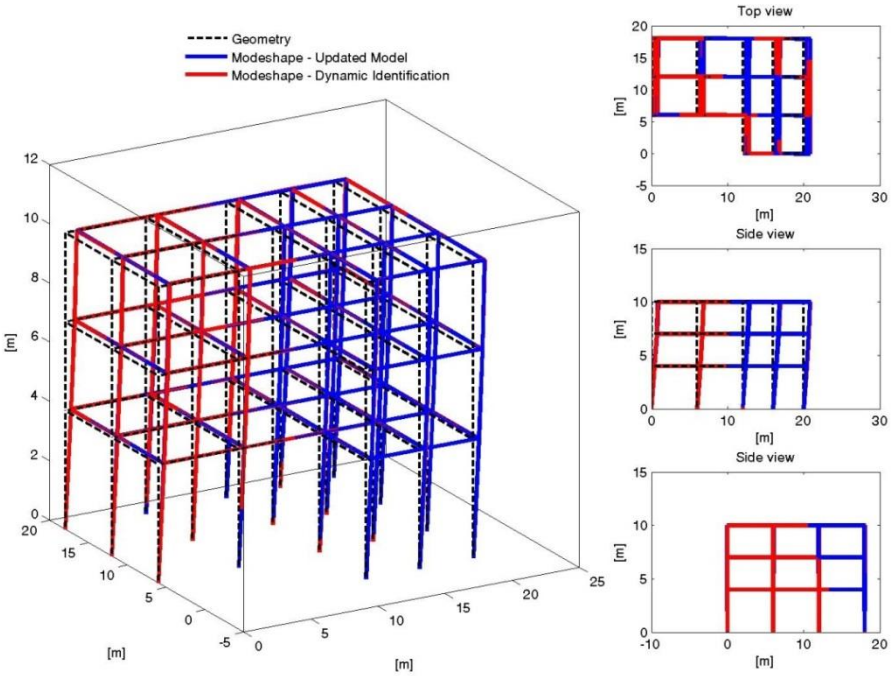

Figure 22 - Mode shape 3 - Comparison between updated model and experimental results - Analysis 4 _ TEST 2

12.2.3 Conclusions
TEST 1

The analysis performed well and the updated model n°2133 exhibited a complete matching with the simulated eigenvalues. The ration between the measured eigenfrequencies and the numerical ones is, for all the 3 considered modes, equal to 1. Comparing with the results of the previous analysis, using the same specifications for the Young's Modulus simulation, the generalized modal error is here three order of magnitude lower than the one obtained considering all the set of 20 eigenmodes and 6 dofs per node.

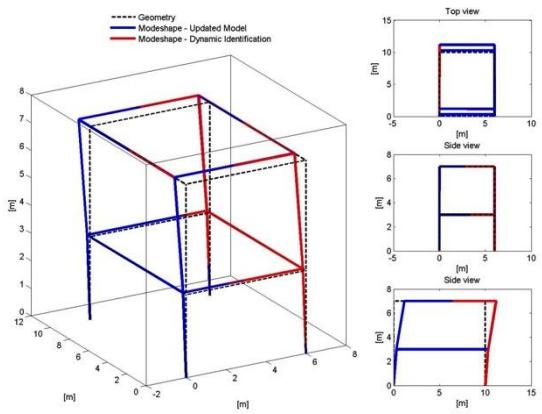

Figure 23 - Mode 1 - Analysis 1

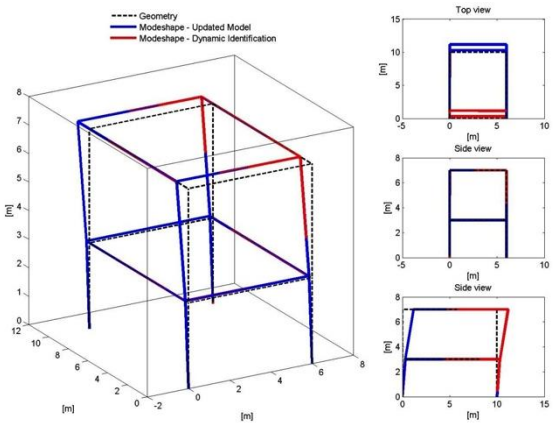

Figure 24 - Mode 1 - Analysis 2

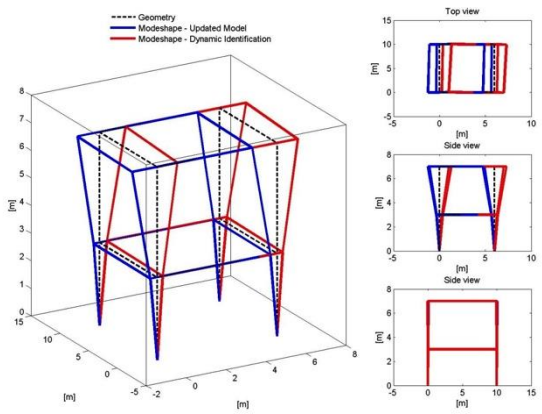

Figure 25 - Mode 2 - Analysis 1

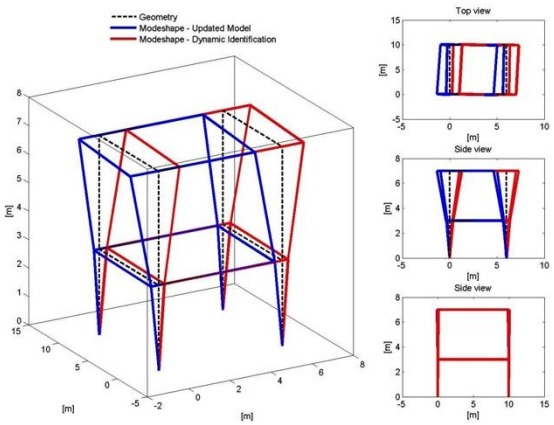

Figure 26 - Mode 2 - Analysis 2

Regarding the comparisons of the mode shapes, for the first 2 modes, the same conclusions of the previous analysis can be considered valid also for this case. The first mode shape entirely match the experimental one while, for the second mode, experimental and numerical mode shapes are opposite between each other.

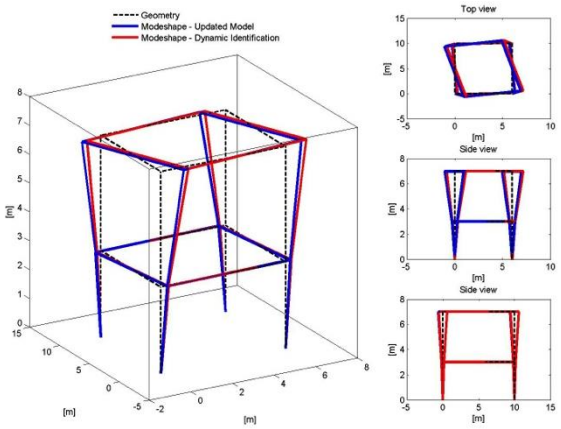

Figure 27 - Mode 3 - Analysis 1

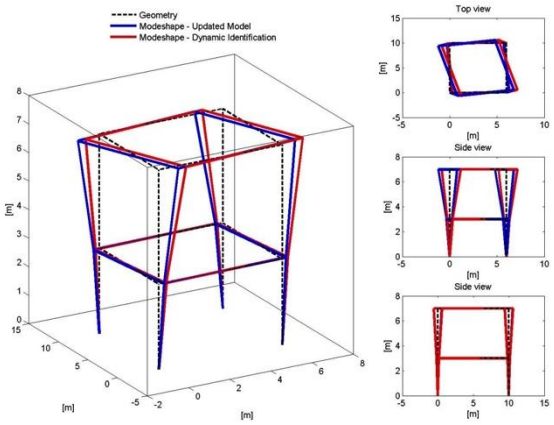

Figure 28 - Mode 3 - Analysis 2

Finally, the third numerical mode seems to be less accurate in matching the experimental results, considering the comparison obtained from the previous analysis. However, also in this case, the updated model qualitatively appears more torsionally rigid than the observed structure.

TEST 2

In tandem with *TEST 1*, the analysis performed a lower generalized modal error comparing to the previous analysis with complete measured data. Model n°615 has been identified as the best updated model. For all the considered modes, the corresponding numerical eigenfrequency improved its value towards the measured ones, and the ratio between measured and numerical eigenfrequencies are practically equal to 1 for each of the 3 modes.

Concerning the comparisons of the deformed shapes, the numerical mode shapes qualitatively match the experimental results for all the first three eigenmodes.

13. Case study – secondary school building at comune di val di sotto (so), italy

The building considered here for the test of the updating methodology, is the Elementary and Secondary School building at *Comune di Val di Sotto* (SO), Italy. The school has to fulfill the energy qualification of buildings and, also, some maintainance is needed to preserve the structure. In order to proceed for these reasons, a characterization of the dynamic parameters was performed, as described in further detail in Deliverable 15.1 of Work Package 15, with the purpose of calibrating the numerical model.

Figure 29 - Building of the Elementary and Secondary School at *Comune di Val di Sotto* (SO), Italy

Figure 30 - Tri-axial seismometer (geophone)

Figure 31 - Installallation of the apparatus for the excitation of the structure and the recording of the displacements

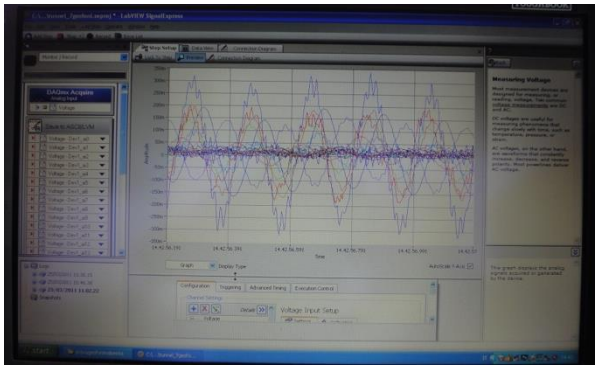

Figure 32 - Analysis of the signals

The measured data obtained from the field monitoring of the school are used to test the updating methodology. The analyses are performed considering the three different type of simulations:

simulated numerical models with one value of Young's Modulus for the entire structure;

simulated numerical models with one value of Young's Modulus for all the elements of the storey;

simulated numerical models with a different value of Young's Modulus for each different element.

For each of the three different types of simulation, an increasing value of generated models are considered for the different tests. The results in terms of generalized modal error are compared in order to understand where the stabilization of the values starts, which means the minimum number of samples which should be generated to obtain satisfactory error index values.

Ones, the type of simulation which exhibites the lowest range of generalized modal error has been identified, the same simulation is used to investigate the results by changing the mean and the standard deviation values for the characteristic compressive strength of the concrete.

13.1 *General description of the building*

The building is a 3-storey RC concrete frame structure, showed in its plan view in Figure 33. The whole building consists in 3 parts, divided by 2 seismic joints (purple lines): *secondary school*, *entrance of the building* and *elementary school*. The dynamic identification measurements were done considering only the schools, without including the entrance. However, only the part represented by the secondary school (Figure 34, Figure 35 and Figure 35), was considered for this specific updating procedure analysis.

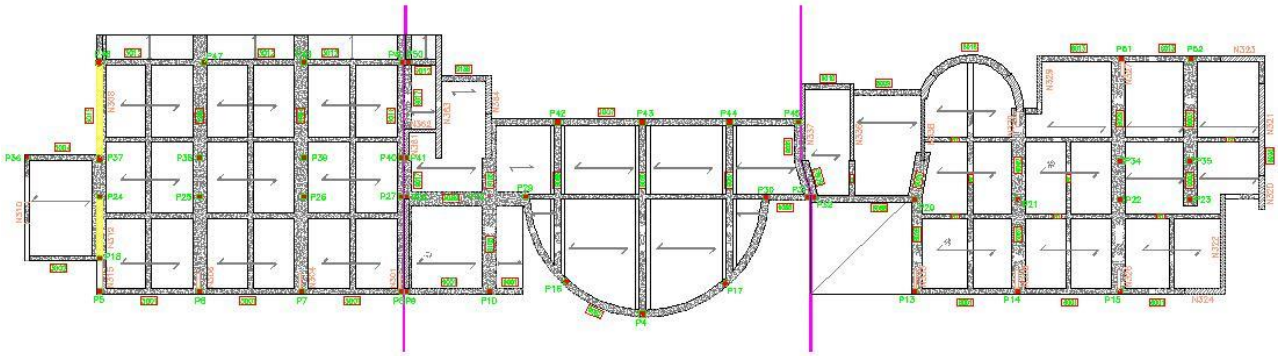

Figure 33 - Plan view of the school's structure (3rd level)

Concerning the structural details, the position of the elements and the orientation of the slabs are indicated in Figure 34 and Figure 35. All the vertical elements are continuos from the foundation up to the top and the slabs are oriented along the longitudinal direction in all the structure. Furthermore, some more specifications regarding the slabs, are listed below for simplicity:

- 1st level (h = 3 m) *RC slab*, height 30 cm;
- 2nd level (h = 6 m) *ribbed slab*, height 24+4 cm;
- 3rd level (h = 9 m) *ribbed slab*, height 24+4 cm.

For the characteristics of the slabs, it's reasonable to consider the slabs themselves with an high stiffness in plane. This assumption simplify the modeling part and also the processing of the results from the field monitoring data. This issue will be discussed more in details afterwards, talking about *mode shape expansion*.

Finally, the frame structure is connected, as showed on the bottom left side of Figure 35, to RC walls which are including the stairs. The walls have a thickness of 40 cm.

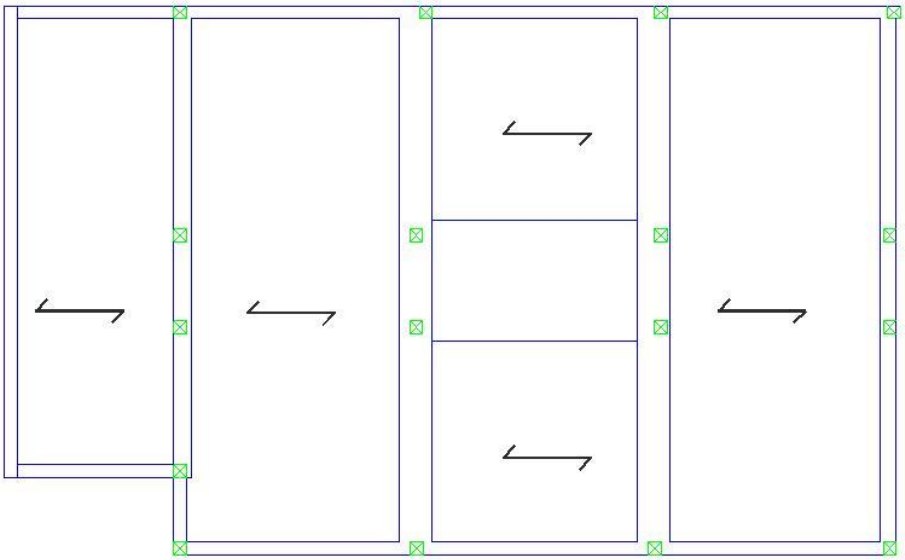

Figure 34 - Secondary School's structure - Plan view 1st level

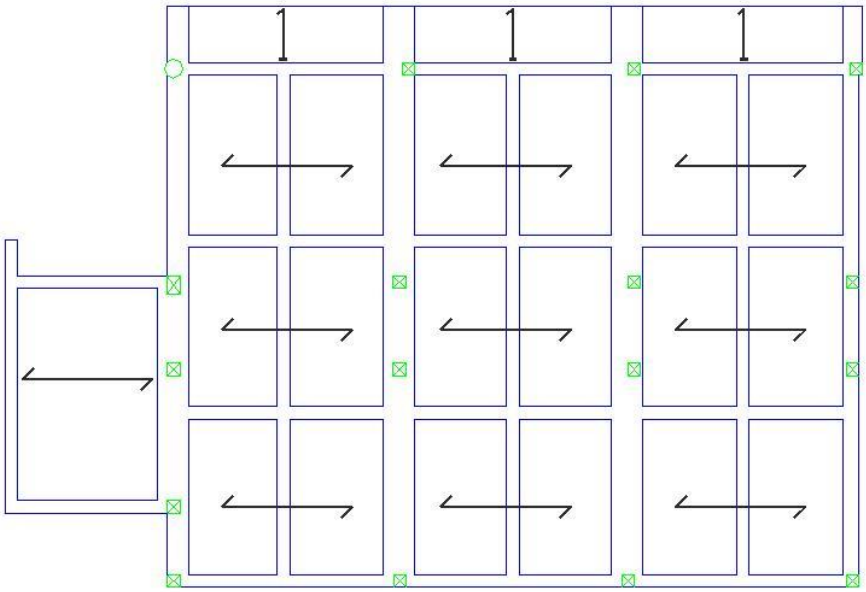

Figure 35 - Secondary School's structure - Plan view 2nd and 3rd level

13.2 *Dynamic identification measurements*

The dynamic identification was performed considering a total of 8 tri-axial seismometers, 2 for the first level and 3 for the second and third level. The first three eigenmodes were identified and the results are indicated in Table 27. All the modes are flexural modes, the first combines both flexural deformed shape along longitudinal and translational directions, the second is a flexural mode along the transversal direction and the third is a flexural mode along the longitudinal direction.

Modes		T [sec]	f [Hz]	ω [rad/sec]
1	Flexural XY	0.166667	6.000	37.69911184
2	Flexural Y	0.135593	7.375	46.33849164
3	Flexural X	0.123077	8.125	51.05088062

Table 27 - Secondary School - Dynamic identification measurements

The monitoring was done by positioning the instruments at the corners of each storey. In this way, the modal displacements of the first three eigenvectors can be reasonably assigned to the nodes at the corners of the frame structure for each level. Under the hypothesis of infinite stiffness in plane of the slab, for each storey, only two instruments are needed to obtain the modal displacements of all the nodes. In fact, both record the displacements and one of the two controls the rigid rotation of the plane. Below, in Figure 36 and Figure 37, the position of the tri-axial seismometers is indicated (blue dots).

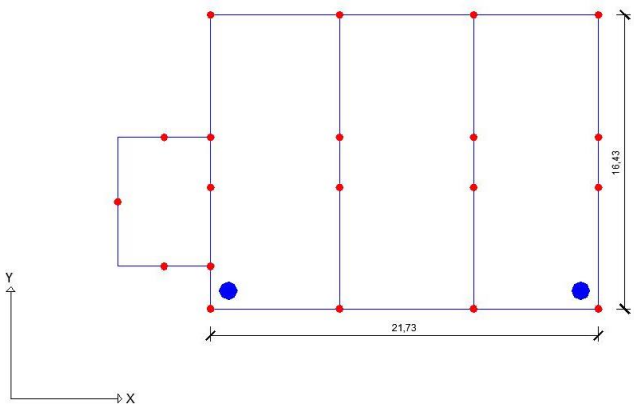

Figure 36 - Position of the tri-axial seismometers - 1st storey

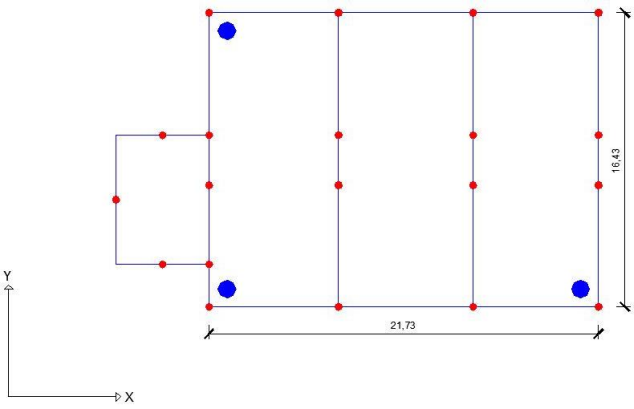

Figure 37 - Position of the tri-axial seismometers - 2nd and 3rd storey

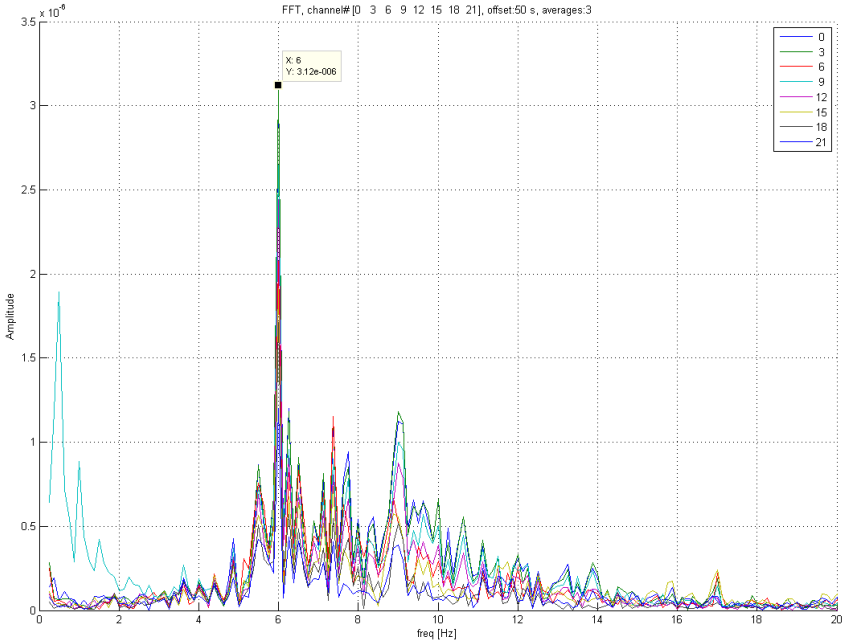

Figure 38 - FFT channels X direction - 6 Hz - Flexural mode shape X and Y direction

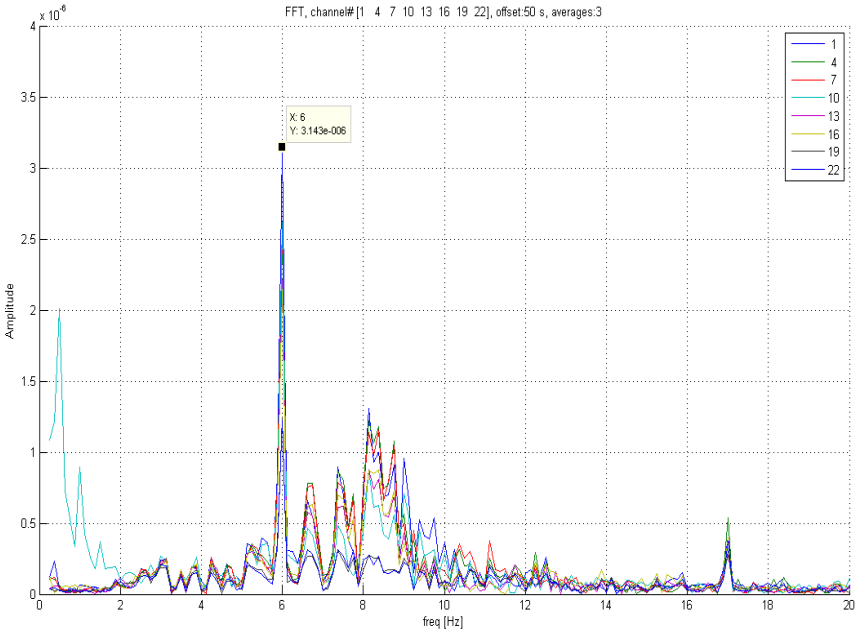

Figure 39 - FFT channels Y direction - 6 Hz - Flexural mode shape X and Y direction

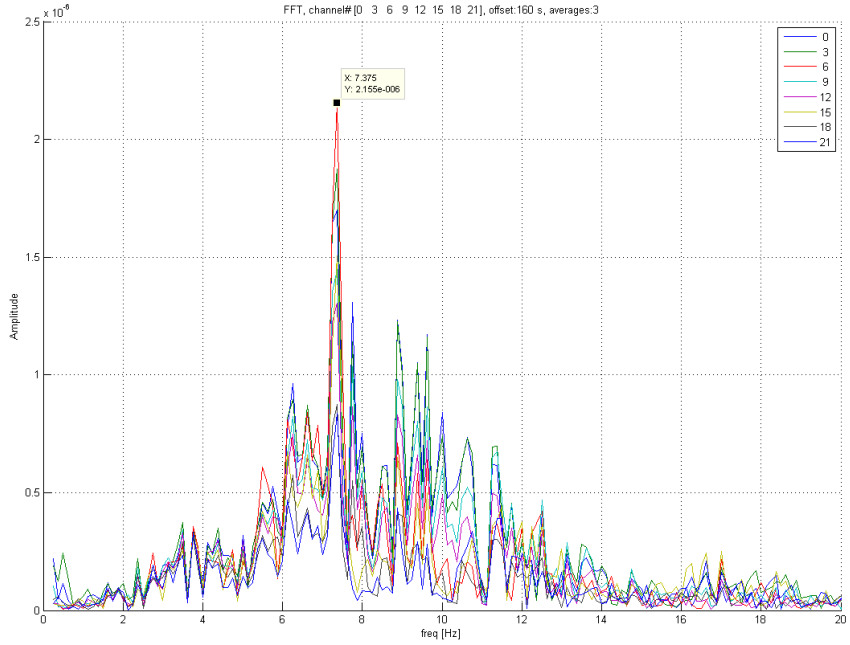

Figure 40 - FFT channels X direction - 7.375 Hz - Flexural mode shape X direction

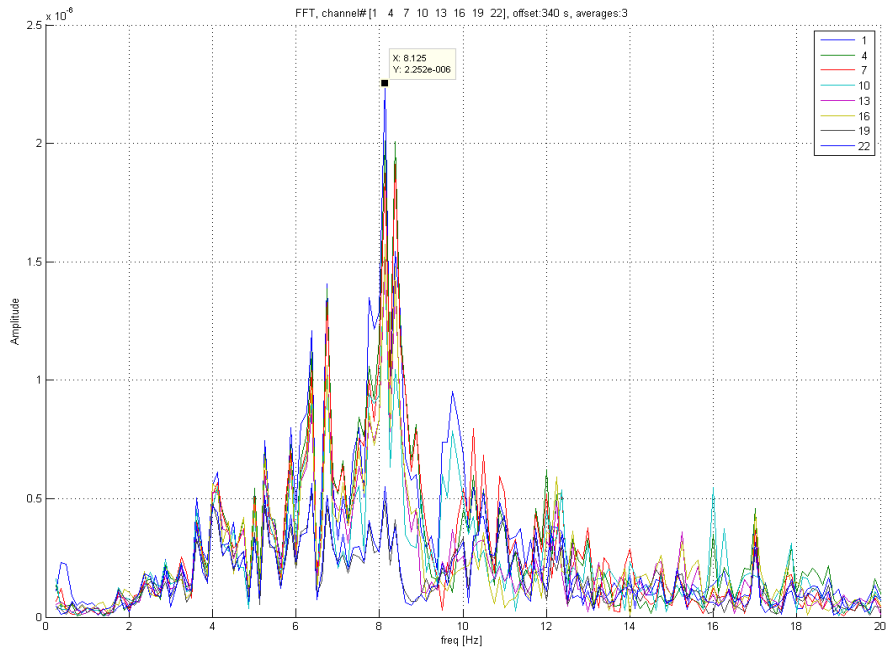

Figure 41 - FFT channels Y direction - 8.125 Hz - Flexural mode shape Y direction

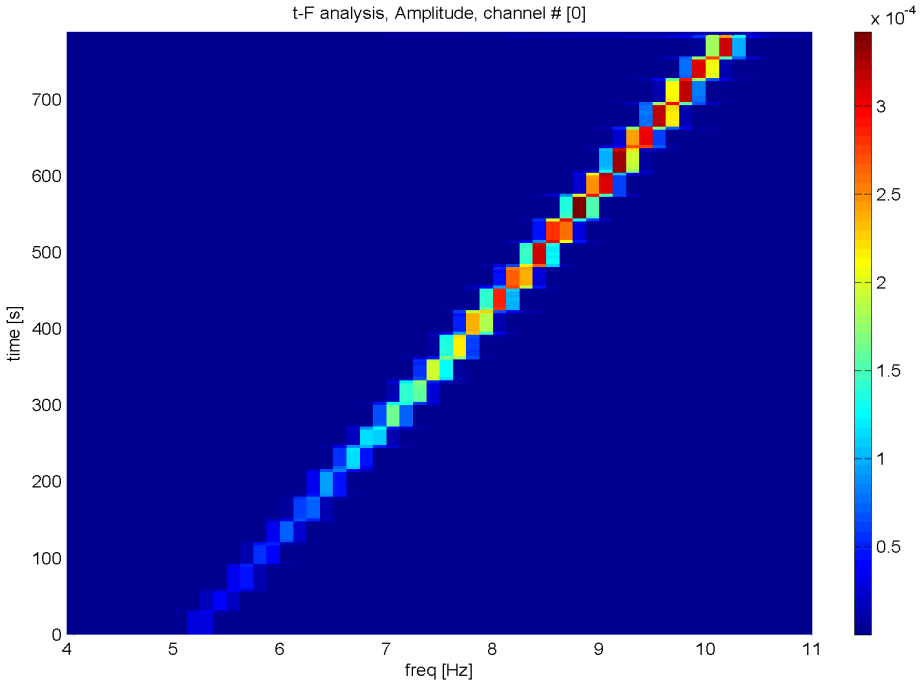

Figure 42 - Harmonic excitation 5-10Hz X direction - Channel 0

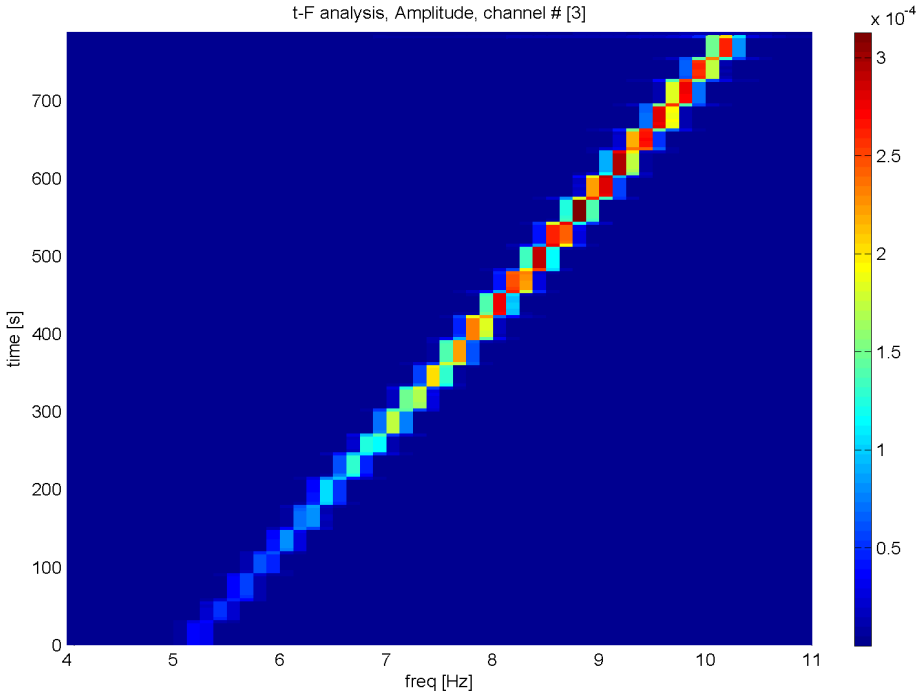

Figure 43 - Harmonic excitation 5-10Hz X direction - Channel 3

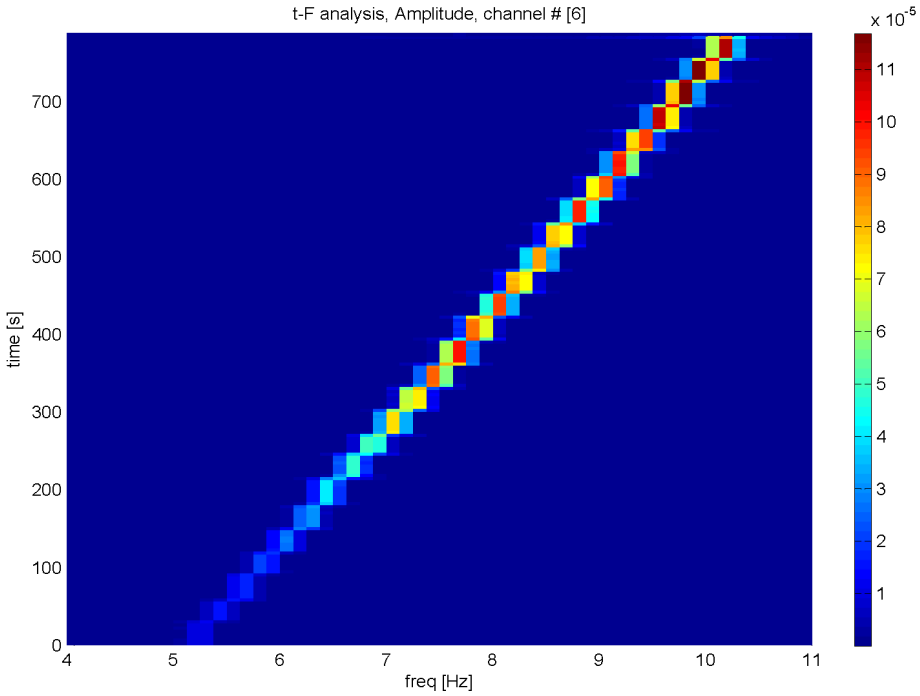

Figure 44 - Harmonic excitation 5-10Hz X direction - Channel 6

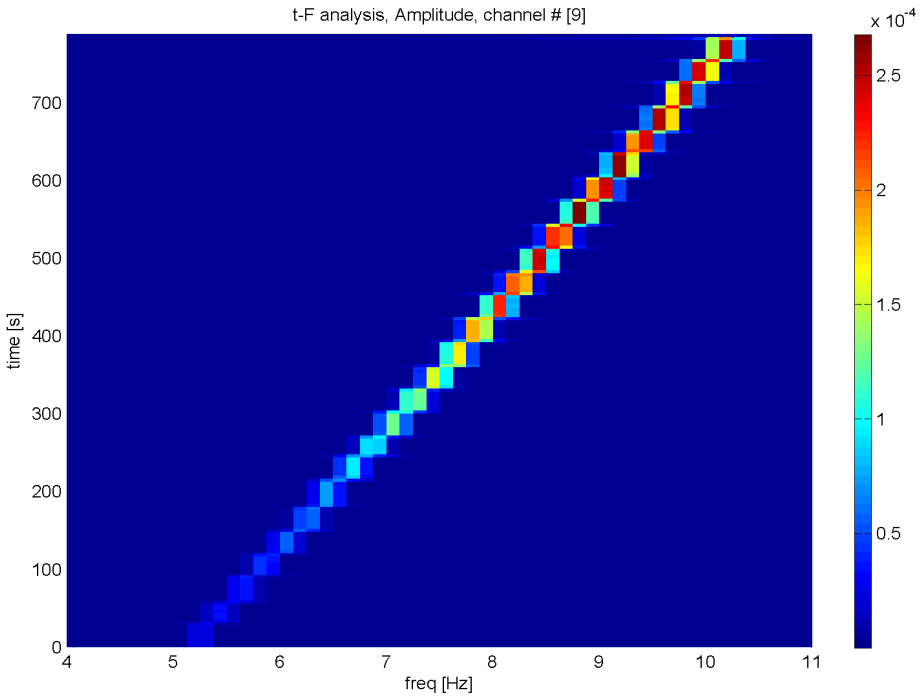

Figure 45 - Harmonic excitation 5-10Hz X direction - Channel 9

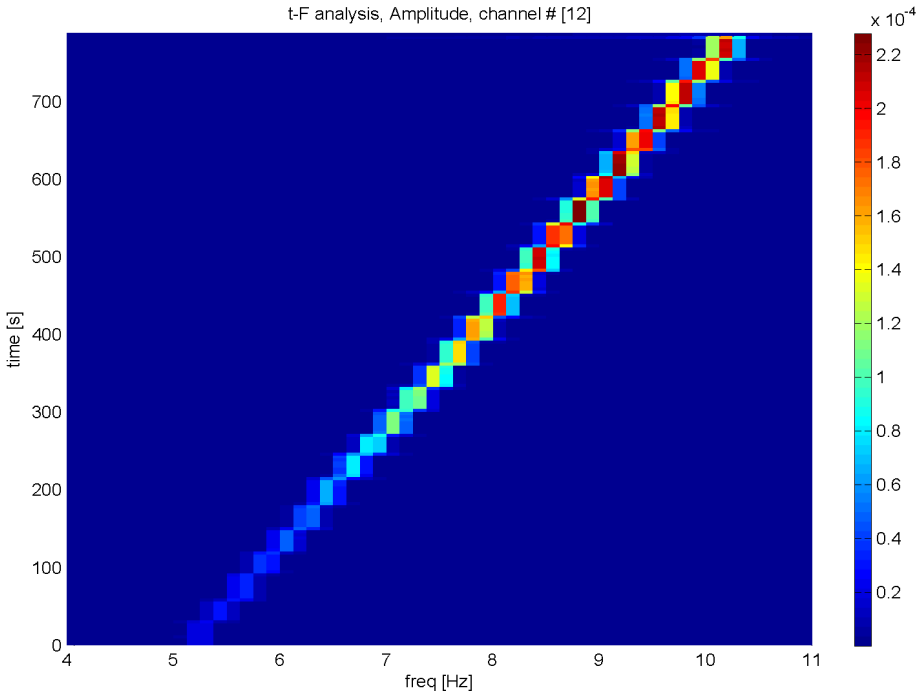

Figure 46 - Harmonic excitation 5-10Hz X direction - Channel 12

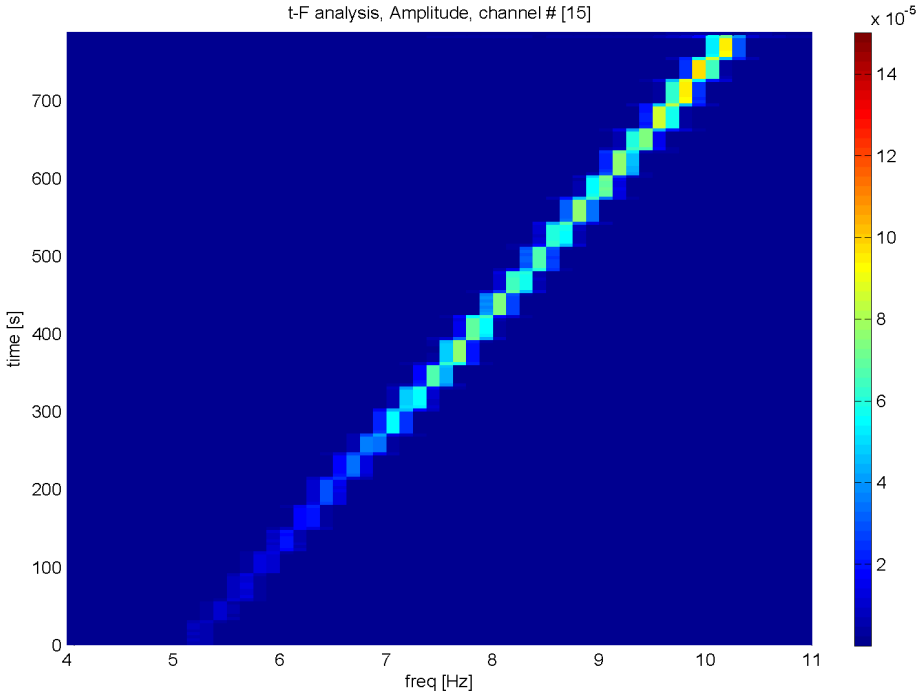

Figure 47 - Harmonic excitation 5-10Hz X direction - Channel 15

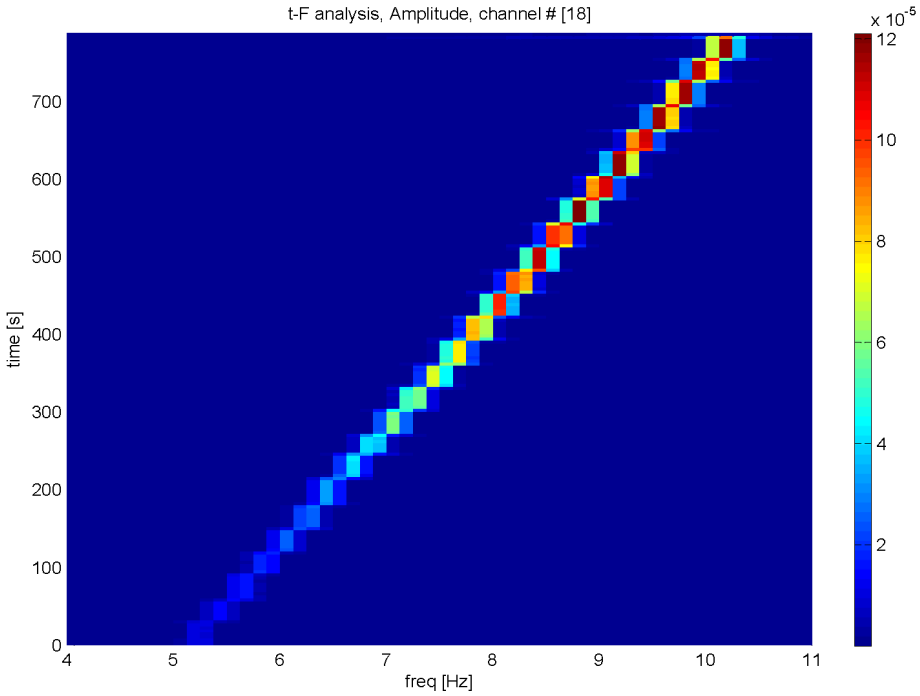

Figure 48 - Harmonic excitation 5-10Hz X direction - Channel 18

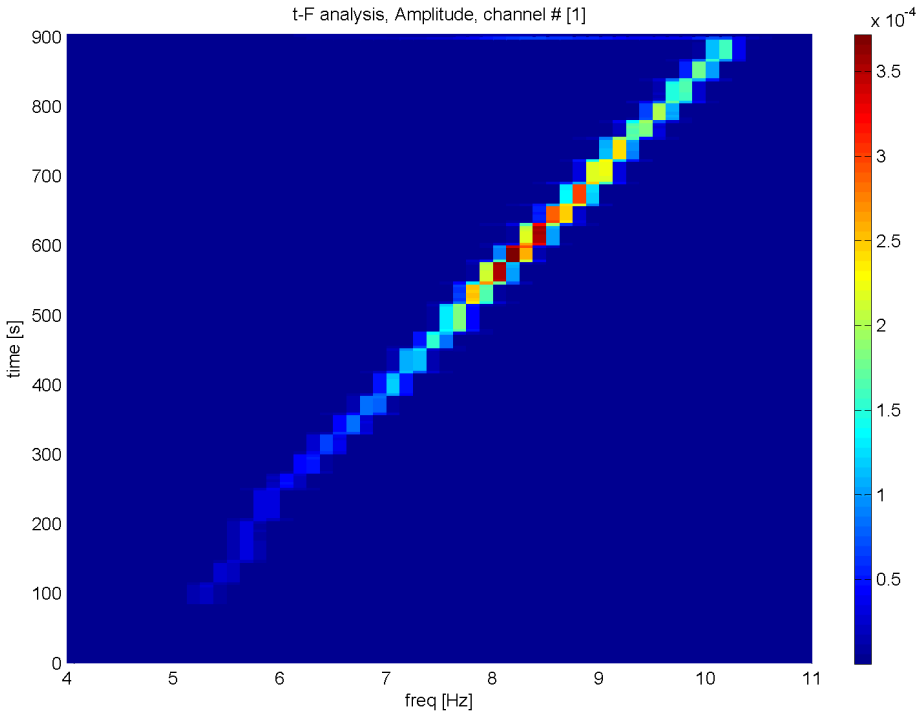

Figure 49 - Harmonic excitation 5-10Hz Y direction - Channel 1

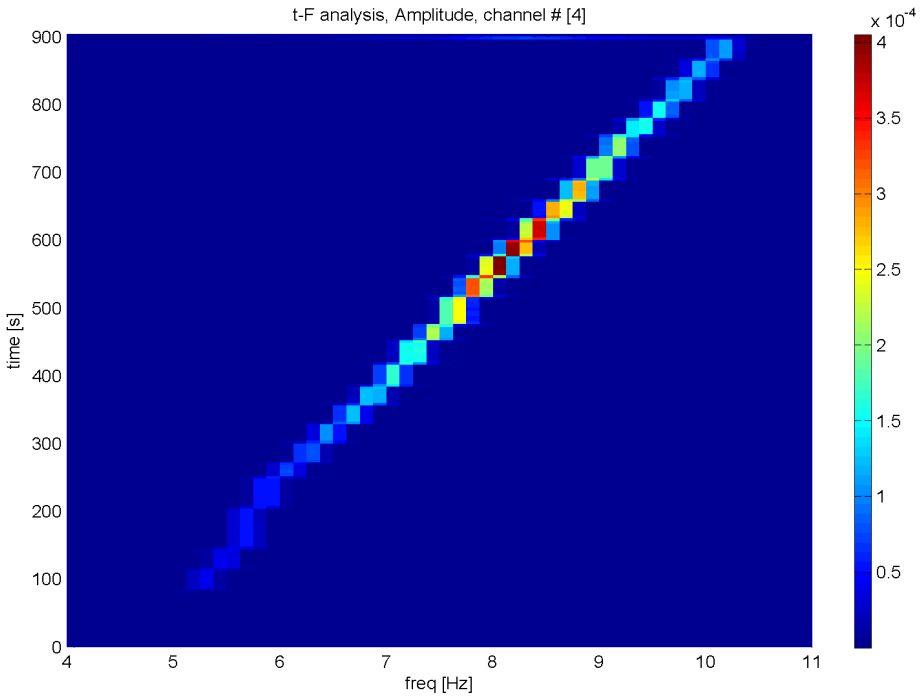

Figure 50 - Harmonic excitation 5-10Hz Y direction - Channel 4

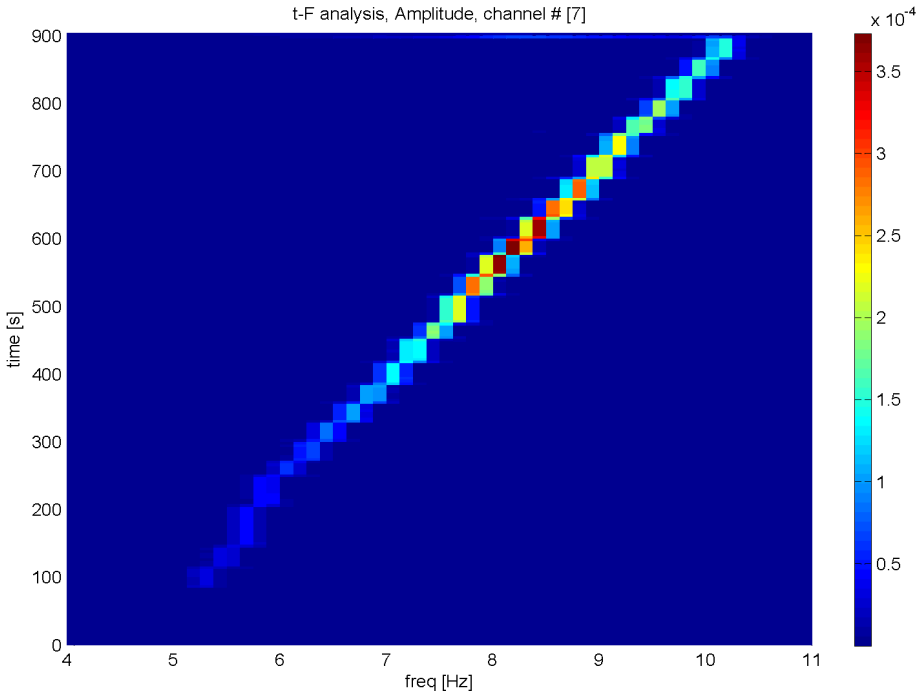

Figure 51 - Harmonic excitation 5-10Hz Y direction - Channel 7

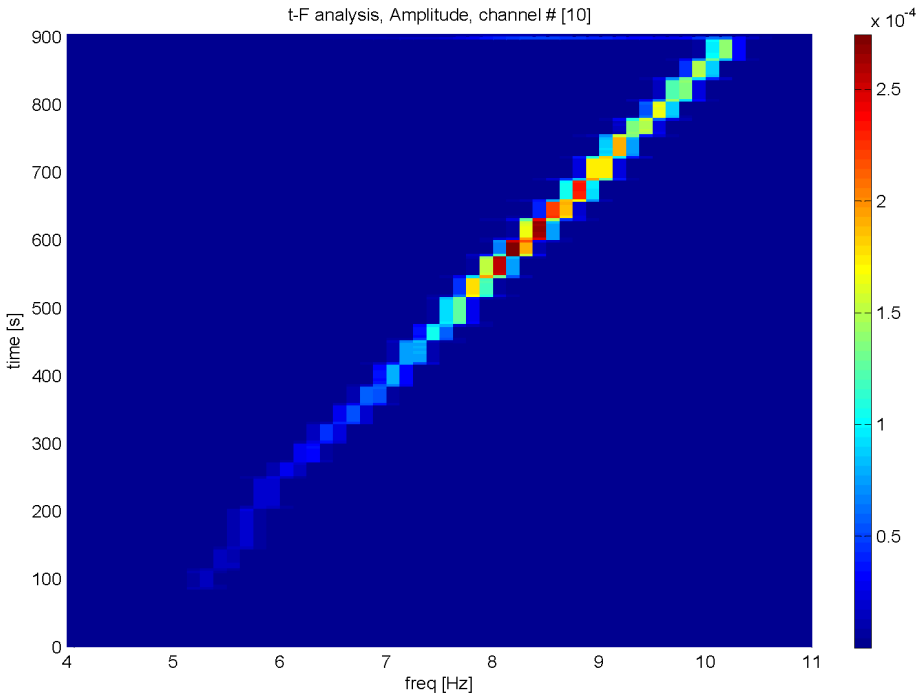

Figure 52 - Harmonic excitation 5-10Hz Y direction - Channel 10

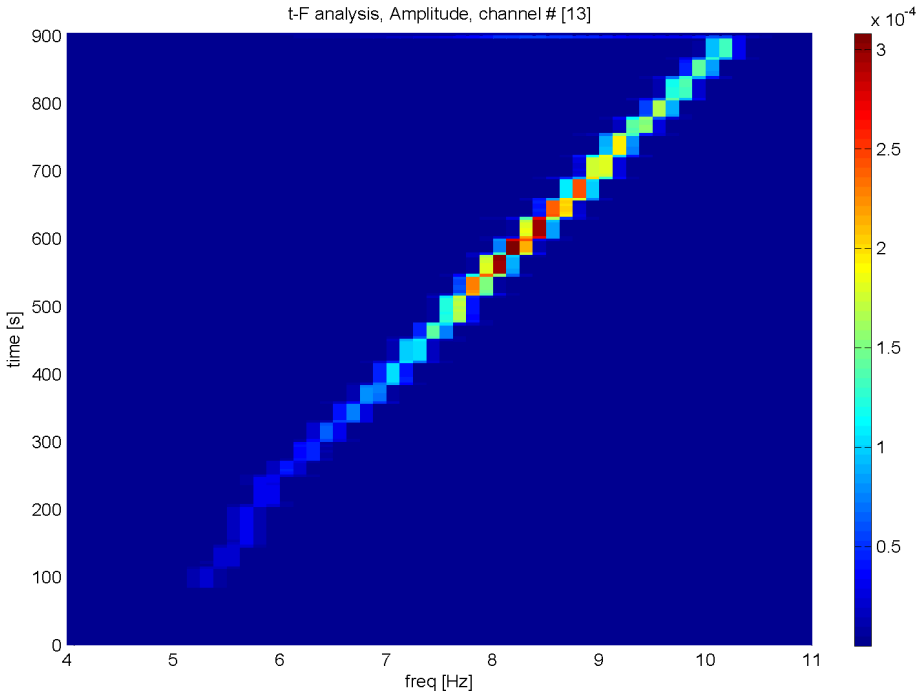

Figure 53 - Harmonic excitation 5-10Hz Y direction - Channel 13

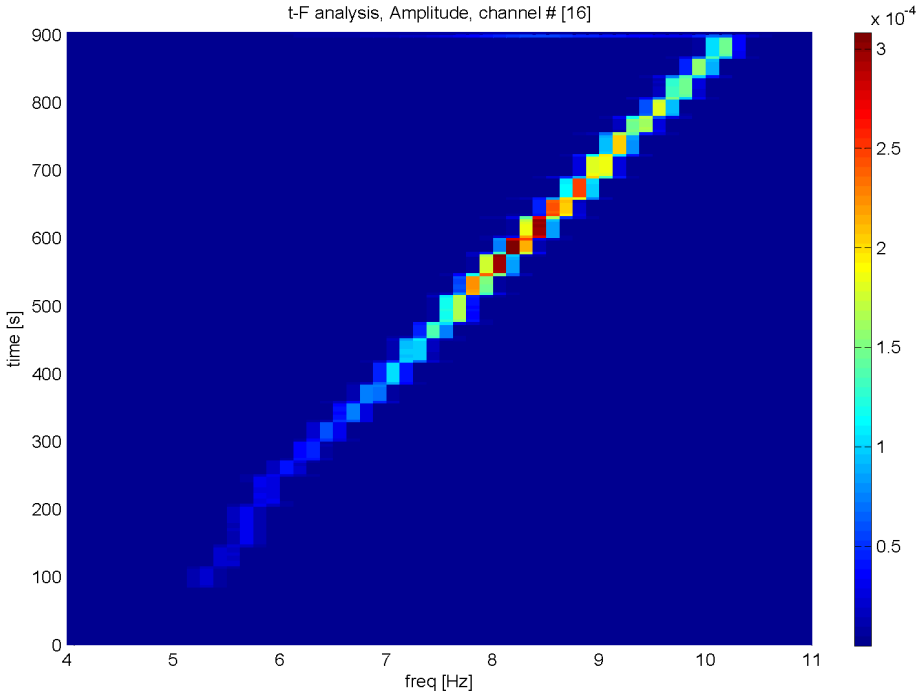

Figure 54 - Harmonic excitation 5-10Hz Y direction - Channel 16

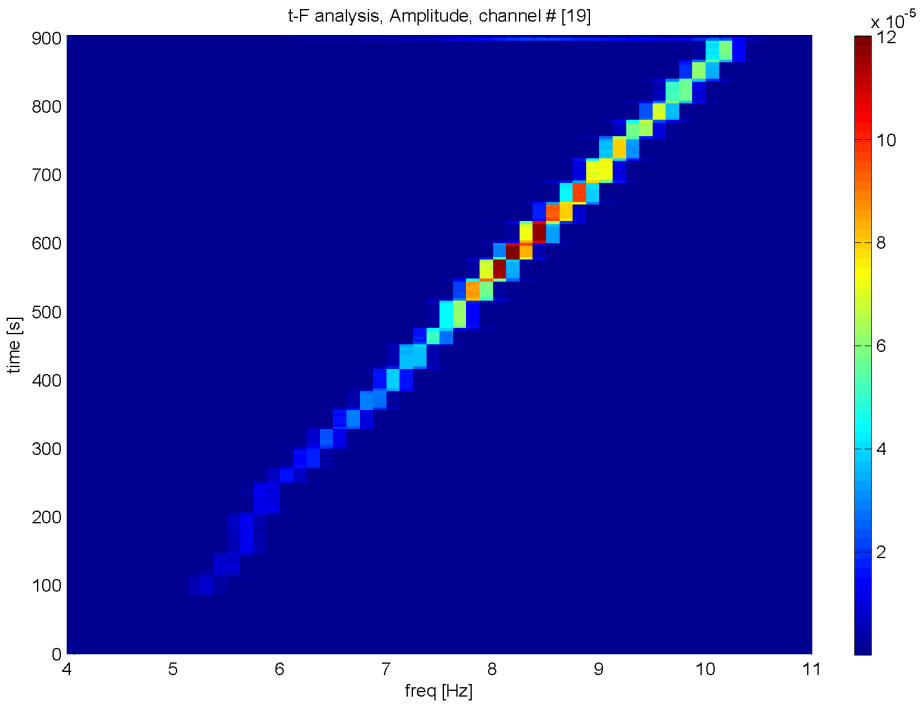

Figure 55 - Harmonic excitation 5-10Hz Y direction - Channel 19

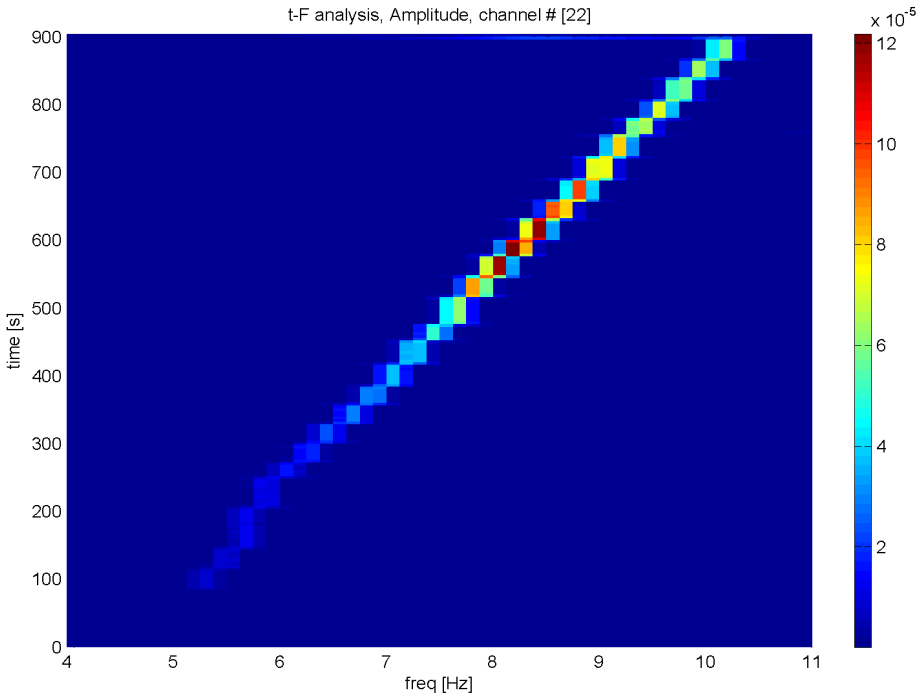

Figure 56 - Harmonic excitation 5-10Hz Y direction - Channel 22

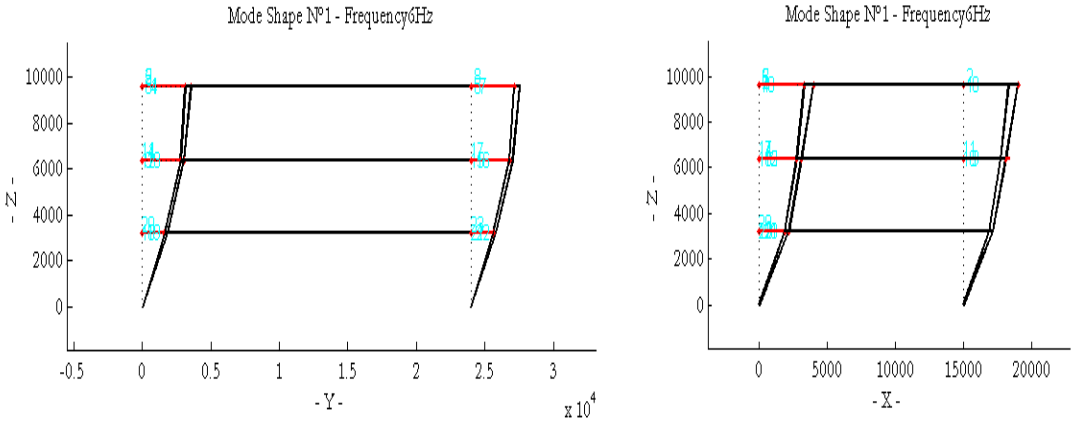

Figure 57 - Mode shape 1 - 6 Hz

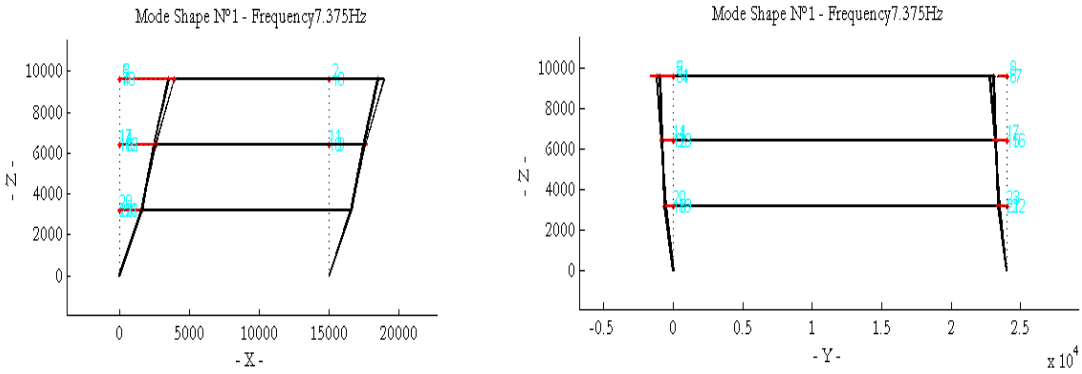

Figure 58 - Mode shape 2 - 7.375 Hz

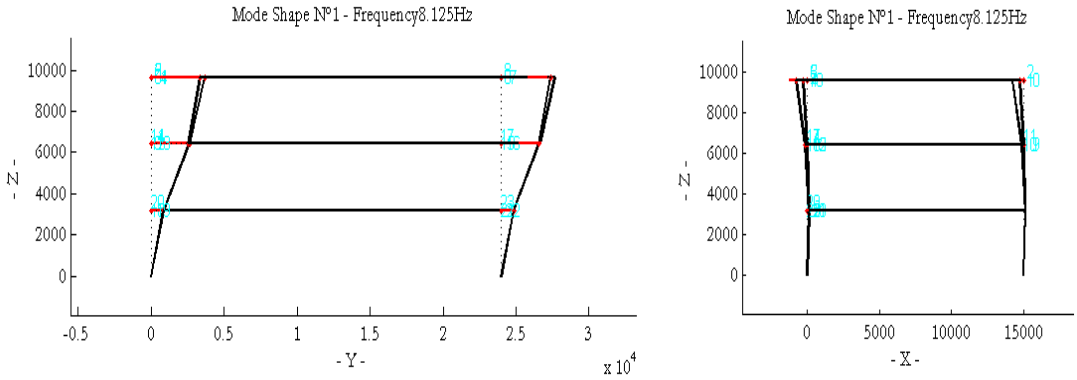

Figure 59 - Mode shape 3 - 8.125 Hz

13.3 *Mode shape expansion*

Based on the fact that measured mode shape information from sensor locations are fewer than the the DOFs in the analytical model, mode shape expansion is employed to extrapolate the measured mode shapes such that they can be compared with the analytical numerical results (Beck and Vanik, 1996).

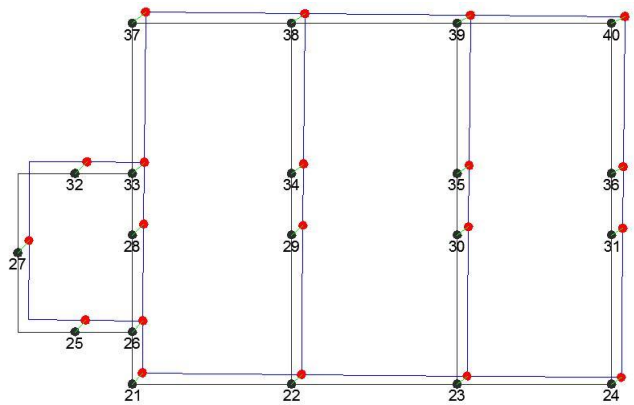

Figure 60 - Normalized modal displacements - Mode 1 - 1st floor

As indicated in the following figures, each of the three mode shapes are obtained from the measured data by plotting the normalized measured displacements of the nodes at the corner of each storey. Consequently, the displacements of the other nodes are obtained. For this specific case, the displacement along X direction of *node 117*, was considered to normalize, respectively, each of the three eigenvectors.

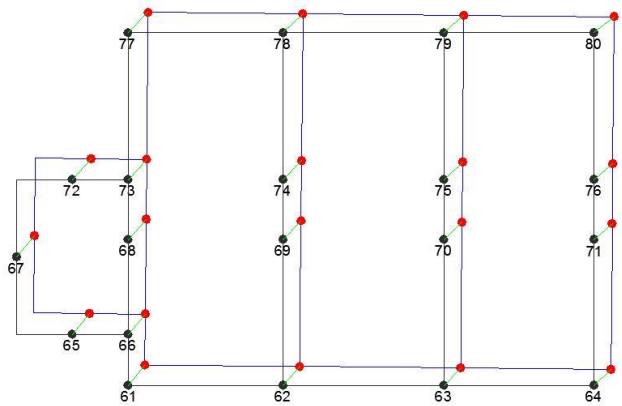

Figure 61 - Normalized modal displacements - Mode 1 - 2nd floor

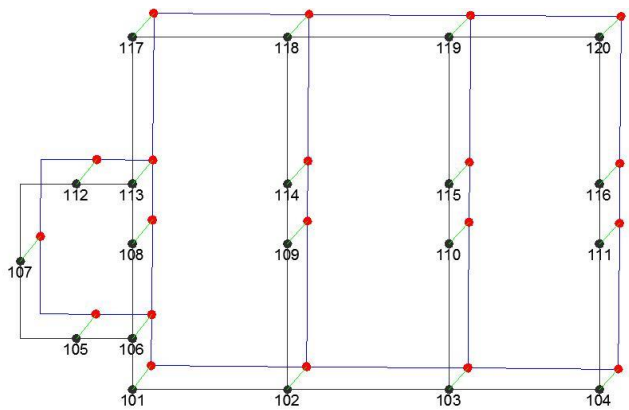

Figure 62 - Normalized modal displacements - Mode 1 - 3rd floor

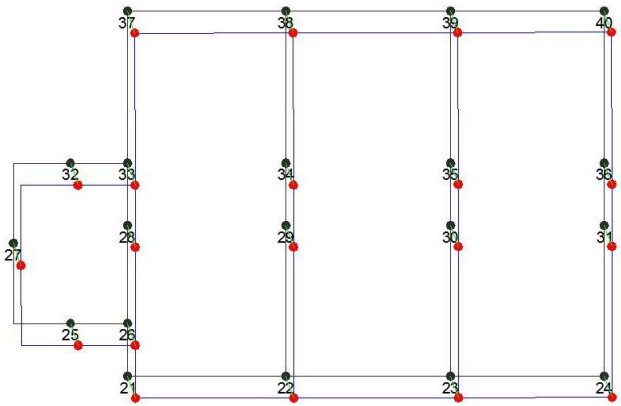

Figure 63 - Normalized modal displacements - Mode 2 - 1st floor

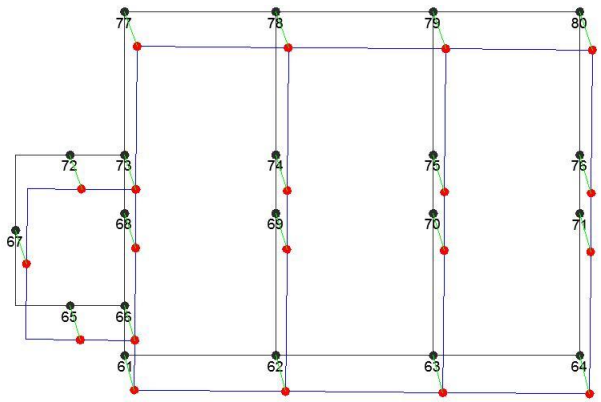

Figure 64 - Normalized modal displacements - Mode 2 - 2nd floor

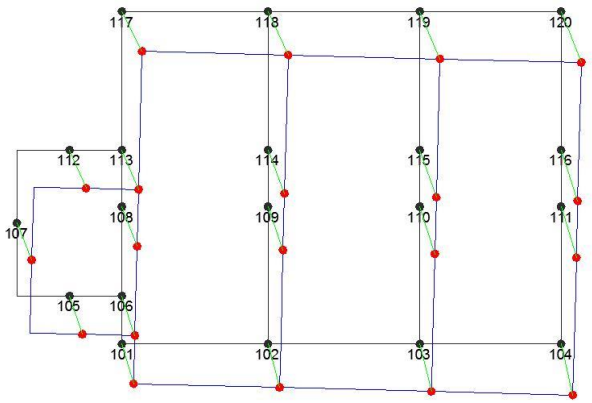

Figure 65 - Normalized modal displacements - Mode 2 - 3rd floor

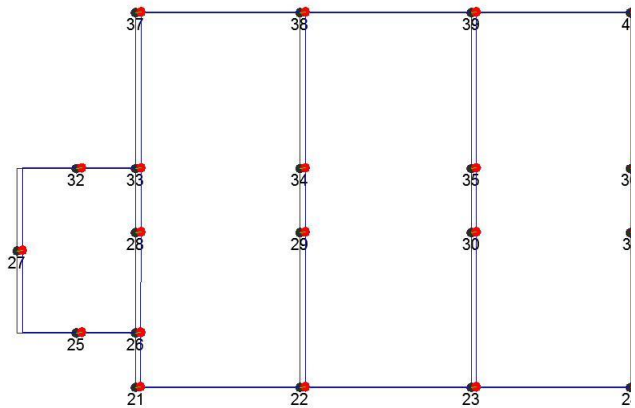

Figure 66 - Normalized modal displacements - Mode 3 - 1st floor

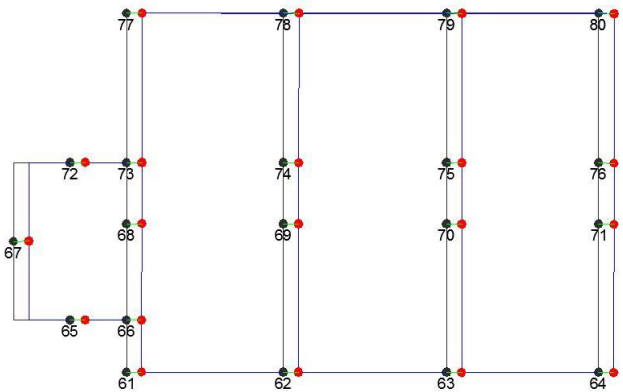

Figure 67 - Normalized modal displacements - Mode 3 - 2nd floor

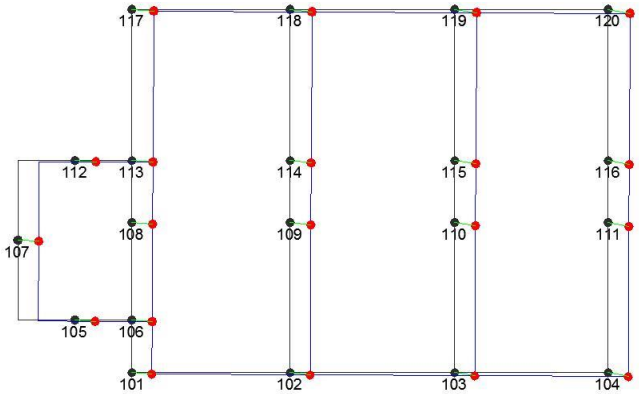

Figure 68 - Normalized modal displacements - Mode 3 - 3rd floor

13.4 *Modeling*

Modeling of the building was done facing several problems due to a lack of informations concerning structural specifications. Drawings are poor in details regarding the characteristics of the slabs and the stairs, no section is indicated for the horizontal elements and there is no clear idea about the mechanical characteristics of the material. However, the basic information in order to perform the modal analysis were available, such as geometry and position of the elements, interstorey height, boundary conditions and masses (Table 28).

Table 28 - Slab masses

Slab Specifications	$Q_{PermanentStructural}$ [ton/m^2]	$Q_{PermanentNonStructural}$ [ton/m^2]	$Q_{Accidental}$ [ton/m^2]
Slab 1st level (h = 30 cm - RC slab)	0.92	0.06	0.35
Slab 2nd level (h = 24+4 cm - ribbed slab)	0.48	0.06	0.35
Slab 3rd level (h = 24+4 cm - ribbed slab)	0.49	-	0.22
Stairs	0.38	-	0.40

The numerical model was initially created with the program *SAP2000*, for a more fast calibration using the measured results from the dynamic identification and the results obtained from the numerical model created for the design of the school. The aforementioned design model, which exhibited as first period T=0.18 sec, includes all the three parts in which the building is divided by the seismic joints. Differently, the numerical model created for the test of the updating methodology, considers only the part of the school represented by the Secondary School building. Hence, the consistency with the performed field monitoring test is maintained and the model represents exactly one of the two part of the structure being characterized by its modal properties.

Several trials, with different modeling specifications, were done in order to find the most representative model of the real building. As a first indicator, the initial design model (T=0.18 sec) appears to be more flexible than the real building which exhibited, from the measurements, T=0.16 sec as a first period.

The main issue related to the modeling is the way of representing the short slender walls sustained by the outer beams and the walls of the stairs. The initial versions of the numerical model, considered first shells and second equivalent trusses to represent those elements. Due to the fact that, the use of shells creates problem in programming the matlab routine and the use of equivalent trusses brings uncertainties in evaluating the section of the trusses themselves, a good compromise was found in modeling the bi-dimensional elements with the use of elastic “beam element” having their proper section and position at the baricenter. Furthermore, this last model showed the closest results to the field measurements. In the following Figure 69 and Figure 70, the numerical modes is indicated.

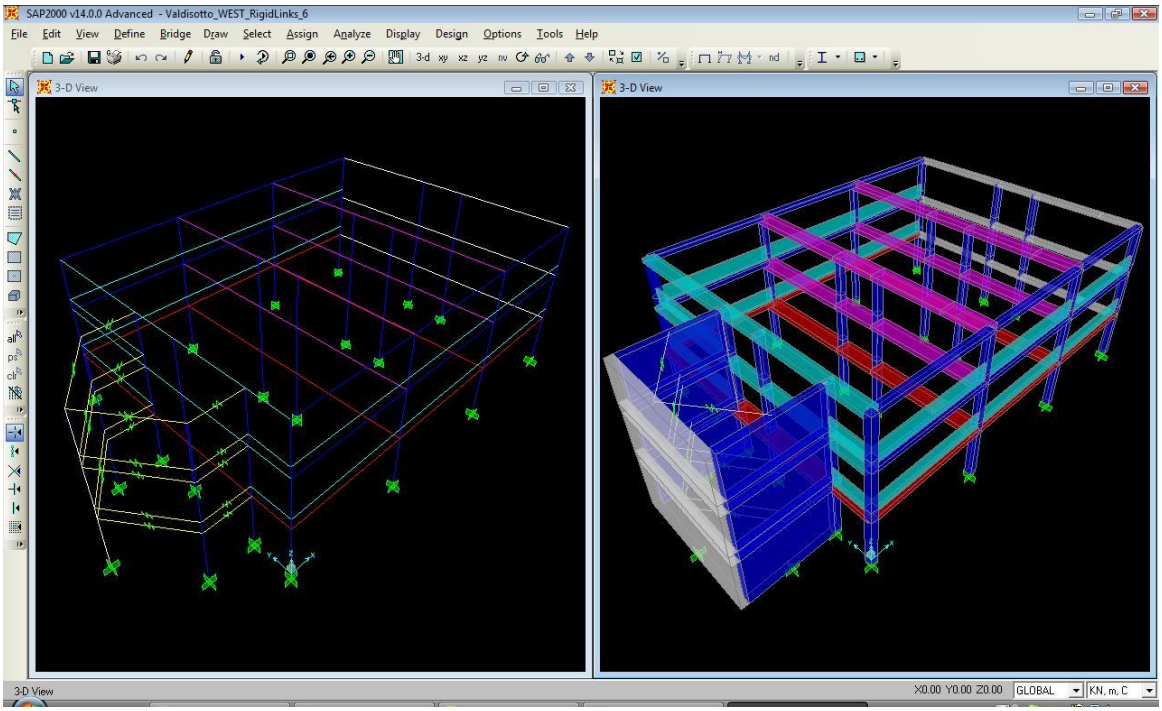

Figure 69 - Initial numerical model (SAP)

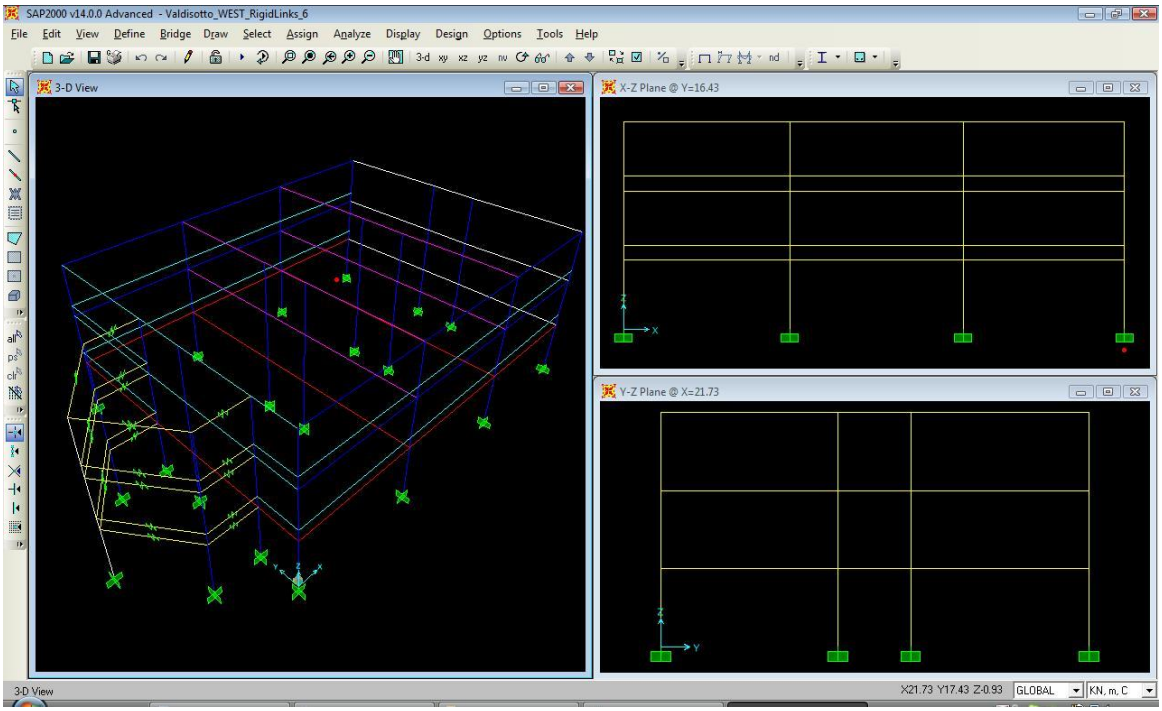

Figure 70 - Initial numerical model - 3D and side views (SAP)

The results of the modal analysis in terms of periods, frequencies and modal participating mass ratios are indicated below. The numerical results don't match the measured data and, in terms of deformed shapes, only the first and the third mode are comparable with the measured mode shapes.

Table 29 - Results modal analysis (SAP) and comparison with the measured values from dynami identification

Mode	T [Sec]	f [Cyc/sec]	ω [rad/sec]	T_E [Sec]	f_E [Cyc/sec]	$ω_E$ [rad/sec]
1	0.275291	3.6325	22.824	0.166667	6.000	37.69911184
2	0.104742	9.5473	59.987	0.135593	7.375	46.33849164
3	0.0927	10.788	67.78	0.123077	8.125	51.05088062
4	0.065229	15.331	96.326	-	-	-
5	0.062028	16.122	101.3	-	-	-
6	0.0509	19.647	123.44	-	-	-
7	0.050891	19.65	123.46	-	-	-
8	0.050109	19.957	125.39	-	-	-
9	0.049768	20.093	126.25	-	-	-
10	0.049735	20.107	126.33	-	-	-
11	0.049122	20.357	127.91	-	-	-
12	0.047198	21.187	133.12	-	-	-
13	0.046282	21.607	135.76	-	-	-
14	0.036322	27.532	172.99	-	-	-
15	0.036319	27.534	173	-	-	-
16	0.035655	28.046	176.22	-	-	-
17	0.034788	28.745	180.61	-	-	-
18	0.034413	29.059	182.58	-	-	-
19	0.033859	29.534	185.57	-	-	-
20	0.033569	29.79	187.17	-	-	-

Table 30 - Modal partecipating mass ratios (SAP)

Period [sec]	UX	UY	UZ	RX	RY	RZ
0.275291	0.0092	0.61634	1.804E-07	0.1818	0.00198	0.67293
0.104742	0.0000966	0.06064	0.000005993	0.00307	0.00064	0.05401
0.0927	0.74158	0.00692	0.00096	0.00566	0.1795	0.16559
0.065229	0.00319	0.05189	0.00005055	0.02073	0.00107	0.04665
0.062028	0.00009946	0.03642	0.0000103	0.01077	0.00003397	0.00058
0.0509	8.001E-07	1.236E-08	0.2777	0.1415	0.25451	1.606E-07
0.050891	4.812E-07	0.000002864	0.00026	0.12822	0.00025	2.089E-07
0.050109	4.249E-08	8.192E-10	0.06159	0.03373	0.09136	3.012E-09
0.049768	0.00000468	0.000001418	0.05758	0.00419	0.00817	1.825E-08
0.049735	0.000004492	0.000001975	0.04661	0.08275	0.0065	0.000002179
0.049122	3.133E-07	3.404E-11	0.08395	0.0449	0.02591	4.126E-08
0.047198	0.000001519	0.000004595	7.974E-10	0.00061	4.008E-08	4.912E-07
0.046282	8.835E-07	0.000006338	1.735E-08	0.0006	2.712E-08	4.431E-07
0.036322	0.00021	0.000003985	0.07348	0.05901	0.18195	0.00005357
0.036319	0.00000499	3.241E-07	0.004	0.01928	0.01004	4.227E-07
0.035655	0.000002339	6.278E-08	0.05512	0.02979	0.13982	6.797E-07
0.034788	0.05076	0.0091	0.00411	0.00408	0.00089	0.02981
0.034413	0.00022	0.00001101	0.00001909	0.0006	0.000003771	0.0000436
0.033859	0.00349	0.000008353	0.02837	0.07086	0.00002788	0.00067
0.033569	0.11043	0.00103	0.02979	0.0066	0.0015	0.00981

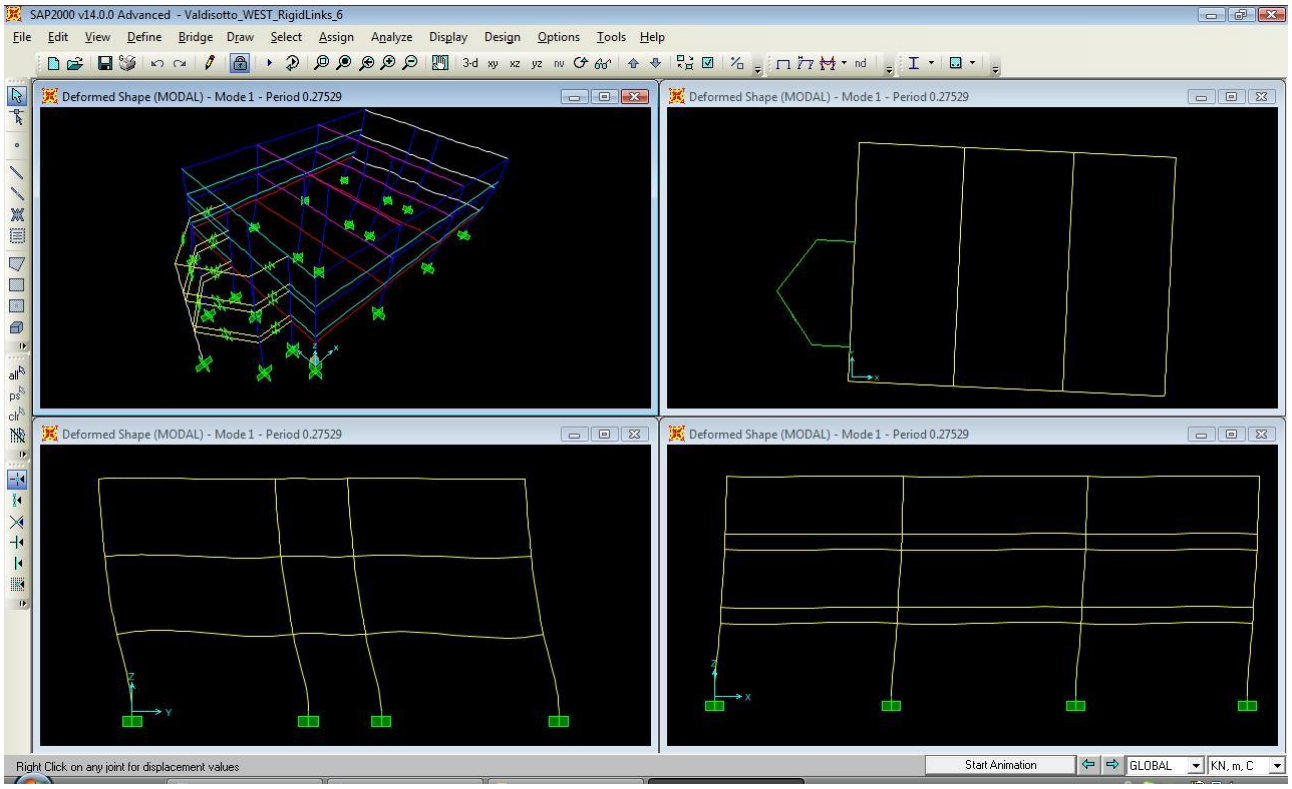

Figure 71 - Initial numerical model - Deformed shape mode 1 (SAP)

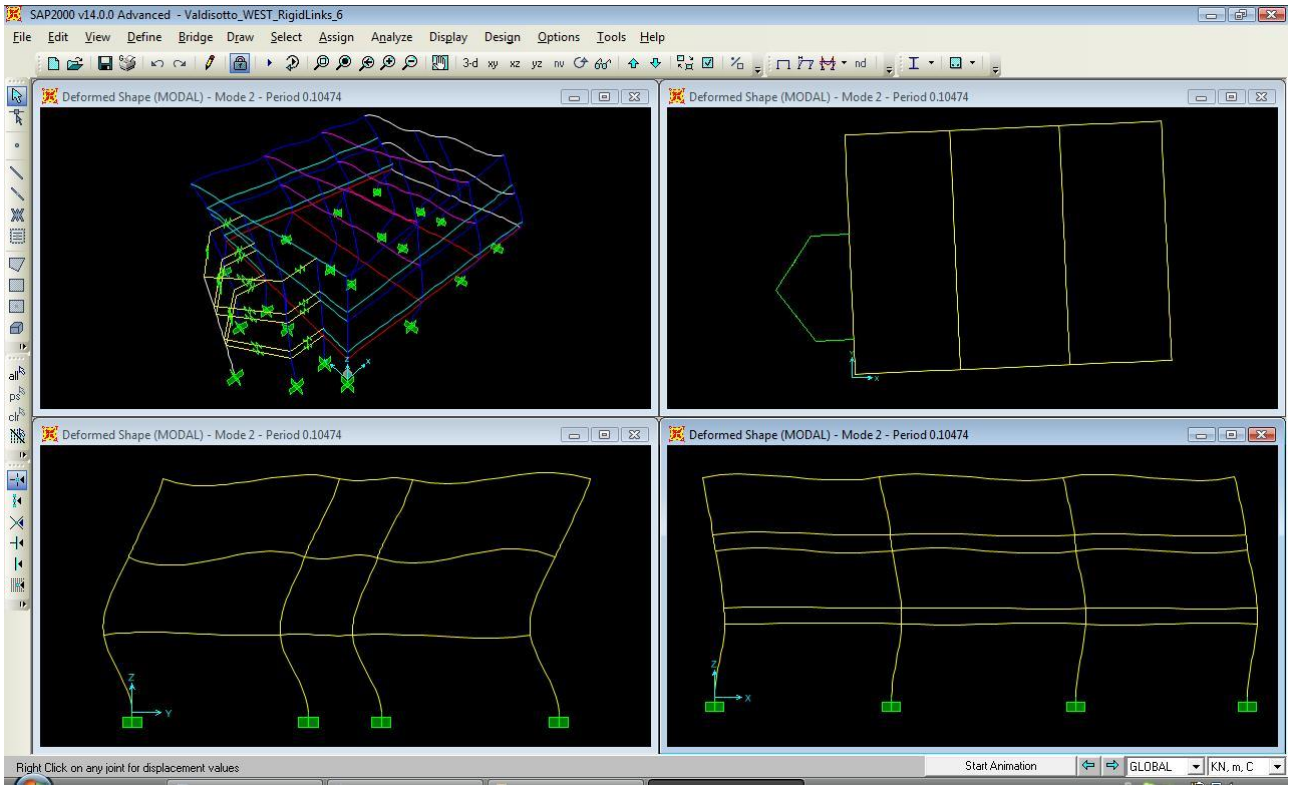

Figure 72 - Initial numerical model - Deformed shape mode 2 (SAP)

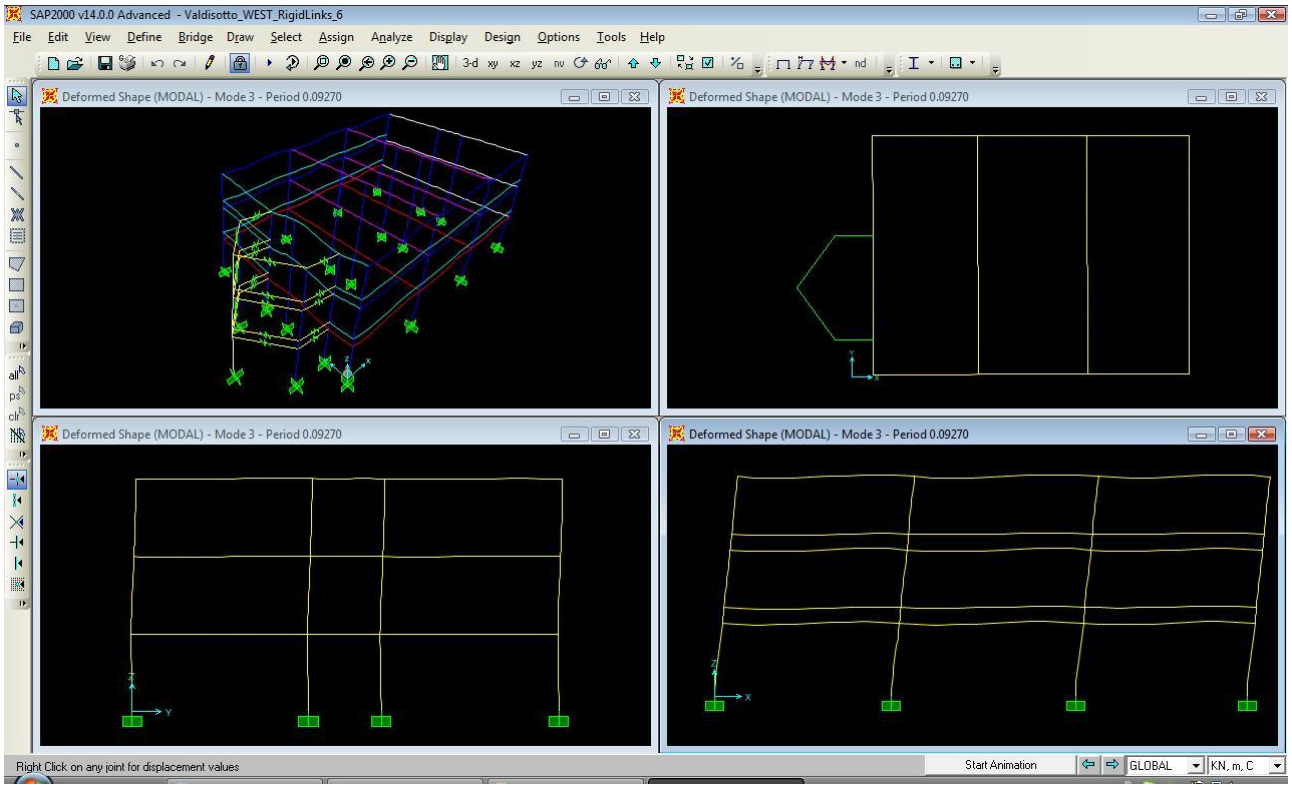

Figure 73 - Initial numerical model - Deformed shape mode 3 (SAP)

The same numerical model was created also with the program OpenSees and a first comparison has been done with the previous numerical results. The figure and the table below indicate the geometry of the builiding and the script written in order to perform the modal analysis.

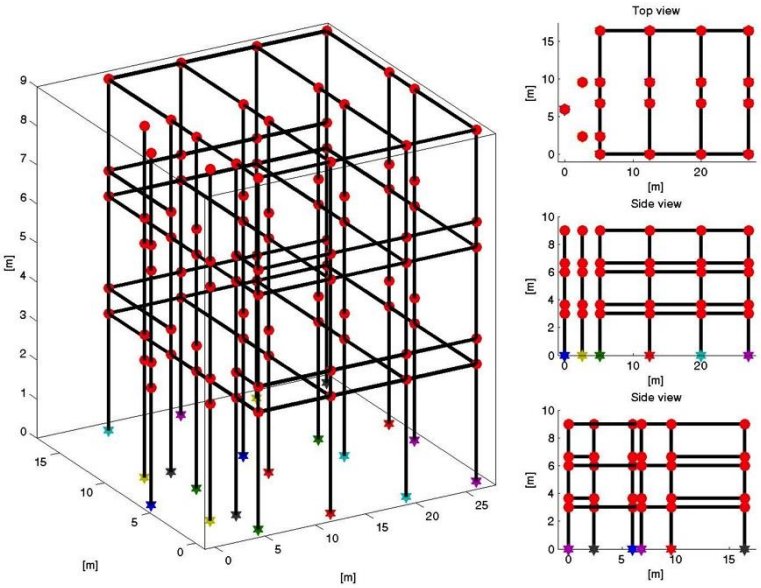

Figure 74 - Initial numerical model (OpenSees)

Table 31 - Script of the initial numerical model (OpenSees)

```
#MODEL GENERATION

wipe all

#UNITS: kN, ton, m, sec

#MODEL BUILDER (analysis dimension and dof of each node)
model BasicBuilder -ndm 3 -ndf 6

#NODES [tag x y z]
node 1 5.2 0 0
node 2 12.42 0 0
node 3 19.93 0 0
node 4 26.93 0 0
node 5 2.6 0 2.38
node 6 5.2 0 2.38
node 7 0 0 5.985
node 8 5.2 0 6.79
node 9 12.42 0 6.79
node 10 19.93 0 6.79
node 11 26.93 0 6.79
node 12 2.6 0 9.59
node 13 5.2 0 9.59
node 14 12.42 0 9.59
node 15 19.93 0 9.59
node 16 26.93 0 9.59
node 17 5.2 0 16.43
node 18 12.42 0 16.43
node 19 19.93 0 16.43
node 20 26.93 0 16.43
node 21 5.2 3 0
node 22 12.42 3 0
node 23 19.93 3 0
node 24 26.93 3 0
node 25 2.6 3 2.38
node 26 5.2 3 2.38
node 27 0 3 5.985
node 28 5.2 3 6.79
node 29 12.42 3 6.79
node 30 19.93 3 6.79
node 31 26.93 3 6.79
node 32 2.6 3 9.59
node 33 5.2 3 9.59
node 34 12.42 3 9.59
node 35 19.93 3 9.59
node 36 26.93 3 9.59
node 37 5.2 3 16.43
node 38 12.42 3 16.43
node 39 19.93 3 16.43
node 40 26.93 3 16.43
node 41 5.2 3.65 0
node 42 12.42 3.65 0
node 43 19.93 3.65 0
node 44 26.93 3.65 0
node 45 2.6 3.65 2.38
node 46 5.2 3.65 2.38
node 47 0 3.65 5.985
node 48 5.2 3.65 6.79
node 49 12.42 3.65 6.79
node 50 19.93 3.65 6.79
node 51 26.93 3.65 6.79
node 52 2.6 3.65 9.59
node 53 5.2 3.65 9.59
node 54 12.42 3.65 9.59
node 55 19.93 3.65 9.59
node 56 26.93 3.65 9.59
node 57 5.2 3.65 16.43
node 58 12.42 3.65 16.43
node 59 19.93 3.65 16.43
node 60 26.93 3.65 16.43
```

```
node 61 5.2 6 0
node 62 12.42 6 0
node 63 19.93 6 0
node 64 26.93 6 0
node 65 2.6 6 2.38
node 66 5.2 6 2.38
node 67 0 6 5.985
node 68 5.2 6 6.79
node 69 12.42 6 6.79
node 70 19.93 6 6.79
node 71 26.93 6 6.79
node 72 2.6 6 9.59
node 73 5.2 6 9.59
node 74 12.42 6 9.59
node 75 19.93 6 9.59
node 76 26.93 6 9.59
node 77 5.2 6 16.43
node 78 12.42 6 16.43
node 79 19.93 6 16.43
node 80 26.93 6 16.43
node 81 5.2 6.65 0
node 82 12.42 6.65 0
node 83 19.93 6.65 0
node 84 26.93 6.65 0
node 85 2.6 6.65 2.38
node 86 5.2 6.65 2.38
node 87 0 6.65 5.985
node 88 5.2 6.65 6.79
node 89 12.42 6.65 6.79
node 90 19.93 6.65 6.79
node 91 26.93 6.65 6.79
node 92 2.6 6.65 9.59
node 93 5.2 6.65 9.59
node 94 12.42 6.65 9.59
node 95 19.93 6.65 9.59
node 96 26.93 6.65 9.59
node 97 5.2 6.65 16.43
node 98 12.42 6.65 16.43
node 99 19.93 6.65 16.43
node 100 26.93 6.65 16.43
node 101 5.2 9 0
node 102 12.42 9 0
node 103 19.93 9 0
node 104 26.93 9 0
node 105 2.6 9 2.38
node 106 5.2 9 2.38
node 107 0 9 5.985
node 108 5.2 9 6.79
node 109 12.42 9 6.79
node 110 19.93 9 6.79
node 111 26.93 9 6.79
node 112 2.6 9 9.59
node 113 5.2 9 9.59
node 114 12.42 9 9.59
node 115 19.93 9 9.59
node 116 26.93 9 9.59
node 117 5.2 9 16.43
node 118 12.42 9 16.43
node 119 19.93 9 16.43
node 120 26.93 9 16.43

#BOUNDARY CONDITIONS [tag x y z rx ry rz]
fix 1 1 1 1 1 1 1
fix 2 1 1 1 1 1 1
fix 3 1 1 1 1 1 1
fix 4 1 1 1 1 1 1
fix 5 1 1 1 1 1 1
fix 6 1 1 1 1 1 1
fix 7 1 1 1 1 1 1
fix 8 1 1 1 1 1 1
fix 9 1 1 1 1 1 1
fix 10 1 1 1 1 1 1
fix 11 1 1 1 1 1 1
```

```
fix 12 1 1 1 1 1 1
fix 13 1 1 1 1 1 1
fix 14 1 1 1 1 1 1
fix 15 1 1 1 1 1 1
fix 16 1 1 1 1 1 1
fix 17 1 1 1 1 1 1
fix 18 1 1 1 1 1 1
fix 19 1 1 1 1 1 1
fix 20 1 1 1 1 1 1

#mpCONSTRAINTS_equalDOF [rNodeTag cNodeTag dof1 dof2 ...]
#There are no constraints between the nodes

#mpCONSTRAINTS_rigidDiaphragm [perpDirn masterNodeTag slaveNodeTag1 slaveNodeTag2 ...]
rigidDiaphragm 2 29 21 22 23 24 25 26 27 28 30 31 32 33 34 35 36 37 38 39 40
rigidDiaphragm 2 69 61 62 63 64 65 66 67 68 70 71 72 73 74 75 76 77 78 79 80
rigidDiaphragm 2 109 101 102 103 104 105 106 107 108 110 111 112 113 114 115 116 117 118 119 120

#NODAL MASSES [tag x y z rx ry rz]
mass 21 15.04 15.04 15.04 0 0 0
mass 22 31.8 31.8 31.8 0 0 0
mass 23 33.1 33.1 33.1 0 0 0
mass 24 16.34 16.34 16.34 0 0 0
mass 25 8.93 8.93 8.93 0 0 0
mass 26 15.04 15.04 15.04 0 0 0
mass 27 14.16 14.16 14.16 0 0 0
mass 28 15.04 15.04 15.04 0 0 0
mass 29 31.8 31.8 31.8 0 0 0
mass 30 33.1 33.1 33.1 0 0 0
mass 31 16.34 16.34 16.34 0 0 0
mass 32 8.93 8.93 8.93 0 0 0
mass 33 15.11 15.11 15.11 0 0 0
mass 34 31.8 31.8 31.8 0 0 0
mass 35 33.1 33.1 33.1 0 0 0
mass 36 16.34 16.34 16.34 0 0 0
mass 37 15.14 15.14 15.14 0 0 0
mass 38 31.8 31.8 31.8 0 0 0
mass 39 33.1 33.1 33.1 0 0 0
mass 40 16.34 16.34 16.34 0 0 0
mass 41 1.83 1.83 1.83 0 0 0
mass 42 2.49 2.49 2.49 0 0 0
mass 43 2.46 2.46 2.46 0 0 0
mass 44 1.5 1.5 1.5 0 0 0
mass 45 7.34 7.34 7.34 0 0 0
mass 46 0.91 0.91 0.91 0 0 0
mass 47 11.63 11.63 11.63 0 0 0
mass 48 0.61 0.61 0.61 0 0 0
mass 49 0.61 0.61 0.61 0 0 0
mass 50 0.61 0.61 0.61 0 0 0
mass 51 0.61 0.61 0.61 0 0 0
mass 52 7.34 7.34 7.34 0 0 0
mass 53 1.79 1.79 1.79 0 0 0
mass 54 0.61 0.61 0.61 0 0 0
mass 55 0.61 0.61 0.61 0 0 0
mass 56 0.61 0.61 0.61 0 0 0
mass 57 2.87 2.87 2.87 0 0 0
mass 58 2.49 2.49 2.49 0 0 0
mass 59 2.46 2.46 2.46 0 0 0
mass 60 1.5 1.5 1.5 0 0 0
mass 61 9.11 9.11 9.11 0 0 0
mass 62 19.08 19.08 19.08 0 0 0
mass 63 19.86 19.86 19.86 0 0 0
mass 64 9.89 9.89 9.89 0 0 0
mass 65 7.34 7.34 7.34 0 0 0
mass 66 9.11 9.11 9.11 0 0 0
mass 67 11.63 11.63 11.63 0 0 0
mass 68 9.11 9.11 9.11 0 0 0
mass 69 19.08 19.08 19.08 0 0 0
mass 70 19.86 19.86 19.86 0 0 0
mass 71 9.89 9.89 9.89 0 0 0
mass 72 7.34 7.34 7.34 0 0 0
mass 73 9.42 9.42 9.42 0 0 0
mass 74 19.08 19.08 19.08 0 0 0
```

```
mass 75 19.86 19.86 19.86 0 0 0
mass 76 9.89 9.89 9.89 0 0 0
mass 77 9.58 9.58 9.58 0 0 0
mass 78 19.08 19.08 19.08 0 0 0
mass 79 19.86 19.86 19.86 0 0 0
mass 80 9.89 9.89 9.89 0 0 0
mass 81 1.83 1.83 1.83 0 0 0
mass 82 2.49 2.49 2.49 0 0 0
mass 83 2.46 2.46 2.46 0 0 0
mass 84 1.5 1.5 1.5 0 0 0
mass 85 7.34 7.34 7.34 0 0 0
mass 86 0.91 0.91 0.91 0 0 0
mass 87 11.63 11.63 11.63 0 0 0
mass 88 0.61 0.61 0.61 0 0 0
mass 89 0.61 0.61 0.61 0 0 0
mass 90 0.61 0.61 0.61 0 0 0
mass 91 0.61 0.61 0.61 0 0 0
mass 92 7.34 7.34 7.34 0 0 0
mass 93 1.79 1.79 1.79 0 0 0
mass 94 0.61 0.61 0.61 0 0 0
mass 95 0.61 0.61 0.61 0 0 0
mass 96 0.61 0.61 0.61 0 0 0
mass 97 2.87 2.87 2.87 0 0 0
mass 98 2.49 2.49 2.49 0 0 0
mass 99 2.46 2.46 2.46 0 0 0
mass 100 1.5 1.5 1.5 0 0 0
mass 101 7.81 7.81 7.81 0 0 0
mass 102 16.4 16.4 16.4 0 0 0
mass 103 17.07 17.07 17.07 0 0 0
mass 104 8.48 8.48 8.48 0 0 0
mass 105 5.75 5.75 5.75 0 0 0
mass 106 7.81 7.81 7.81 0 0 0
mass 107 9.11 9.11 9.11 0 0 0
mass 108 7.81 7.81 7.81 0 0 0
mass 109 16.4 16.4 16.4 0 0 0
mass 110 17.07 17.07 17.07 0 0 0
mass 111 8.48 8.48 8.48 0 0 0
mass 112 5.75 5.75 5.75 0 0 0
mass 113 8.05 8.05 8.05 0 0 0
mass 114 16.4 16.4 16.4 0 0 0
mass 115 17.07 17.07 17.07 0 0 0
mass 116 8.48 8.48 8.48 0 0 0
mass 117 8.18 8.18 8.18 0 0 0
mass 118 16.4 16.4 16.4 0 0 0
mass 119 17.07 17.07 17.07 0 0 0
mass 120 8.48 8.48 8.48 0 0 0

#GEOMETRIC TRANSFORMATIONS
geomTransf Linear 1 0 0 1
geomTransf Linear 2 0 1 0

#ELEMENTS [eleType eleTag iNode jNode ... ]
element elasticBeamColumn 1 1 21 0.16 3e+007 1.25e+007 0.003605 0.00213333 0.00213333 1
element elasticBeamColumn 2 2 22 0.16 3e+007 1.25e+007 0.003605 0.00213333 0.00213333 1
element elasticBeamColumn 3 3 23 0.16 3e+007 1.25e+007 0.003605 0.00213333 0.00213333 1
element elasticBeamColumn 4 4 24 0.16 3e+007 1.25e+007 0.003605 0.00213333 0.00213333 1
element elasticBeamColumn 5 5 25 1.92 3e+007 1.25e+007 0.097 0.0256 3.6864 1
element elasticBeamColumn 6 6 26 0.16 3e+007 1.25e+007 0.003605 0.00213333 0.00213333 1
element elasticBeamColumn 7 7 27 3.04 3e+007 1.25e+007 0.157 14.6904 0.0405867 1
element elasticBeamColumn 8 8 28 0.16 3e+007 1.25e+007 0.003605 0.00213333 0.00213333 1
element elasticBeamColumn 9 9 29 0.16 3e+007 1.25e+007 0.003605 0.00213333 0.00213333 1
element elasticBeamColumn 10 10 30 0.16 3e+007 1.25e+007 0.003605 0.00213333 0.00213333 1
element elasticBeamColumn 11 11 31 0.16 3e+007 1.25e+007 0.003605 0.00213333 0.00213333 1
element elasticBeamColumn 12 12 32 1.92 3e+007 1.25e+007 0.097 0.0256 3.6864 1
element elasticBeamColumn 13 13 33 0.16 3e+007 1.25e+007 0.003605 0.00213333 0.00213333 1
element elasticBeamColumn 14 14 34 0.16 3e+007 1.25e+007 0.003605 0.00213333 0.00213333 1
element elasticBeamColumn 15 15 35 0.16 3e+007 1.25e+007 0.003605 0.00213333 0.00213333 1
element elasticBeamColumn 16 16 36 0.16 3e+007 1.25e+007 0.003605 0.00213333 0.00213333 1
element elasticBeamColumn 17 17 37 0.16 3e+007 1.25e+007 0.003605 0.00213333 0.00213333 1
element elasticBeamColumn 18 18 38 0.16 3e+007 1.25e+007 0.003605 0.00213333 0.00213333 1
element elasticBeamColumn 19 19 39 0.16 3e+007 1.25e+007 0.003605 0.00213333 0.00213333 1
element elasticBeamColumn 20 20 40 0.16 3e+007 1.25e+007 0.003605 0.00213333 0.00213333 1
element elasticBeamColumn 21 21 41 0.16 3e+007 1.25e+007 0.003605 0.00213333 0.00213333 1
```

```
element elasticBeamColumn 22 22 42 0.16 3e+007 1.25e+007 0.003605 0.00213333 0.00213333 1
element elasticBeamColumn 23 23 43 0.16 3e+007 1.25e+007 0.003605 0.00213333 0.00213333 1
element elasticBeamColumn 24 24 44 0.16 3e+007 1.25e+007 0.003605 0.00213333 0.00213333 1
element elasticBeamColumn 25 25 45 1.92 3e+007 1.25e+007 0.097 0.0256 3.6864 1
element elasticBeamColumn 26 26 46 0.16 3e+007 1.25e+007 0.003605 0.00213333 0.00213333 1
element elasticBeamColumn 27 27 47 3.04 3e+007 1.25e+007 0.157 14.6904 0.0405867 1
element elasticBeamColumn 28 28 48 0.16 3e+007 1.25e+007 0.003605 0.00213333 0.00213333 1
element elasticBeamColumn 29 29 49 0.16 3e+007 1.25e+007 0.003605 0.00213333 0.00213333 1
element elasticBeamColumn 30 30 50 0.16 3e+007 1.25e+007 0.003605 0.00213333 0.00213333 1
element elasticBeamColumn 31 31 51 0.16 3e+007 1.25e+007 0.003605 0.00213333 0.00213333 1
element elasticBeamColumn 32 32 52 1.92 3e+007 1.25e+007 0.097 0.0256 3.6864 1
element elasticBeamColumn 33 33 53 0.24 3e+007 1.25e+007 0.007512 0.0072 0.0032 1
element elasticBeamColumn 34 34 54 0.16 3e+007 1.25e+007 0.003605 0.00213333 0.00213333 1
element elasticBeamColumn 35 35 55 0.16 3e+007 1.25e+007 0.003605 0.00213333 0.00213333 1
element elasticBeamColumn 36 36 56 0.16 3e+007 1.25e+007 0.003605 0.00213333 0.00213333 1
element elasticBeamColumn 37 37 57 0.28 3e+007 1.25e+007 0.0127 0.00636173 0.00636173 1
element elasticBeamColumn 38 38 58 0.16 3e+007 1.25e+007 0.003605 0.00213333 0.00213333 1
element elasticBeamColumn 39 39 59 0.16 3e+007 1.25e+007 0.003605 0.00213333 0.00213333 1
element elasticBeamColumn 40 40 60 0.16 3e+007 1.25e+007 0.003605 0.00213333 0.00213333 1
element elasticBeamColumn 41 41 61 0.16 3e+007 1.25e+007 0.003605 0.00213333 0.00213333 1
element elasticBeamColumn 42 42 62 0.16 3e+007 1.25e+007 0.003605 0.00213333 0.00213333 1
element elasticBeamColumn 43 43 63 0.16 3e+007 1.25e+007 0.003605 0.00213333 0.00213333 1
element elasticBeamColumn 44 44 64 0.16 3e+007 1.25e+007 0.003605 0.00213333 0.00213333 1
element elasticBeamColumn 45 45 65 1.92 3e+007 1.25e+007 0.097 0.0256 3.6864 1
element elasticBeamColumn 46 46 66 0.16 3e+007 1.25e+007 0.003605 0.00213333 0.00213333 1
element elasticBeamColumn 47 47 67 3.04 3e+007 1.25e+007 0.157 14.6904 0.0405867 1
element elasticBeamColumn 48 48 68 0.16 3e+007 1.25e+007 0.003605 0.00213333 0.00213333 1
element elasticBeamColumn 49 49 69 0.16 3e+007 1.25e+007 0.003605 0.00213333 0.00213333 1
element elasticBeamColumn 50 50 70 0.16 3e+007 1.25e+007 0.003605 0.00213333 0.00213333 1
element elasticBeamColumn 51 51 71 0.16 3e+007 1.25e+007 0.003605 0.00213333 0.00213333 1
element elasticBeamColumn 52 52 72 1.92 3e+007 1.25e+007 0.097 0.0256 3.6864 1
element elasticBeamColumn 53 53 73 0.24 3e+007 1.25e+007 0.007512 0.0072 0.0032 1
element elasticBeamColumn 54 54 74 0.16 3e+007 1.25e+007 0.003605 0.00213333 0.00213333 1
element elasticBeamColumn 55 55 75 0.16 3e+007 1.25e+007 0.003605 0.00213333 0.00213333 1
element elasticBeamColumn 56 56 76 0.16 3e+007 1.25e+007 0.003605 0.00213333 0.00213333 1
element elasticBeamColumn 57 57 77 0.28 3e+007 1.25e+007 0.0127 0.00636173 0.00636173 1
element elasticBeamColumn 58 58 78 0.16 3e+007 1.25e+007 0.003605 0.00213333 0.00213333 1
element elasticBeamColumn 59 59 79 0.16 3e+007 1.25e+007 0.003605 0.00213333 0.00213333 1
element elasticBeamColumn 60 60 80 0.16 3e+007 1.25e+007 0.003605 0.00213333 0.00213333 1
element elasticBeamColumn 61 61 81 0.16 3e+007 1.25e+007 0.003605 0.00213333 0.00213333 1
element elasticBeamColumn 62 62 82 0.16 3e+007 1.25e+007 0.003605 0.00213333 0.00213333 1
element elasticBeamColumn 63 63 83 0.16 3e+007 1.25e+007 0.003605 0.00213333 0.00213333 1
element elasticBeamColumn 64 64 84 0.16 3e+007 1.25e+007 0.003605 0.00213333 0.00213333 1
element elasticBeamColumn 65 65 85 1.92 3e+007 1.25e+007 0.097 0.0256 3.6864 1
element elasticBeamColumn 66 66 86 0.16 3e+007 1.25e+007 0.003605 0.00213333 0.00213333 1
element elasticBeamColumn 67 67 87 3.04 3e+007 1.25e+007 0.157 14.6904 0.0405867 1
element elasticBeamColumn 68 68 88 0.16 3e+007 1.25e+007 0.003605 0.00213333 0.00213333 1
element elasticBeamColumn 69 69 89 0.16 3e+007 1.25e+007 0.003605 0.00213333 0.00213333 1
element elasticBeamColumn 70 70 90 0.16 3e+007 1.25e+007 0.003605 0.00213333 0.00213333 1
element elasticBeamColumn 71 71 91 0.16 3e+007 1.25e+007 0.003605 0.00213333 0.00213333 1
element elasticBeamColumn 72 72 92 1.92 3e+007 1.25e+007 0.097 0.0256 3.6864 1
element elasticBeamColumn 73 73 93 0.24 3e+007 1.25e+007 0.007512 0.0072 0.0032 1
element elasticBeamColumn 74 74 94 0.16 3e+007 1.25e+007 0.003605 0.00213333 0.00213333 1
element elasticBeamColumn 75 75 95 0.16 3e+007 1.25e+007 0.003605 0.00213333 0.00213333 1
element elasticBeamColumn 76 76 96 0.16 3e+007 1.25e+007 0.003605 0.00213333 0.00213333 1
element elasticBeamColumn 77 77 97 0.28 3e+007 1.25e+007 0.0127 0.00636173 0.00636173 1
element elasticBeamColumn 78 78 98 0.16 3e+007 1.25e+007 0.003605 0.00213333 0.00213333 1
element elasticBeamColumn 79 79 99 0.16 3e+007 1.25e+007 0.003605 0.00213333 0.00213333 1
element elasticBeamColumn 80 80 100 0.16 3e+007 1.25e+007 0.003605 0.00213333 0.00213333 1
element elasticBeamColumn 81 81 101 0.16 3e+007 1.25e+007 0.003605 0.00213333 0.00213333 1
element elasticBeamColumn 82 82 102 0.16 3e+007 1.25e+007 0.003605 0.00213333 0.00213333 1
element elasticBeamColumn 83 83 103 0.16 3e+007 1.25e+007 0.003605 0.00213333 0.00213333 1
element elasticBeamColumn 84 84 104 0.16 3e+007 1.25e+007 0.003605 0.00213333 0.00213333 1
element elasticBeamColumn 85 85 105 1.92 3e+007 1.25e+007 0.097 0.0256 3.6864 1
element elasticBeamColumn 86 86 106 0.16 3e+007 1.25e+007 0.003605 0.00213333 0.00213333 1
element elasticBeamColumn 87 87 107 3.04 3e+007 1.25e+007 0.157 14.6904 0.0405867 1
element elasticBeamColumn 88 88 108 0.16 3e+007 1.25e+007 0.003605 0.00213333 0.00213333 1
element elasticBeamColumn 89 89 109 0.16 3e+007 1.25e+007 0.003605 0.00213333 0.00213333 1
element elasticBeamColumn 90 90 110 0.16 3e+007 1.25e+007 0.003605 0.00213333 0.00213333 1
element elasticBeamColumn 91 91 111 0.16 3e+007 1.25e+007 0.003605 0.00213333 0.00213333 1
element elasticBeamColumn 92 92 112 1.92 3e+007 1.25e+007 0.097 0.0256 3.6864 1
element elasticBeamColumn 93 93 113 0.24 3e+007 1.25e+007 0.007512 0.0072 0.0032 1
element elasticBeamColumn 94 94 114 0.16 3e+007 1.25e+007 0.003605 0.00213333 0.00213333 1
```

```
element elasticBeamColumn 95 95 115 0.16 3e+007 1.25e+007 0.003605 0.00213333 0.00213333 1
element elasticBeamColumn 96 96 116 0.16 3e+007 1.25e+007 0.003605 0.00213333 0.00213333 1
element elasticBeamColumn 97 97 117 0.28 3e+007 1.25e+007 0.0127 0.00636173 0.00636173 1
element elasticBeamColumn 98 98 118 0.16 3e+007 1.25e+007 0.003605 0.00213333 0.00213333 1
element elasticBeamColumn 99 99 119 0.16 3e+007 1.25e+007 0.003605 0.00213333 0.00213333 1
element elasticBeamColumn 100 100 120 0.16 3e+007 1.25e+007 0.003605 0.00213333 0.00213333 1
element elasticBeamColumn 101 21 22 0.12 3e+007 1.25e+007 0.001944 0.0009 0.0016 2
element elasticBeamColumn 102 22 23 0.12 3e+007 1.25e+007 0.001944 0.0009 0.0016 2
element elasticBeamColumn 103 23 24 0.12 3e+007 1.25e+007 0.001944 0.0009 0.0016 2
element elasticBeamColumn 104 37 38 0.12 3e+007 1.25e+007 0.001944 0.0009 0.0016 2
element elasticBeamColumn 105 38 39 0.12 3e+007 1.25e+007 0.001944 0.0009 0.0016 2
element elasticBeamColumn 106 39 40 0.12 3e+007 1.25e+007 0.001944 0.0009 0.0016 2
element elasticBeamColumn 107 21 26 0.12 3e+007 1.25e+007 0.001944 0.0009 0.0016 2
element elasticBeamColumn 108 26 28 0.3 3e+007 1.25e+007 0.0073 0.00225 0.025 2
element elasticBeamColumn 109 28 33 0.3 3e+007 1.25e+007 0.0073 0.00225 0.025 2
element elasticBeamColumn 110 33 37 0.3 3e+007 1.25e+007 0.0073 0.00225 0.025 2
element elasticBeamColumn 111 22 29 0.3 3e+007 1.25e+007 0.0073 0.00225 0.025 2
element elasticBeamColumn 112 29 34 0.3 3e+007 1.25e+007 0.0073 0.00225 0.025 2
element elasticBeamColumn 113 34 38 0.3 3e+007 1.25e+007 0.0073 0.00225 0.025 2
element elasticBeamColumn 114 23 30 0.3 3e+007 1.25e+007 0.0073 0.00225 0.025 2
element elasticBeamColumn 115 30 35 0.3 3e+007 1.25e+007 0.0073 0.00225 0.025 2
element elasticBeamColumn 116 35 39 0.3 3e+007 1.25e+007 0.0073 0.00225 0.025 2
element elasticBeamColumn 117 24 31 0.15 3e+007 1.25e+007 0.002817 0.001125 0.003125 2
element elasticBeamColumn 118 31 36 0.15 3e+007 1.25e+007 0.002817 0.001125 0.003125 2
element elasticBeamColumn 119 36 40 0.15 3e+007 1.25e+007 0.002817 0.001125 0.003125 2
element elasticBeamColumn 120 61 62 0.11 3e+007 1.25e+007 0.001662 0.000731733 0.00149333 2
element elasticBeamColumn 121 62 63 0.11 3e+007 1.25e+007 0.001662 0.000731733 0.00149333 2
element elasticBeamColumn 122 63 64 0.11 3e+007 1.25e+007 0.001662 0.000731733 0.00149333 2
element elasticBeamColumn 123 77 78 0.11 3e+007 1.25e+007 0.001662 0.000731733 0.00149333 2
element elasticBeamColumn 124 78 79 0.11 3e+007 1.25e+007 0.001662 0.000731733 0.00149333 2
element elasticBeamColumn 125 79 80 0.11 3e+007 1.25e+007 0.001662 0.000731733 0.00149333 2
element elasticBeamColumn 126 61 66 0.2 3e+007 1.25e+007 0.003834 0.00128053 0.00800333 2
element elasticBeamColumn 127 66 68 0.2 3e+007 1.25e+007 0.003834 0.00128053 0.00800333 2
element elasticBeamColumn 128 68 73 0.2 3e+007 1.25e+007 0.003834 0.00128053 0.00800333 2
element elasticBeamColumn 129 73 77 0.2 3e+007 1.25e+007 0.003834 0.00128053 0.00800333 2
element elasticBeamColumn 130 62 69 0.28 3e+007 1.25e+007 0.006027 0.00182933 0.0233333 2
element elasticBeamColumn 131 69 74 0.28 3e+007 1.25e+007 0.006027 0.00182933 0.0233333 2
element elasticBeamColumn 132 74 78 0.28 3e+007 1.25e+007 0.006027 0.00182933 0.0233333 2
element elasticBeamColumn 133 63 70 0.28 3e+007 1.25e+007 0.006027 0.00182933 0.0233333 2
element elasticBeamColumn 134 70 75 0.28 3e+007 1.25e+007 0.006027 0.00182933 0.0233333 2
element elasticBeamColumn 135 75 79 0.28 3e+007 1.25e+007 0.006027 0.00182933 0.0233333 2
element elasticBeamColumn 136 64 71 0.14 3e+007 1.25e+007 0.002378 0.000914667 0.00291667 2
element elasticBeamColumn 137 71 76 0.14 3e+007 1.25e+007 0.002378 0.000914667 0.00291667 2
element elasticBeamColumn 138 76 80 0.14 3e+007 1.25e+007 0.002378 0.000914667 0.00291667 2
element elasticBeamColumn 139 101 102 0.11 3e+007 1.25e+007 0.001662 0.000731733 0.00149333 2
element elasticBeamColumn 140 102 103 0.11 3e+007 1.25e+007 0.001662 0.000731733 0.00149333 2
element elasticBeamColumn 141 103 104 0.11 3e+007 1.25e+007 0.001662 0.000731733 0.00149333 2
element elasticBeamColumn 142 117 118 0.11 3e+007 1.25e+007 0.001662 0.000731733 0.00149333 2
element elasticBeamColumn 143 118 119 0.11 3e+007 1.25e+007 0.001662 0.000731733 0.00149333 2
element elasticBeamColumn 144 119 120 0.11 3e+007 1.25e+007 0.001662 0.000731733 0.00149333 2
element elasticBeamColumn 145 101 106 0.2 3e+007 1.25e+007 0.003834 0.00128053 0.00800333 2
element elasticBeamColumn 146 106 108 0.2 3e+007 1.25e+007 0.003834 0.00128053 0.00800333 2
element elasticBeamColumn 147 108 113 0.2 3e+007 1.25e+007 0.003834 0.00128053 0.00800333 2
element elasticBeamColumn 148 113 117 0.2 3e+007 1.25e+007 0.003834 0.00128053 0.00800333 2
element elasticBeamColumn 149 102 109 0.28 3e+007 1.25e+007 0.006027 0.00182933 0.0233333 2
element elasticBeamColumn 150 109 114 0.28 3e+007 1.25e+007 0.006027 0.00182933 0.0233333 2
element elasticBeamColumn 151 114 118 0.28 3e+007 1.25e+007 0.006027 0.00182933 0.0233333 2
element elasticBeamColumn 152 103 110 0.28 3e+007 1.25e+007 0.006027 0.00182933 0.0233333 2
element elasticBeamColumn 153 110 115 0.28 3e+007 1.25e+007 0.006027 0.00182933 0.0233333 2
element elasticBeamColumn 154 115 119 0.28 3e+007 1.25e+007 0.006027 0.00182933 0.0233333 2
element elasticBeamColumn 155 104 111 0.14 3e+007 1.25e+007 0.002378 0.000914667 0.00291667 2
element elasticBeamColumn 156 111 116 0.14 3e+007 1.25e+007 0.002378 0.000914667 0.00291667 2
element elasticBeamColumn 157 116 120 0.14 3e+007 1.25e+007 0.002378 0.000914667 0.00291667 2
element elasticBeamColumn 158 41 42 0.1 3e+007 1.25e+007 0.0003123 0.00833333 8.33333e-005 2
element elasticBeamColumn 159 42 43 0.1 3e+007 1.25e+007 0.0003123 0.00833333 8.33333e-005 2
element elasticBeamColumn 160 43 44 0.1 3e+007 1.25e+007 0.0003123 0.00833333 8.33333e-005 2
element elasticBeamColumn 161 81 82 0.1 3e+007 1.25e+007 0.0003123 0.00833333 8.33333e-005 2
element elasticBeamColumn 162 82 83 0.1 3e+007 1.25e+007 0.0003123 0.00833333 8.33333e-005 2
element elasticBeamColumn 163 83 84 0.1 3e+007 1.25e+007 0.0003123 0.00833333 8.33333e-005 2
element elasticBeamColumn 164 57 58 0.1 3e+007 1.25e+007 0.0003123 0.00833333 8.33333e-005 2
element elasticBeamColumn 165 58 59 0.1 3e+007 1.25e+007 0.0003123 0.00833333 8.33333e-005 2
element elasticBeamColumn 166 59 60 0.1 3e+007 1.25e+007 0.0003123 0.00833333 8.33333e-005 2
element elasticBeamColumn 167 97 98 0.1 3e+007 1.25e+007 0.0003123 0.00833333 8.33333e-005 2
```

```
element elasticBeamColumn 168 98 99 0.1 3e+007 1.25e+007 0.0003123 0.00833333 8.33333e-005 2
element elasticBeamColumn 169 99 100 0.1 3e+007 1.25e+007 0.0003123 0.00833333 8.33333e-005 2
element elasticBeamColumn 170 53 57 0.1 3e+007 1.25e+007 0.0003123 0.00833333 8.33333e-005 2
element elasticBeamColumn 171 93 97 0.1 3e+007 1.25e+007 0.0003123 0.00833333 8.33333e-005 2
element elasticBeamColumn 172 46 41 0.1 3e+007 1.25e+007 0.0003123 0.00833333 8.33333e-005 2
element elasticBeamColumn 173 86 81 0.1 3e+007 1.25e+007 0.0003123 0.00833333 8.33333e-005 2

#mpCONSTRAINTS_rigidLink [rigidLink $type $masterNodeTag $slaveNodeTag]
rigidLink bar 25 27
rigidLink bar 32 27
rigidLink bar 25 26
rigidLink bar 32 33
rigidLink bar 65 67
rigidLink bar 72 67
rigidLink bar 65 66
rigidLink bar 72 73
rigidLink bar 105 107
rigidLink bar 112 107
rigidLink bar 105 106
rigidLink bar 112 113
rigidLink bar 52 47
rigidLink bar 45 47
rigidLink bar 52 53
rigidLink bar 45 46
rigidLink bar 92 87
rigidLink bar 85 87
rigidLink bar 92 93
rigidLink bar 85 86

#ANALYSIS GENERATION

#MODAL ANALYSIS
set nameScript "TEST"
set nameFolderOut "Results_Modal_Analysis_$nameScript"
file mkdir $nameFolderOut
set numModes 20
set eigenvalues [eigen $numModes]
for { set k 1 } { $k <= $numModes } { incr k } { recorder Node -file [format "$nameFolderOut/mode%i.txt" $k] -
nodeRange 1 120 -dof 1 2 3 "eigen $k" }
set omega {}
set f {}
set T {}
set pi 3.141593
foreach lambda $eigenvalues {
    lappend omega [expr sqrt($lambda)]
    lappend T [expr (2*$pi)/sqrt($lambda)]
    lappend f [expr sqrt($lambda)/(2*$pi)]
}
puts ">> eigenfrequencies are $omega"
puts ">> eigenperiods are $T"

set output1 "$nameFolderOut/eigenfrequencies.txt"
set outfile [open $output1 w]
puts $outfile $omega
close $outfile
set output2 "$nameFolderOut/eigenperiods.txt"
set outfile [open $output2 w]
puts $outfile $T
close $outfile

#Run one step gravity load with no loading (to record eigenvectors)
integrator LoadControl 0 1 0 0
#Create the convergence test (tolerance maxIter displayCode)
test EnergyIncr 1.0e-10 100 0
#Create the solution algorithm
algorithm Newton
#Create the DOF numberer using reverse Cuthill-McKee algorithm
numberer RCM
#Create the constraint handler
constraints Transformation
#System of equation solver
system ProfileSPD
analysis Static
```

analyze 1

Althought the models are the same, the differences in the results between *SAP2000* and *OpenSees* are significant. For this reason, the two models were create step-by-step in order to understand what specification in modeling is affecting the results. After the initial check of geometry and masses, the frames are compared. The results showed qualitatively the same values in terms of periods and the biggest difference for the first three modes is about 1.50%. The second step was adding the rigid diaphragm to the models. In *SAP2000* this is modeled constraining X, Y and the rotation about the vertical axis Z for all the nodes of the storey, while in *OpenSees* this has to be written giving, as instruction, the normal direction of the plane and the nodes belonging to the slab. The differences in this case remained below the 3% for the first three modes. The problem arise when the short slender walls sustained by the beams at the borders and mainly the walls of the stairs are added to the model. The connection between the walls of the stairs and the frame is made with rigid links for both models, but while *SAP2000* requires only the definition of the dofs to be constrained by the rigid link, *OpenSees* requires also the specification of master and slave node. Since the mode shapes show primarly flexural modes along the longitudinal direction, the nodes corresponding to the two walls with the plane oriented along the same direction were selected to be the master node. In the following Table 32, the results of the final models and the measured field data are compared. The introduction of the rigid connection between walls and frame played the major role in creating the differences among the results of the numerical models.

Table 32 - Results modal analysis (OpenSees) and comparison with the results obtained from SAP2000 and with the measured values from dynami identification

Mode	T_{SAP} [Sec]	f_{SAP} [Cyc/sec]	ω_{SAP} [rad/sec]	$T_{OpenSees}$ [Sec]	$f_{OpensSees}$ [Cyc/sec]	$\omega_{OpenSees}$ [rad/sec]	T_E [Sec]	f_E [Cyc/sec]	ω_E [rad/sec]
1	0.275291	3.6325	22.824	**0.182749**	**5.471994**	**34.38155**	0.166667	6.000	37.69911
2	0.104742	9.5473	59.987	**0.116302**	**8.598332**	**54.024911**	0.135593	7.375	46.33849
3	0.0927	10.788	67.78	**0.076861**	**13.01057**	**81.747807**	0.123077	8.125	51.05088
4	0.065229	15.331	96.326	**0.050877**	**19.65533**	**123.49806**	-	-	-
5	0.062028	16.122	101.3	**0.050868**	**19.65879**	**123.5198**	-	-	-
6	0.0509	19.647	123.44	**0.050104**	**19.95854**	**125.40319**	-	-	-
7	0.050891	19.65	123.46	**0.04973**	**20.10841**	**126.34489**	-	-	-
8	0.050109	19.957	125.39	**0.049695**	**20.12266**	**126.43441**	-	-	-
9	0.049768	20.093	126.25	**0.049116**	**20.35984**	**127.92463**	-	-	-
10	0.049735	20.107	126.33	**0.047115**	**21.22474**	**133.35895**	-	-	-
11	0.049122	20.357	127.91	**0.046209**	**21.64086**	**135.97356**	-	-	-
12	0.047198	21.187	133.12	**0.044694**	**22.37426**	**140.58161**	-	-	-
13	0.046282	21.607	135.76	**0.036559**	**27.35315**	**171.86492**	-	-	-
14	0.036322	27.532	172.99	**0.036304**	**27.54507**	**173.07079**	-	-	-
15	0.036319	27.534	173	**0.036295**	**27.55209**	**173.11488**	-	-	-
16	0.035655	28.046	176.22	**0.035651**	**28.04938**	**176.23944**	-	-	-
17	0.034788	28.745	180.61	**0.034371**	**29.09412**	**182.80377**	-	-	-
18	0.034413	29.059	182.58	**0.033878**	**29.51734**	**185.46291**	-	-	-
19	0.033859	29.534	185.57	**0.033037**	**30.26939**	**190.1882**	-	-	-
20	0.033569	29.79	187.17	**0.03193**	**31.31805**	**196.77711**	-	-	-

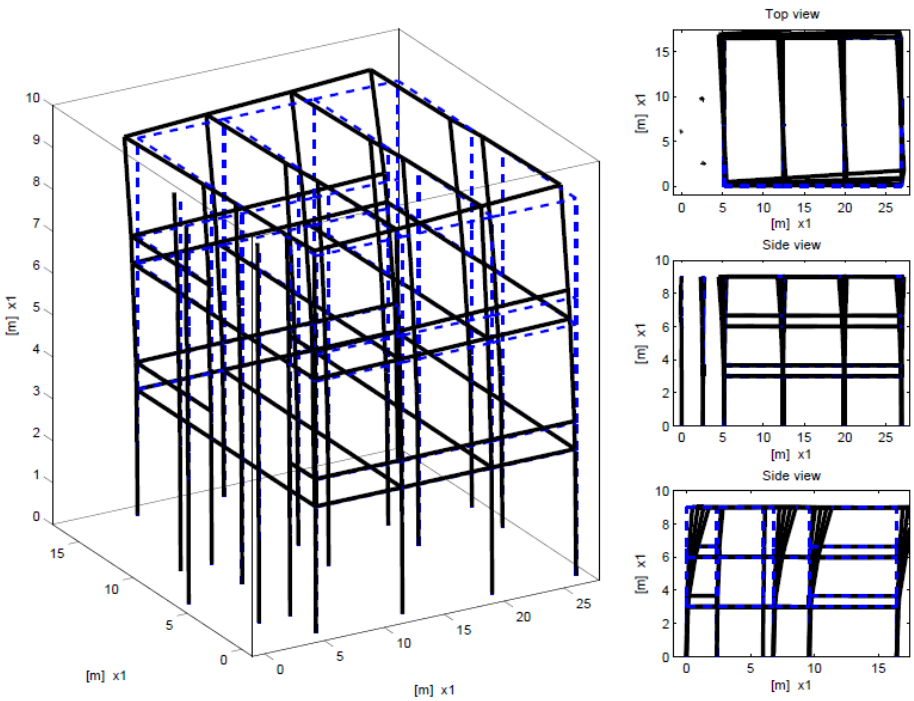

Figure 75 - Initial numerical model - Deformed shape mode 1 (OpenSees)

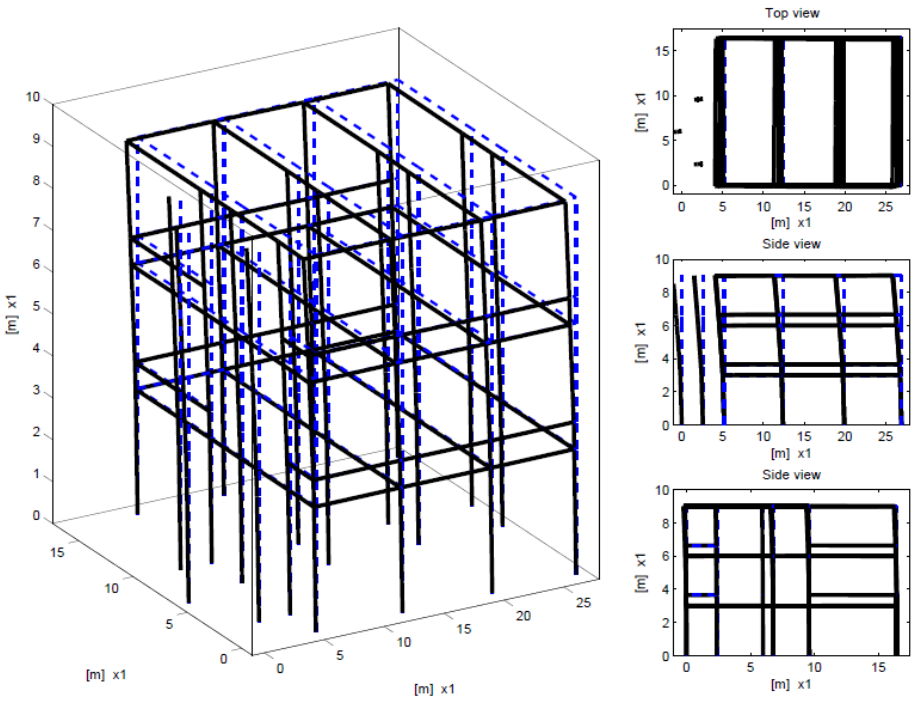

Figure 76 - Initial numerical model - Deformed shape mode 2 (OpenSees)

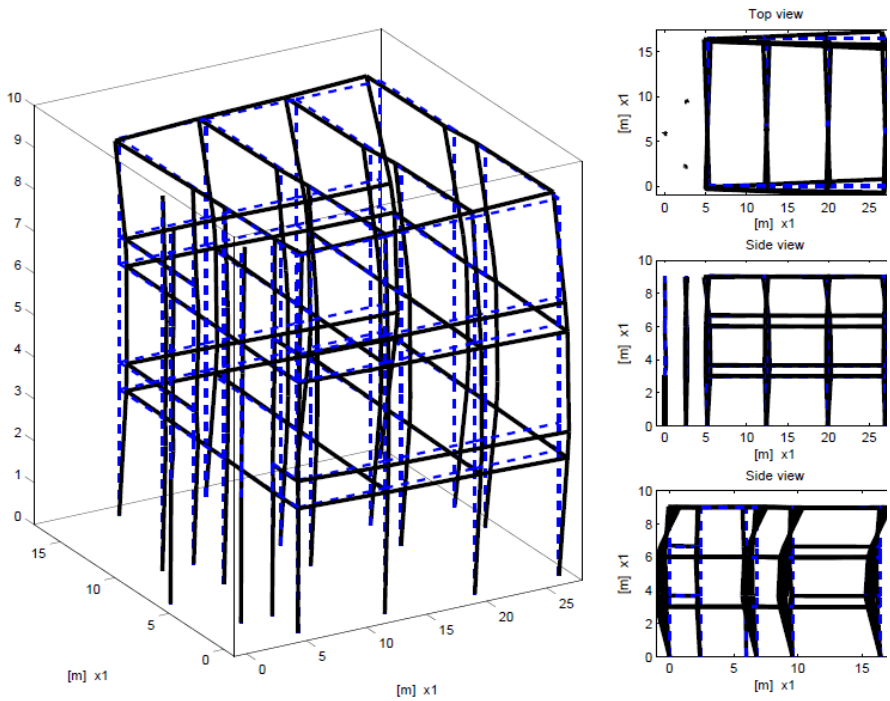

Figure 77 - Initial numerical model - Deformed shape mode 3 (OpenSees)

Finally, it is clear the differences between the results of the numerical models created with the two programs. Moreover, the deformed shapes appear the same with a disagreement in the order of them: mode shape 2 in *OpenSees* corresponds to mode shape 3 in *SAP2000* and viceversa. Considering only the model with *OpenSees* and the measured mode shapes, only the first modes can be compared. For this reason, only this mode will be involved in the finite element model updating procedure.

13.5 *Results*

The results of the performed analyses are showed below. First, all the type of simulations are investigated, then from the one that exhibites the lowest error index curve, other analysis are repeated in order to see the variability of the results by changing the mean and standard deviation of characteristic compressive strength of the concrete.

13.5.1 Simulation type 1 (μ_{fck}=18 N/mm^2, σ_{fck}=6 N/mm^2)

Table 33 - Result of the simulations (type 1) - Generalized modal errors

Simulation	Type	Models	μ_{fck} [N/mm^2]	σ_{fck} [N/mm^2]	Updated Model n°	Generalized Modal Error	E [kN/m^2]
1	3	1000	18	6	756	1.234	3.3931e+007
2	3	2000	18	6	1338	0.26053	3.4881e+007
3	3	3000	18	6	2811	0.17115	3.5242e+007
4	**3**	**4000**	**18**	**6**	**2355**	**0.13711**	**3.5327e+007**
5	3	5000	18	6	3667	0.20078	3.5175e+007
6	3	6000	18	6	2487	0.16736	3.5251e+007
7	3	7000	18	6	5463	0.21867	3.5137e+007
8	3	8000	18	6	5811	0.17115	3.5242e+007

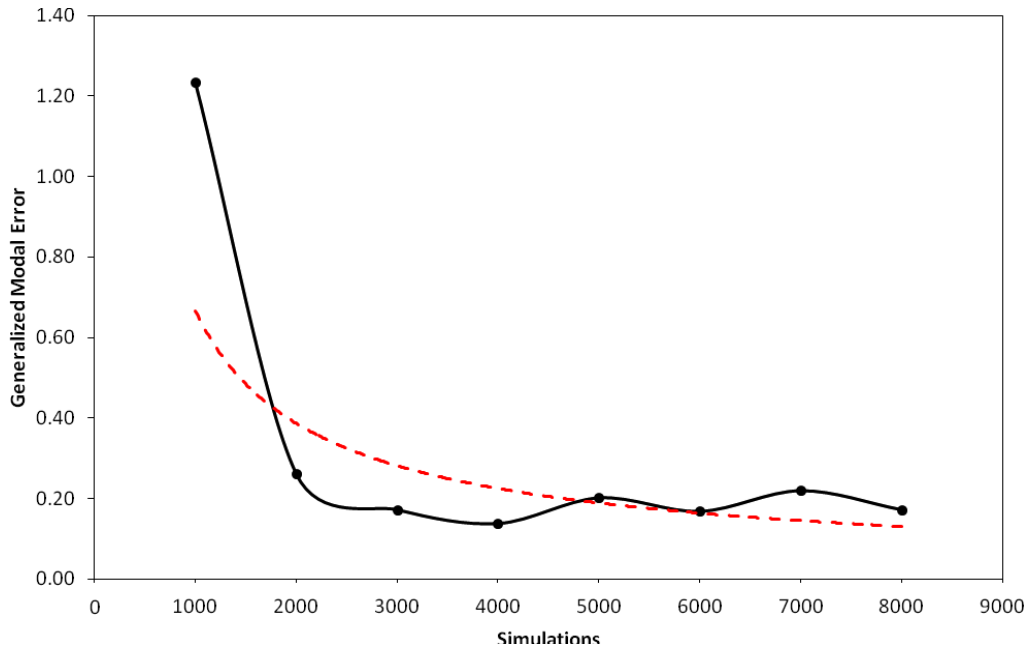

Figure 78 - Result of the simulations (type 1) - Generalized modal errors

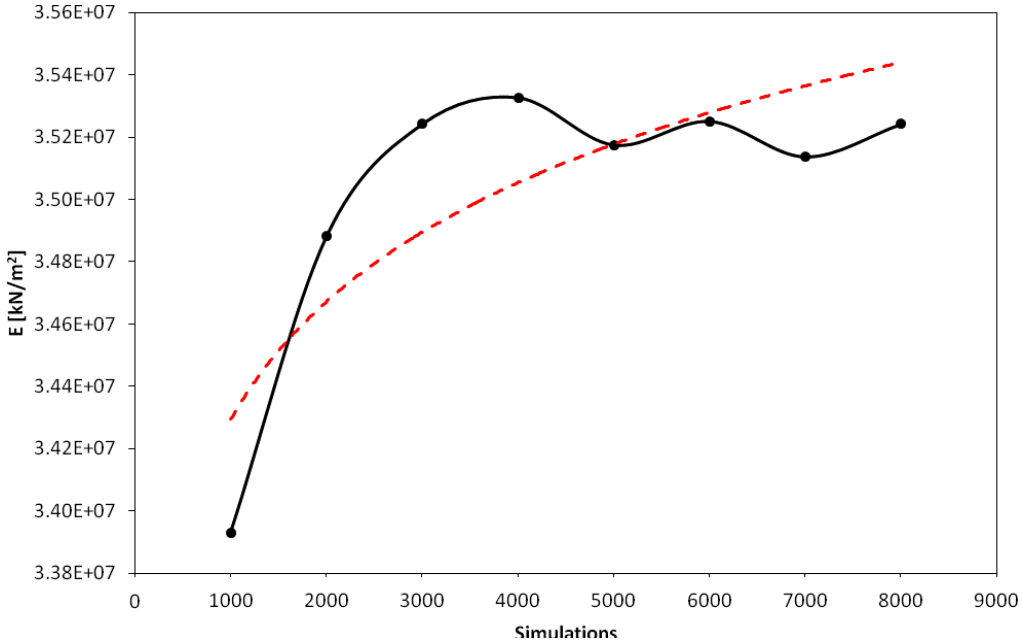

Figure 79 - Result of the simulations (type 1) - Young's Modulus

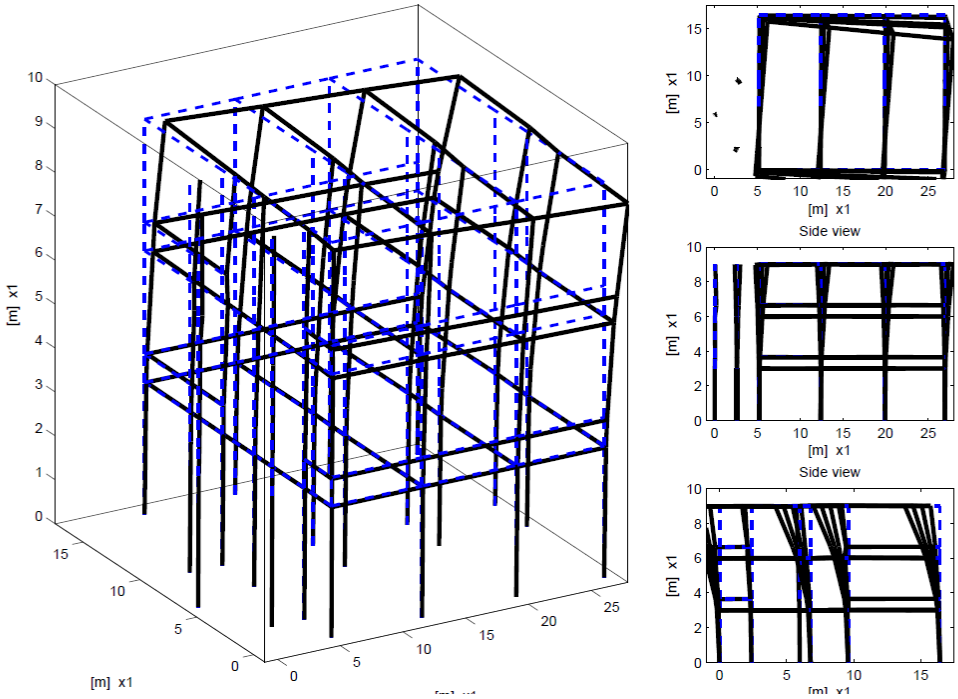

Figure 80 - Deformed shape mode 1 (normalized according to node 117) - Initial model

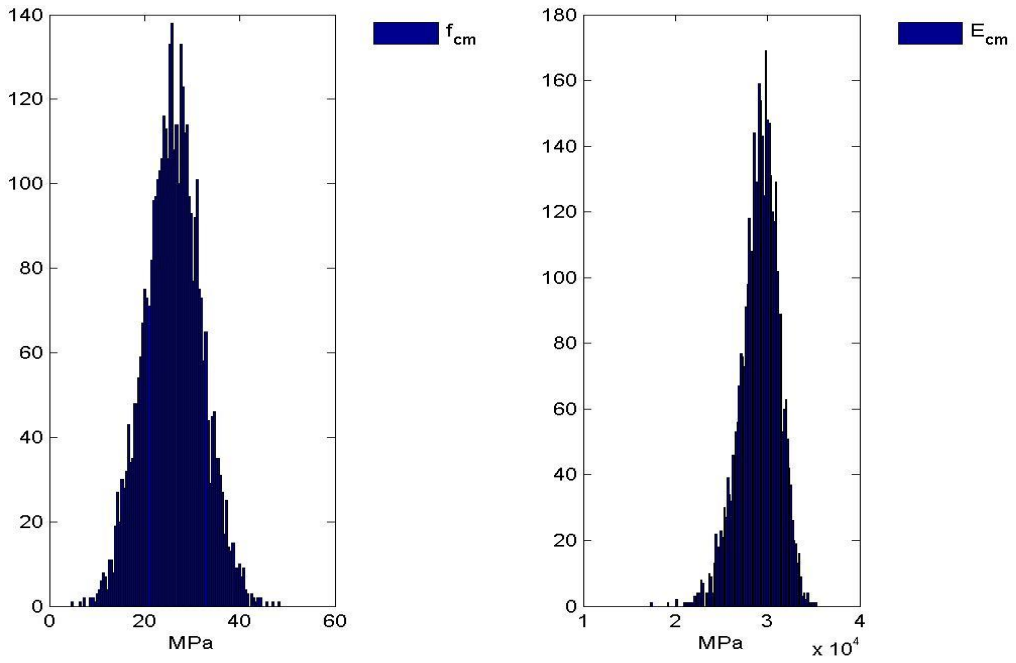

Figure 81 - Generation of the mechanical properties f_{cm} and E_{cm} for the 4000 samples simulation (type 1)

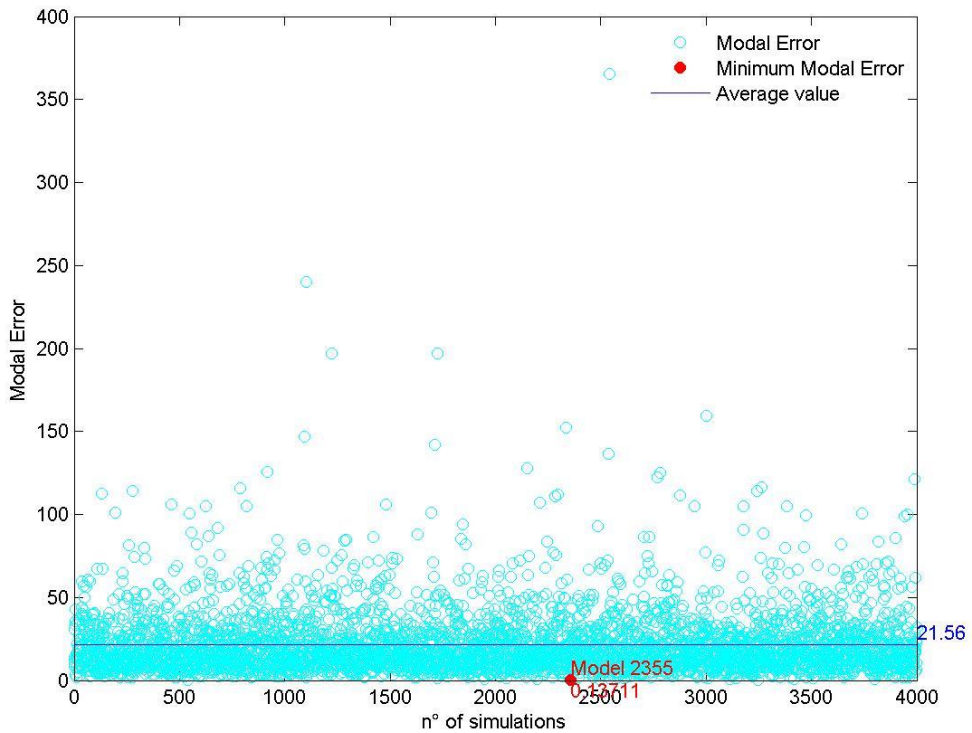

Figure 82 - Generalized modal errors for the 4000 samples simulation (type 1) - Updated model n°2355

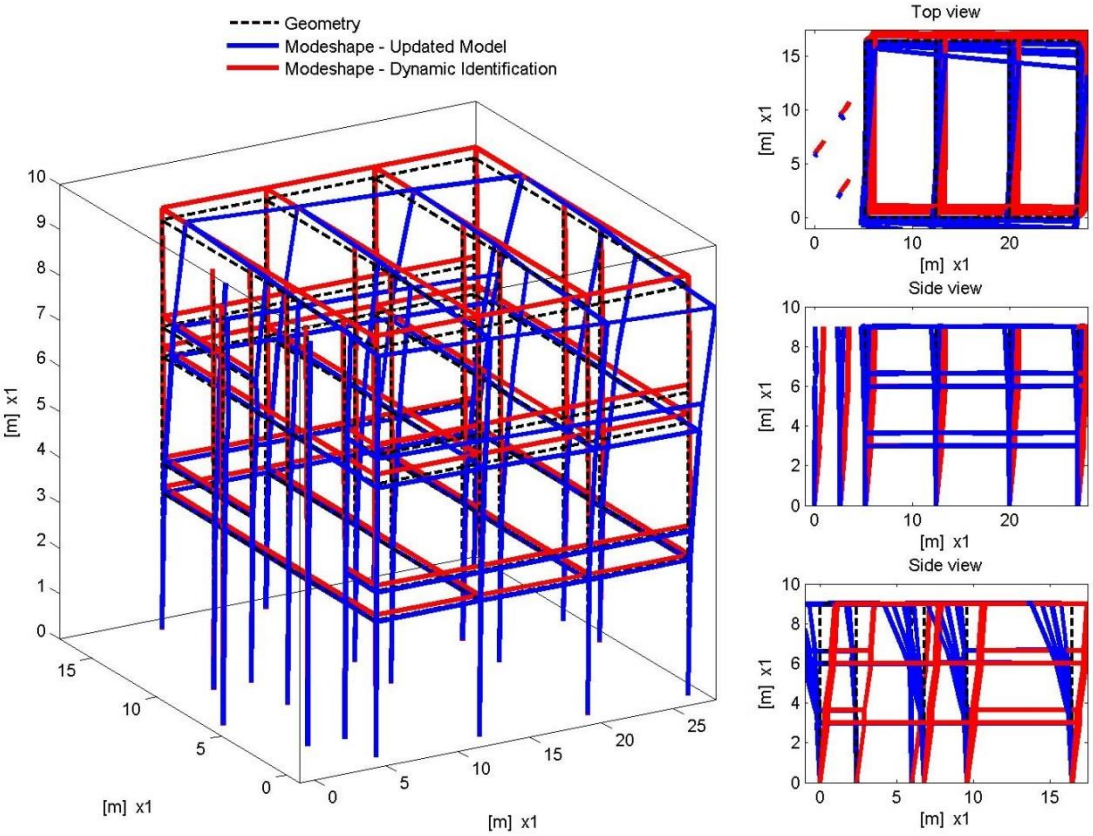

Figure 83 - Comparison between numerical updated (model n°2355) and measured modal displacements - Deformed shape mode 1

Table 34 - Comparison between numerical results from the initial and updated model and measured values - Updated model n° 2355

Mode	ω_i [rad/sec]	ω_U [rad/sec]	ω_E [rad/sec]	ω_i/ω_E	ω_U/ω_E
1	34.381	37.309	37.699	0.912	0.990
2	-	-	46.338	-	-
3	-	-	51.051	-	-

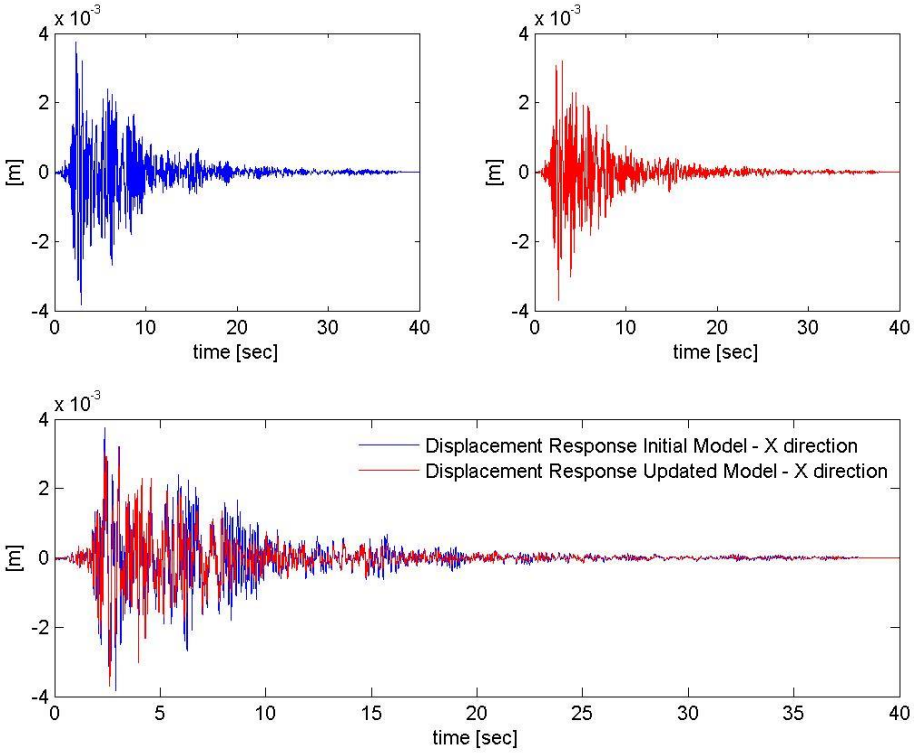

Figure 84 - Elastic THA - Comparison between initial and updated model - X direction (longitudinal)

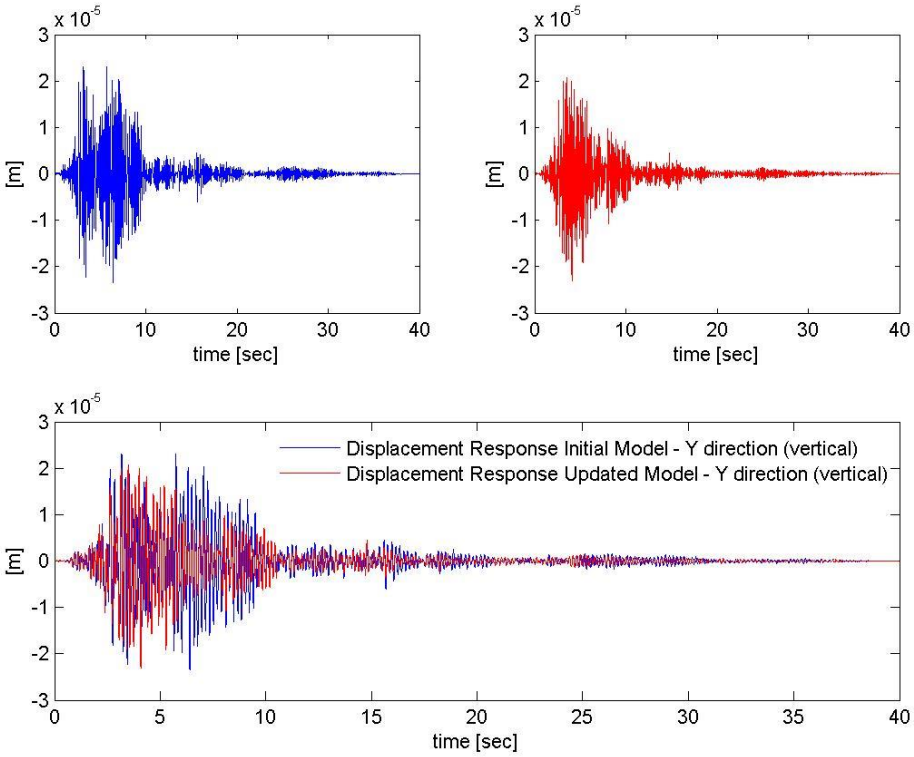

Figure 85 - Elastic THA - Comparison between initial and updated model - Y direction (vertical)

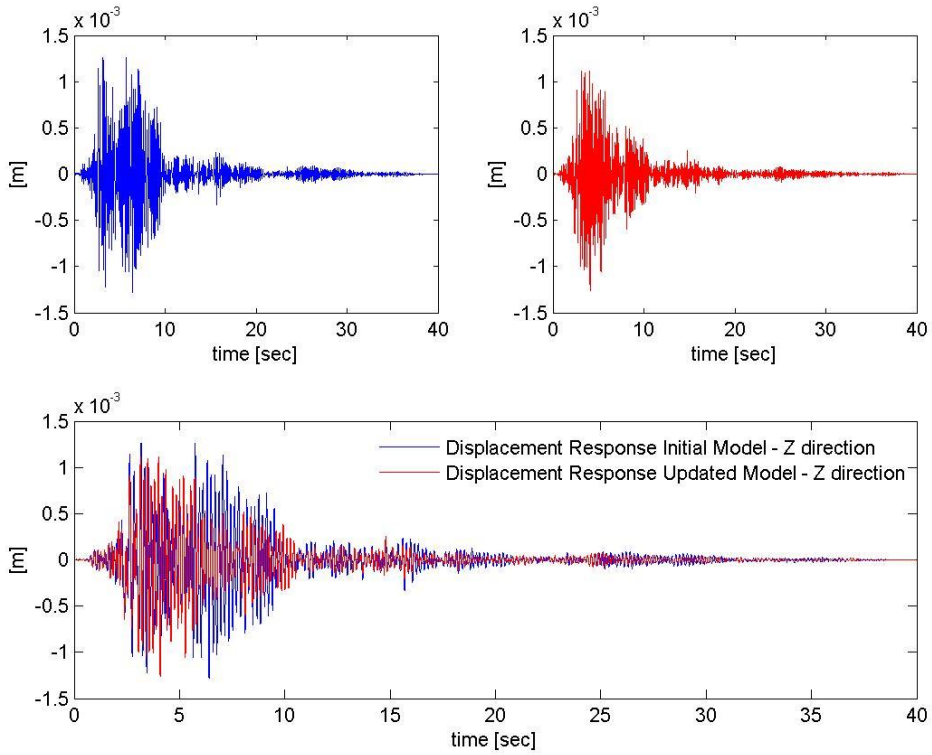

Figure 86 - Elastic THA - Comparison between initial and updated model - Z direction (transversal)

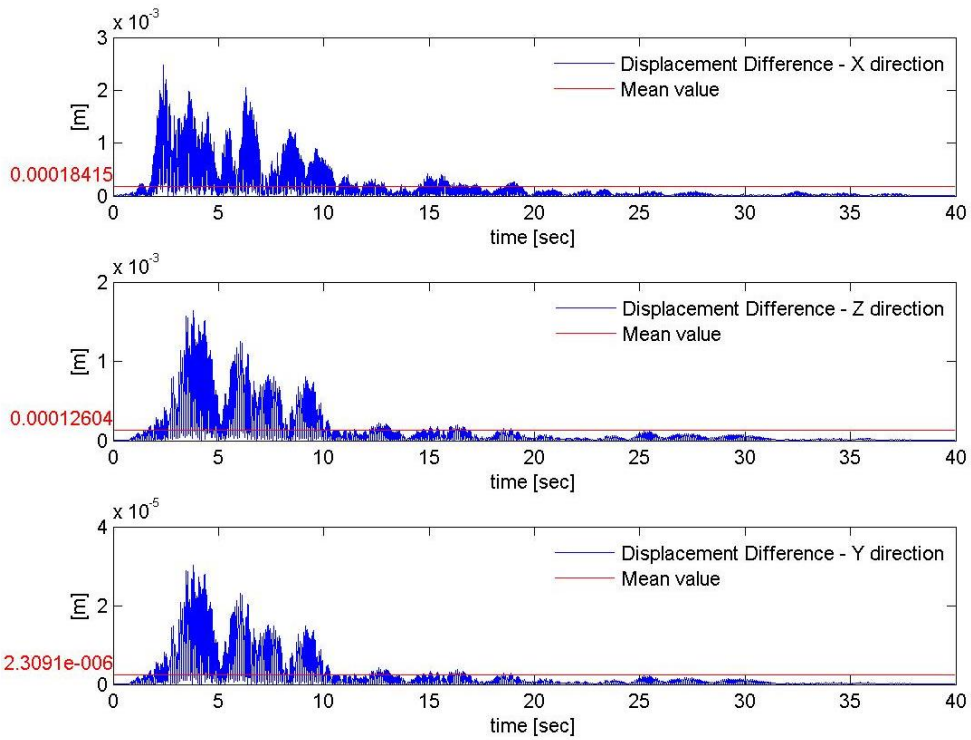

Figure 87 - Absolute value of the displacement responses between initial and updated numerical models for each of the 3 directions

13.5.2 A.4.5.2 Simulation type 2 (μ_{fck}=18 N/mm^2, σ_{fck}=6 N/mm^2)

Table 35 - Result of the simulations (type 2) - Generalized modal errors

Simulation	Type	Models	μ_{fck} [N/mm^2]	σ_{fck} [N/mm^2]	Updated Model n°	Generalized Modal Error
1	3	1000	18	6	748	5.7868
2	3	2000	18	6	1329	3.4714
3	3	3000	18	6	916	3.9096
4	3	4000	18	6	3885	4.2469
5	3	5000	18	6	997	3.2437
6	3	6000	18	6	4729	3.4714
7	3	7000	18	6	316	3.9096
8	**3**	**8000**	**18**	**6**	**997**	**3.2437**

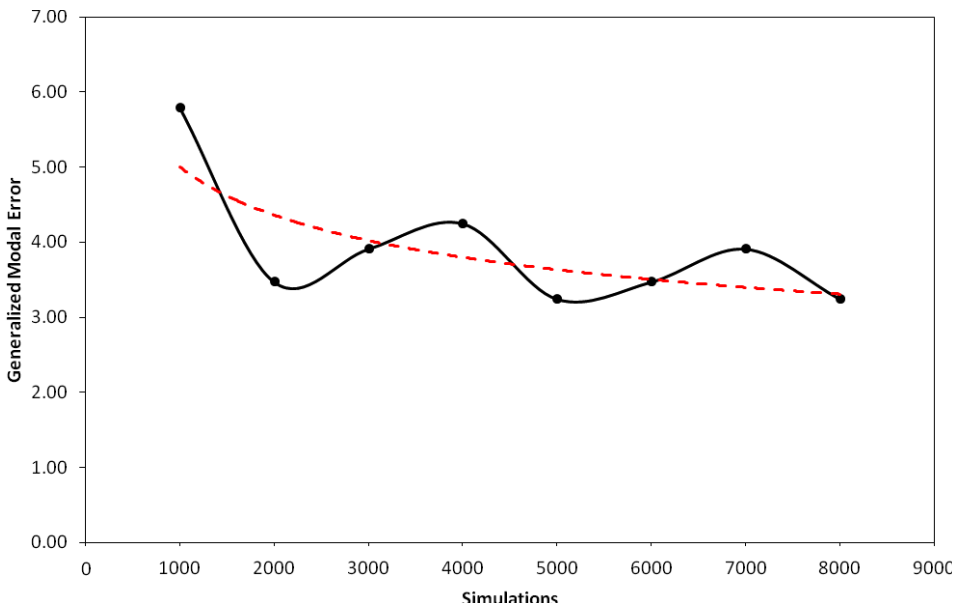

Figure 88 - Result of the simulations (type 2) - Generalized modal errors

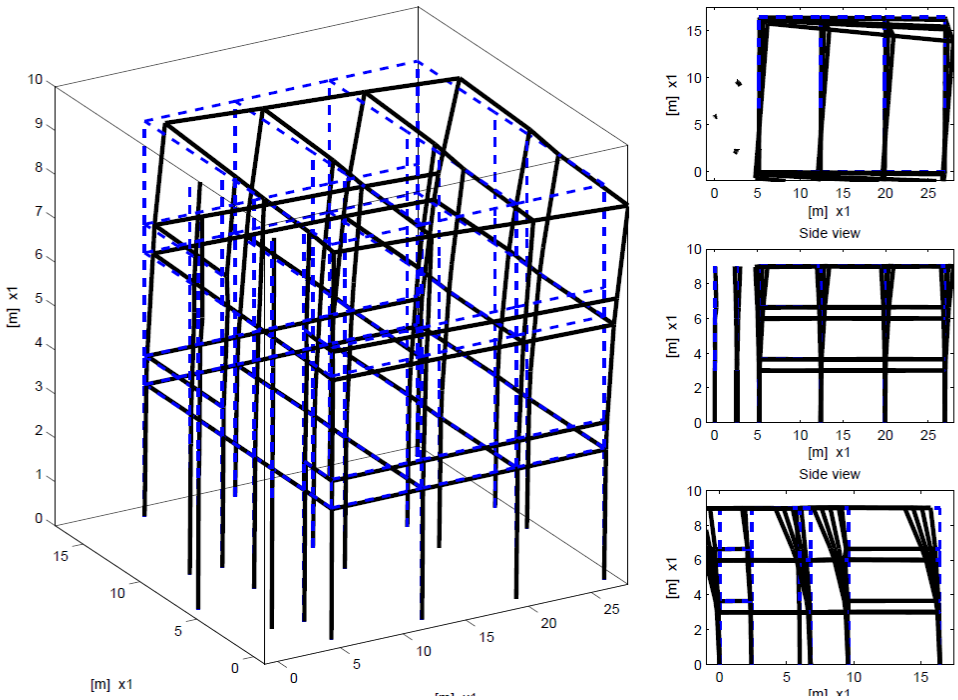

Figure 89 - Deformed shape mode 1 (normalized according to node 117) - Initial model

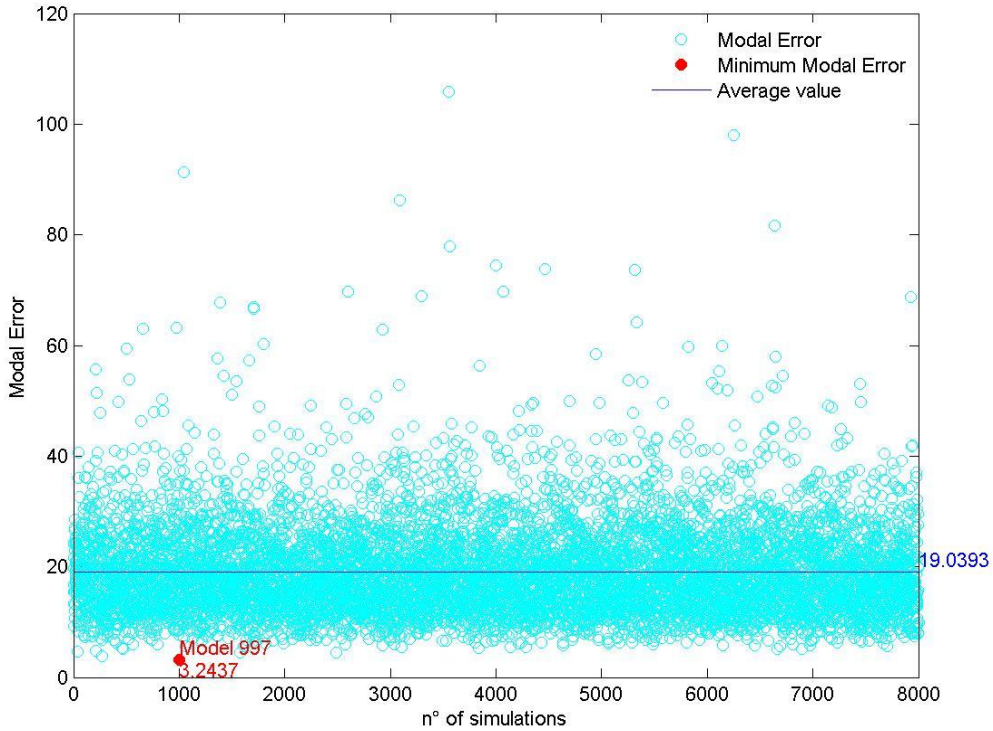

Figure 90 - Generalized modal errors for the 8000 samples simulation (type 2) - Updated model n°997

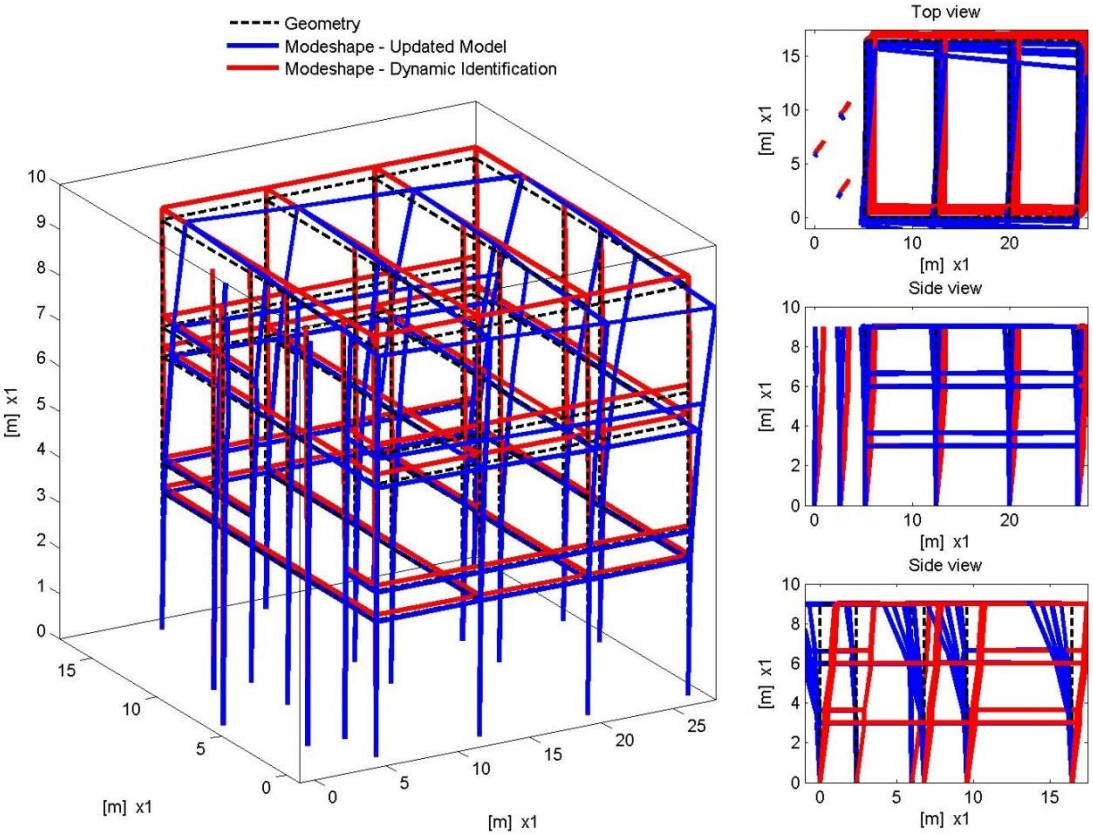

Figure 91 - Comparison between numerical updated (model n°977) and measured modal displacements - Deformed shape mode 1

Table 36 - Comparison between numerical results from the initial and updated model and measured values - Updated model n° 977

Mode	ω_i [rad/sec]	ω_U [rad/sec]	ω_E [rad/sec]	ω_i/ω_E	ω_U/ω_E
1	34.381	35.909	37.699	0.912	0.953
2	-	-	46.338	-	-
3	-	-	51.051	-	-

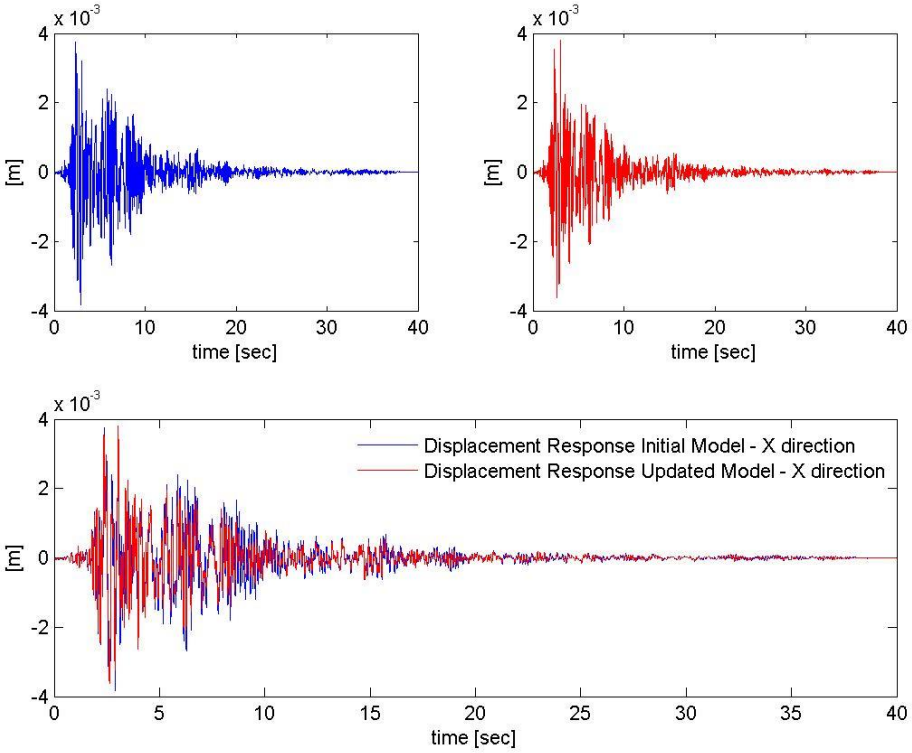

Figure 92 - Elastic THA - Comparison between initial and updated model - X direction (longitudinal)

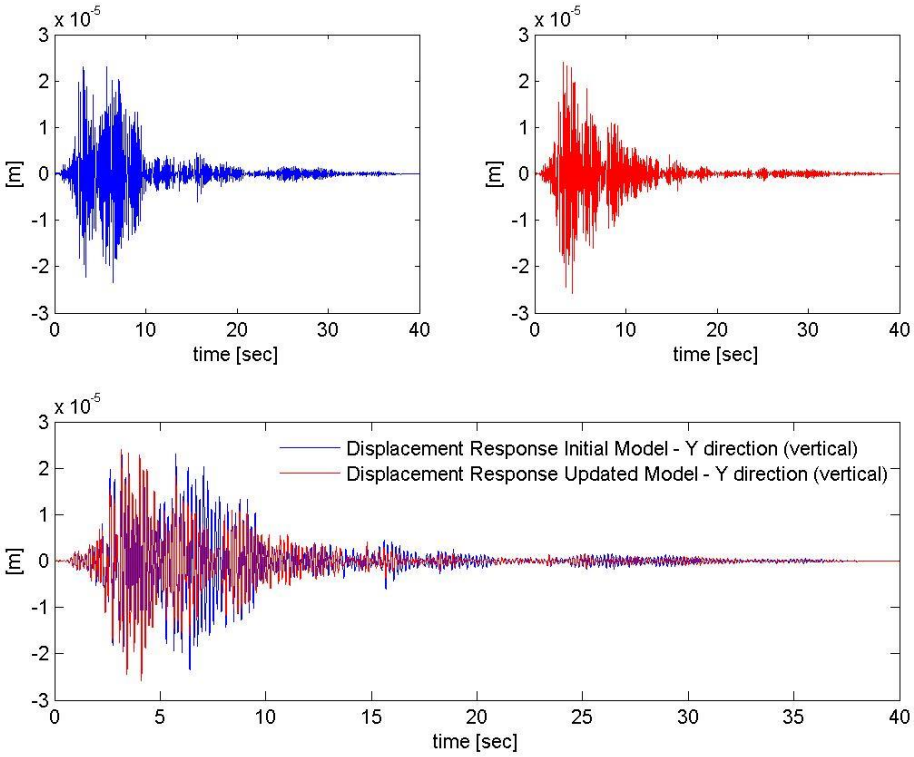

Figure 93 - Elastic THA - Comparison between initial and updated model - Y direction (vertical)

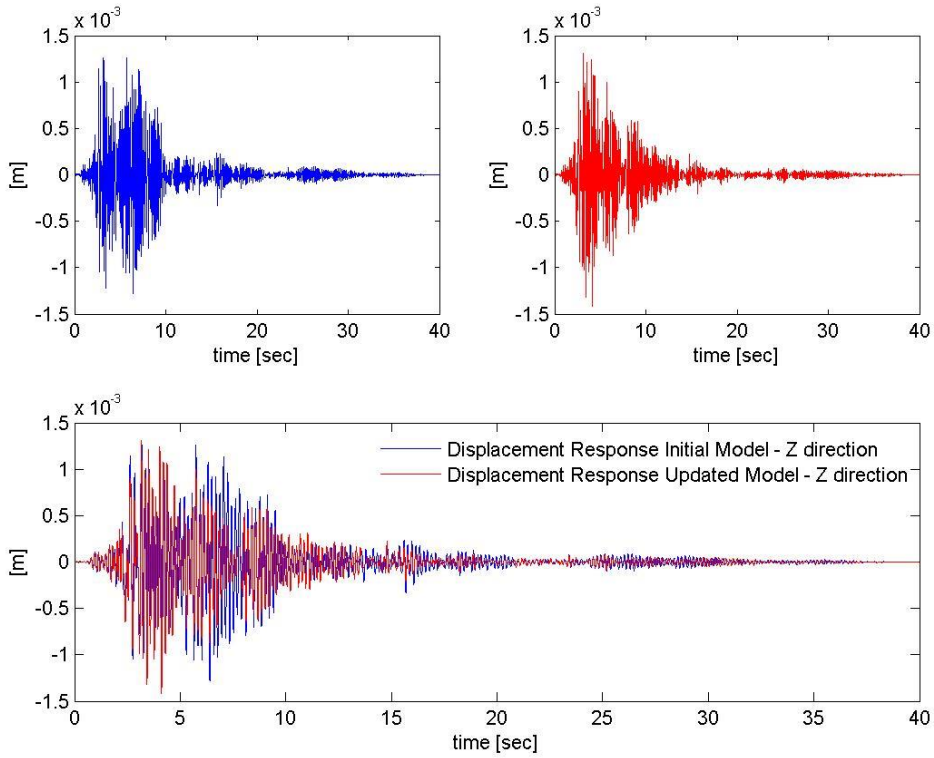

Figure 94 - Elastic THA - Comparison between initial and updated model - Z direction (transversal)

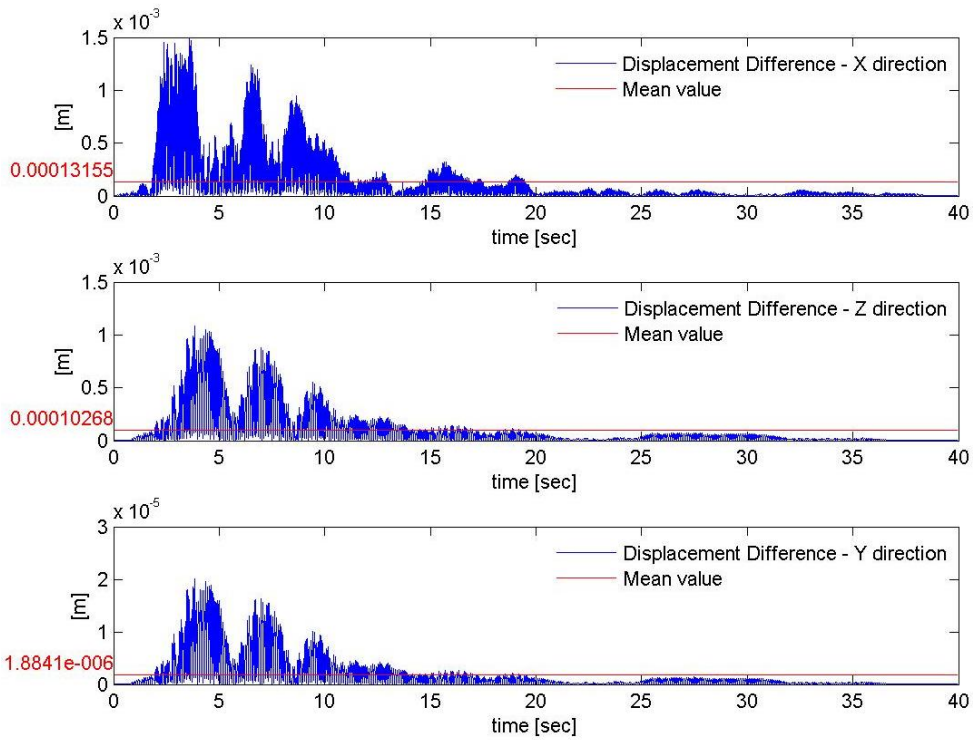

Figure 95 - Absolute value of the displacement responses between initial and updated numerical models for each of the 3 directions

13.5.3 A.4.5 3 Simulation type 3 (μ_{fck}=18 N/mm^2, σ_{fck}=6 N/mm^2)

Simulation	Type	Models	μ_{fck} [N/mm^2]	σ_{fck} [N/mm^2]	Updated Model n°	Generalized Modal Error
1	3	1000	18	6	15	9.0707
2	3	2000	18	6	180	9.8107
3	3	3000	18	6	1140	9.793
4	3	4000	18	6	3700	9.3882
5	3	5000	18	6	2900	8.5293
6	3	6000	18	6	4044	9.5245
7	3	7000	18	6	1310	8.8147
8	**3**	**8000**	**18**	**6**	**7784**	**8.1432**

Table 37 - Result of the simulations (type 3) - Generalized modal errors

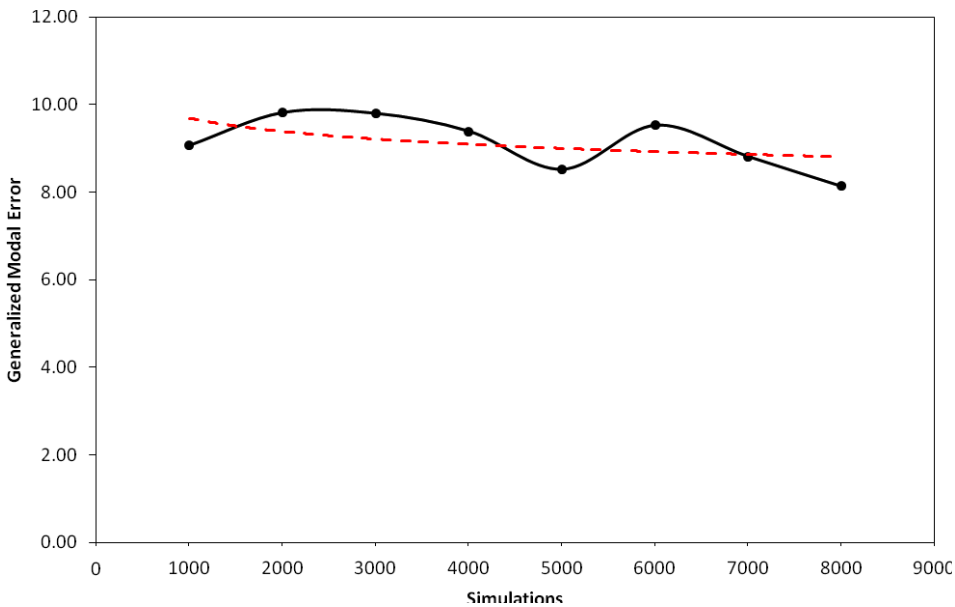

Figure 96 - Result of the simulations (type 3) - Generalized modal errors

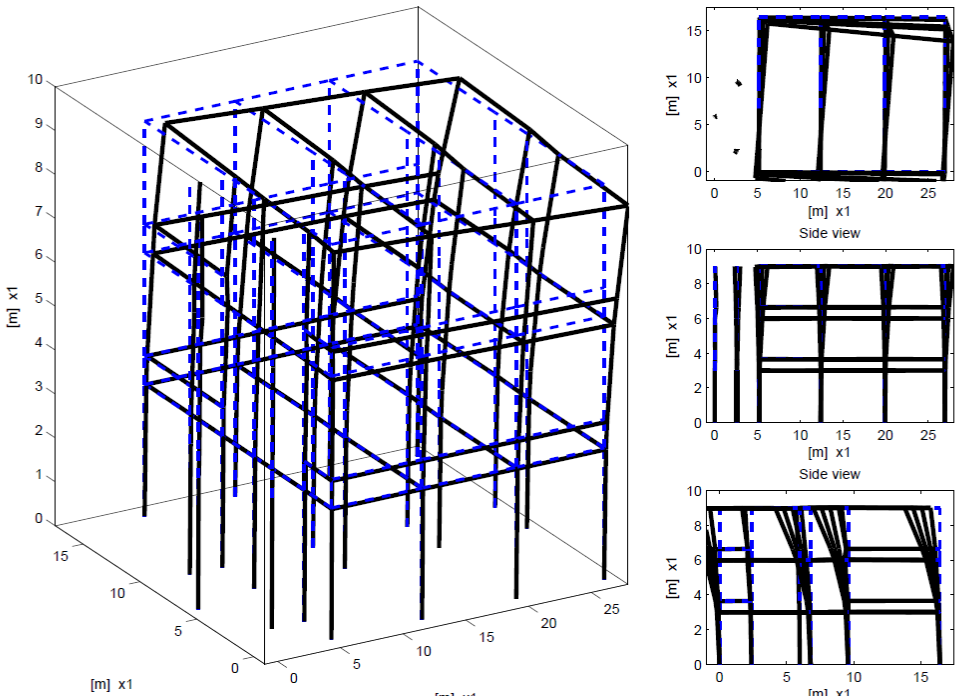

Figure 97 - Deformed shape mode 1 (normalized according to node 117) - Initial model

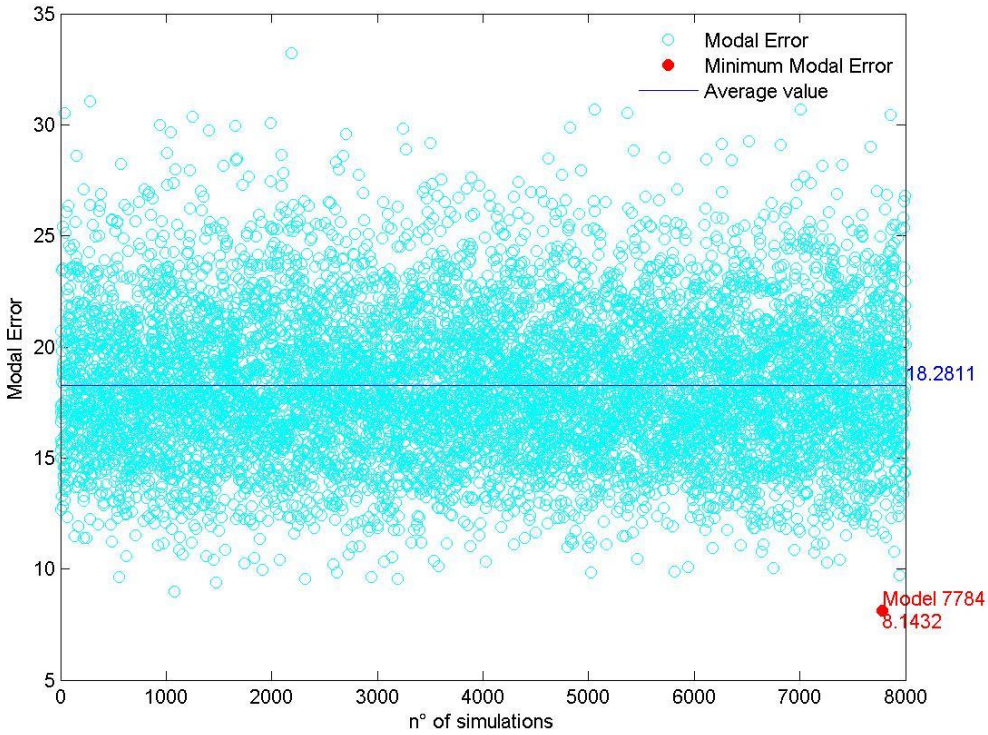

Figure 98 - Generalized modal errors for the 8000 samples simulation (type 3) - Updated model n°7784

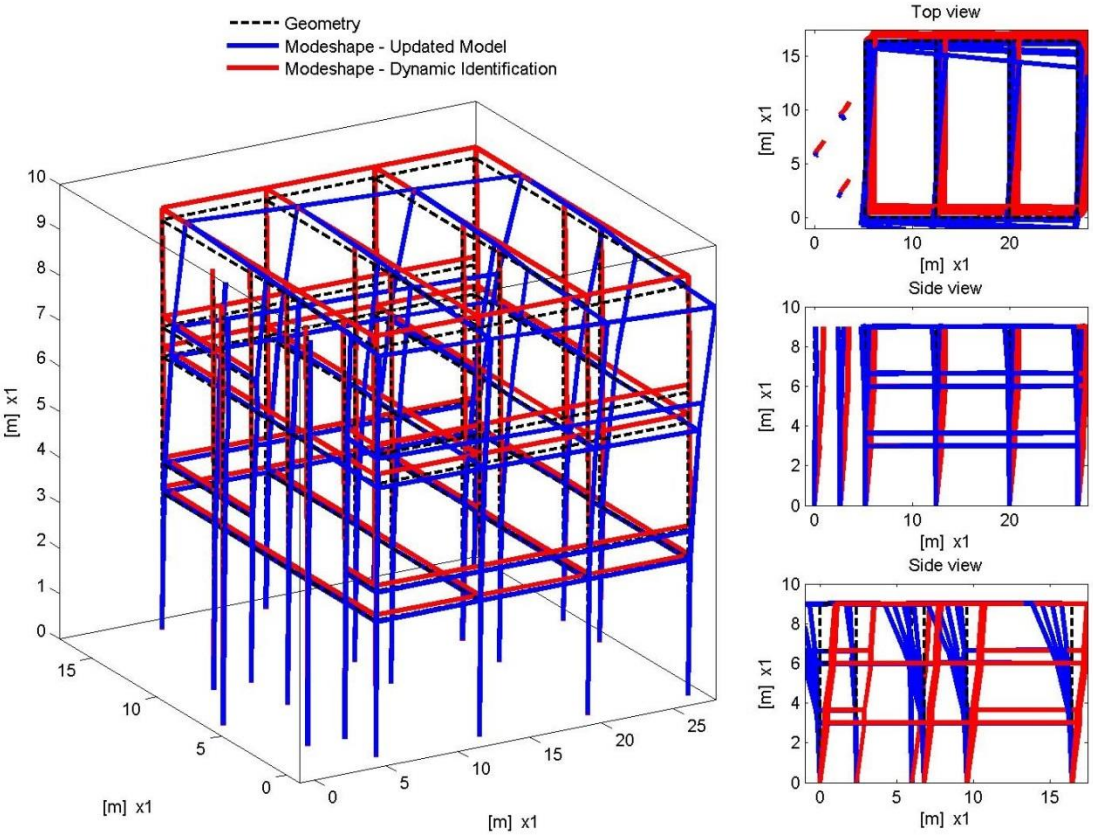

Figure 99 - Comparison between numerical updated (model n°7784) and measured modal displacements - Deformed shape mode 1

Table 38 - Comparison between numerical results from the initial and updated model and measured values - Updated model n° 7784

Mode	ω_i [rad/sec]	ω_U [rad/sec]	ω_E [rad/sec]	ω_i/ω_E	ω_U/ω_E
1	34.381	34.868	37.699	0.912	0.925
2	-	-	46.338	-	-
3	-	-	51.051	-	-

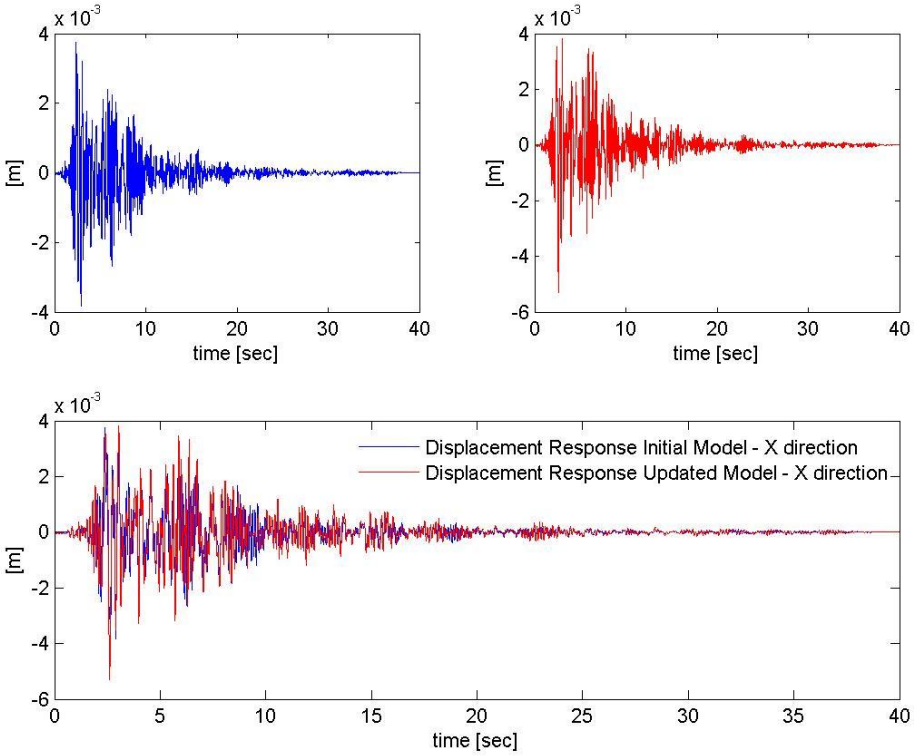

Figure 100 - Elastic THA - Comparison between initial and updated model - X direction (longitudinal)

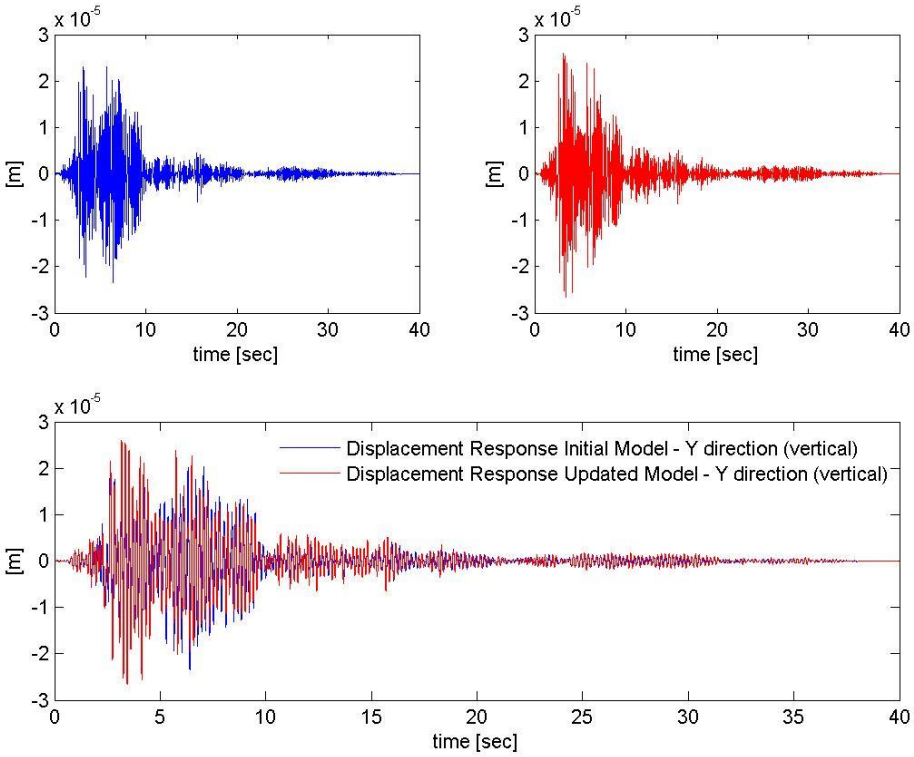

Figure 101 - Elastic THA - Comparison between initial and updated model - Y direction (vertical)

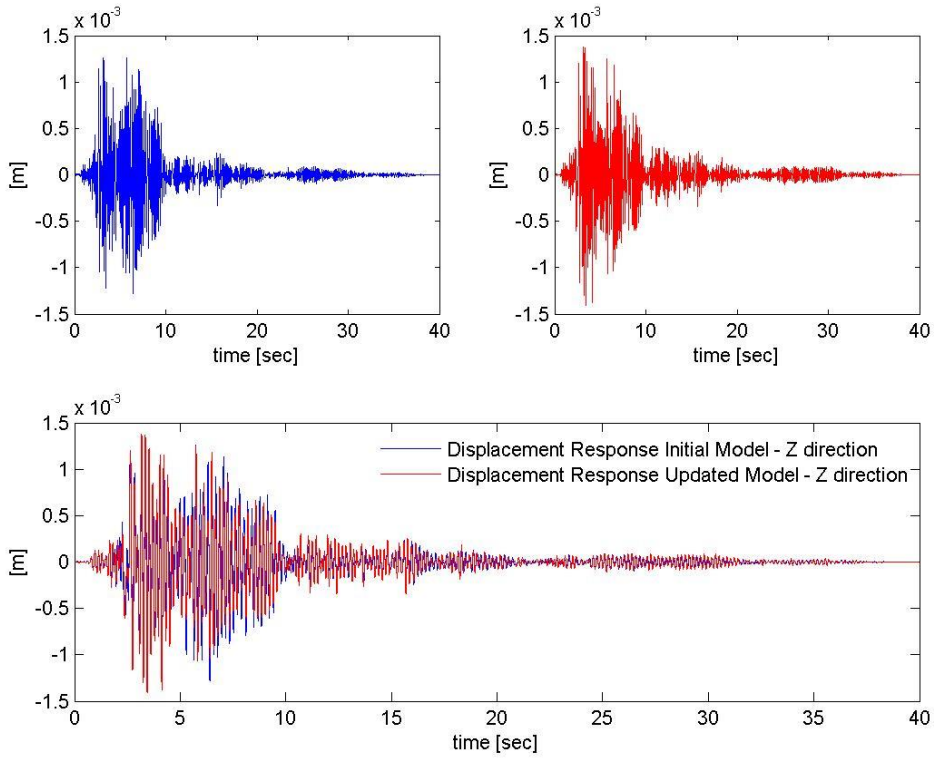

Figure 102 - Elastic THA - Comparison between initial and updated model - Z direction (transversal)

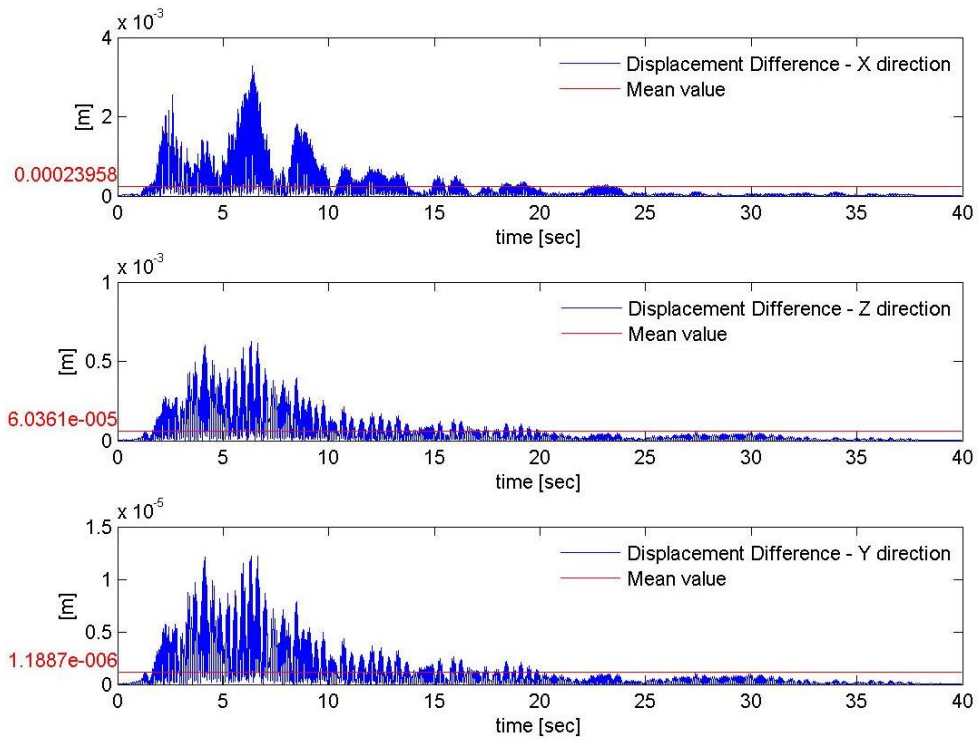

Figure 103 - Absolute value of the displacement responses between initial and updated numerical models for each of the 3 directions

13.5.4 A.4.5.4 Simulation type 1 - Calibration of the mechanical characteristic generation

Table 39 - Calibration of the mechanical characteristic generation (Sim. type 1) - Generalized modal errors

Simulation	Type	Models	μ_{fck} [N/mm^2]	σ_{fck} [N/mm^2]	Updated Model n°	Generalized Modal Error	E [kN/m^2]
1	1	8000	20	6	1781	0.0013138	35995000
2	**1**	**8000**	**21**	**6**	**852**	**0.0000864**	**36050000**
3	1	8000	22	6	759	0.0026489	35964000

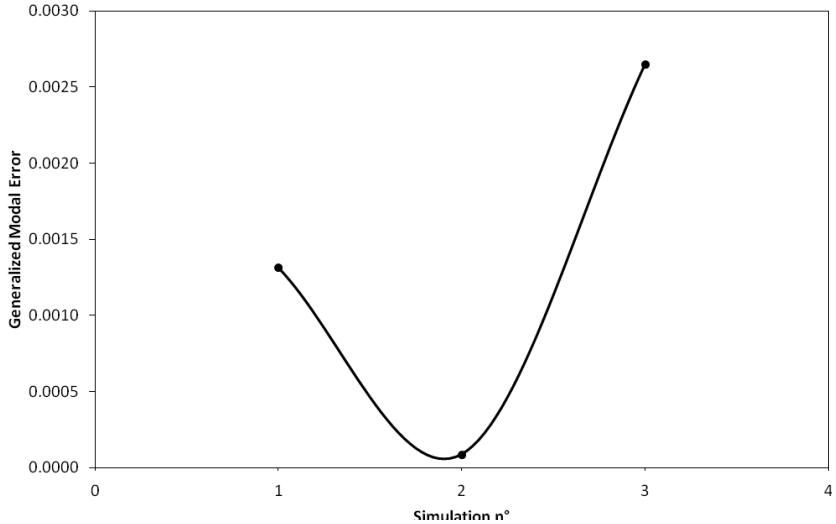

Figure 104 - Calibration of the mechanical characteristic generation (Sim. type 1) - Generalized modal errors

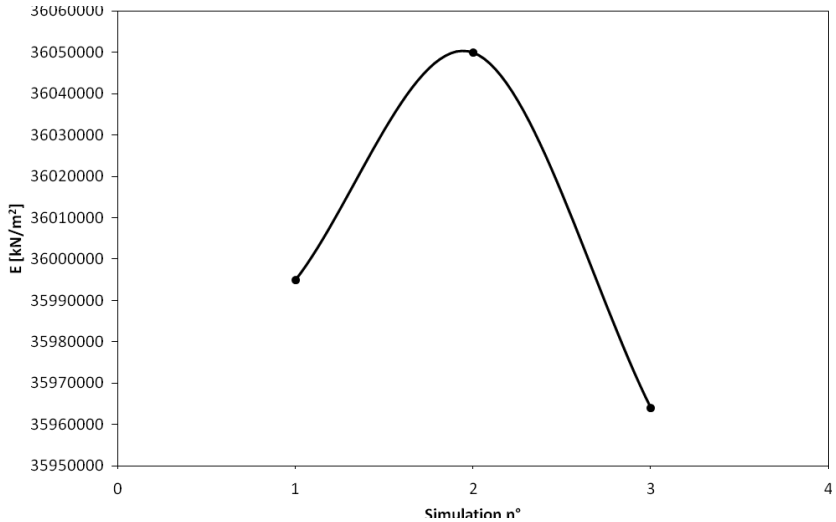

Figure 105 - Calibration of the mechanical characteristic generation (Sim. type 1) - Young's Modulus

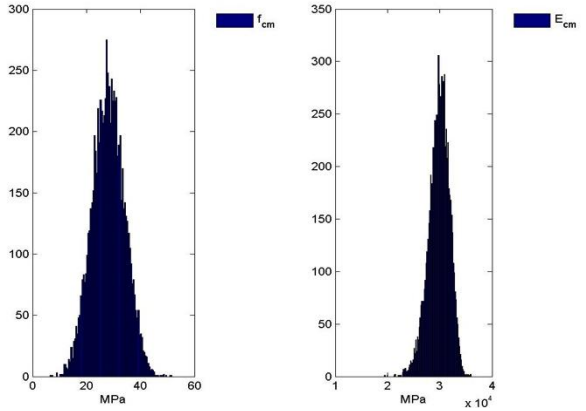

Figure 106 - Calibration of the mechanical characteristic generation 1 - f_{cm} and E_{cm} (Sim 1)

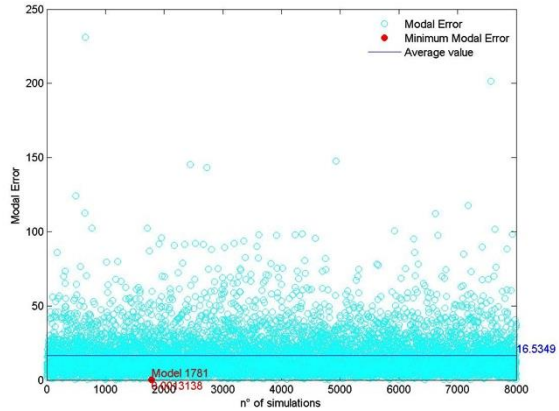

Figure 107 - Calibration of the mechanical characteristic generation 1 - Generalized modal errors (Sim. 1) - Updated model n°1781

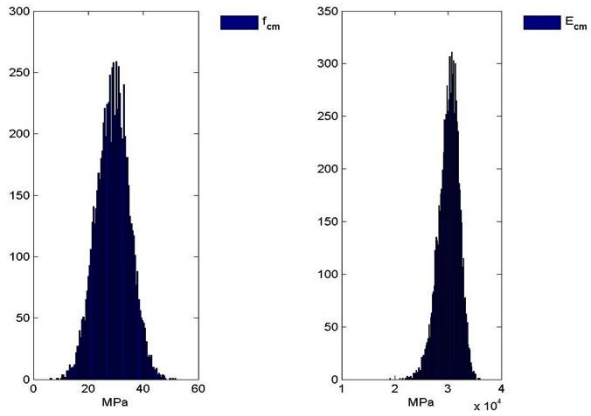

Figure 108 - Calibration of the mechanical characteristic generation 2 - f_{cm} and E_{cm} (Sim. 1)

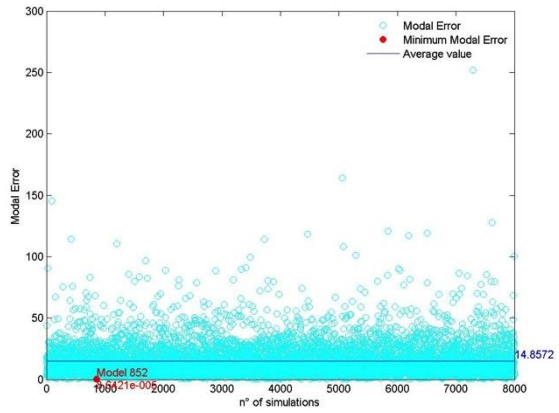

Figure 109 - Calibration of the mechanical characteristic generation 2 - Generalized modal errors (Sim. 1) - Updated model n°852

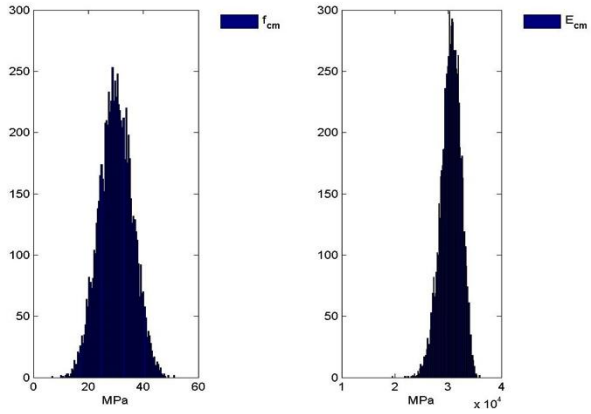

Figure 110 - Calibration of the mechanical characteristic generation 3 - f_{cm} and E_{cm} (Sim. 1)

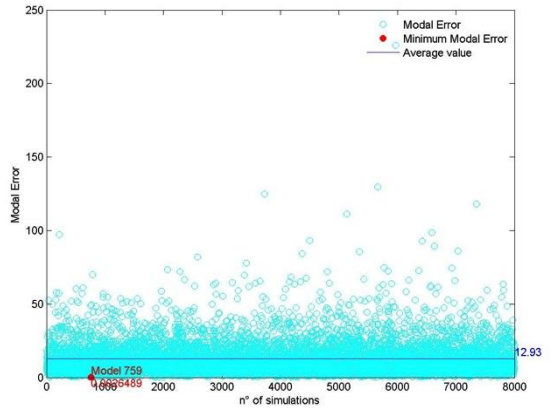

Figure 111 - Calibration of the mechanical characteristic generation 3 - Generalized modal errors (Sim. 1) - Updated model n°759

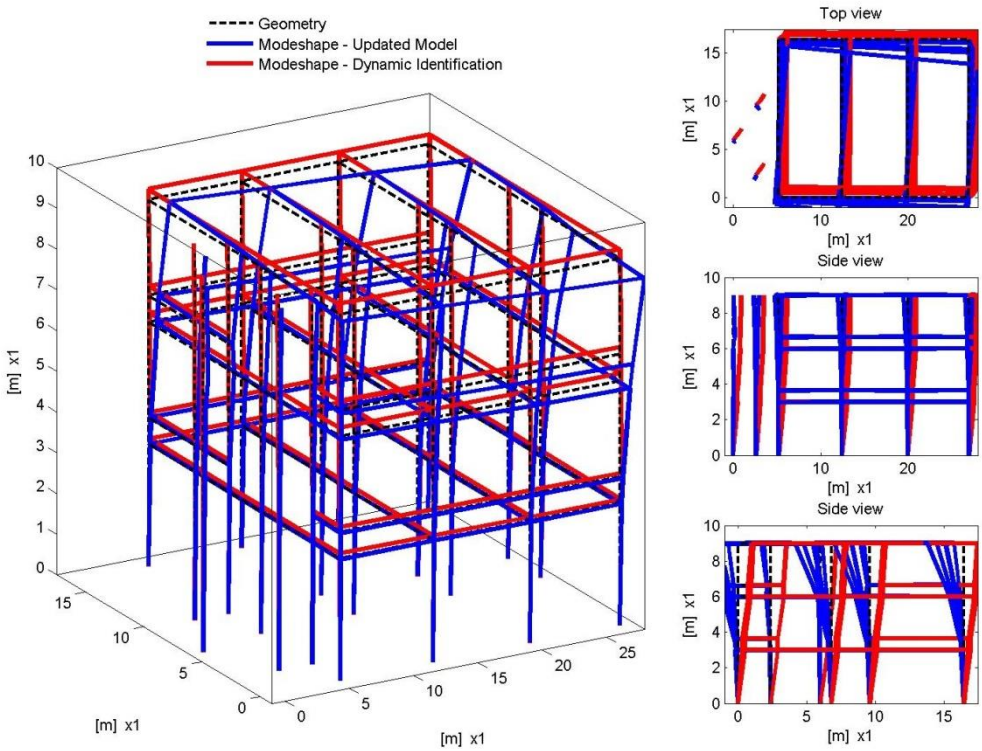

Figure 112 - Calibration of the mechanical characteristic generation 1 - Comparison between numerical updated (model n°1781) and measured modal displacements - Deformed shape mode 1

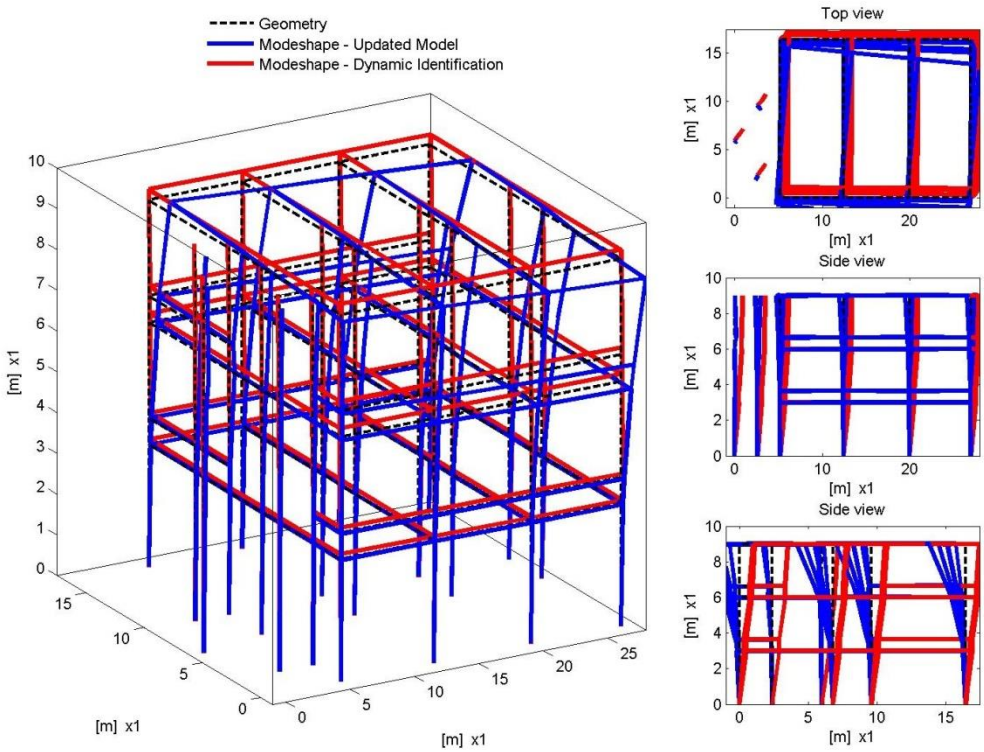

Figure 113 - Calibration of the mechanical characteristic generation 2 - Comparison between numerical updated (model n°852) and measured modal displacements - Deformed shape mode 1

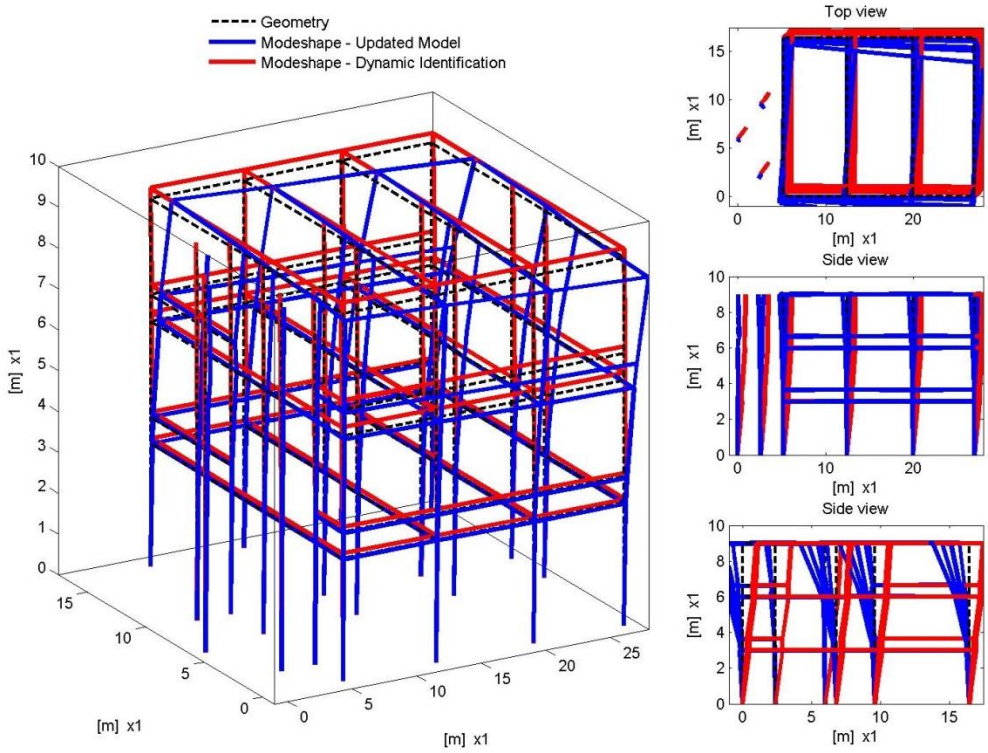

Figure 114 - Calibration of the mechanical characteristic generation 3 - Comparison between numerical updated (model n°759) and measured modal displacements - Deformed shape mode 1

Table 40 - Calibration of the mechanical characteristic generations - Comparison between numerical results from the initial and updated model and measured values

Simulation	Mode	ω_i [rad/sec]	ω_U [rad/sec]	ω_E [rad/sec]	ω_i/ω_E	ω_U/ω_E
1	1	34.381	37.660	37.699	0.912	0.998965
2	**1**	**34.381**	**37.689**	**37.699**	**0.912**	**0.999735**
3	1	34.381	37.644	37.699	0.912	0.998541

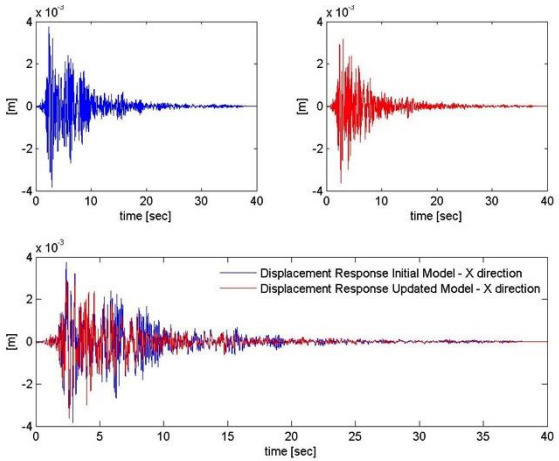

Figure 115 - Elastic THA - Comparison between initial and updated model 1781- X direction (long)

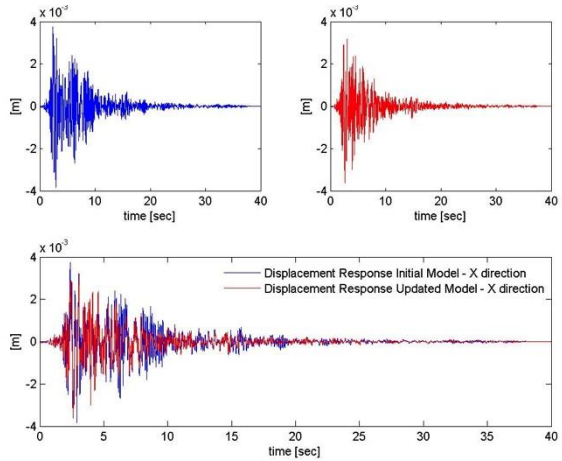

Figure 116 - Elastic THA - Comparison between initial and updated model 852- X direction (long)

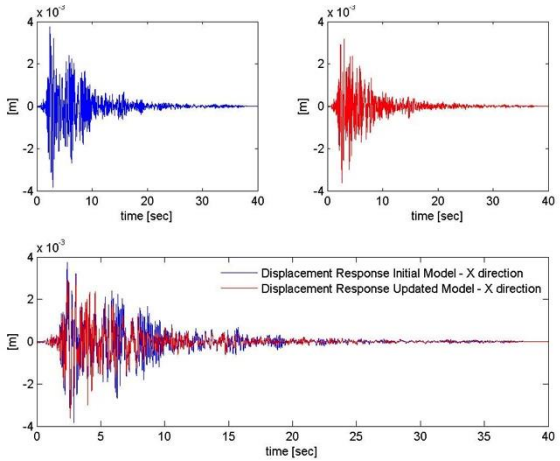

Figure 117 - Elastic THA - Comparison between initial and updated model 759- X direction (long)

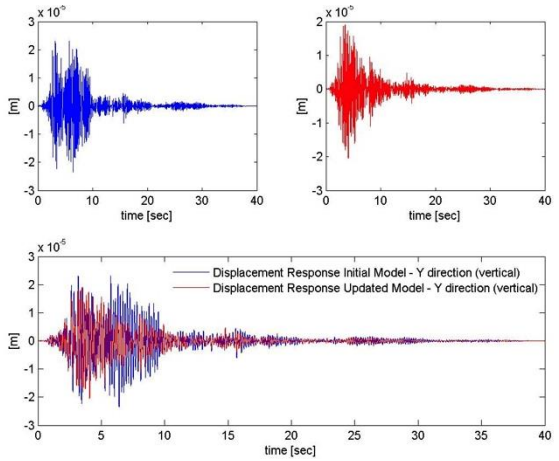

Figure 118 - Elastic THA - Comparison between initial and updated model 1781- Y direction (vert)

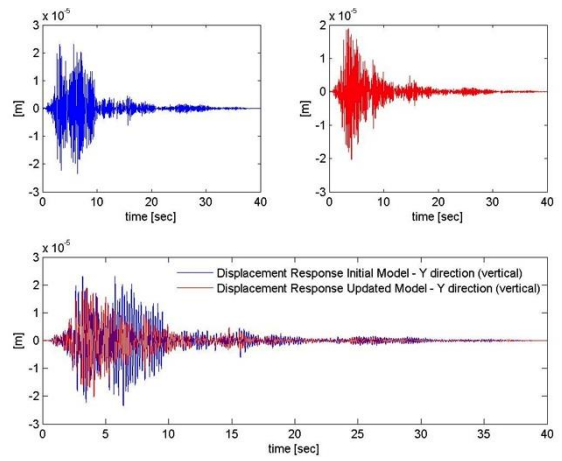

Figure 119 - Elastic THA - Comparison between initial and updated model 852- Y direction (vert)

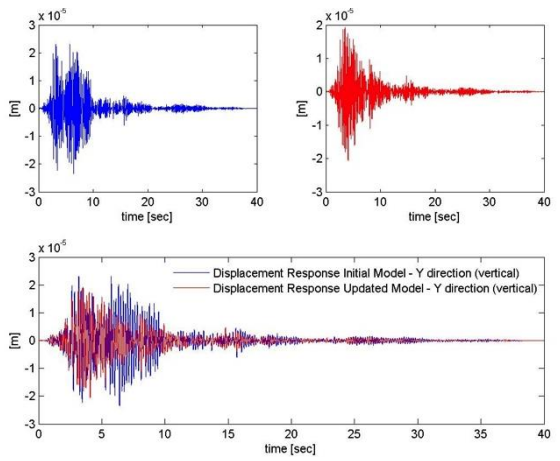

Figure 120 - Elastic THA - Comparison between initial and updated model 759- Y direction (vert)

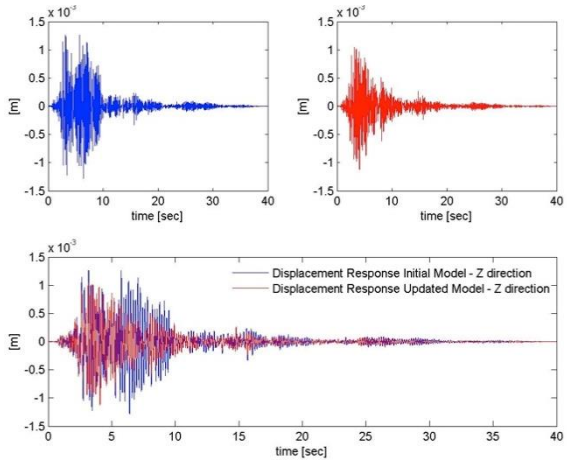

Figure 121 - Elastic THA - Comparison between initial and updated model 1781- Z direction (transv)

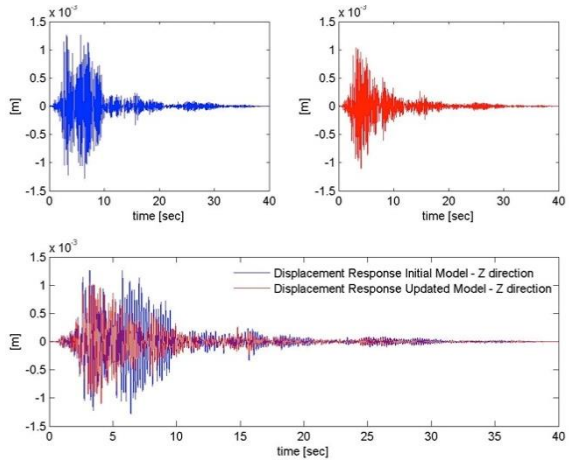

Figure 122 - Elastic THA - Comparison between initial and updated model 852- Z direction (transv)

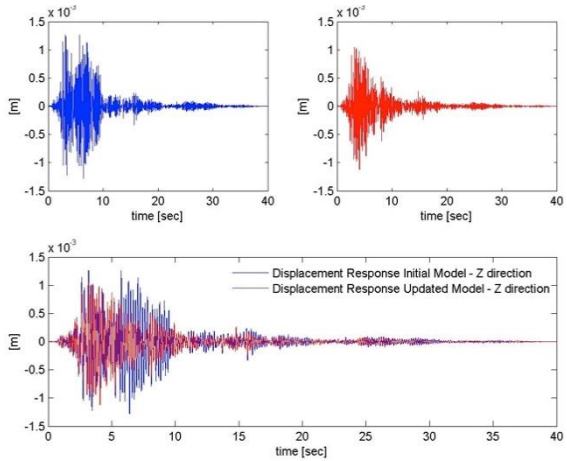

Figure 123 - Elastic THA - Comparison between initial and updated model 759- Z direction (transv)

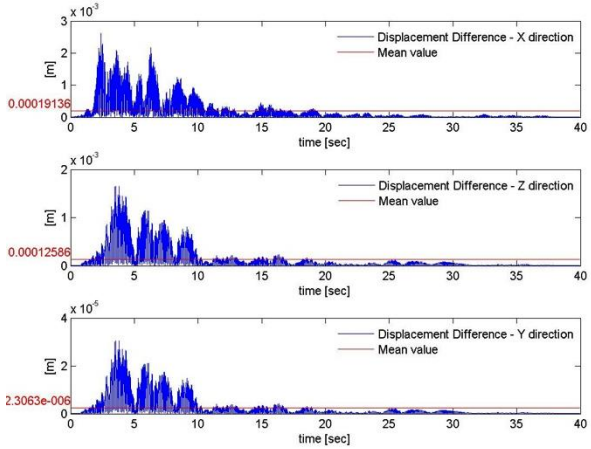

Figure 124 - Absolute value of the displacement responses between initial and updated numerical model 1781

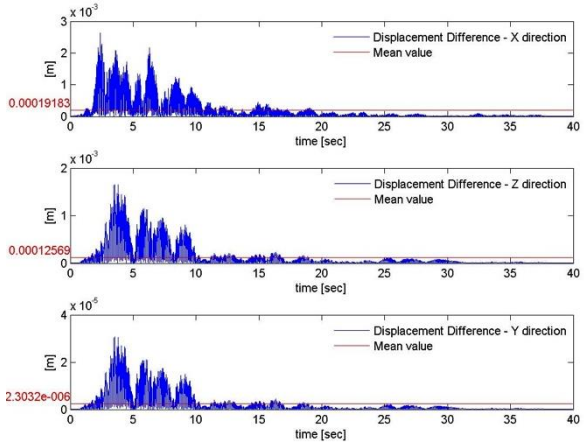

Figure 125 - Absolute value of the displacement responses between initial and updated numerical model 852

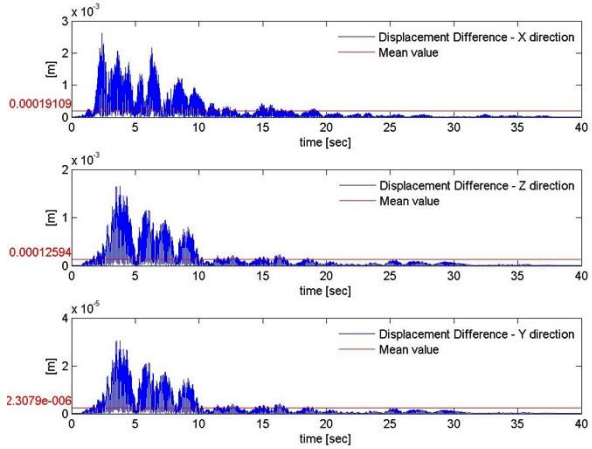

Figure 126 - Absolute value of the displacement responses between initial and updated numerical model 759

13.6 *Conclusions*

Stabilization of the generalized modal error according to the different simulations of the mechanical characteristics

It can be notice from Figure 127, which shows the results from the three different types of simulation in term of modal error index, tha *Simulation 1* (same Young's Modulus for all the structural elements) exhibited the best results, considering the amount of analysis that the memory of the server allows to performe (no more than 8000 generated numerical models). The curve corresponding to *Simulation 1* is rapidly decrising after a number of 2000 generated samples, and the trend is stable right after the same value. For the specific case, an amount of 4000 generated numerical models could be enough to update the numerical model and to obtain satisfactory results.

However, for *Simulation 2* and *3*, which correspond to Young's Modulus equal for each storey and Young's Modulus different for each structural member respectively, a larger amount of numerical models are needed in order to obtain reasonable results. A number of 8000 samples were not enough to appreciate a stabilization of the modal error index.

Finally, if numerical results and the measured data are comparable concerning the mode shapes, Simulation 1 is the most powerful and rapid approach, among the aforementioned possibility of simulation, for a good matching of the modal response of the numerical model with the real building.

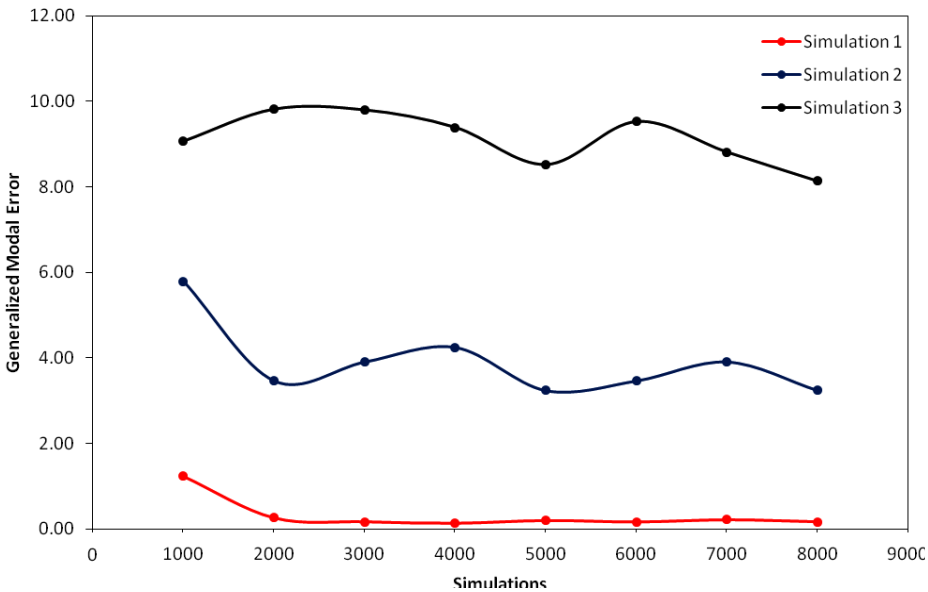

Figure 127 - Comparison between the results of Simulation 1, 2 and 3 - Generalized modal error

Initial differences between the numerical and experimental mode shapes

In case numerical and measured mode shapes do not corresponde, only the use of the elastic modulus is not enough to update the numerical model in order to find the matching between numerical and experimental modal behavior. For this reason, in this specific case, only the first mode shape was used to test the methodology.

Confidence of the experimental results

The building is divided into three parts by a number of two seismic joints. It was not possible to investigate if the structural parts are really disconnected by the joints, hence the dynamic identification has been performed with the assumption that there is a gap between the three structures and those are behaving indipendently. In case this cannot be assume, the joints will transfer the forces and the structure being identified for its dynamic characteristics, is just 1/3 of the whole building. There is no certainty in the experimental results, and the introduction of some confidence parameters (see bayesian updating) could be helpful for the reliability of the results.

Calibration of mean and standard deviation of the sensitivity parameter

There is the need to implement in the routine an automatic calibration of mean and standard deviation for the simulation of the characteristic compressive strength of the concrete, needed to simulate subsequently the Young's Modulus. This can be done, in case of *Simulation 3*, by comparing the mean and standard deviation of the distribution of Young's Modulus in the updated model and compare those values with the initial mean and standard deviation of the same parameter used to generate the entire set of numerical models.

Updated model n°852

The numerical model that more closely matches the measured eigenfrequencies has been identified from *Simulation 1 (model n°852)* by using $\boldsymbol{\mu_{fck}}$**=21 N/mm^2** and $\boldsymbol{\sigma_{fck}}$**=6 N/mm^2** to generate the samples. The difference between the measured and the numerical eigenfrequency is about **0.03%** while the updated **Young's Modulus increased about 20%** of the initial value E=30000000 kN/m^2. Finally, comparing the elastic time history analyses of both initial and updated models, the maximum difference among the responses remains **below 3 mm**.

14. Closing remarks and further developments

The work developed under this work package focused the use of dynamic identification measurements in the FE model updating of buildings. A methodology based on Montecarlo simulation scheme to update numerical models was proposed and calibrated by means of a parametric study using simulated testing structures and a real case-study.

When considering simulated field monitoring results, a good matching between experimental and numerical modal response has been encountered. Among the aforementioned analyses, the fact of considering incomplete simulated experimental data, i.e. reducing the number of modes from 20 modes up to the first three fundamental ones and considering only 3 (translational) modal DOFs per node, lead the algorithm to improve the matching with the experimental data in terms of a better comparison between experimental and numerical eigenfrequencies. Lower Generalized Modal Error values were obtained and this can be explained by the fact that a fewer number of parameters have to match the experimental quantities. However, concerning the modal deformed shape, the analysis showed poorer results comparing the same analysis using complete measured data.

In case numerical and experimental mode shapes do not correspond, such as the second and the third modes, considering the Young's Modulus as the only sensitivity parameter is not enough for matching the dynamic identification measurements. The addition of confidence parameters to the field monitoring results (e.g., through Bayesian updating), in case the detail of the information on the structure is poor, will help the algorithm to find more reliable matching of the field measurements.

Generally, the response in terms of eigenfrequencies always enabled good improvements towards the observed behaviour at the end of the updating process. However, from what it could be observed in the case-study building, the updated numerical deformed shapes didn't present a good matching with the field monitoring mode shapes. In order to overcome this problem a higher number of simulations or introducing a more efficient type of sampling at the beginning of the algorithm is needed. Latin Hypercube Sampling (LHS) might be implemented in the routine, in addition to the Montecarlo Simulation, in order to optimize the size of the samples for matching between the numerical models and experimental quantities.

With respect to further developments, the proposed updating methodology will yield more reliable models, using field monitoring data, which can be used for subsequent updating of fragility curves, according to the methodology proposed in Deliverable 14.2. This will also allow one to understand how much the changes in the properties of the numerical model will actually influence the vulnerability of the building. If a similar simulation scheme would be carried out in terms of fragility analysis, a direct correlation between monitored parameters, undamaged and damaged building fragility might be sought, with the contribution of shaking table test results.

15. Reference List

[1] Alvin, KF. (1997). Finite element model update via bayesian estimation and minimization of dynamic residuals. AIAA Journal 35(5), 879-886.

[2] Beck, JL., Vanik, MW. (1996) Structural model updating using expanded modeshapes. Proceedings of the 11th Engineering Mechanics Conference, ASCE, NY. 152-155.

[3] Decreto Ministeriale (2008) NTC-08 Norme Tecniche per le Costruzioni (in Italian).

[4] Farhat, C., Hemez, PM. (1993). Updating finite element dynamics models using an element-by-element sensitivity methodology. AIAA Journal 31(9), 1702-1711.

[5] Lekidis, V., Karakostas, C., Christodoulou, K., A. Karamanos, S., Papadimitriou, C., Panetsos, P. (2004). Investigation of dynamic response and model updating of instrumented R/C bridges. Proceedings of the 13th World Conference on Earthquake Engineering, Vancouver, Canada. Paper No. 2591.

[6] MathWorks, Inc (2009) MATLAB, R2009a.

[7] McKenna, F., Fenves, G. L., Scott, M. H., Jeremic, B. (2000). Open System for Earthquake Engineering Simulation (OpenSees). Pacific Earthquake Engineering Research Center, University of California, Berkeley, CA.

[8] Papadimitriou, C., Levine-West, M., Milman, M. (1997). Structural damage detection using modal test data. Proceedings of the International Workshop on Structural Health Monitoring, Stanford, California.

Appendix B:

Spittelbreitengasse

VCE

16. Introduction

The mostly unpredictable and random characteristics of ground motions regarding their intensity features as well as the frequency of occurrence have secured a great challenge in the seismic design and performance evaluation of the infrastructures, exposed to such sources of excitation. However, the analysis of the past earthquakes and their devastating impacts over tens of years, taking place in various places of the world has provided the investigators and the engineers of the field with an undeniably enriched source of remarks and precious lessons, on which the theoretical, analytical and eventually statistical procedures have resulted into notable improvements towards the seismic design and protection of structures. In the light of such a view and with the aim of improving the seismic safety of the structures, several large scale research programs on the concepts of seismic risk assessment, mitigation and managements have been defined of which the focus is on the estimation of the future earthquake hazards, the consequent structural damage states and the plausible retrofitting and safety enhancement methods. Consequently and aligned with the defined expectations of the modern structural and earthquake engineering fields, this document is to present the analytical procedures, recommended to derive the "Real Time Fragility Curves" of a typical masonry residential building based on the "In-Site" measured dynamic records of the structures.

As long as the specific derived graphs in this document correspond to the recorded data of "Fendigasse" building, the specific characteristics of the measured dynamic histories of the structure and specially the existence of a great number of "white noise" records could have had its own effects on the obtained final results, though a huge amount of efforts had been dedicated to the purification of the measured data and the selection of the best possible recorded sets. Nevertheless, in case of any unforeseen but possible future modifications on the numerical results, the introduced analytical steps in this document will hold the applicability without the loss of the theoretical generality.

16.1 *Fragility Curves Derivation*

As previously introduced and based on the definitions, "fragility curves" are to represent the probability of the occurrence of a specific damage state to a structure, under a certain level of ground motion shaking [1],[2],[3],[4],[5]. As a result, any phenomena, such as degrading of the structural material properties due to aging or probable damages by various events during the lifetime of the structure could inherently influence the extent of response of the building to any arbitrary excitations in comparison to the original intact state. This is to imply that the "fragility curves" of a specific structure might not potentially hold their initial configuration and could need an upgrade to the "real time" condition.

Accordingly, the procedures described below have been followed to derive the "fragility curves" of the specific masonry structure located at "Fendigasse 20/1050Wien/Austria" based on the latest dynamic characteristics, measured in-site. Hence, the input data are assumed to reflect the most updated condition of the building in comparison to the nominal theoretically derived models.

16.2 *Structural Response Evaluation*

Since the exact evaluation of the response of the structures to any arbitrary time history excitation in a linear scheme requires the solution of the "Duhamel Integral", as represented in equation (1) below, the accuracy of the eigen frequencies and mode shapes of the building as well as the modal participation factors and damping coefficients are of undeniable importance[6]. Consequently, application of the measured "real time" modal parameters can be the best way to reflect the "as-of-the-date" dynamic performance of the structure.

$$y_i(t) = \frac{P_i}{\omega_i}\int_0^t \ddot{U}_g(\tau)e^{-\xi_i\omega_i(t-\tau)}\sin(\omega_{Di}(t-\tau))\,d\tau \quad (1)$$

$$P_i = \frac{\overline{k_\iota}}{M_i} \quad (2)$$

$$\overline{k_\iota} = \{\phi\}_i{}^T[M]\{l\} \quad (3)$$

$$M_i = \{\phi\}_i{}^T[M]\{\phi\}_i \quad (4)$$

$$\omega_{Di} = \omega_i\sqrt{1-\xi^2{}_i} \quad (5)$$

In the equations introduced above, $y_i(t)$ is the time dependent response of a single degree of freedom (SDOF) oscillator to the ground acceleration, $\ddot{U}(t)_g$, with the structural natural and damped angular frequencies, ω_i and ω_{Di}, mass, M_i, and the critical damping ratio, ξ_i. Furthermore, the term P_i refers to the modal participation factor defined per equation (2) belonging to the ith mode of vibration of the real multi degree of freedom (MDOF) system with the corresponding mode shape vectors, $\{\phi\}_i$ and the mass participation factor, $\overline{k_\iota}$. In addition, $\{l\}$ is the global influence vector and t and τ are the time parameters of the convolution equation (1). Eventually, the index *i* in all the terms defined in the equations above specifies the corresponding mode of response.

Consequently, once the time dependent part of the response of the original MDOF system, $y_i(t)$, is derived, the total response of the structure in a linear elastic situation, $\{x(t)\}$, can be obtained applying equation (5) to combine the effects of all the modes, equal to the total number of the degrees of freedom, *n*, as given below.

$$\{x(t)\} = \sum_{i=1}^{n}\{\phi\}_i\, y_i(t) \quad (5)$$

Hence, as long as the main objective is to derive the response of the structure under certain different levels of ground motion hazard and the estimation of the exceedance probability based on specific damage state thresholds as closely as possible to the real-time condition of the building, the following dynamic characteristics can be directly obtained from the "In-Site" measurements and used in equations (1) through (5) to eventually assess the response of the structure under the selected excitation.

16.3 *Eigen Angular Frequencies ωi*

Once the "In-Sight" ambient and/or the properly forced excitation amplitudes of the building have been recorded and processed, the derivation of the Fast Fourier Transform (FFT) diagrams will result into the modal frequencies of the structure. Since the peaks of the FFT curves in a real scale structural measurements might not be ideally and sufficiently decomposed and obvious at the first glance, an estimation of the expected frequencies as *a priori* could serve to be a great bonus at the expense of the calculation time. However, based on the existing scientific literature at hand, some approaches such as the FDD is already capable of decomposing the modes in ambient vibration measurements[4]. Nevertheless, some issues with the actual recorded data at "Fendigasse" building and the existence of various noises within the records prevented the author of this document from applying the aforementioned method. Hence, the sub-steps defined below were followed to eventually derive the eigen frequencies of the structure from the ambient recorded data.

Calculation of the mass of the structure

For this purpose, the mass of the floors were estimated based on the existing drawings of the building in the "4-story" configuration, using the dead weight of the structure as shown per Table (1). Since the measurements were recorded at a time where most of the residential units were evacuated for the rehabilitation procedures, the live load effects on the building mass were assumed to be negligible. Furthermore, as long as the "Keller" floor, located below the zero datum ground level possesses both the thickest bearing walls as shown per the configurations in Appendix (I) and surrounded by the soil, a comparison procedures between the approximate "5" degree of freedom (DOF) model and a "6" one was made of which the outcome was convincing enough to handle the rest of the analytical procedures with the "5" DOF model. The mass per unit area of the floors and the specific weight of the walls were assumed to be $175\ kg/m^2$ and $18\ kN/m^3$, in the order of appearance in this entire Appendix B[7].

Table (1). The lumped masses of the floors- left: 5DOF- right: 6DOF

Story	Lumped Mass (ton)
1	449,64
2	380,06
3	361,67
4	359,15
Roof	183,93

Story	Lumped Mass (ton)
Erdg	518,63
1	449,64
2	380,06
3	361,67
4	359,15
Roof	183,93

Estimation of the stiffness of the structure

Referring to the attached maps in the Appendix (I), the lateral bearing system of this building is composed of unreinforced masonry walls. Although the actual performance of the building will involve the torsional behaviors as well as the lateral motions, the level of accuracy of the aimed "fragility curves" at the defined "Phase 0" would accommodate the negligence of the torsional modes of response.

Moreover and in the absence of the required detailed information on the condition of the bearing wall-ceiling connections, the equivalent stiffness of the lateral bearing system was estimated by the application of the well-known equation of structural mechanics (6), assuming full-fixity of the wall-ceiling joints. The material mechanical properties of the building, mostly obtained from references [7],[8] are summarized per Table (2).

$$K_e = \left(\frac{h^3}{\beta E I_e} + \frac{\kappa h}{G A_w}\right)^{-1} \tag{6}$$

In equation (6), K_e is the equivalent stiffness of the masonry bearing wall with the rectangular section and fully fixed conditions at the both end supports, $\kappa = 1.5$ and $\beta = 12$. A_w also refers to the effective shear resistance area of the wall section, as a function of the nominal section area, A_n, per equation (7). In addition, G is the shear modulus of the material and all the other terms hold their definitions as clarified elsewhere.

$$A_w = \frac{A_n}{\kappa} \tag{7}$$

Table (2). The experimentally reported material properties of Fendigasse masonry building[7],[8]

Young Modulus	Shear Modulus	Poisson's Ratio
(Pa)	(Pa)	-
1,80E+09	512820513	0.17

Furthermore, it needs to be reminded that as long as there are some non-negligible openings in the continuous bearing walls as schematically shown in Fig. (1), the lateral stiffens of these elements have been approximated using the equivalent moment of inertia, I_e, per equation (8)[9].

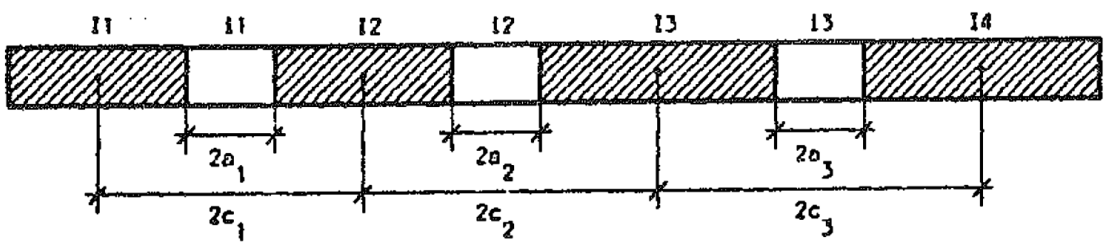

Fig (1). Schematic continuous bearing wall with openings[9]

$$I_e = \frac{I}{1 + \frac{8I\psi}{(I_1 + I_2 + I_3 + \cdots)\alpha^2}} \tag{8}$$

$$\alpha = \omega \mathrm{H} \tag{9}$$

$$\omega^2 = \frac{6\acute{E}}{Eh(I_1+I_2+I_3+\cdots)}\left(\frac{i_1 c_1^2}{a_1^3}+\frac{i_2 c_2^2}{a_2^3}+\cdots\right) \tag{10}$$

In equations (8) to (10), I is the moment of inertia of the whole wall should it contain no openings, I_i refers to the moment of inertia of the partially continuous parts of the wall and i_i is the moment of inertia of the openings, taken to be positive rather than negative. a_i and c_i also define half of the width of the openings and the center to center distance between the adjacent partially continuous walls, in the order of appearance and as sketched in Fig. (1). In all the introduced notations, the index i, acts as the number identifier in the original equations. The parameter ψ, considering both the geometrical and material properties of the bearing walls with openings, is derived from the empirical curves, schematically shown per Fig. (2). As noticed, such curves are a function of the terms α and ω by equations (9) and (10) and the term J_l as the ratio of the length of the wall to the height of the structure. Moreover, the terms H, h, $\acute{E}$ and E in equations (9) and (10) are to represent the total height of the building, the center to center distance between the two consequent openings along the height of the structure, the modulus of elasticity of the connecting beam at the top of the opening and of the wall itself, respectively. The final lumped lateral stiffness of the building in both the X and Y directions and for the two "5DOF" and "6DOF" models are presented in Tables (3) and (4), in the order of appearance. Once again, it needs to be emphasized that these equivalent spring stiffness values do not reflect either the torsional properties of the building or the soil-structure interaction at the supports, but the existence of the openings within the walls. In addition, the effects of the adjacent buildings on the dynamic properties of the structure have not been directly included into the stiffness approximation.

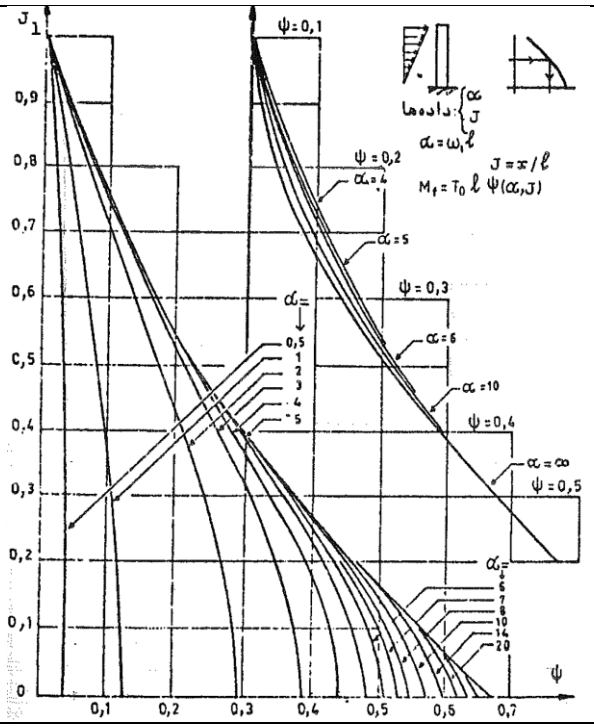

Fig (2). Graphs of the parameter ψ of the building based on α and J_l [9]

Table (3). Approximate lumped stiffness of the 5DOF model

Story	Lumped Stiffness X (kN/m)	Lumped Stiffness Y (kN/m)
1	1993664,62	2439224,719
2	1963019,98	2006311,141
3	1723771,35	1831176,268
4	1739337,35	1847591,053
Roof	1683446,62	1789144,371

Table (4). Approximate lumped stiffness of the 6DOF model

Story	Lumped Stiffness X (kN/m)	Lumped Stiffness Y (kN/m)
Erdg	2871113,65	3972161,192
1	1993664,62	2439224,719
2	1963019,98	2006311,141
3	1723771,35	1831176,268
4	1739337,35	1847591,053
Roof	1683446,62	1789144,371

- ***Approximation of the eigen frequencies***

As well specified and known in the technical literature, the eigen values of the mass and stiffness matrices of the defined linear elastic mass-spring system will yield the eigen angular frequencies of the structure[6],[10]. Hence, once the mass and stiffness of the structure have been estimated through the procedures explained above, solution to equation (11) will provide the analytically expected values of the eigen frequencies

$$|[K - M\omega^2]| = 0 \qquad (11)$$

where $[K]$ and $[M]$ respectively refer to the stiffness and mass matrices of the defined system, where the mass matrix remains the same though the stiffness matrix varies for the two orthogonal horizontal directions, *X* and *Y*.

Once the analytical eigen frequencies have been derived, the corresponding peaks detected in the measured FFT curves will provide the real time modal frequencies of the structure to be applied to the fundamental equation (1). Samples of such a spectrum are represented per Fig. (3).

The following Tables (5) and (6) represent the analytically approximated and the averaged measured frequencies of the system in each direction and for the two defined DOF classes. As noticed per the numerically represented data, the difference between the calculated eigen frequencies of the 5DOF and 6DOF mass-spring systems are sufficiently small in the accuracy scale of the defined "Phase 0" stage to continue with just the 5DOF model for the rest of the calculations. Moreover and clearly, the following relationship between the linear frequency and the angular one has been consistently used for the entire calculations.

$$\omega_i = 2\pi f_i \tag{12}$$

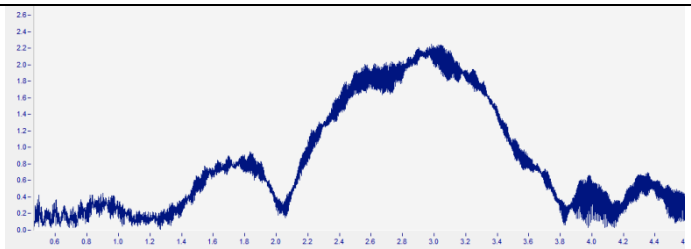

Fig (3). Sample FFT spectral analysis for the eigen frequency determination[11]

Table (5). The approximated analytical eigen frequencies- left: 5DOF- right: 6DOF

Mode X #	Freq (Hz)	Mode Y #	Freq (Hz)
1	3,67	1	3,76
2	9,82	2	10,38
3	15,28	3	15,89
4	19,39	4	19,94
5	21,6	5	22,25

Mode X #	Freq (Hz)	Mode Y #	Freq (Hz)
1	3,24	1	3,4
2	8,49	2	9,14
3	13,51	3	14,28
4	17,11	4	18,38
5	19,9	5	21,05
6	21,64	6	22,37

Table (6). The averaged measured eigen frequencies for the 5DOF model

Mode X #	Freq (Hz)	Mode Y #	Freq (Hz)
1	3,18	1	2,86
2	9,41	2	10,80
3	15,60	3	15,35
4	20,23	4	19,85
5	23,23	5	23,03

16.4 *Mode Shapes*

As sufficiently well-known from the principles of dynamics of structures, once the eigen frequencies of the system are known, the solution to equation (13) will result into the analytical mode shapes of the structure[10]

$$[K - M\omega_i{}^2]\{\phi\}_i = 0 \tag{13}$$

where all the terms have been previously defined. However, as long as the main motivation of this current research program is to obtain the so-called real dynamic properties of the building by the in-site measurement methods, a well-equipped recording set up where each degree of freedom possesses at least one accelerometer unit must provide the eigen vectors of the system along with the eigen frequencies at the same time.

Nevertheless, in the absence of such measurement set up, the following analytical procedures will theoretically result into the real-time mode shapes of the structure using a single story recorded data set.

Referring to the sub-steps taken to derive the analytical eigen frequencies of the structure by the application of equation (11), the actual stiffness of the structure can be back calculated by the same methodology, should the actual stiffness matrix $[K]$ be taken as the unknown and the real-time measured frequencies of the system, ω_i, be back substituted as the known elements. The solution to the derived nonlinear system of *n* equations will result into the elements of the actual stiffness matrix of the structure. Hence, in a subsequent step, the "real-time" mode shapes of the structure could be derived, applying equation (13), in which all the engaged terms $[K]$, $[M]$ and ω_i are updated for the actual condition. It could also be expected that by such a back calculation methodology, the derived actual stiffness matrix could reflect the effects of the adjacent structures, the torsional movements and to some extents the soil-structure interactions brought up by the application of the measured eigen frequencies. As a result, once the first bracket in equation (13) is updated, its analytical solution will end up with the "real-time" lateral mode shapes of the structure.

Despite the fact that all the detailed required steps described to first derive the actual stiffness matrix of the structure and consequently calculate the mode shapes have been followed for the specific case at "Fendigasse" where all the sensors were placed at one level, the derivation of the correct solution to the system of nonlinear equations could not be completed due to a lack of the required sufficiently strong mathematical tools to handle the equations. However, skipping the procedure to update the stiffness matrix and applying the same approximately calculated analytical one, equation (13) was solved by the combination of the measured eigen frequencies with all the other terms for the unknown eigen vectors of the building in the two orthogonal directions. The values of the mode shapes for "Fendigasse" are summarized in Tables (7) to (11), as well as the Fig. (4).

Table (7). First mode shape of the building in the X and Y directions

Mode X #1	Mode Shape	Mode Y # 1	Mode Shape
5	1	5	1
4	0,8473	4	0,8636
3	0,6299	3	0,6773
2	0,3578	2	0,4463
1	0,18589	1	0,2082

Table (8). Second mode shape of the building in the X and Y directions

Mode X #2	Mode Shape	Mode Y #2	Mode Shape
5	1	5	1
4	-0,219	4	0,7107
3	-1,2403	3	-0,204
2	-1,363	2	-0,942
1	-1,1207	1	-0,794

Table (9). Third mode shape of the building in the X and Y directions

Mode X #3	Mode Shape	Mode Y #3	Mode Shape
5	1	5	1
4	0,3154	4	-0,298
3	-0,972	3	-1,016
2	-0,3142	2	0,1254
1	1,7262	1	0,9467

Table (10). Fourth mode shape of the building in the X and Y directions

Mode X #4	Mode Shape	Mode Y #4	Mode Shape
5	1	5	1
4	1,115	4	-0,678
3	-2,4868	3	-0,253
2	2,2939	2	0,9538
1	-1,3667	1	-0,752

Table (11). Fifth mode shape of the building in the X and Y directions

Mode X #5	Mode Shape	Mode Y #5	Mode Shape
5	1	5	1
4	-0,502	4	-0,665
3	0,25	3	0,428
2	-0,106	2	-0,237
1	0,0372	1	0,0959

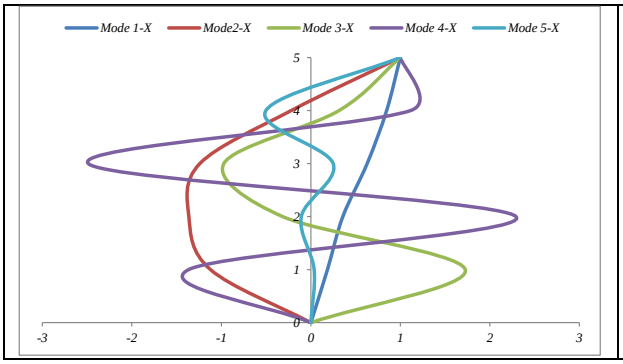

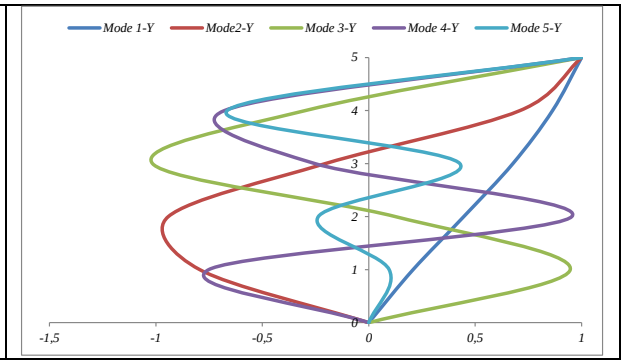

Fig (4). Mode shapes of the structure- left: X direction- right: Y direction

16.5 *Modal Damping Coefficients*

In the preceding parts, all the required structural characteristics in the fundamental equation (1) were determined besides the modal damping coefficient values. Hence, the following is to represent one of the practical methods to estimate the aforementioned quantities from the measured data.

- Application of the half-power band width method

According to the theories of dynamics of structures, the maximum amplitude of the steady-state response of an oscillator, X, and static stiffness K, to a harmonic excitation with the amplitude F_0 and angular frequency ω can be estimated by the following relationship[6].

$$X = \frac{F_0/K}{\sqrt{\left[1-\left(\frac{\omega}{\omega_n}\right)^2\right]^2+\left(2\xi\frac{\omega}{\omega_n}\right)^2}} \tag{14}$$

In equation (14), ω_n and ξ are the angular natural frequencies and damping coefficients of the SDOF oscillator, in the order of appearance. As noticed per equation (14), the oscillator will reach its maximum range when the frequency of excitation falls close enough to the vicinity of the natural frequency of the dynamic system, as shown by equation (15) below[6].

$$X_{max} = \frac{F_0/K}{2\xi} \tag{15}$$

As long as equation (14) holds for any arbitrary maximum amplitude of vibration a certain dynamic system may undergo, the so-called "half-power band width" method essentially tries to derive a relationship between Lehr's critical damping coefficient, ξ, and the eigen frequency of the system when the maximum amplitude of vibration is equal to $X_{max}/\sqrt{2}$. Hence, multiplying equation (15) by $1/\sqrt{2}$ and equating it with the right hand side of equation (14) and further simplifying the relationship for small values of Lehr's damping coefficient, the following expression enables the engineers to approximate the damping properties of the system, using the experimental displacement spectrum in the frequency domain by the following expression

$$\xi = \frac{\omega_2-\omega_1}{\omega_n} = \frac{f_2-f_1}{f_2+f_1} \tag{16}$$

where ω_2 and ω_1 are the angular frequencies corresponding to the amplitude values in the spectrum equal to $X_{max}/\sqrt{2}$[6].

Application of the aforementioned procedures to the measured data in a real scale structure subjected to a series of artificially induced harmonic excitations under

controlled conditions may result into a sufficiently smooth FFT spectrum which will be turned into the displacement amplitudes, dividing the recorded accelerations by the corresponding squared angular frequencies at each and every point. Derivation of such a displacement spectrum will consequently serve as the base for the application of equation (16). However, in the absence of the well recorded sets of data where the harmonic frequency of excitation was swept through a reasonably wide range to capture all the modal frequencies of the structure, the best set of data obtained from the ambient vibrations first needs to be recognized and subsequently smoothed out to reflect the desirable amplitude peaks in the FFT spectrum. Nevertheless, since the measured vibrations in the real condition is usually accompanied by inevitable noises from the surrounding environments, the corresponding modal peaks and frequencies might not be eventually reflected into the obtained FFT diagrams with the expected resolutions. That is to say that should the quality of the recorded data allow for the application of the aforementioned procedures, the modal damping coefficients will be estimated using equation (16).

However, it has to be declared that neither of the measured histories at "Fendigasse" building as of July 2011 resulted into a sufficiently smooth FFT curve and the numerical results obtained by the application of equation (16) were not in the expected range of civil engineering applications. Hence, a conservative value $\xi = 0$ for all the modes of the structure was assumed in the derivation of the "Phase 0" fragility curves.

Based on the calculations, undertaken in sub-sections (2.1.1) through (2.1.3), the required dynamic structural characteristics of the system for the derivation of the response of the structure applying equation (1) have already been derived. Consequently, the selection of the proper earthquakes, $\ddot{U}(t)_g$, for the structural response derivation will be brushed up as follows.

16.6 *Ground Motion Hazard Level Selection*

As declared earlier, the determination of the "fragility curves" requires the estimation of the response of the structure under certain various hazard levels and further relating the obtained results to the specified damage states in a probabilistic scheme. Since the fundamentals of the structural response derivation by the application of a time history analysis as the most exact method were sufficiently entailed in the preceding section, the major outlines of the selection of the appropriate ground motions as the second essential step will be briefly reviewed as follows.

According to the outlines mentioned in reference [1], there are certain challenges to be conquered in the selection of the proper group of earthquakes, representing each level of the ground motion hazard[1]. Based on the numerous recent investigations on the probable parameters affecting the devastating characteristics of an earthquake, "the demand intensity of the earthquake on the structures generally is not quantitatively unique, as the same value of peak ground acceleration (PGA) as a common representation of the seismic demand does not guarantee the similarity of the structural responses by any ways. Hence, in order to classify the ground motions, representing the same level of hazard, the localized special effects such as the faulting mechanism, the path of the seismic wave, the directivity and fling-step effects in addition to the soil amplifications and its interactions with the structure foundation have to be reflected into

the derived fragility curves, as affecting the longitudinal axes of the graph, potentially noticeably"[1],[5],[12],[13],.

In addition, "scaling the set of the ground motions representing the certain hazard level to the current code-based spectra might serve as an ad-hock solution, however, in more advanced cases and special structures and lifelines, special seismic hazard analysis has to specify and describe the seismicity of the area"[1].

Moreover, "based on the widely available research results on the damage indices and measurements, this is a difficulty to find the most appropriate quantitative representation of the seismic demand, as it is usually coupled with the specific structural behavior. In the other word, although some analytical researches have shown the sensitivity of specific types of the structures to certain ground motion parameters, derivation of a general conclusion might not be applicable as long as some other types of structures may show different degrees of sensitivity to other characteristics parameters of the ground-motion"[1],[12].

Although the aforementioned issues have already been detected and clarified, the solution to such matters, sourcing from the unknown random nature of the earthquakes cannot be deterministically found. Hence, as long as the order of accuracy of the "Phase 0" curves could leave some rooms for further possible future modifications regarding the by-the-time detected shortcomings, the following major characteristics were taken as the appropriate base to detect and selelct the earthquake group at each hazard level.

i) Since Vienna is not potentially prone to highly destructive ground motions, the earthquakes were intensively selected in a way not to possess any obvious Near-Field characteristics, specifically high amplitude pulses in the velocity and displacement records or long period motions in the acceleration time histories[8],[15].

ii) The recording station of the seismic data has to be at least 10 *km* away from the source of faulting.

iii) In order to keep the smoothness of the final fragility curves for all the defined hazard levels, in this research project only one set of earthquakes, satisfying the two above conditions was selected and consequently linearly scaled to different hazard levels. In the other word, the basic earthquake group remained the same while the amplitudes of the acceleration data were multiplied by a factor, representing the hazard level of interest.

Once the proper group of earthquakes was selected of which the characteristics are summarized in Table (12), the acceleration records have been first normalized for the unit of ground motion accelerations in the *g* scale and consequently modified for the PGA in the range of 0.05*g* to 1.5*g*, with a 0.05*g* acceleration increments. That is to say that the structure has been subjected to 30 defined hazard levels based on the PGA classifications where each hazard level contains 8 ground motions. Moreover, in Table (12), the terms PGV and PGD refer to the peak ground velocity and peak ground displacement, in the order of appearance. All the recorded time histories are retrieved from Peer Berkeley Strong Ground Motion Database[14].

Table (12). As recorded characteristics of the selected earthquakes[14]

Earhtquake	Recording Station	Array	PGA (g)	PGV (cm/s)	PGD (cm)	Energy Density (cm^2/s)
Imperial Valley 1979	Elcentro Calipatra Fire Station	225	0.128	15.37	11.3	653.5
Imperial Valley 1979	Elcentro Calipatra Fire Station	315	0.078	13.62	13.85	445.069
Imperial Valley 1979	Elcentro 13	140	0.117	14.67	8.05	453.18
Imperial Valley 1979	Elcentro 13	230	0.139	13	5.94	422.33
Imperial Valley 1979	Elcentro Coachella Canal	4045	0.115	12.46	2.51	106.85
Imperial Valley 1979	Elcentro Coachella Canal	4135	0.128	15.61	3.1	152.853
Imperial Valley 1979	Elcentro Delta	262	0.238	26.015	12.79	4942.61
Imperial Valley 1979	Elcentro Delta	352	0.351	35	347.2	7791.2

16.7 *Numerical Evaluations and Arithmetic Statistics*

The procedures entailed in the preceding sub-sections suffice the numerical evaluation of the structural response by the application of the fundamental equations (1) and (5) in a time history scheme, using the scaled ground motion records referred in Table (12). Hence, the proceeding parts are to summarize the obtained numerical structural responses and the arithmetic statistical procedures accomplished to derive the "definition-based real-time" fragility curves of the specified building at "Fendigasse".

As attached per Appendix (II) to this document, a computer code in "Fortran 95" programing environment, capable of assessing the linear response time history of the structure in both the forced and free phases of vibration, was developed and the maximum inter story drifts of the one-dimensionally modeled building in the two orthogonal directions were extracted as the parameters of interest[16]. In the next step, the obtained responses of the structure in each defined hazard level were purified for the maximum three values, implying that though in each ground motion hazard state defined by the corresponding scaled PGA of the record, the structure was subjected to eight separate ground motions in the two horizontal orthogonal directions, only the three highest inter story drifts of the building were selected to represent the structural behavior for the rest of the statistical calculations.

Consequently, the mean and standard deviation of the structural response in each hazard level are evaluated and the continuous probability of exceedance of each defined damage state is calculated, applying equation (17) as follows[5],[17].

$$Fragility = P(R_s > L_{DS}|HL_G) = 1 - P(R_s < L_{DS}|HL_G) \quad (17)$$

In the equation above, P is to represent the probability calculation function, R_s, the structural response, L_{DS}, the defined damage state limit corresponding to the type of the structural response evaluated and HL_G is the ground motion hazard level. Based on the

theories of probability and statistics, the notation used in equation (17) is clearly referring to a conditional probability.

Furthermore, in order to derive the fragility values as a continuous quantity for each damage state instead of a set of discrete numbers, it is a common practice to assume a normal distribution density function for the obtained structural responses in each hazard level with the specific calculated mean and standard deviation values and assess the fragility as the cumulative distributed probability function. Implementation of the described procedure into equation (17) will render the following expressions[18].

$$f(R_s;\mu,\sigma^2) = \frac{1}{\sigma\sqrt{2\pi}} e^{\frac{-(R_S-\mu)^2}{2\sigma^2}} \tag{18}$$

$$F(L_{DS};\mu,\sigma^2) = \phi\left(\frac{L_{DS}-\mu}{\sigma}\right) = \frac{1}{2}\left[1 + erf\left(\frac{L_{DS}-\mu}{\sigma\sqrt{2}}\right)\right] \tag{19}$$

$$erf(x) = \frac{2}{\sqrt{\pi}}\int_0^x e^{-t^2}dt \tag{20}$$

$$Fragility = P(R_s > L_{DS}|HL_G) = 1 - \phi\left(\frac{L_{DS}-\mu}{\sigma}\right) \tag{21}$$

In equations (18) to (21), f and F refer to the probability density and the cumulative probability distributions in the order of appearance. In addition, μ and σ are the mean and the standard deviations of the obtained structural responses in each defined hazard levels. Moreover, the terms ϕ and erf represent the cumulative distribution probability and error functions, respectively and t and x are the dummy variables to define the error function. All the other terms hold their definitions as stated elsewhere.

The final numerical values of the introduced terms, parameters and functions are summarized and represented per Tables (13) and (14) for the two orthogonal directions. It needs to be clarified that in this project, four different levels of the damage state, namely the slight, moderate, extensive and complete have been defined of which the numerical inter-story drift ratio limits, L_{DS}, are reproduced in an ascending order in the aforementioned tables, obtained from FEMA HAZUS[5].

In addition and as declared earlier, all the maximum structural inter-story drift ratios were assessed using a linear time history analysis. However, the obtained results have been consequently applied towards the fragility derivation in the damage state levels "moderate", "extensive" and "complete", where at least the materials plasticity will invalidate the general applicability of the linear dynamic theories. Nevertheless, this is to emphasize that as long as the monitored structural response is selected to be the inter-story drifts and not the force-based actions, assuming the equality of the linear and nonlinear inelastic displacements could sufficiently fulfill the preciseness level of the derived fragility curves in the defined "Phase 0"[6],[10]. Notwithstanding, the detailed effects of such an assumption could be further investigated in the future, should the specific data on the material plastic performance be available. The obtained definition-

based real-time fragility curves of the building in the X and Y directions are shown in Figs. (5) and (6), respectively.

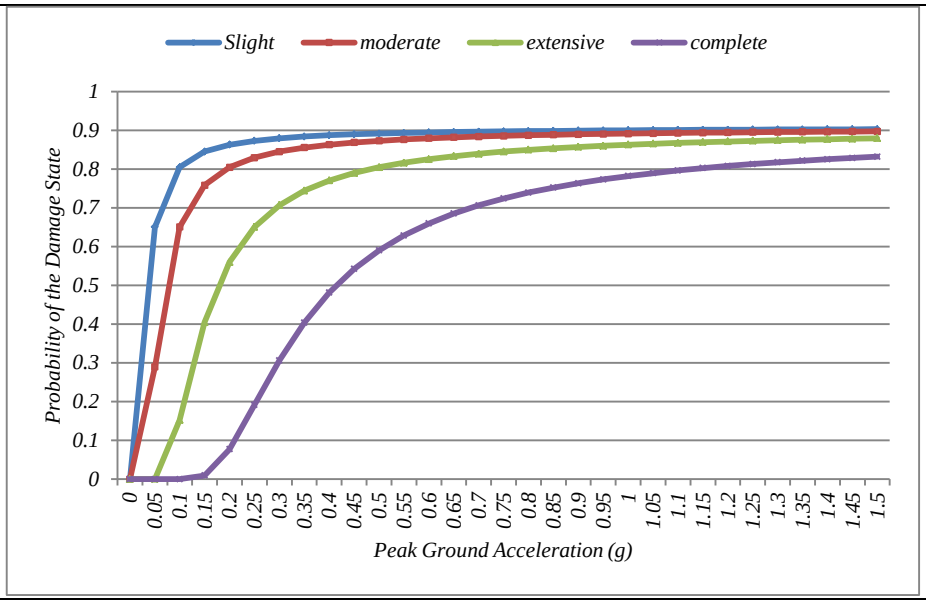

Fig (5). Definitions-based fragility curves of the building in the X direction

Table (13). The fragility calculations for different levels of damage states in the X direction

Hazard Level	0	0.05	0.1	0.15	0.2	0.25	0.3	0.35	0.4	0.45	0.5	0.55	0.6	1.1	1.15	1.2	1.25	1.3	1.35	1.4	1.45	1.5	PGA(g)	
Structural Inter-Story Drift Ratio	0	0.0021	0.0042	0.0063	0.0084	0.0105	0.0126	0.0147	0.0168	0.0189	0.0210	0.0231	0.0252	0.0461	0.0482	0.0503	0.0524	0.0545	0.0566	0.0587	0.0608	0.0629	Elcentro Calipatra Fire Station 225	Earthquake
	0	0.0040	0.0081	0.0121	0.0161	0.0202	0.0242	0.0282	0.0323	0.0363	0.0403	0.0444	0.0484	0.0887	0.0927	0.0968	0.1008	0.1048	0.1089	0.1129	0.1169	0.1210	Elcentro Calipatra Fire Station 315	
	0	0.0006	0.0013	0.0019	0.0026	0.0032	0.0039	0.0045	0.0052	0.0058	0.0065	0.0071	0.0077	0.0142	0.0148	0.0155	0.0161	0.0168	0.0174	0.0181	0.0187	0.0194	Elcentro Delta	
Mean	0	0.0023	0.0045	0.0068	0.0090	0.0113	0.0135	0.0158	0.0181	0.0203	0.0226	0.0248	0.0271	0.0497	0.0519	0.0542	0.0565	0.0587	0.0610	0.0632	0.0655	0.0677	μ	
Standard Deviation	0	0.0017	0.0034	0.0051	0.0068	0.0085	0.0102	0.0119	0.0136	0.0153	0.0170	0.0187	0.0204	0.0374	0.0391	0.0408	0.0425	0.0442	0.0459	0.0476	0.0493	0.0510	σ	
Fragility (Eq 21)	0	0.6507	0.8046	0.8449	0.8629	0.8730	0.8794	0.8838	0.8871	0.8896	0.8915	0.8931	0.8944	0.9008	0.9011	0.9014	0.9017	0.9019	0.9022	0.9024	0.9026	0.9028	L_{DS}=0.0016	Damage States
	0	0.2897	0.6507	0.7584	0.8046	0.8295	0.8449	0.8554	0.8629	0.8686	0.8730	0.8765	0.8794	0.8931	0.8938	0.8944	0.8950	0.8955	0.8960	0.8964	0.8969	0.8973	L_{DS}=0.0032	
	0	0.0004	0.1527	0.4050	0.5604	0.6507	0.7068	0.7442	0.7705	0.7898	0.8046	0.8162	0.8255	0.8675	0.8695	0.8713	0.8730	0.8745	0.8758	0.8771	0.8783	0.8794	L_{DS}=0.008	
	0	0	0.00002	0.0097	0.0775	0.1916	0.3067	0.4039	0.4814	0.5422	0.5903	0.6287	0.6597	0.7963	0.8024	0.8079	0.8129	0.8174	0.8215	0.8253	0.8288	0.8320	L_{DS}=0.0187	

≈continues≈

Table (14). The fragility calculations for different levels of damage states in the Y direction

Hazard Level	0	0.05	0.1	0.15	0.2	0.25	0.3	0.35	0.4	0.45	0.5	0.55	0.6	1.1	1.15	1.2	1.25	1.3	1.35	1.4	1.45	1.5	PGA(g)	
Structural Inter-Story Drift Ratio	0	0.0007	0.0015	0.0022	0.0030	0.0037	0.0045	0.0052	0.0059	0.0067	0.0074	0.0082	0.0089	0.0163	0.0171	0.0178	0.0185	0.0193	0.0200	0.0208	0.0215	0.0223	Elcentro Calipatra Fire Station 225	Earthquake
	0	0.0029	0.0059	0.0088	0.0117	0.0147	0.0176	0.0205	0.0235	0.0264	0.0294	0.0323	0.0352	0.0646	0.0675	0.0705	0.0734	0.0763	0.0793	0.0822	0.0851	0.0881	Elcentro Calipatra Fire Station 315	
	0	0.0012	0.0023	0.0035	0.0046	0.0058	0.0070	0.0081	0.0093	0.0105	0.0116	0.0128	0.0139	0.0255	0.0267	0.0279	0.0290	0.0302	0.0314	0.0325	0.0337	0.0348	Elcentro Delta	
Mean	0	0.0016	0.0032	0.0048	0.0065	0.0081	0.0097	0.0113	0.0129	0.0145	0.0161	0.0177	0.0194	0.0355	0.0371	0.0387	0.0403	0.0419	0.0435	0.0452	0.0468	0.0484	μ	
Standard Deviation	0	0.0012	0.0023	0.0035	0.0047	0.0058	0.0070	0.0082	0.0093	0.0105	0.0116	0.0128	0.0140	0.0256	0.0268	0.0279	0.0291	0.0303	0.0314	0.0326	0.0338	0.0349	σ	
Fragility (Eq 21)	0	0.5044	0.7574	0.8231	0.8512	0.8666	0.8762	0.8828	0.8875	0.8911	0.8939	0.8962	0.8981	0.9070	0.9075	0.9079	0.9083	0.9086	0.9089	0.9092	0.9095	0.9098	L_{DS}=0.0016	Damage States
	0	0.0864	0.5044	0.6805	0.7574	0.7983	0.8231	0.8395	0.8512	0.8599	0.8666	0.8719	0.8762	0.8962	0.8972	0.8981	0.8989	0.8996	0.9003	0.9010	0.9015	0.9021	L_{DS}=0.0032	
	0	0.0000	0.0202	0.1827	0.3698	0.5044	0.5949	0.6568	0.7007	0.7330	0.7574	0.7765	0.7918	0.8583	0.8614	0.8641	0.8666	0.8688	0.8709	0.8728	0.8746	0.8762	L_{DS}=0.008	
	0	0	0.00000	0.0000	0.0043	0.0339	0.0983	0.1817	0.2669	0.3449	0.4126	0.4702	0.5187	0.7438	0.7539	0.7630	0.7712	0.7786	0.7853	0.7915	0.7971	0.8023	L_{DS}=0.0187	

≈continues≈

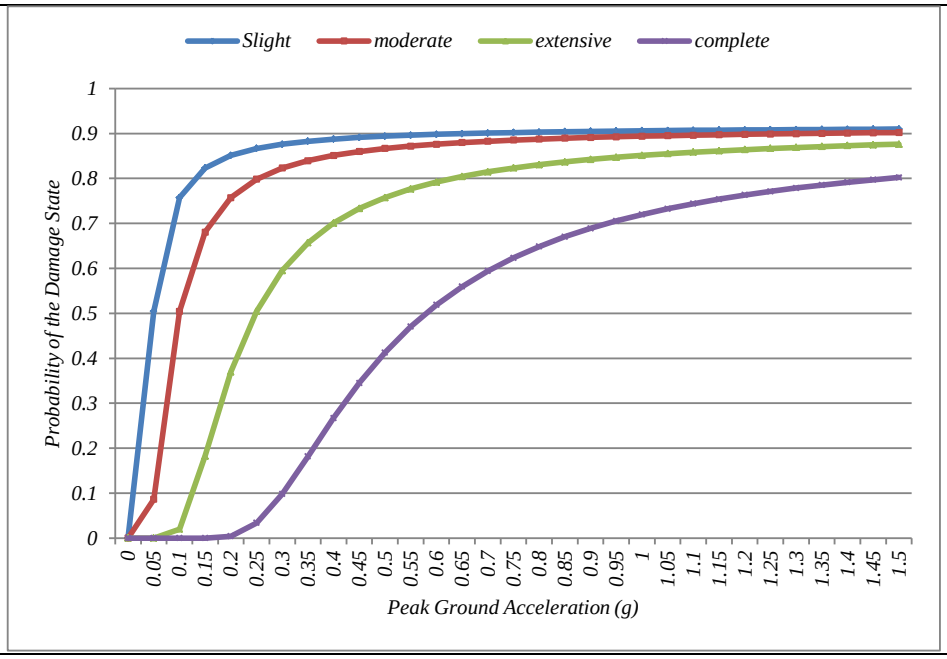

Fig (6). Definitions-based fragility curves of the building in the Y direction

17. Curve Fitting and Fragility Functions

As noticed per the configuration of the derived curves in Figs. (5) and (6), and according to the technical literature at hand, the fragility curves could be idealized and generalized by a lognormal distribution function in terms of the intensity parameter, used to define the ground motion hazard levels[2],[3],[5],[19]. In the other word, the aim of this section is to introduce the family of the lognormal distribution functions which could sufficiently exactly approximate the trend of the fragility curves, derived analytically and based on the definitions as shown in Figs. (5) and (6).

According to probability theories, a lognormal cumulative distribution function, F, is defined by equation (22), below

$$F(\ln(PGA);\mu,\sigma) = \phi\left(\frac{\ln(PGA)-\mu}{\sigma}\right) = \frac{1}{2}erfc\left(-\frac{\ln(PGA)-\mu}{\sigma\sqrt{2}}\right) \tag{22}$$

where μ and σ are known as the location and scale parameters, corresponding to the mean and standard deviation of the natural logarithm of the ground motion hazard level intensity index, here referred as PGA[20]. In addition, the term $erfc$ represents the complementary error function[21].

In compliance with the eventual objective of this section and in order to relate the derived probabilities of exceedance known as the fragilities directly to the ground motion intensity parameter, PGA, via a lognormal distribution curve fitting, the procedures described below have been followed. All the terms have been already defined in the preceding parts[22].

$$erfc\left(-\frac{\ln(PGA)-\mu}{\sigma\sqrt{2}}\right) = Fragility \times 2 \tag{23}$$

$$erf\left(-\frac{\ln(PGA)-\mu}{\sigma\sqrt{2}}\right) = 1 - erfc\left(-\frac{\ln(PGA)-\mu}{\sigma\sqrt{2}}\right) = 1 - Fragility \times 2 = z \tag{24}$$

$$erf^{-1}(z) = \frac{1}{2}\sqrt{\pi}\left(z + \frac{\pi}{12}z^3 + \frac{7\pi^2}{480}z^5 + \frac{127\pi^3}{40320}z^7 + \frac{4369\pi^4}{5806080}z^9 + \frac{34807\pi^5}{182476800}z^{11} + \cdots\right) \tag{25}$$

$$-\frac{\ln(PGA)-\mu}{\sigma\sqrt{2}} = erf^{-1}(z) \tag{26}$$

According to equation (26), the terms μ and σ can be derived based on the slope and the intersection of a line, connecting every two points of the pairs $\left(\ln(PGA), erf^{-1}(z)\right)$. Should the obtained definition-based fragility curves in Figs. (5) and (6) inherently follow a lognormal distribution function, equation (26) will turn out to be a unique line in terms of the $\ln(PGA)$ and $erf^{-1}(z)$ for the entire pairs of each specific damage state. However, as long as the definition-based curves schematically resemble a lognormal distribution function, though not necessarily analytically, the solution to equation (26) will not result in a single (μ, σ) pair and a couple of "statistical fragility functions", defined per equation (22) will be achieved. Consequently and in essence, the engineer in charge may select the best fitted curve for any generalization purposes.

Regarding the descriptions given above, the statistical fragility functions in this specific project could be referred as "self-induced". That is to imply that for every two points of the definition-based fragility curves at each hazard level shown per Figs. (5) and (6), a separate statistical fragility function with a specific (μ, σ) pair was first calculated, as the Figs. (7) to (14) depict the numerical convolution results, accomplished in "Fortran 95" programing media and Microsoft Excel 2010[16], [22]. As observed per the aforementioned figures, there are above four hundred possibilities of statistical lognormal fragility functions for each hazard level and the direction of interest, enveloping the real definition-based fragility curves. As long as the selection of the best statistical lognormal curve fitting the original real definition-based fragility function is greatly dependent on the type of the structure and the seismicity of the area in addition to the required degree of conservatism, the samples of the best fitting curves from this document author's point of view have been shown in Figs. (15) and (16) with the corresponding calculated mean and standard deviations, (μ, σ), despite the fact that the selection of the most appropriate statistical fragility function could not be unique. In the two latter referred figures, the analytical fragility curves are shown by continuous lines and the fitted lognormal one by the dotted line.

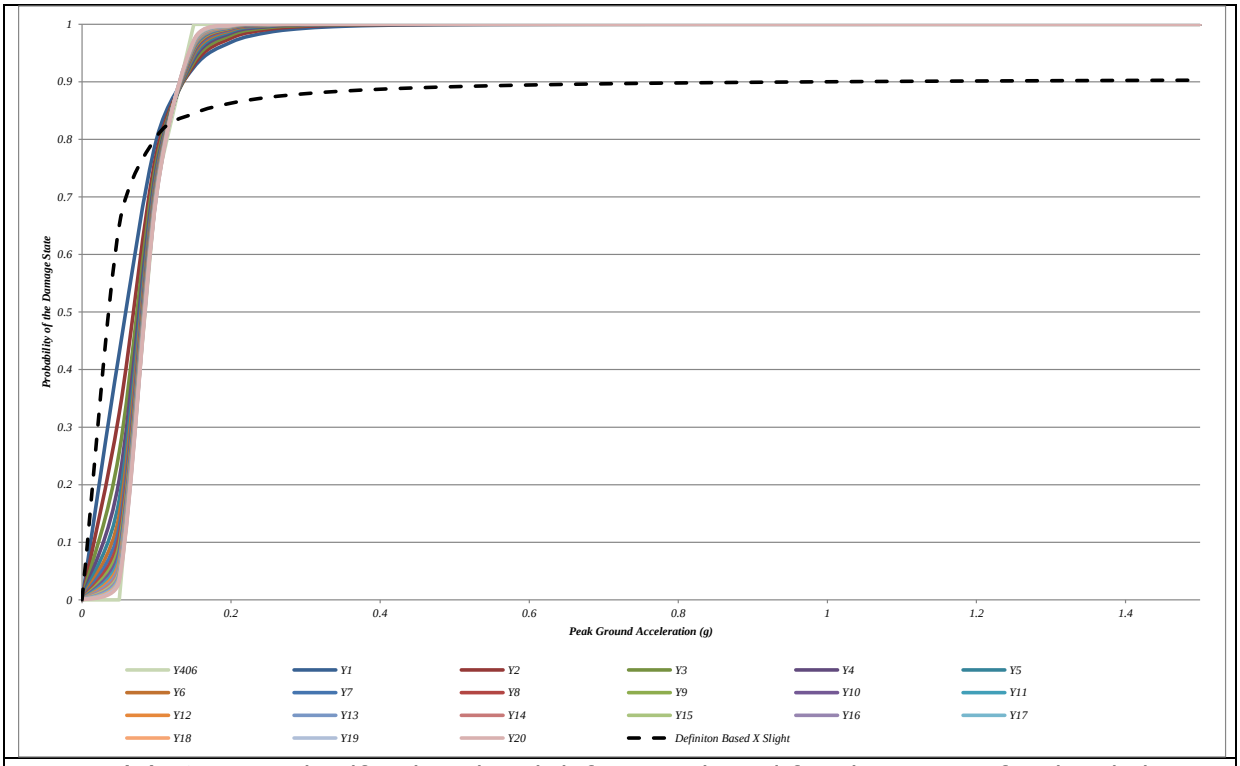

Fig (7). Statistical self-induced and definitions-based fragility curves for the slight damage state- X direction

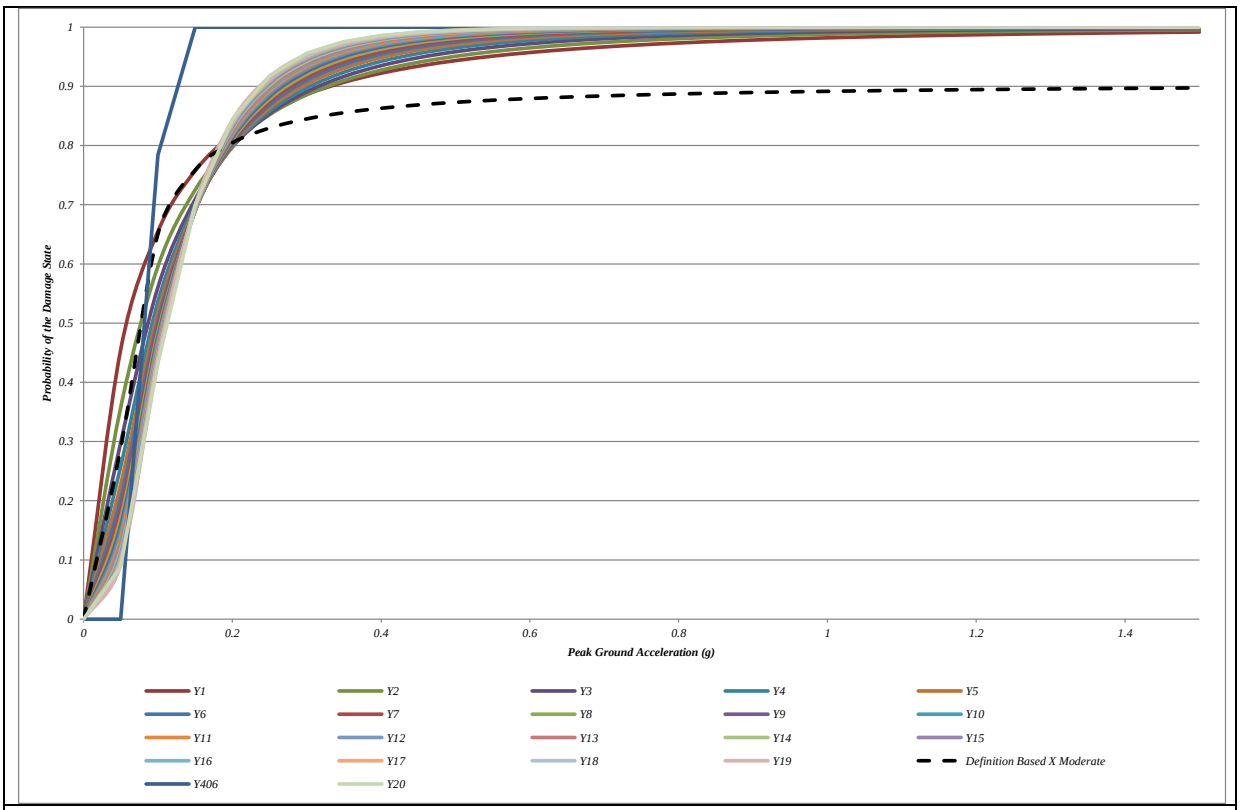

Fig (8). Statistical self-induced and definitions-based fragility curves for the moderate damage state- X direction

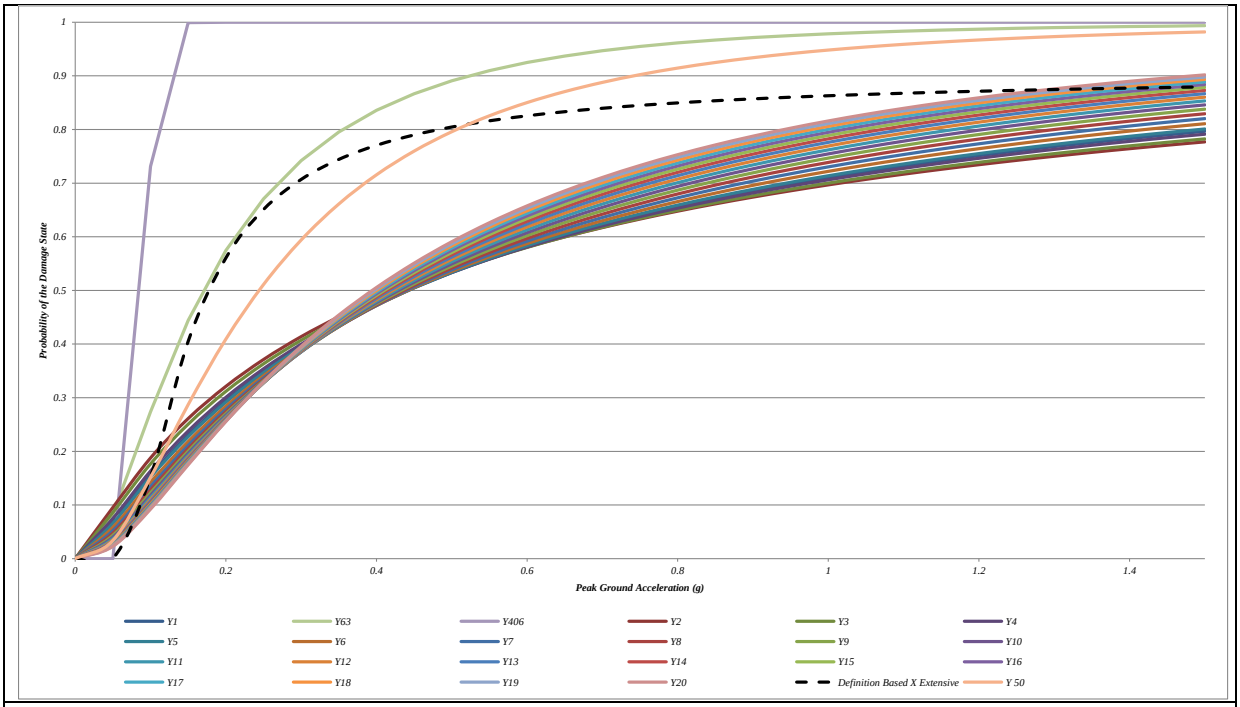

Fig (9). Statistical self-induced and definitions-based fragility curves for the extensive damage state- X direction

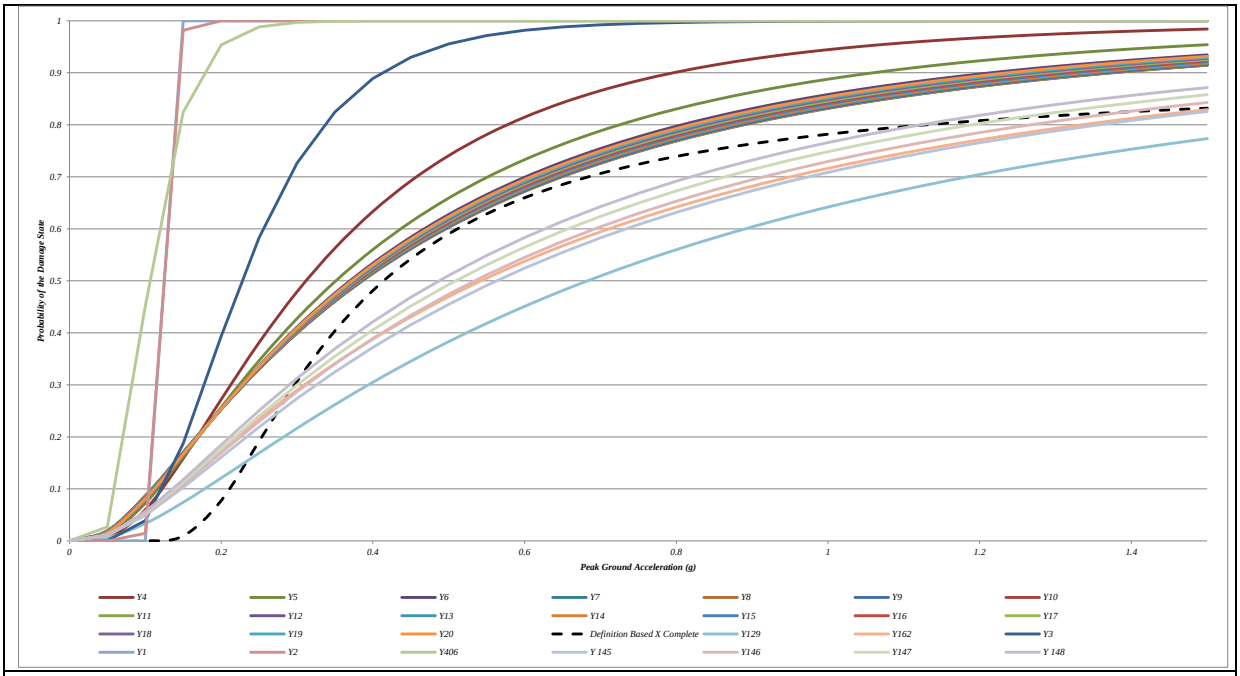

Fig (10). Statistical self-induced and definitions-based fragility curves for the complete damage state X direction

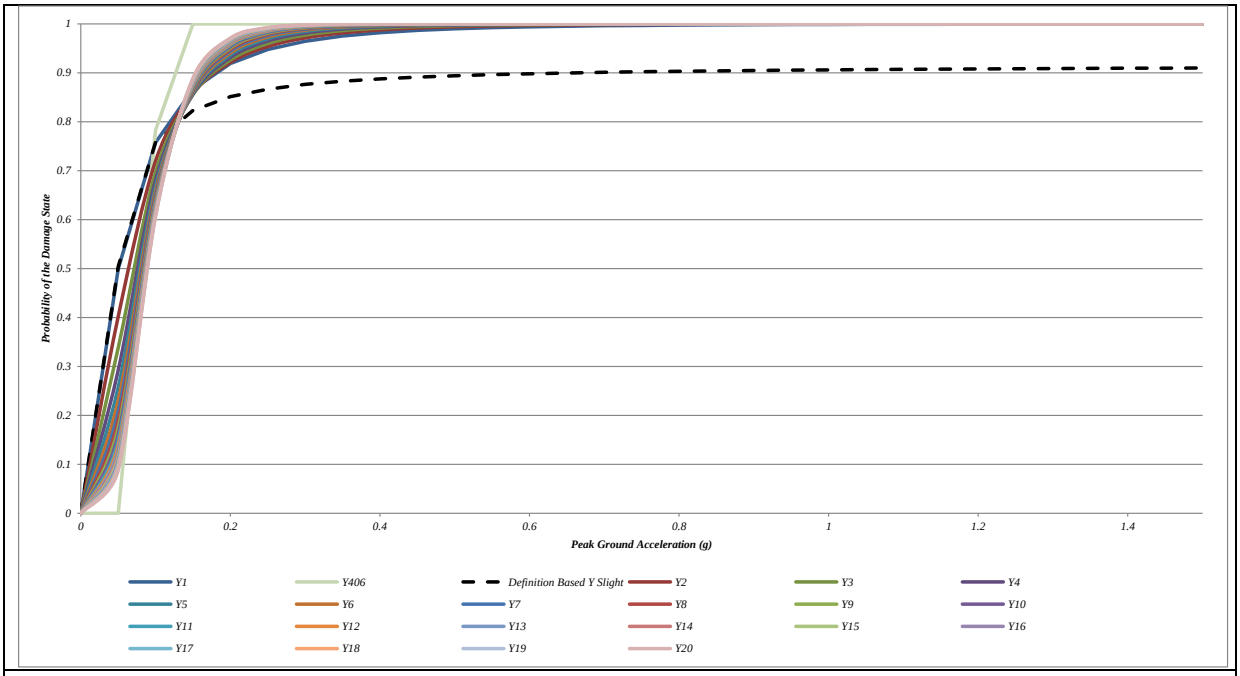

Fig (11). Statistical self-induced and definitions-based fragility curves for the slight damage state- Y direction

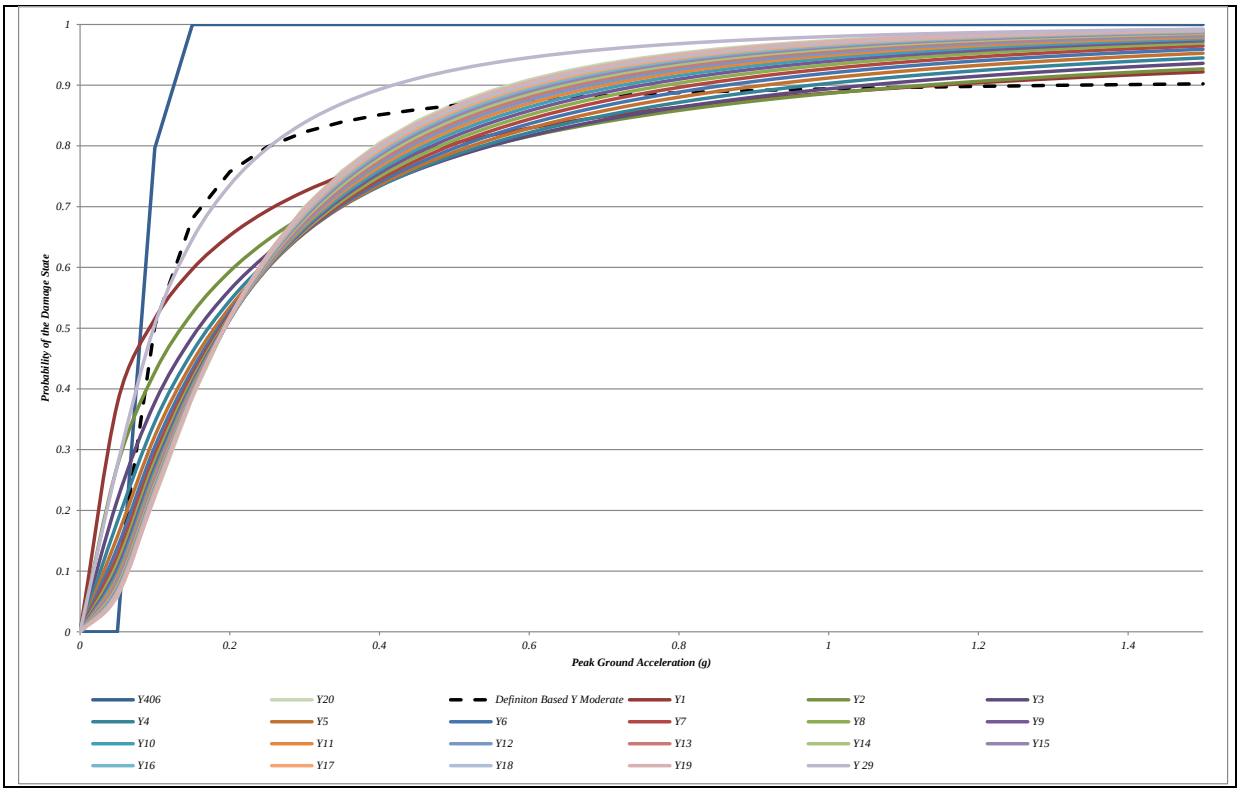

Fig (12). Statistical self-induced and definitions-based fragility curves for the moderate damage state Y direction

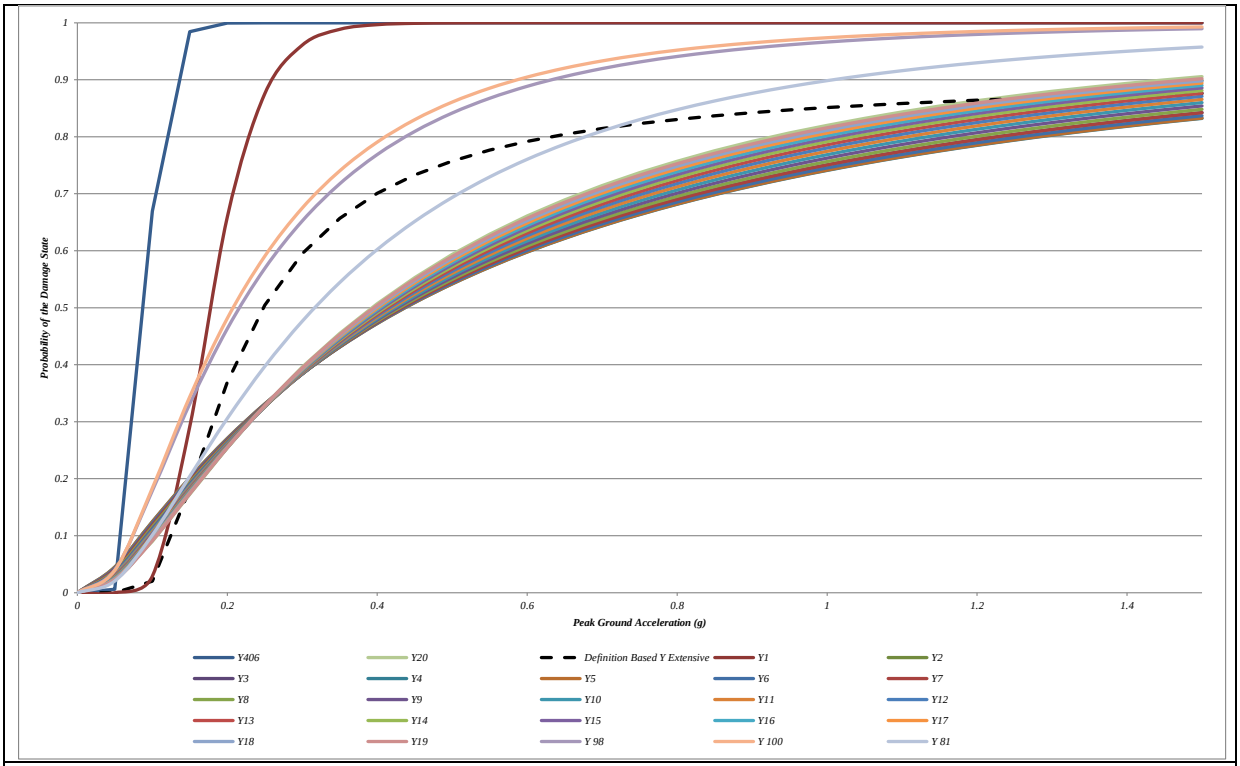

Fig (13). Statistical self-induced and definitions-based fragility curves for the extensive damage state Y direction

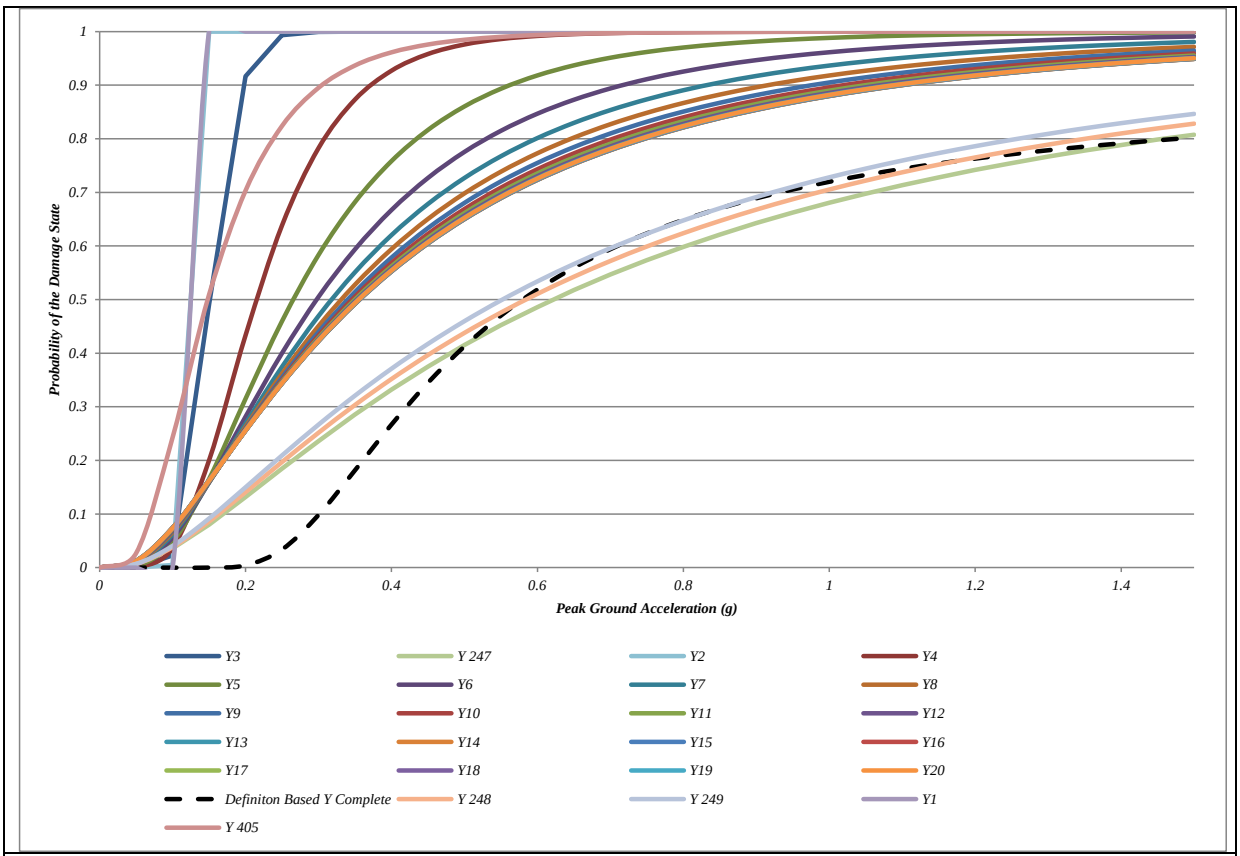

Fig (14). Statistical self-induced and definitions-based fragility curves for the complete damage state Y direction

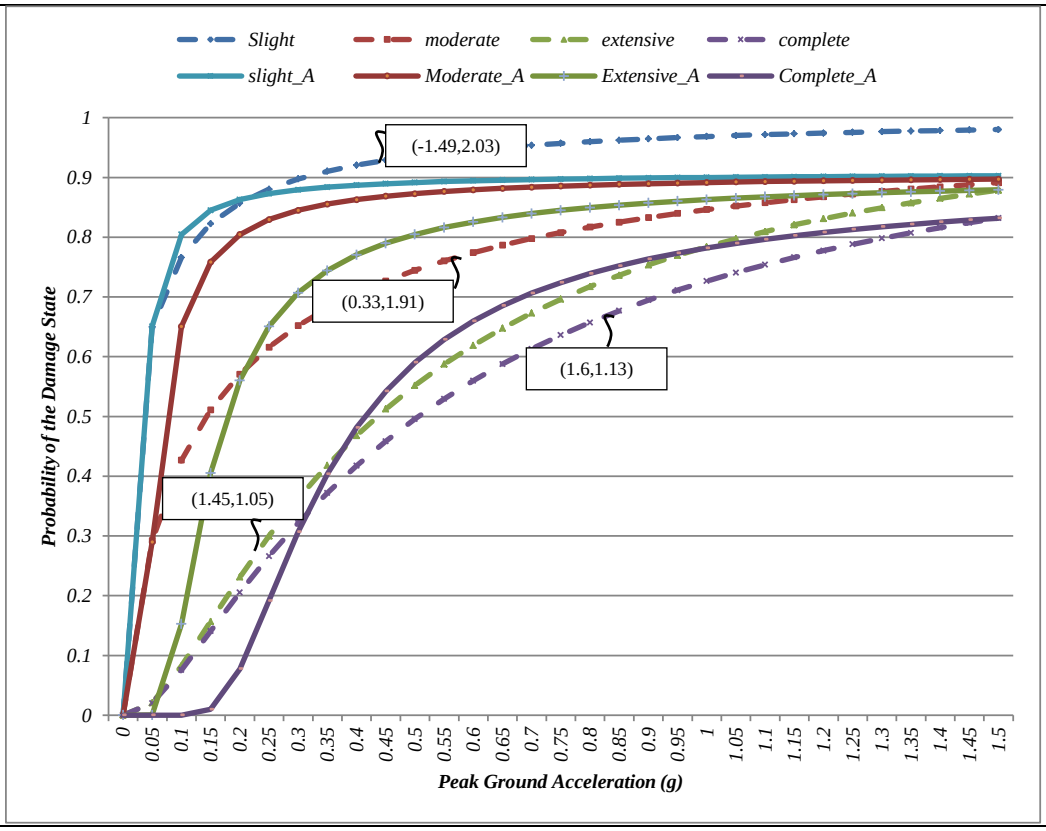

Fig (15). Comparison of the fitted Statistical self-induced (dotted) and definitions-based (continuous) fragility curves in the X direction with (μ, σ)

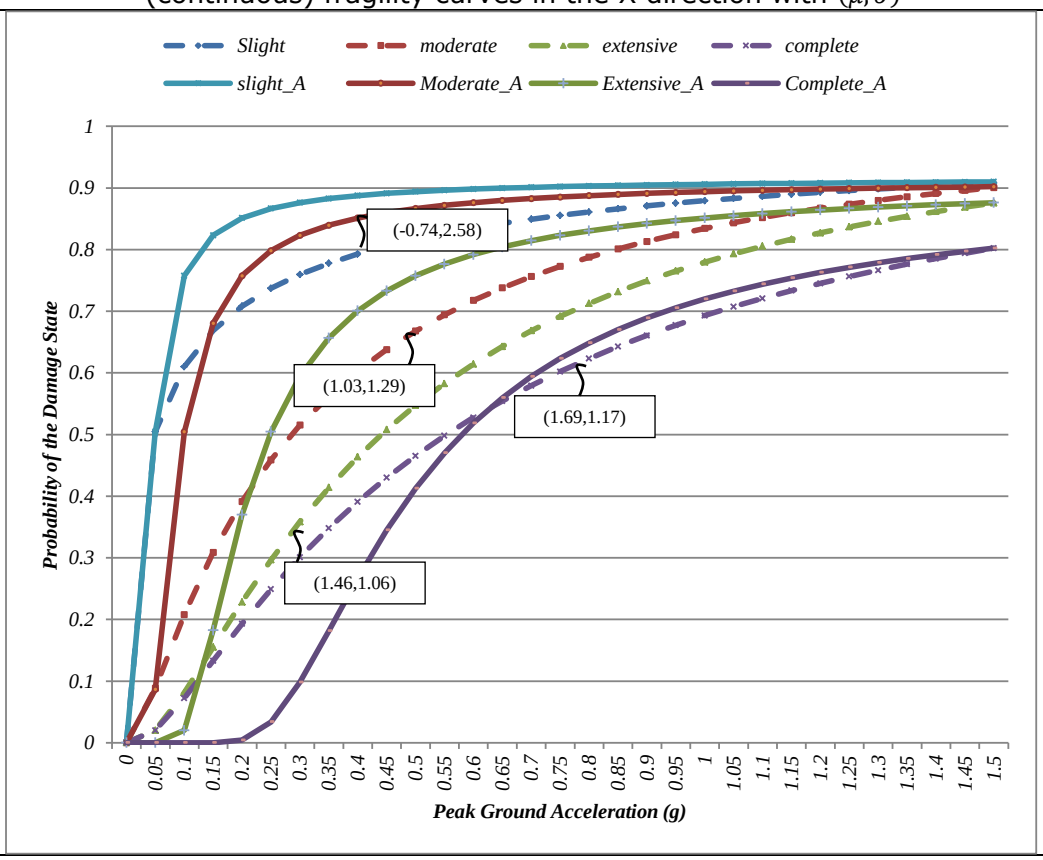

Fig (16). Comparison of the fitted Statistical self-induced (dotted) and definitions-based (continuous) fragility curves in the Y direction with (μ, σ)

18. Example: Spittelbreitengasse

18.1 *Introduction*

The existence of natural phenomena such as fatigue, creep and degradation of material properties during the life time of the structures as well as the plausible damages due to the occurrence of the external hazards including but not limited to the ground motions, may result into a notable deviation in the global characteristics and dynamic performance of the buildings at real-time from the initial, theoretically assumed, design values.

Moreover and based on the philosophy of the definition and development of fragility curves as abstract damage intensity predictors of various structures and life lines under different demand levels, such functions have to be derived in a way to reflect the most analytically possible, realistic view of the performance of the structure under certain levels of the predicted hazard. As a consequence, the estimation of the most updated structural characteristics towards such a damage intensity evaluation remains inevitable [1]. Accordingly and aligned with the expectations from the modern structural and earthquake engineering fields, this manuscript aims to recommend a clear path on the derivation of the analytical fragility curves of structures of which the dynamic properties of the finite element model have already been synchronized with the real-time conditions, measured "In-Site" [2], [3]. Hence, applying the system identification methods and updating the linear dynamic properties of an existing masonry residential building located in Vienna, Austria, the full-scale finite element model of the structure is first calibrated through the match of the analytical and experimentally-recorded linear frequencies and damping parameters, and further subjected to nonlinear seismic time-history analysis. All the analyses include the effects of the adjacent buildings interactions, applying appropriate stiffener elements in ANSYS 10.0 [4]. In addition, the masonry material has been simulated, using the macro-scale equivalent properties of the tested specimens [2], [3], [5]. Eventually, accomplishing the required arithmetic statistics procedures on the derived demands and acceptance criteria, the preliminary, unfinalized "Real-Time" fragility curves of the building under a resampled-smoothed group of ground motions have been worked out.

18.2 *System Identification*

As shown per Figs. (A.1) to (A.5) in the Appendix part of this document, the building under consideration is an old three-story unreinforced masonry structure, located at Spittelbreitengasse, Vienna, Austria. Furthermore and according to the procedures briefly outlined in the 'Introduction' section, the linear dynamic properties of the structure, namely the natural frequencies belonging to the linear mode shapes and the modal damping values of the building, required for the estimation of the linear structural response under any arbitrary excitations per equations (27) to (31), have been derived based on the data processing of the 'In-Site' measurement records by the engaged staff at 'Vienna Consulting Engineers' (vce holding GmbH) [6], [7], [8].

$$y_i(t) = \frac{P_i}{\omega_i}\int_0^t \ddot{U}_g(\tau)e^{-\xi_i\omega_i(t-\tau)}\sin(\omega_{Di}(t-\tau))\,d\tau \qquad (27)$$

$P_i = \frac{\overline{k_i}}{M_i}$
(28)

$\overline{k_i} = \{\phi\}_i^T [M]\{l\}$ (29)

$M_i = \{\phi\}_i^T [M]\{\phi\}_i$ (30)

$\omega_{Di} = \omega_i \sqrt{1 - \xi^2{}_i}$ (31)

"In the equations introduced above, $y_i(t)$ is the time dependent response of a single degree of freedom (SDOF) oscillator to the ground acceleration, $\ddot{U}(t)_g$, with the structural natural and damped angular frequencies, ω_i and ω_{Di}, mass, M_i, and the critical damping ratio, ξ_i. Furthermore, the term P_i refers to the modal participation factor defined per equation (2) belonging to the ith mode of vibration of the real multi degree of freedom (MDOF) system with the corresponding mode shape vectors, $\{\phi\}_i$ and the mass participation factor, $\overline{k_i}$. In addition, $\{l\}$ is the global influence vector and t and τ are the time parameters of the convolution equation (27). Eventually, the index *i* in all the terms defined in the equations above specifies the corresponding mode of response" [1].

"Consequently, once the time dependent part of the response of the original MDOF system, $y_i(t)$, is derived, the total response of the structure in a linear elastic situation, $\{x(t)\}$, can be obtained applying equation (32) to combine the effects of all the modes, equal to the total number of the degrees of freedom, *n*, as given below" [1].

$\{x(t)\} = \sum_{i=1}^{n} \{\phi\}_i \, y_i(t)$ (32)

Hence, although the finalized fragility curves of the buildings have to be derived by the nonlinear analysis of a finite element model (FEM) built in ANSYS 10.0 [4], the initial boundary conditions of the modeled structure have been calibrated in a way, so that the linear properties of the numerical model match the real-time recorded ones, as further clarified [7], [8].

18.2.1 Eigenfrequencies and Eigenvectors

Since the longitudinal modes of vibrations are expected to have the dominant influence on the response of the three-story modeled building, in the first step, the linear frequencies of the structures are detected by the analysis of the 'ambient In-site measurements', as shown per Fig. (1) and summarized per Table (1), below [7], [8].

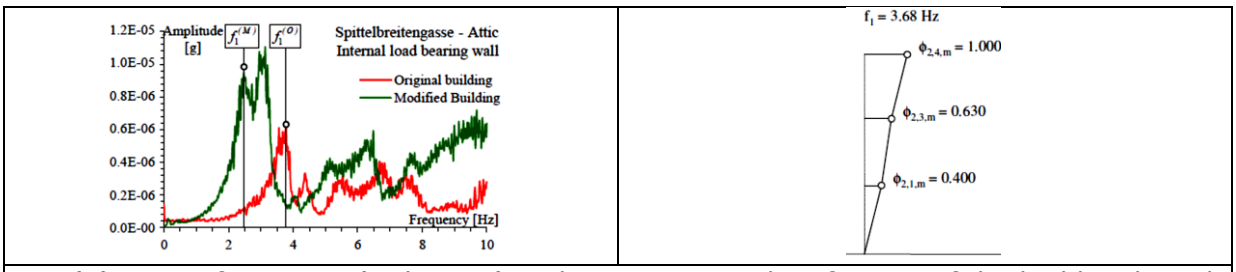

Fig (1). Eigen frequency (red curve) and eigen vector identification of the building based on the in-site measurments [7], [8]

Table (1). The experimentally recorded eigen frequencies of the building [8]

Mode No#	Frequency (Hz)
1	3.8
2	4.2
3	4.6

Once the eigen frequencies of the structure is derived, the calibration procedures will lead to an FEM model of which the linear properties correspond to the recorded real-time characteristics of the structure. This is to further imply that all the phenomena and interactions, having the potential to deviate the global behavior of the structure from the theoretically and initially assumed conditions are expected to be reflected in the numerical model, as well.

18.2.2 Modal Damping

Due to the information provided per reference [8], the averaged result of the damping values obtained from the decay trend of five separate records indicates Lehr's critical damping coefficient to be equal to $= 3.37\%$.

18.3 Numerical Finite Element Modeling

As aforementioned, the numerical analysis of the structural performance has been conducted, using ANSYS 10.0, where the macro-scale behavior of the masonry material have been modeled by the application of Shell 43 elements with inelastic capabilities [4], [5]. In addition, the floor slabs were simulated using Shell 63 elements and the structural interactions with the adjacent buildings have been introduced into the model by the insertion of Combin 14 elements, acting as the stiffeners. The geometry of the building in ANSYS 10.0 environment is reproduced per Fig. (2) [4].

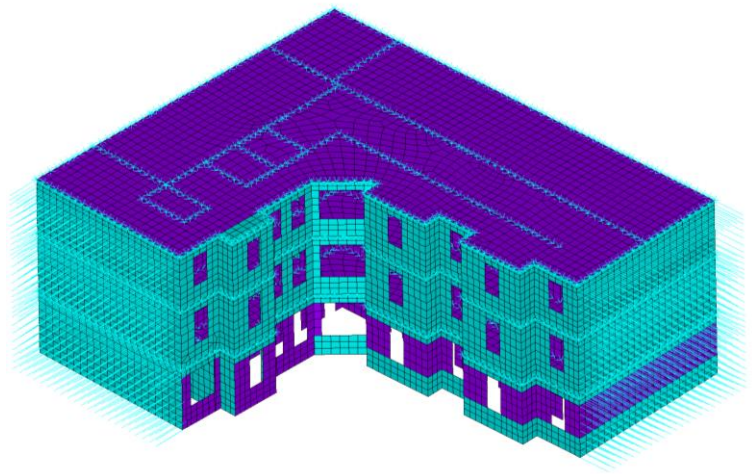

Fig (2). Geometry of the finite element model in ANSYS10.0 [4]

18.3.1 Finite Element Model Calibration

Since the initial theoretical values of the frequencies obtained by the finite element model varied slightly from the experimentally recorded ones summarized per Table (1),

the modulus of elasticity of the material was tuned in a way, so that the three longitudinal eigen frequencies of the structure fell within a tolerable vicinity of the recorded data, as documented per Table (2) [7]. For the sake of ease of comparison, the experimental values are reported in Table (2), once again and as well.

Table (2). The numerically and experimentally derived eigen frequencies of the building[7]

Mode No#	Frequency (Hz)	
	Recorded	Numerical
1	3.8	3.78
2	4.2	4.29
3	4.6	4.67

Figs. (2) and (3) show the first two calibrated mode shapes of the modeled structure using the finite element approach [7].

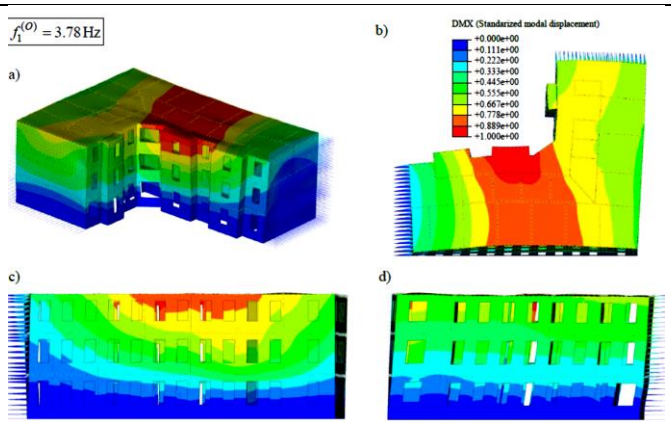

Fig (2). First longitudinal mode and eigen frequency of the calibrated model in ANSYS 10.0 [4], [7]

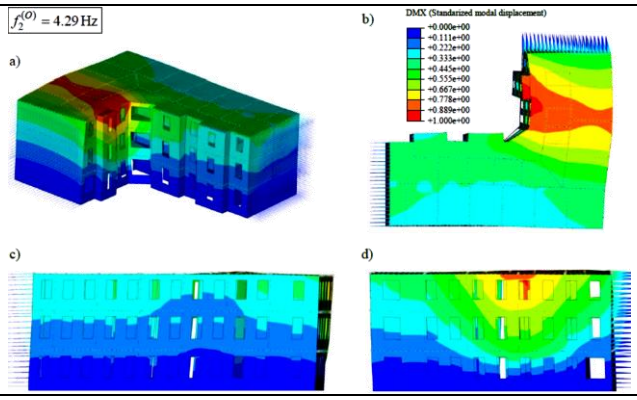

Fig (3). Second longitudinal mode and eigen frequency of the calibrated model in ANSYS 10.0 [4], [7]

18.3.2 Material Properties

The elastic properties of the masonry material, fitted to the desired frequencies of the building and the plastic Drucker- Prager criterion used to model the inelastic behavior of the structure are summarized in Table (3), where f_c, ϕ and ψ are the cohesion

coefficient, the angle of friction and dilatancy in the order of appearance and E is the modulus of elasticity. In this table, Poisson's ratio is also represented by the term υ[2] ,[3], [5], [7], [9], [10], [11].

Table (3). The material properties of the masonry structure[2], [3], [5], [11]

E	f_c	ϕ	φ	ν
(Pa)	(Pa)	Degree		-
1.15E+09	3.50E+05	30	30	0.2

18.3.3 Time History Analysis

In order to assess the vulnerability of the structure through the derivation of the fragility curves, the described calibrated model is subjected to the following seismic excitations per Table (4), where PGA, PGV and PGD parameters refer to the peak ground acceleration, velocity and displacement, respectively. However, since the fragility derivation is still in the trial and error procedures, the developed preliminary ones are constructed based on the performance of the model under smoothed resampled ground motions which might be the subject of modifications in the future. Moreover, it needs to be reminded that based on the seismicity of Austria, the earthquakes are chosen in a way not to reflect any obvious characteristics of a strong Near-Field one. In the other word, all the recording stations are at least $10\,km$ away from the ruptured fault and do not have any long period, high amplitude velocity and displacement records, as documented per Peer Berkeley Strong Ground Motion Database [12], [13], [14], [15]. Eventually, the numerical time history integration scheme has been set up to be "Newmark", incorporating the simultaneous effects of the two horizontal components of the ground motion excitation [4], [6], [16].

Table (4). Characteristics of the selected ground motions

Earthquake	Recording Station	Array	PGA (g)	PGV (cm/s)	PGD (cm)	Energy Density (cm^2/s)
Imperial Valley 1979	Elcentro Calipatra Fire Station	225	0.128	15.37	11.3	653.5
Imperial Valley 1979	Elcentro Calipatra Fire Station	315	0.078	13.62	13.85	445.069
Imperial Valley 1979	Elcentro 13	140	0.117	14.67	8.05	453.18
Imperial Valley 1979	Elcentro 13	230	0.139	13	5.94	422.33
Imperial Valley 1979	Elcentro Delta	262	0.238	26.015	12.79	4942.61
Imperial Valley 1979	Elcentro Delta	352	0.351	35	347.2	7791.2

18.4 *Numerical Evaluations and Arithmetic Statistics*

As entailed in the preceding sections, the up-to-date numerical model performance under the resampled-smoothed and scaled ground motions per Table (4), forms the basis of judgment of the intensity of damage within the structural elements under certain levels of hazard demand. Accordingly and based on the state-of-the-art on the

development of fragility curves at least in the preliminary phases, the interstory drifts and the PGA parameter of the ground motion have served to act as the response and demand indcators in the definition of the fragility calculations, as follows [17], [18], [19].

Referring to the definitions of the fragility functions as the probability of the occurrence or exceedance of a specific damage state to a structure under a certain level of ground motion, equation (34) will render the values, here after referred to as the fragility of the building [17], [20], [21].

$$Fragility = P(R_s > L_{DS}|HL_G) = 1 - P(R_s < L_{DS}|HL_G) \tag{34}$$

In equation (34), P refers to the probability function, R_s, the structural response, L_{DS}, the defined damage state limit corresponding to the type of the structural response evaluated and HL_G is the ground motion hazard level. Based on the theories of probability and statistics, the notation used in the aforementioned equation is representing a conditional probability [22].

In addition, the fragility discrete values are turned into a continuous function for each damage state, using a normal distribution density function for the obtained structural responses in each hazard level with the specific calculated mean and standard deviation. The following expressions mathematically formulate the statistical, explained procedures [23]

$$f(R_s; \mu, \sigma^2) = \frac{1}{\sigma\sqrt{2\pi}} e^{\frac{-(R_S-\mu)^2}{2\sigma^2}} \tag{35}$$

$$F(L_{DS}; \mu, \sigma^2) = \phi\left(\frac{L_{DS}-\mu}{\sigma}\right) = \frac{1}{2}\left[1 + erf\left(\frac{L_{DS}-\mu}{\sigma\sqrt{2}}\right)\right] \tag{36}$$

$$erf(x) = \frac{2}{\sqrt{\pi}} \int_0^x e^{-t^2} dt \tag{37}$$

$$Fragility = P(R_s > L_{DS}|HL_G) = 1 - \phi\left(\frac{L_{DS}-\mu}{\sigma}\right) \tag{38}$$

where f and F denote the probability density and the cumulative probability distributions, respectively. Moreover, μ and σ represent the mean and the standard deviations of the obtained structural responses in each defined hazard levels and the terms ϕ and erf are to refer to the cumulative distribution probability and error functions, in the order of appearance with t and x as the dummy variables to define the error function. All the other terms hold their definitions as stated elsewhere.

As previously clarified in the 'Introduction' to this document, since the analysis verification procedures have not been finalized yet, the obtained structural responses and the corresponding fragility curves represented in this document could only serve as a preliminary indicator of the expected damage intensity. Nevertheless, the numerical values required in the calculation procedures per equations (34) to (38) are summarized in Tables (5) and (6) below and the corresponding fragility curves are further depicted in Figs. (4) and (5). The term L_{DS} in the aforementioned tables refers to the acceptance limit state of each damage state in terms of interstroy drift ratios, as defined per FEMA HAZUS [17].

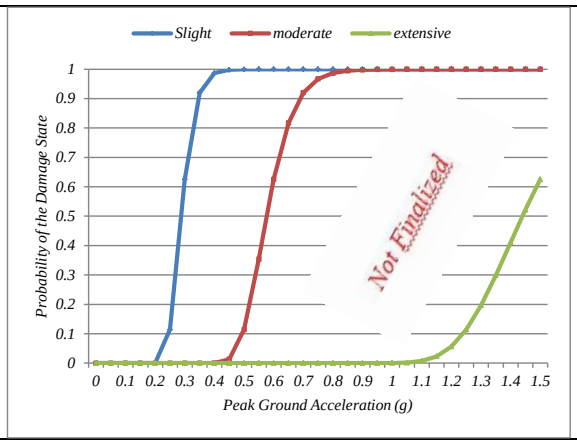

Fig (4). Preliminary fragility curves of the building in the X direction

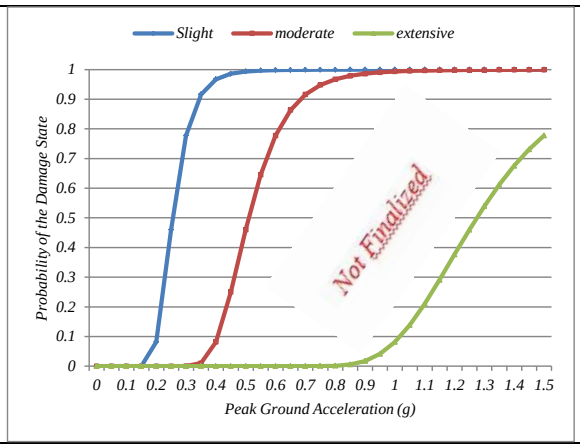

Fig (5). Preliminary fragility curves of the building in the Y direction

Table (5). The fragility calculations for different levels of damage states in the X direction

Hazard Level	0	0.05	0.1	0.15	0.2	0.25	0.3	0.35	0.4	0.45	0.9	0.95	1	1.05	1.1	1.15	1.2	1.25	1.3	1.35	1.4	1.45	1.5	PGA(g)	
Structural Inter-Story Drift Ratio	0	0.0002	0.0005	0.0007	0.0010	0.0012	0.0014	0.0017	0.0019	0.0021	0.0043	0.0045	0.0048	0.0050	0.0052	0.0055	0.0057	0.0060	0.0062	0.0064	0.0067	0.0069	0.0071	Elcentro Calipatra Fire Station 225	Earthquake
	0	0.0003	0.0006	0.0009	0.0012	0.0015	0.0018	0.0021	0.0024	0.0027	0.0055	0.0058	0.0061	0.0064	0.0067	0.0070	0.0073	0.0076	0.0079	0.0082	0.0085	0.0088	0.0091	Elcentro 13-140	
	0	0.0003	0.0006	0.0009	0.0012	0.0015	0.0017	0.0020	0.0023	0.0026	0.0052	0.0055	0.0058	0.0061	0.0064	0.0067	0.0070	0.0073	0.0076	0.0078	0.0081	0.0084	0.0087	Elcentro Delta 262	
Mean	0	0.0003	0.0045	0.0068	0.0090	0.0113	0.0135	0.0158	0.0181	0.0203	0.0406	0.0429	0.0452	0.0474	0.0497	0.0519	0.0542	0.0565	0.0587	0.0610	0.0632	0.0655	0.0677	μ	
Standard Deviation	0	0.000035	0.000035	0.000035	0.000035	0.000035	0.000035	0.000035	0.000035	0.000035	0.000035	0.000035	0.000035	0.000035	0.000035	0.000035	0.000035	0.000035	0.000035	0.000035	0.000035	0.000035	0.000035	σ	
Fragility (Eq 11)	0	0.0000	0.0000	0.0000	0.0002	0.1139	0.6250	0.9204	0.9869	0.9979	1.0000	1.0000	1.0000	1.0000	1.0000	1.0000	1.0000	1.0000	1.0000	1.0000	1.0000	1.0000	1.0000	L_{DS}=0.0016	Damage States
	0	0.0000	0.0000	0.0000	0.0000	0.0000	0.0000	0.0000	0.0002	0.0131	0.9979	0.9991	0.9996	0.9998	0.9999	1.0000	1.0000	1.0000	1.0000	1.0000	1.0000	1.0000	1.0000	L_{DS}=0.0032	
	0	0.0000	0.0000	0.0000	0.0000	0.0000	0.0000	0.0000	0.0000	0.0000	0.0000	0.0000	0.0002	0.0016	0.0071	0.0227	0.0562	0.1139	0.1965	0.2986	0.4106	0.5222	0.6250	L_{DS}=0.008	

≈continues≈

Table (6). The fragility calculations for different levels of damage states in the Y direction

Hazard Level	0	0.05	0.1	0.15	0.2	0.25	0.3	0.35	0.4	0.95	1	1.05	1.1	1.15	1.2	1.25	1.3	1.35	1.4	1.45	1.5	PGA(g)	
Structural Inter-Story Drift Ratio	0	0.0003	0.0005	0.0008	0.0011	0.0013	0.0016	0.0019	0.0021	0.0051	0.0053	0.0056	0.0059	0.0061	0.0064	0.0067	0.0069	0.0072	0.0075	0.0077	0.0080	Elcentro Calipatra Fire Station 225	Earthquake
	0	0.0004	0.0008	0.0012	0.0015	0.0019	0.0023	0.0027	0.0031	0.0073	0.0077	0.0081	0.0084	0.0088	0.0092	0.0096	0.0100	0.0104	0.0107	0.0111	0.0115	Elcentro 13-140	
	0	0.0003	0.0006	0.0009	0.0012	0.0015	0.0017	0.0020	0.0023	0.0055	0.0058	0.0061	0.0064	0.0067	0.0070	0.0073	0.0076	0.0078	0.0081	0.0084	0.0087	Elcentro Delta 262	
Mean	0	0.0003	0.0003	0.0003	0.0003	0.0003	0.0003	0.0003	0.0003	0.0003	0.0003	0.0003	0.0003	0.0003	0.0003	0.0003	0.0003	0.0003	0.0003	0.0003	0.0003	μ	
Standard Deviation	0	0.000062	0.000062	0.000062	0.000062	0.000062	0.000062	0.000062	0.000062	0.000062	0.000062	0.000062	0.000062	0.000062	0.000062	0.000062	0.000062	0.000062	0.000062	0.000062	0.000062	σ	
Fragility (Eq 11)	0	0.0000	0.0000	0.0002	0.0816	0.4605	0.7776	0.9163	0.9674	0.9999	0.9999	0.9999	1.0000	1.0000	1.0000	1.0000	1.0000	1.0000	1.0000	1.0000	1.0000	L_{DS}=0.0016	Damage Sta
	0	0.0000	0.0000	0.0000	0.0000	0.0000	0.0002	0.0102	0.0816	0.9907	0.9936	0.9955	0.9968	0.9977	0.9983	0.9987	0.9990	0.9992	0.9994	0.9995	0.9996	L_{DS}=0.0032	
	0	0.0000	0.0000	0.0000	0.0000	0.0000	0.0000	0.0000	0.0000	0.0414	0.0816	0.1388	0.2102	0.2913	0.3764	0.4605	0.5398	0.6120	0.6757	0.7308	0.7776	L_{DS}=0.008	

≈continues≈

18.5 *Summary and Future Work*

As explicitly entailed in the preceding sections, this manuscript focuses on the derivation of the "real-time" fragility curves of the masonry structures via the tuning of the built up analytical model to the recorded identified dynamic characteristics of the building. Hence, first processing the 'In-Site' ambient vibration measurements of the old three-story masonry building located at "Spittelbreitengasse", Vienna, Austria, the as-of-the-date eigen frequencies and damping parameters of the linear system have been derived [7], [8]. In the second step, once the linear elastic finite element model of the building, simulated in ANSYS 10.0 environment, is modified in a way such that the modal frequencies and damping ratios of the FE model match those obtained by the measurements, the whole structure is subjected to nonlinear seismic time history analyses under the "scaled-resampled-smoothed" excitations built on the basis of three different earthquakes retrieved from Peer Berkeley Strong Ground Motion Data Base [4], [15]. Accordingly, the comparison of the performance of the structure with the defined acceptance criteria corresponding to each level of the damage intensity per FEMA HAZUS, forms the basis of the subsequent statistical calculations towards the derivation of the fragility curves, depicted in Figs. (4) and (5) [17]. Clearly, for any further information not covered in details in this summary section, the reader may refer to the main body of the text and/or directly consult the referred documents.

Although the fragility curves shown per Figs. (4) and (5) are derived following the above procedures, the numerical calculations are not declared finalized as long as the coupled seismic performance of the structure under the defined nonlinear scheme is still under additional investigations. This is to further imply and emphasize on the fact that the represented preliminary curves might be the subject of future modifications.

As more detailed information regarding the simulation of the specific masonry material characteristics is being examined, the future contributions by the technical engaged staff at "Vienna Consulting Engineers" could include the verification of the derived fragility curves, applying the most updated material properties of the masonry specimens under the actual and non-resampled, non-smoothed earthquake excitations. Upon the validity of the required information, the task may extend to involve the performance of the building in a modified situation where some walls and partitions have been removed [7], [8].

19. Conclusion

Since the first introduction of the concept of fragility curves in the safety assessment of nuclear power plants, there has been an ongoing effort towards the generalization of the methodology for the vulnerability and risk assessment of various structures, specially but not specifically within the Civil Engineering applications[22],[23],[24],[25].

Furthermore and based on the definition of the seismic fragility of any arbitrary object, the analytical procedures should target the evaluation of the probability of reaching or exceeding a certain damage level under a specific demand state, here taken to be the ground motion hazard level[26],[27],[28],. As abundantly declared in the preceding sections and with the aim of first deriving the "definition-based real time" fragility curves of the structure for the "as-of-the-date" condition and consequently idealizing the derived

curve, serving as the exact reference, by a lognormal distributed cumulative function, the following steps were taken of which the results were carefully presented in sections (2) and (3). It needs to be reminded that all the numerical evaluations have been specifically performed, using the actual recorded data of the unreinforced masonry building at "Fendigasse" so that the derived diagrams and functions could be interpreted as the 'real-time' properties of the structure under consideration. Clearly, for any detailed information not entailed in this summary section, the reader may consult the main body of the text and/or further the referred manuscripts and technical literature.

Quoting from the structural fragility definition, the following three elements are the main components of constructing such curves by analytical approaches.

- The ground motion hazard level

Based on the vast literature at hand, the bizarre nature of the earthquakes, all categorized under the same natural hazard class though with far different characteristics might not easily allow for the determination of the best parameter to characterize the ground motion destructive potential. However, in this specific case, the PGA of the earthquakes was selected to serve as the ground motions hazard level indicators[12],[14],[15],[29],[30],[31]. The selected acceleration time histories were chosen in a way not to possess any significant Near-Field effects regarding the seismicity of the area.

- The evaluated structural response

Since the calculation of the probability of reaching or exceeding a certain damage state undeniably calls for the assessment of the structural behavior either in terms of the force-based actions or displacement-based reactions, the inter-story drift ratio of the structure derived by a direct linear time history analysis for both the forced and free phases of vibration was selected to form the base of justice for the structural dynamic performances. The two points of emphasis could be first the application of the updated frequencies, masses, mode shapes and damping coefficients of the building into the "Duhamel" integral, equation (5), according to the in-site measurements recorded by the "Vienna Consulting Engineers" staff, and second, the implementation of the linear time history analysis results towards the derivation of the fragility curves for the damage states higher than the "slight" one where the materials plasticity are playing an important role. However, this matter has been justified by the author of this Appendix B that the similarity of the displacements in the linear and nonlinear analyses could be a sufficiently accurate assumptions for the defined level of the project, as "Phase 0". Should sufficient information regarding the inelastic behavior of the material be at hand, the latter assumption could be relaxed and be re-validated via the plastically analyzed responses[32]. As aforementioned, the linear time history analysis of the one-dimensional mass-spring modeled system in "Fortran 95" programing environment resulted into the derivation of the maximum inter-story drift of the structure under each hazard level and applied towards the derivation of probability density function of the structural response and consequently the cumulative probability distribution function of which the adjoin is taken to be the structural fragility at the defined ground motion hazard level verses different structural damage states.

- The damage state limits

The damage state thresholds in the ordinary structural applications are defined based on the evaluation of the capacity curves of the structure in a nonlinear static scheme which by and large needs the analysis of a sufficiently large group of buildings, all of the same type. Though even such detailed time consuming analysis results have been well challenged regarding the compatibility of the responses with those obtained by a dynamic time history analysis, the inter-story damage state limits defined per FEMA HAZUS and obtained by the application of the push over analysis to buildings of the same type have been used in the current project[5],[30].

Once the "definition-based real-time" fragility curves were derived using equation (21), the idealization of the obtained curves by lognormal cumulative probability functions in terms of the defined ground motion hazard level and the corresponding mean and standard deviations of the logarithmized parameter resulted into a family of statistic "self-induced" fragility functions by the application of equation (22) with the back calculated data from equation (26). As noticed per Figs. (7) to (14), the "definition-based" fragility curves do not resemble a unique lognormal cumulative probability function, hence, instead of a single pair of the mean and standard deviations, a family of such pairs have been calculated at each defined damage state and for the two horizontal orthogonal directions. Despite the fact that the selection of the best statistically fitted curve essentially requires an engineering judgment, oriented towards the specific matters of considerations in the specially defined project, the samples of the so-called best fitted curves and the statistical characteristics have been shown in Figs. (15) and (16).

Moreover, the following flow chart in Fig. (17) once again summarizes the taken steps towards the derivation of the both the "definition-based real time" fragility curves and the corresponding "self-induced" fragility functions.

20. Reference list

[1] Boroumand, P., "Real-Time Fragility Curves: Outlines of the plausibility considerations", Vienna Consulting Engineers Internal Report

[2] Burningham, C., Mosqueda, G., and Saavedra, R.R., "COMPARISON OF SEISMIC FRAGILITY OF FREE STANDING EQUIPMENT USING CURRENT TESTING PROTOCOLS AND RECORDED BUILDING FLOOR MOTIONS", Retrieved online from http://mceer.buffalo.edu/education/reu/2007/content/20Burningham.pdf on 16/3/2012

[3] Chon, Y-S., and Elnashai, A.S., "A simplified framework for probabilistic earthquake loss estimation", *J. Prob. Eng. Mech.,* 25 (2010) 355-364

[4] Michel, C., and Gueguen, P., and Causse, M., "Seismic vulnerability assessment to slight damage based on experimental modal parameters", *J. Earthquake Engng Struct. Dyn.*, 41(2012) 81-98

[5] FEMA. HAZUS-MH MR3 Technical Manual. Federal Emergency Management Agency, Washington, DC, U.S.A., 2003

[6] Chopra, A.K., "Dynamics of Structures - Theory and applications to Earthquake Engineering", Pearson Education Asia Limited and Tsinghua University Press, Beijing, 2001

[7] Schäfer, D., "Report on the measurements at Fendigasse", Vienna Consulting Engineers Internal Report

[8] Achs, G. *et al*, "Erdbeben im Wiener Becken", Vienna Consulting Engineers, Vienna, Austria, Oct 2011

[9] Rahai, A.R., "DESIGN and CALCULATION REINFORCED CONCERETE STRUCTURES", (Persian), Amirkabir University of Technology (Tehran Polytechnic), Tehran, Iran, 2004

[10] R. W. Clough, J. Penzien, Dynamics of Structures, Mc-Graw Hill Inc., New York, 1975

[11] "Famos Data Analysis Software", imc Meßsysteme GmbH Company, Germany

[12] Cosenza, E., and Manfredi, G., "Damage indices and damage measures", Prog. Struct. Engng Mater. 2 (2000) 50–59

[13] Rossetto T., and Elnashai, A., "A new analytical procedures for the derivation of displacement-based vulnerability curves for populations of RC structures", *J. Engng Struct.*, 27 (2005) 397-409

[14] "Peer Berkeley Strong Ground Motion Data Base", Retrieved online from http://peer.berkeley.edu/smcat/ on 20/5/2012

[15] "Impulsive Near-Field Earthquake Ground Motions", Retrieved online from http://nisee.berkeley.edu/data/strong_motion/sacsteel/motions/nearfault.html on 20/5/2012

[16] Silverfrost FTN95: "Fortran for Windows", http://www.silverfrost.com/default.aspx

[17] Hosseini, M., and Majd, M., "Developing Fragility Curves for Regular Steel Buildings with X-Bracing Using Nonlinear Time History" (Persian), *Sharif J Civil Engng*., 27 (2011) 3-13

[18] McPherson, G. "Statistics in scientific investigation: its basis, application and interpretation", Springer-Verlag. ISBN 0-387-97137-8, 1990

[19] Porter, K., Kennedy, R., Bachman, R., "Creating Fragility Functions for Performance-Based Earthquake Engineering", *Earthquake Spectra*, 23(2007) 471-489

[20] Aitchison, J., and Brown, J.A.C., "The Lognormal Distribution, Cambridge University Press, 1957

[21] Andrews, Larry C., "Special functions of mathematics for engineers"

[22] Zenter, I., Nadjarian, A., Humbert, N., and Viallet, E., "NUMERIAL CALCULATION OF FRAGILITY CURVES FOR PROBABILISTIC SRISMIC RISK ASSERSSMENT", the 14th World Conference on Earthquake Engineering, Beijing, China, 2008

[23]. Schultz, M.T., Gouldby, B.P., Simm, J.D., and Wibowo, J.L., "Beyond the Factor of Safety: Developing Fragility Curves to Characterize System Reliability- ERDC SR-10-1", US Army Corps of Engineers, Engineer Research and Development Center, Washington D.C, USA, 2010

[24] Kaplan, S., Perla, H. G., and Bley, D. C., "A methodology for seismic analysis at nuclear power plants", *Risk Analysis,* 3(1983) 169–180

[25] Kennedy, R. P., Cornell, C. A., Campbell, R. D, S. Kaplan, and Perla, H. F. "Probabilistic seismic safety study of an existing nuclear power plant", *Nuclear Engineering and Design*, 59(1980) 315–338.

[26] Antl, P., Achs, G., and Wenzel, H., "Assessment of historic residential buildings using fragility curves", International Conference on Performance-Based Design in Earthquake Geotechnical Engineering – from case history to practice, Tsukuba, Japan, 2009

[27] Lumantarna, E., Vaculik, J., Griffith, M., Lam, N., and Wilson, J., "Seismic fragility curves for un-reinforced masonry walls", Earthquake Engineering in Australia, Canberra, Australia, 2006

[28] Lin, A-L., Elnashai, A.S., and Spencer, Jr., "AN INTEGRATED EATHQUAKE IMPACT ASSESSMNET SYSTEM", 8th International Conference on Urban Earthquake Engineering, Tokyo, Japan, 2011

[29] Michel, C., and Philippe, G., "Seismic vulnerability analysis of moderate seismicity areas using in situ experimental techniques: from the building to the city scale-Application to Grenoble and Pointe-a-Pitre (France)", Retrieved online from http://arxiv.org/ftp/arxiv/papers/0907/0907.1735.pdf on 19/4/2012

[30] Boroumand, P., "Application of Performance-Based Design in Base-Isolated Steel Structures Under Near-Field Ground Motions"(Persian), MSc Thesis, Amirkabir University of Technology (Tehran Polytechnic), Tehran, Iran, 2008

[31] Ghodrati Amiri, G., ABDOLLAHZADE DARZI, G., and RAZAVIAN AMREI, S.A., "NEAR-FIELD EARTHQUAKE EFFECTS ON IRANIAN DESIGN BASIS ACCELERATION FOR TEHRAN", 13th World Conference on Earthquake Engineering Vancouver, B.C., Canada, 2004

[32] ASCE (2000). "FEMA 356 Prestandard and Commentary for the Seismic Rehabilitation of Buildings", ASCE for the Federal Emergency Management Agency, Washington, D.C., November 2000

[33] Rota, M., Penna, A., and Magenes, G., "A PROCEDURE FOR DERIVING ANALYTICAL FRAGILITY CURVES FOR MASONRY BUILDINGS", the 14th World Conference on Earthquake Engineering, Beijing, China, 2008

[34] Kwon, O-S., and Elnashai, A.S., "The effect of material and ground motion uncertainty on the seismic vulnerability curves of RC structure", *J. Engng. Struct*., 28 (2006) 289-303

Appendix C:

AHEPA hospital in Thessaloniki

KU Leuven

21. Introduction

The AHEPA hospital in Thessaloniki, Greece is a seven-story reinforced concrete structure with basement.

The building is instrumented with the purpose of an early earthquake warning system and structural health monitoring.

There are 13 triaxial accelerometers available. For the time being they are installed as follows: one at the basement, one at the 1st floor, 4 at the middle and 7 at the top floor (Figure 1).

This study aims to apply an Optimal Sensor Location (OSL) algorithm to see if relevant modes could be identified with the available set of accelerometers and to investigate other (better) sensor distributions.

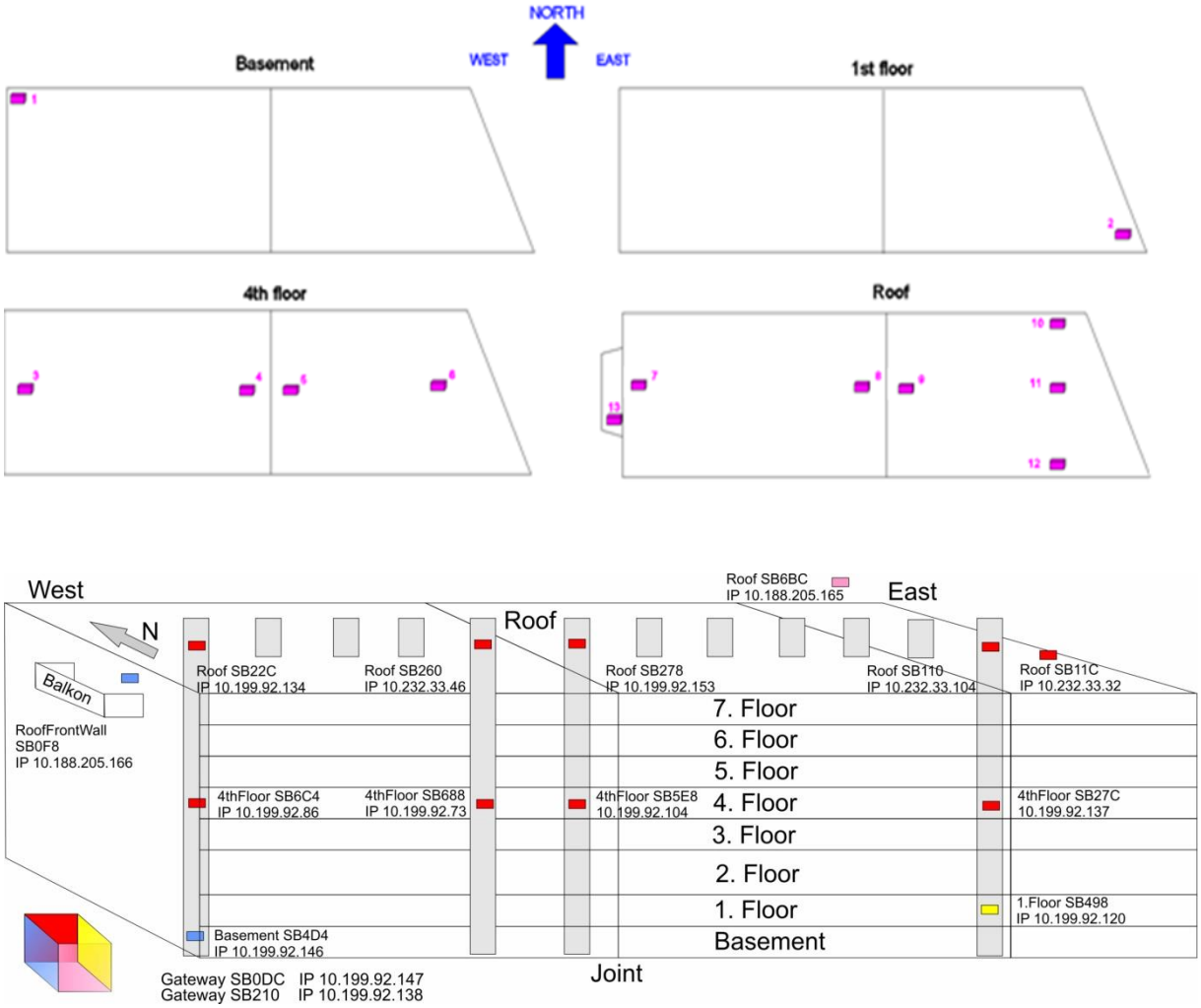

Figure 1: The instrumented building.

The various sensors communicate with each other via a wireless system that exploits the routing concept. All acquired data are transferred to the Seiscomp3 server through the seedlink real-time data acquisition protocol.

A numerical model of the hospital is built with SAP2000. The first seven modes that correspond to the 90% modal participation mass ratio have been extracted. The objective of the instrumentation is to capture as many of these modes as possible.

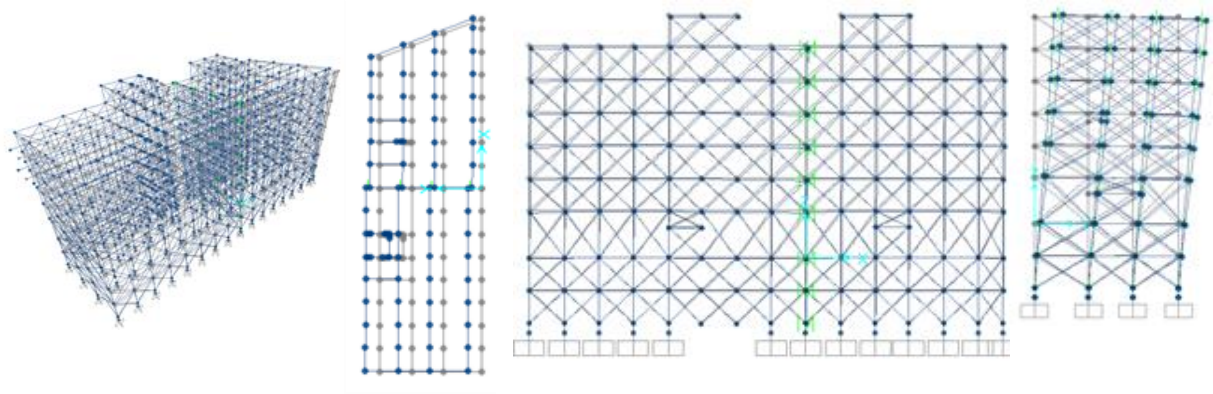

(a) (b) (c) (d)

Figure 2: Mode 1, f = 1.48 Hz, bending mode in the face direction. (a) 3D view, (b) top view, (c) face view, (d) side view.

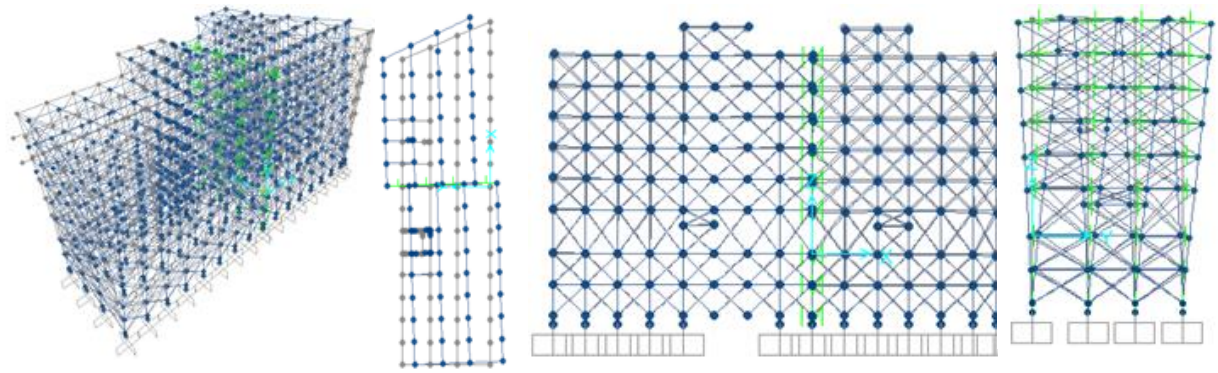

(a) (b) (c) (d)

Figure 3: Mode 2, f = 1.61 Hz, bending mode in the face direction. (a) 3D view, (b) top view, (c) face view, (d) side view.

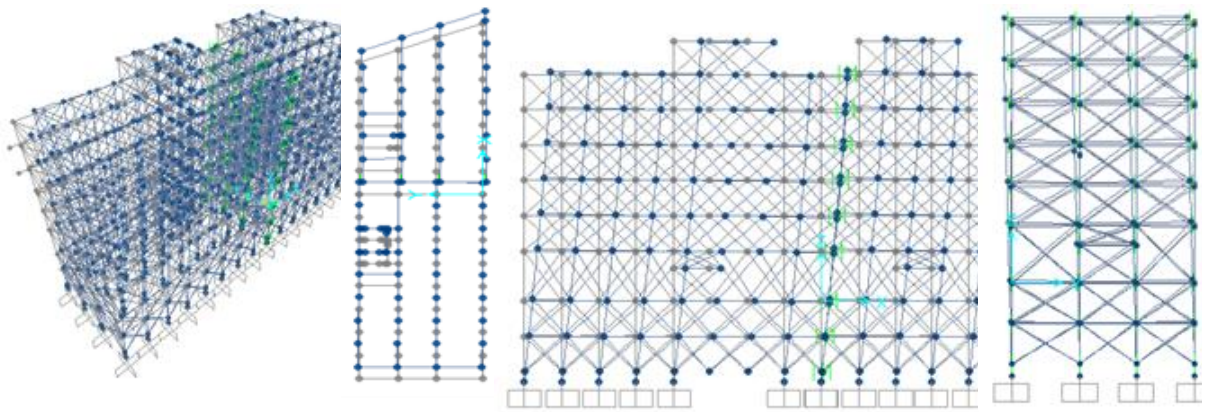

(a) (b) (c) (d)

Figure 4: Mode 3, f = 2.06 Hz, bending mode in the side direction. (a) 3D view, (b) top view, (c) face view, (d) side view.

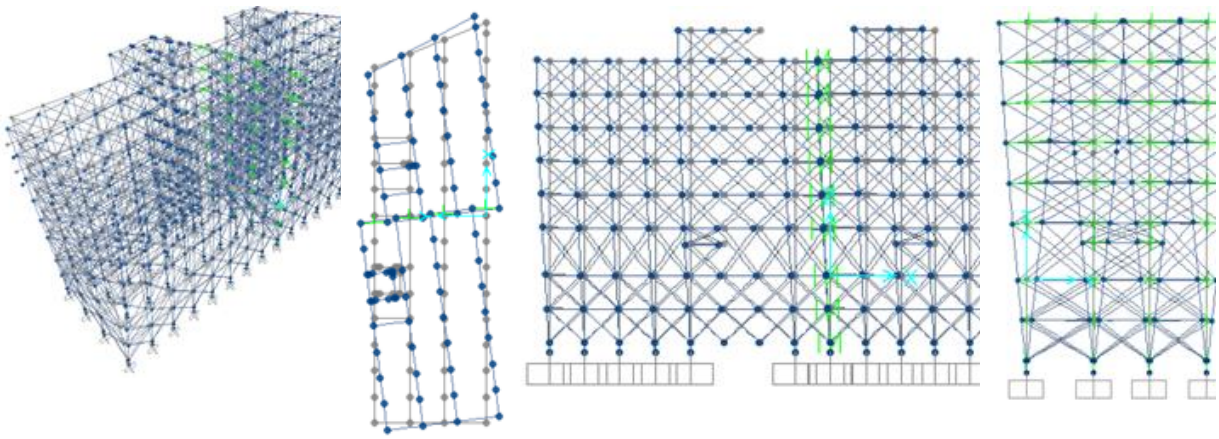

(a) (b) (c) (d)

Figure 5: Mode 4, f = 2.87 Hz, torsion mode. (a) 3D view, (b) top view, (c) face view, (d) side view.

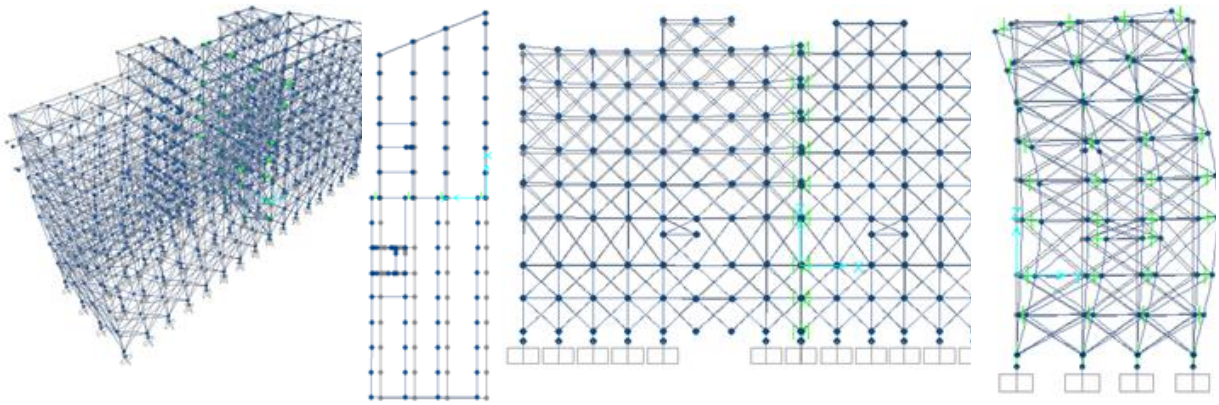

(a) (b) (c) (d)

Figure 6: Mode 5, f = 4.49 Hz, bending mode in the side direction. (a) 3D view, (b) top view, (c) face view, (d) side view.

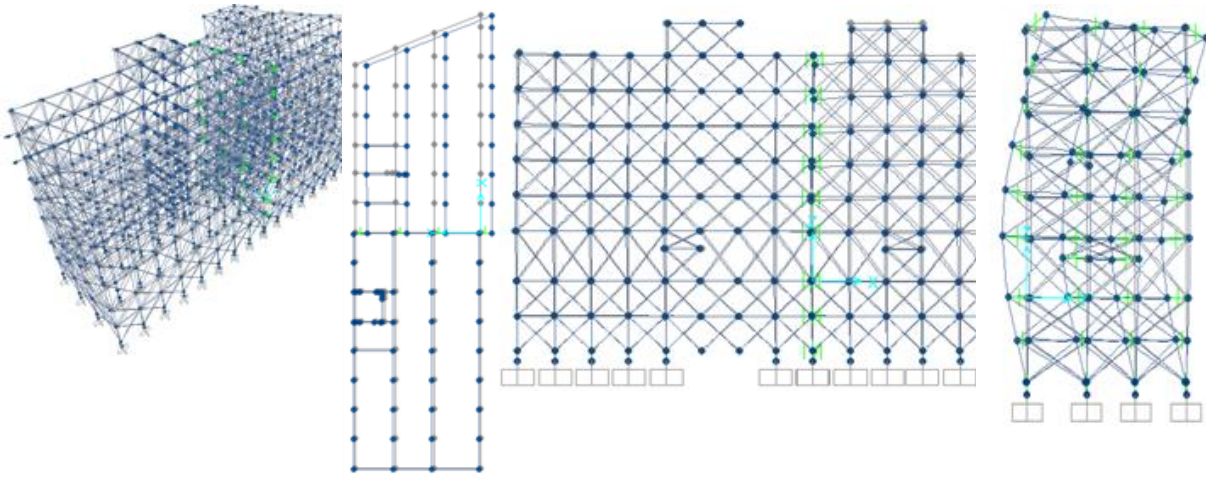

(a) (b) (c) (d)

Figure 7: Mode 6, f = 4.62 Hz, bending mode in the side direction. (a) 3D view, (b) top view, (c) face view, (d) side view.

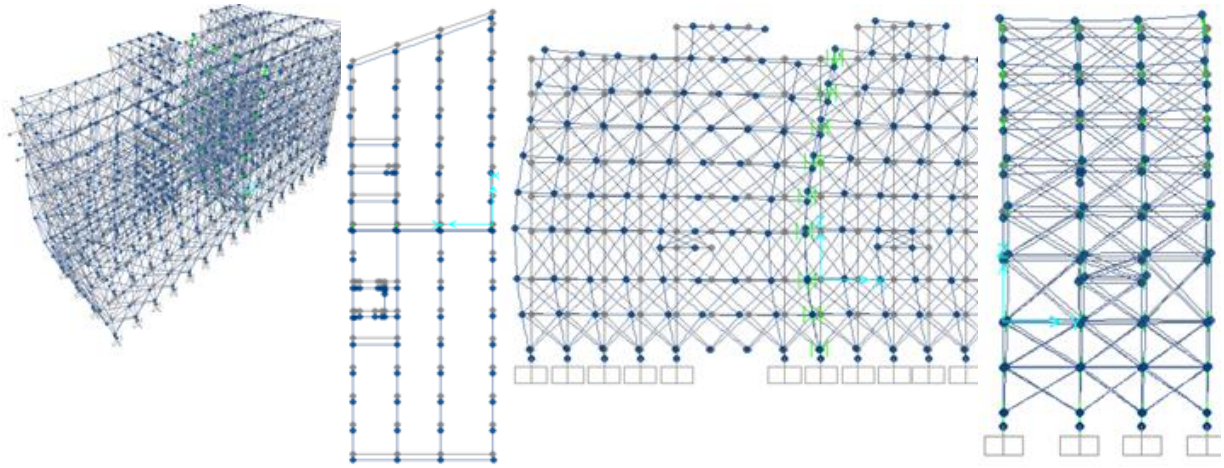

(a) (b) (c) (d)

Figure 8: Mode 7, f = 60.4 Hz, bending mode in the face direction. (a) 3D view, (b) top view, (c) face view, (d) side view.

22. Optimal sensor location

22.1 *Algorithm*

Papadimitriou and Lombaert[1] propose to choose the sensor locations so that the uncertainty of the identified modal coordinates, as measured by their information entropy, is minimized. When $\boldsymbol{y}_k$ denotes the measured response, $\boldsymbol{\Phi}$ the matrix with mode shapes computed from the preliminary finite element model, $\boldsymbol{\xi}_k$ the modal coordinates corresponding to this model and $\boldsymbol{e}_k$ the prediction error due to both modeling inaccuracies and measurement errors, the relationship between the measured response and the modal coordinates of the finite element model is

$$\boldsymbol{y}_k = \boldsymbol{L}[\Phi\boldsymbol{\xi}_k + \boldsymbol{e}_k] \quad (1)$$

where $\boldsymbol{L}$ denotes the observation matrix. This matrix is comprised of ones and zeros and maps, for a given configuration, the measured DOFs to the DOFs of the finite element model. Determining the optimal sensor configuration boils down to choosing the observation matrix $\boldsymbol{L}$ in such a way that the information entropy of the estimated modal coordinates ξk is minimized. This is equivalent to maximizing the determinant of the Fisher information matrix of $\boldsymbol{\xi}_k$ (as a function of $\boldsymbol{L}$), which reads

$$\boldsymbol{Q}(\boldsymbol{L};\boldsymbol{\Sigma}) = (\boldsymbol{L\Phi})^T\ (\boldsymbol{L\Sigma L}^T\ )^{-1}(\boldsymbol{L\Phi}) \quad (2)$$

where $\boldsymbol{\Sigma}$ denotes the covariance matrix of the prediction error $\boldsymbol{e}_k$.

Since the objective function det($\boldsymbol{L}$;$\boldsymbol{\Sigma}$) depends on the covariance of the prediction error $\boldsymbol{e}_k$, the same holds for the optimal sensor configuration. The following model for the prediction error covariance was proposed in [1]:

$$\Sigma_{ij} = \mathrm{E}[e_{k,i}e_{k,j}] = \sqrt{(\Sigma_{ii}\Sigma_{jj})}\ \exp(-\delta_{ij}/\lambda) \quad (3)$$

where δ_{ij} denotes the distance between DOFs i and j, and λ is a scalar defining the degree of spatial correlation, called the correlation length. A value of $\lambda = 0$ means there is no correlation in the prediction error between any two measurement DOFs. A low value of λ means that the prediction error in two close DOFs is highly correlated, while the correlation is low for DOFs that are spatially far apart. A high value of λ denotes a large degree of correlation amongst all DOFs. The correlation length is a priori assumed within the characteristic length of the highest contributing mode.

Two heuristic sequential sensor placement (SSP) algorithms, the forward (FSSP) and the backward (BSSP), were proposed for solving the optimal sensor configuration problem as formulated in Equation (2). FSSP initiates with no sensor. The positions of sensors are computed sequentially by placing one sensor at a time in the structure at a position that results in the highest reduction in information entropy, i.e., in the most informative DOF. Specifically, at each iteration, combinations with an additional sensor to the previous configuration are considered, and the information entropies of all new sensor configurations are evaluated. The configuration with a minimal information entropy value is selected. On the contrary, BSSP is accomplished in an reverse order, starting with sensors placed at all measurable DOFs on the structure and removing successively one sensor at a time from the position that results in the smallest increase in the information entropy. It is advisable to combine results of both SSP algorithms.

[1] C. Papadimitriou, G. Lombaert, ***The effect of prediction error correlation on optimal sensor placement in structural dynamics***, Mechanical Systems and Signal Processing 28 (2012) 105-127.

An information entropy index (IEI) was also introduced as a normalized value to compare the difference between any configuration to the full configuration $\boldsymbol{L}_{full}$ where all possible measurement locations are equipped with sensors:

$$\mathrm{IEI} = \left[\frac{\det \boldsymbol{Q}(\boldsymbol{L}_{\boldsymbol{full}}, \boldsymbol{\Sigma})}{\det \boldsymbol{Q}(\boldsymbol{L}, \boldsymbol{\Sigma})}\right]^{1/2} \tag{4}$$

As from Equation (4), IEI is a function of three variables that are unknown in the design stage. These variables are the number of sensors employed, their configuration and the prediction error correlation matrix among different channels. A large value of IEI means that the information content is small in relation to reference configuration. IEI should go down to unity as the number of sensors deployed approaches the reference mesh.

22.2 *Measurement design of the hospital building*

The building is simplified to a 'plane' structure as in Figure 2. The sensors are assumed only instrumented on that plane only.

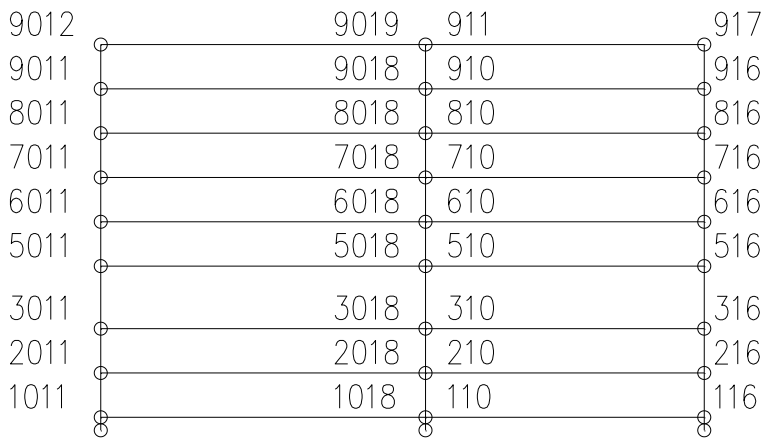

Figure 2: The location mesh for instrumentation.

If classical uni-directional sensors are used, intuition may guide the installation design. However, with the advent of triaxial sensors, designing for permanent monitoring based on engineering judgment is more challenging since one has to look at mode shapes in three directions. From this viewpoint, the optimal sensor placement strategy can be a very useful design tool in (i) reasoning how many sensors are enough to acquire the intended information; (ii) to locate them in an optimal configuration.

The correlation length is chosen within the distance between three consecutive floors, that is 5.01 m. It is assumed that there is no correlation among the vertical and two lateral directions.

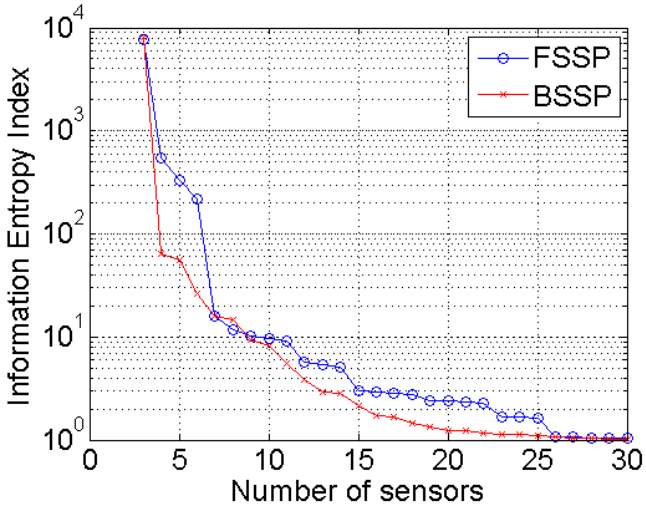

Figure 3: The IEI when using 7 modes for two connected buildings.

The IEI in Figure 3 suggests that at least 20 triaxial sensors have to be used in order to get a good quality of the information content for mode prediction. However, the less sensors are available. The following figures show the arrangement of triaxial sensors (from 1 to 14).

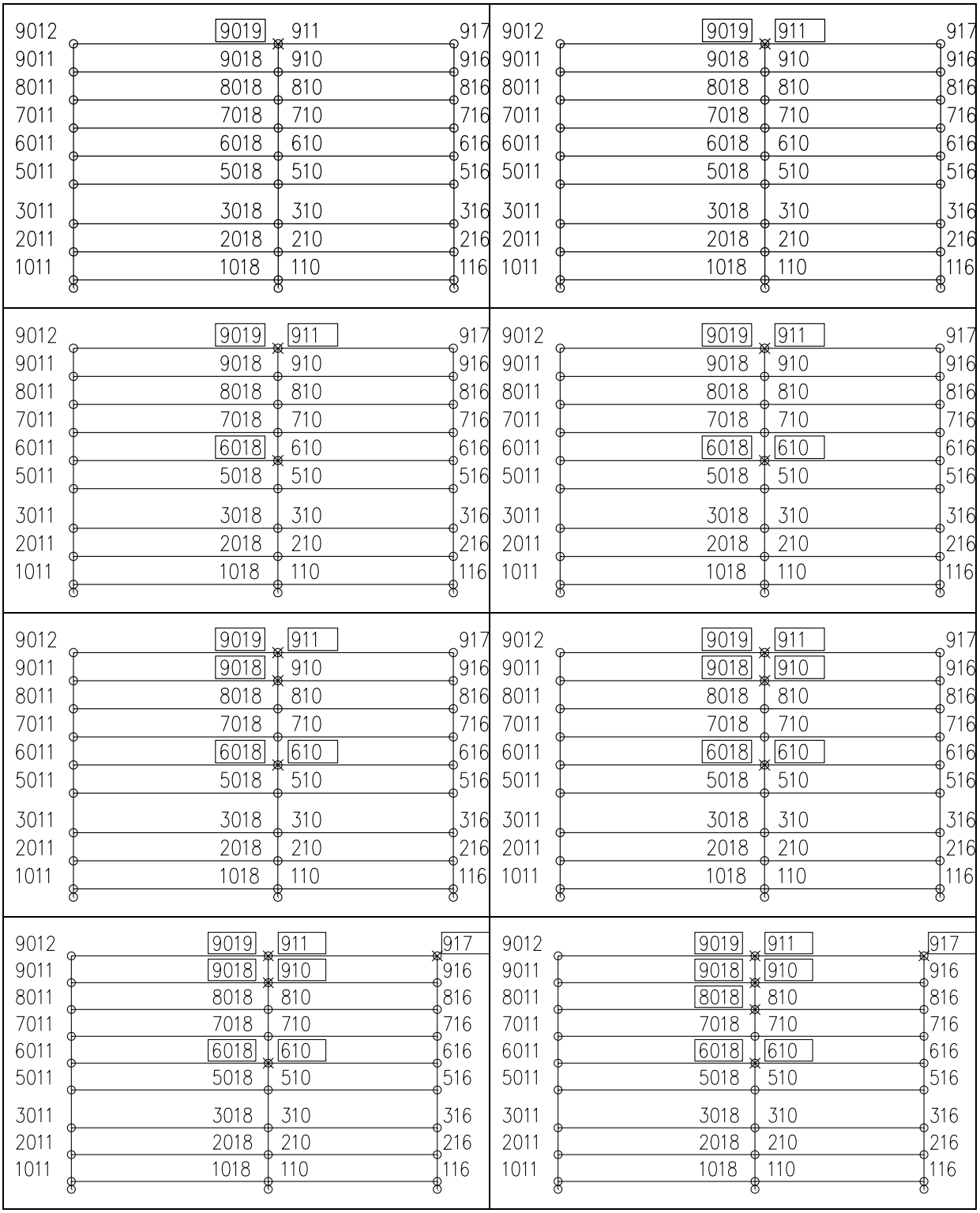
9012 9019 911 917
9011 9018 910 916
8011 8018 810 816
7011 7018 710 716
6011 6018 610 616
5011 5018 510 516
3011 3018 310 316
2011 2018 210 216
1011 1018 110 116
9012 9019 911 917
9011 9018 910 916
8011 8018 810 816
7011 7018 710 716
6011 6018 610 616
5011 5018 510 516
3011 3018 310 316
2011 2018 210 216
1011 1018 110 116
9012 9019 911 917
9011 9018 910 916
8011 8018 810 816
7011 7018 710 716
6011 6018 610 616
5011 5018 510 516
3011 3018 310 316
2011 2018 210 216
1011 1018 110 116
9012 9019 911 917
9011 9018 910 916
8011 8018 810 816
7011 7018 710 716
6011 6018 610 616
5011 5018 510 516
3011 3018 310 316
2011 2018 210 216
1011 1018 110 116
9012 9019 911 917
9011 9018 910 916
8011 8018 810 816
7011 7018 710 716
6011 6018 610 616
5011 5018 510 516
3011 3018 310 316
2011 2018 210 216
1011 1018 110 116
9012 9019 911 917
9011 9018 910 916
8011 8018 810 816
7011 7018 710 716
6011 6018 610 616
5011 5018 510 516
3011 3018 310 316
2011 2018 210 216
1011 1018 110 116
9012 9019 911 917
9011 9018 910 916
8011 8018 810 816
7011 7018 710 716
6011 6018 610 616
5011 5018 510 516
3011 3018 310 316
2011 2018 210 216
1011 1018 110 116
9012 9019 911 917
9011 9018 910 916
8011 8018 810 816
7011 7018 710 716
6011 6018 610 616
5011 5018 510 516
3011 3018 310 316
2011 2018 210 216
1011 1018 110 116
9012 9019 911 917
9011 9018 910 916
8011 8018 810 816
7011 7018 710 716
6011 6018 610 616
5011 5018 510 516
3011 3018 310 316
2011 2018 210 216
1011 1018 110 116

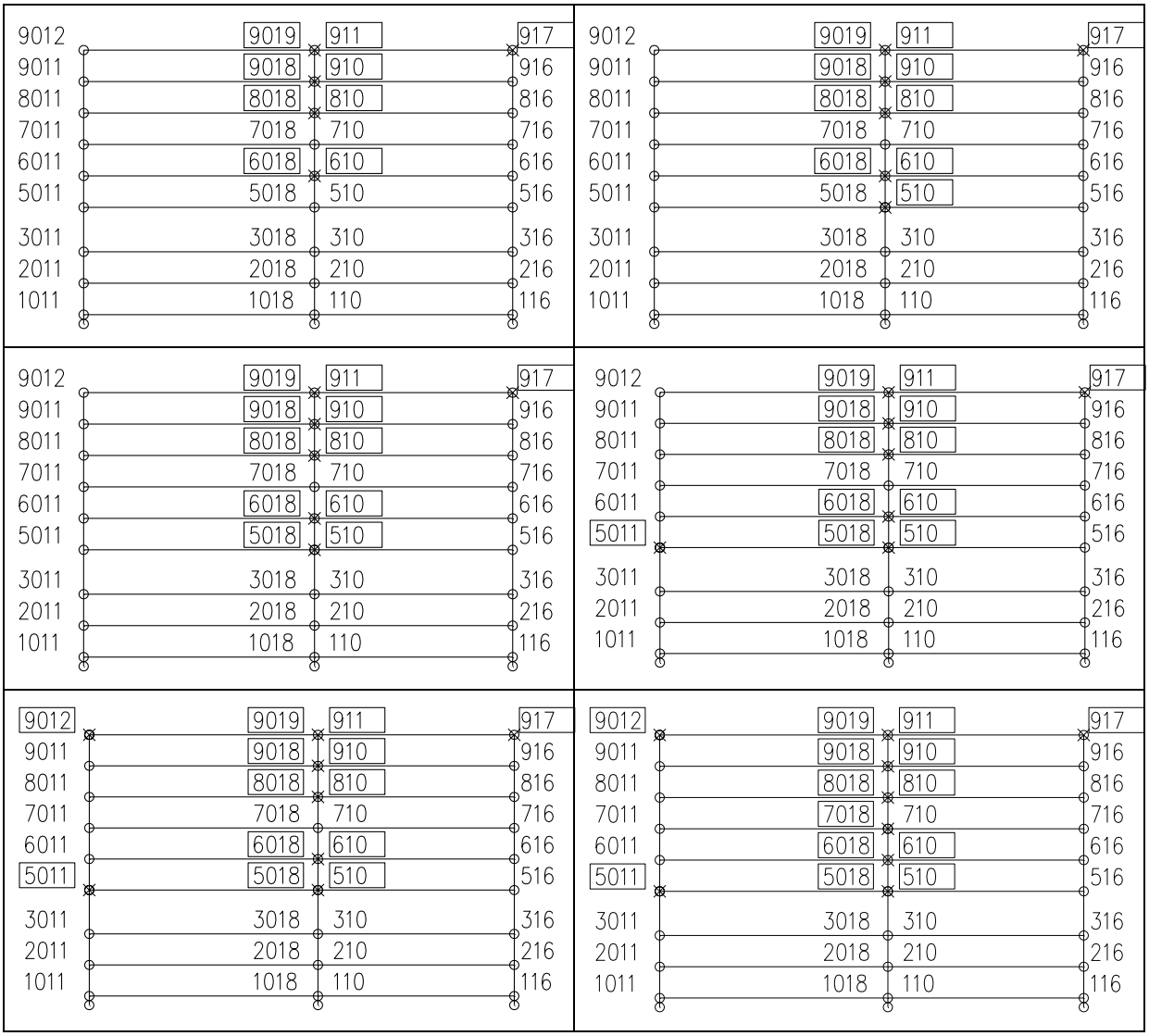

Figure 4: Optimal sensor location when using 7 modes.

Appendix D:

Bossigasse

Austrian Institute of Technology

23. Introduction

Fragility functions indicate the probability that a structure reaches or exceed a specific damage level (called Limit State (LS)) when it is excited by an earthquake characterized by a given intensity. These functions are an effective tool to estimate the probability of losses in case a seismic event occurs, as well to effectiveness of the quality of retrofitting and strengthening interventions in reducing the seismic vulnerability of a structure. This tool can be used not only to estimate the damages after the occurrence of an earthquake but also to plan strengthening of existing structures and infrastructures preventing losses in prospective of future seismic events. A similar method and for some aspect the precursor of the fragility curves are the Damage Probability Matrices that are still used in case of post-event damage estimation. In this report their description will be omitted for the sake of brevity. The estimation of the structural damage level caused by an earthquake is a hard task because of decrease of the capacity of structures during their life-time. The reliability of the vulnerability assessment of existing structures depends on two aspects: the quality of the model describing the structure and the definition a seismic scenario of the area where the structure is located. The analytical/numerical model of the structure might describe the real static and dynamic behavior in the best possible way. The definition of a analytical/numerical model of an existing structure is a hard task due to the lack of knowledge of material characteristics, manufacture and boundary conditions. Furthermore a analytical/numerical model of a real structure includes vagueness, imprecision and ambiguity ensuing from the modelling process. In order to reduce the model uncertainty and improve the estimation of the structural capacity material tests and non-destructive field tests could be carried out. Therefore the fragility functions for single buildings could be easily improved by using field testing data, while the ones defined for classes of buildings need extensive field testing campaigns to define for each class the characteristics common to the quasi-totality of the structures included in it and located in the same area..

Fragility functions defined for building classes are used to define the loss and risk maps of an area [Calvi et al., 2006] and therefore they could be used for a rapid estimation of losses after the occurrence of a seismic event. Fragility function defined for building classes were estimated in the last two decades using data derived from expert observations of structural damages caused by earthquakes [Calvi et al., 2006]: this method to estimate the fragility curves is called empiric. The relation between the occurred structural damage and the earthquake intensity was hard to define with this empiric method, as well to estimate a continuous fragility curves. In order to get over these difficulties, analytical methods were developed. These methods are used to estimate the continuous fragility functions [Calvi et al., 2006] of both building classes and singles structures.

The analytical methods are based on analytical/numerical models of the structures, so they are affected by uncertainty.

The typical method used to calculate the fragility function is based on the classification of structures in categories defined in tools, like HAZUS [HazUS], that list also the uncertainty of the structural capacity. In most of the tools this uncertainty was estimated

through a wide post-earthquake check, so those tools are useful to estimate the fragility of structures with the same characteristics in case of stability post-quake check of large stock of structures.

The analytical fragility functions defined for a single structure are accurate and indicate how much the structure is safe in case of a seismic event characterized by a given intensity and therefore the necessity to retrofit or strength it. The American structures, which most of the tools for the fragility estimation were set for, are quite different from the European ones:the design and construction methods adopted and the materials used vary from a country to the other. These differences are even larger for structures of the architectonical heritages. In order to get through this limit, data of damage caused by earthquakes are gathered in worldwide projects, like GEM [GEM].

The analysis of single structure is essential for the development of specific analytical methods for the estimation of the fragility of each class of structures of the building stock of a geographical/political region. These single structures are specimens to identify the most effective methods for the fragility assessment for each structural typology. The efficiency of the methods is clear if the uncertainty related to the analytical/numerical model and the aging of the single structure is reduced by field testing data.

The European seismic hazard map was recently updated as follow-on from the results of EU FP7 projects the seismic hazard of some densely populated cities was increased from low to almost moderate, so suitable methods to estimate the fragility of typical kinds of building stock of these cities should be developed.

In the city of Vienna approximately 20% of the buildings were built before 1920 and most of them are today strengthened and additional floors are built up to the existing structure, so the method proposed from AIT within NERA JRA5 is directed to calculate fragility functions for this kind of buildings. They are UnReinforced Masonry (URM) structures with wooden slabs (GEM taxonomy = MUR+MUN99/LWAL/////////). In order to develop the method a case study is proposed: a real URM located in the thirteenth district of Vienna was tested with forced vibration method (see D15.1 of the project NERA), its numerical model improved with field testing data and finally its seismic fragility estimated.

24. Fragility functions

24.1 *From the field test data to the updated FE model of the structure*

The estimation of the real structural capacity is central for the seismic vulnerability assessment of existing structures. It depends on the knowledge of the real characteristics and behavior of the structure. This knowledge can be improved by testing the structure. The European standards for the assessment and retrofitting of structures resisting to earthquake [EN 1998-3, 2005] define as elements for a full knowledge of the structure (KL3)

1. the availability of the detailed drawings and the description of all the modifications done during the life-time of the structure,
2. the in-situ inspections to check the correspondence of the drawings details with the actual current state of the structure and
3. the availability of information about the construction materials verified by means of comprehensive in-situ testing.

The European standards give only general indications about field tests to carry out on the materials of the structure to improve its knowledge level. No instructions are given in these standards about the use of dynamic field testing of the full structure to improve the knowledge level. However in the last years some guidelines for the use of dynamic field testing were developed in past European research projects, like LESSLOSS focused on Risk Mitigation for Earthquakes and Landslides [LESSLOSS R02/2007, 2007] and SAMCO focused on Structural Monitoring Assessment and Control ([SAMCo F08a, 2006], [SAMCo F08b, 2006]). The EU FP7 project NERA also developed guidelines for the optimal design of dynamic field tests[NERA D6.2, D6.3]. The estimation of the accuracy enhancement of the structural capacity assessment obtained by the dynamic field testing is still a research subject. Furthermore the work done in the project NERA is not comprehensive in investigating the improvement of the knowledge of the structures using a combination of local destructive and non-destructive in-situ testing of the materials and non-destructive dynamic field testing of all the structure.

The dynamic field tests carried out either through ambient vibration or forced vibration, provide information about the dynamic behavior of the structure. Analyses either in time domain or in frequency domain can be carried out on the testing data: the first kind of data analyses are mostly used for damage investigation, while the second ones lead to the estimation of modal characteristics of the structure (see appendix 2 of the D6.3 of the project NERA). The modal characteristics of the structure provide information about the structural response to a dynamic excitation, including ground motion. The knowledge of the natural frequencies and the mass participation factor to each vibration mode indicates which frequency components of the ground motion signal excite the structure and the mass portion excited by them. Furthermore the knowledge of the mass participation factor and frequency of each vibration mode is extremely important to calibrate the non-linear dynamic analysis of the full structure that is the most common method for the structural capacity assessment used by practitioners.

24.1.1 Field testing data

The natural frequencies and mode shapes of the structure are the most important results obtained from the analysis of dynamic field testing data. These characteristics of the structure could be used to calibrate the analytical/numerical model of the structure. A case study is hereafter presented, in which the numerical FE model of the structure is calibrated by field testing data. The tested and analyzed structure is an UnReinforced Masonry (URM) building in the thirteen district of Vienna. It was tested with forced vibration method. The excitation was applied by a servohydraulic shaker. A multi-sessions measurement was carried out with velocity sensors. The description of the position of the sensors and the point of load application were reported in the D15.1 of the project NERA. The force applied by the shaker was a broad band signal approximating a

white noise with intensity 4 KN(±1KN) and frequency range 0.1-20 Hz. . The sensitivity of the velocity sensors used is 10v/1mm/s. The testing data were analyzed with Stochastic Subspace Identification algorithm (Figure 1). The first five natural frequencies with the higher participating mass were identified (table 1). More details about the forced field testing and the test data and the system identification algorithm are presented in the D6.3 and D6.2 of the project NERA.

Table (1). Natural frequency identified.

Mode	Frequency [Hz]
1	2.64
2	4.4
3	6.09
4	8.18
5	9.44

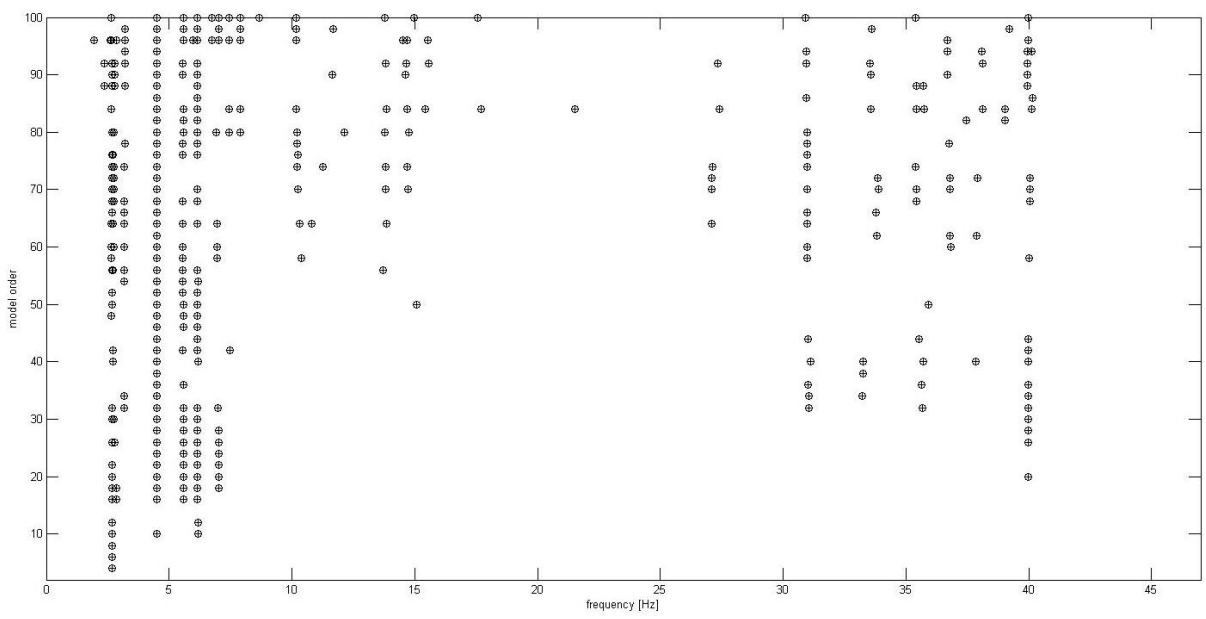

Fig (1). Stabilization diagram showing the frequency of the structure

24.1.2 ***From the initial model of the structure to the updated one***

The commercial FE code ANSYS 14.0 was used to build a FE model of the building (Figure 2). Both masonry walls and the floor slabs were modelled with linear elastic shell elements to carry out the modal analysis. The building has three floors, a cellar partially underground and an attic covered by a timber roof. Three different kinds of floor slabs characterize the structure: jack arch masonry slab between the cellar and the ground floor, which was modelled with isotropic plate, simple timber slab between the ground floor and the first floor and between the first floor and second floor and slab with full wooden joists between the second floor and the attic, which were modelled with orthotropic plates. The diaphragms modelling the timber slabs are not fixed to the walls

on all the sides, but only along two sides. Furthermore spring elements control the mutual rotation between the plate modelling the wooden slab and the plate modelling the walls in order to simulate the flexible behavior of the wooden floor.

The Winkler model was used to represent the soil-structure interaction. The interaction between the tested building and the nearby one was also modelled by unidirectional springs.

The characteristics of the masonry wall were calculated as indicated in the EN 1996 [EN 1996-1-1, 2006]. Therefore the elastic modulus of the masonry was calculated combining the resistances of the brick and the mortar given in previous studies about the old masonry buildings of the city of Vienna ([Zimmermann, 2012], [Furtmüller, 2011]).

This initial model was updated by using the identified natural frequencies of the structure. An optimization problem was formulated to minimize the difference between the values of the identified frequencies and the ones estimated from the FE model. The variables of the problem were the masonry elastic modulus, the stiffness of the rotational spring modelling the flexible behavior of the wooden floor, the stiffness of the wooden floor and the stiffness of the spring simulating the interaction with the close building [Morga et al, 2013]. The values of the natural frequencies estimated from the best solution are shown in the Table 2. The frequencies calculated with the updated FE model do not match perfectly the natural frequencies calculated from the field testing data because of the model uncertainty that could not be reduced by the use of field testing data.

Table (2). Natural frequency estimated with the updated FE model.

Mode	Frequency [Hz]
1	2.6
2	4.54
3	6.4
4	8.5
5	9.9

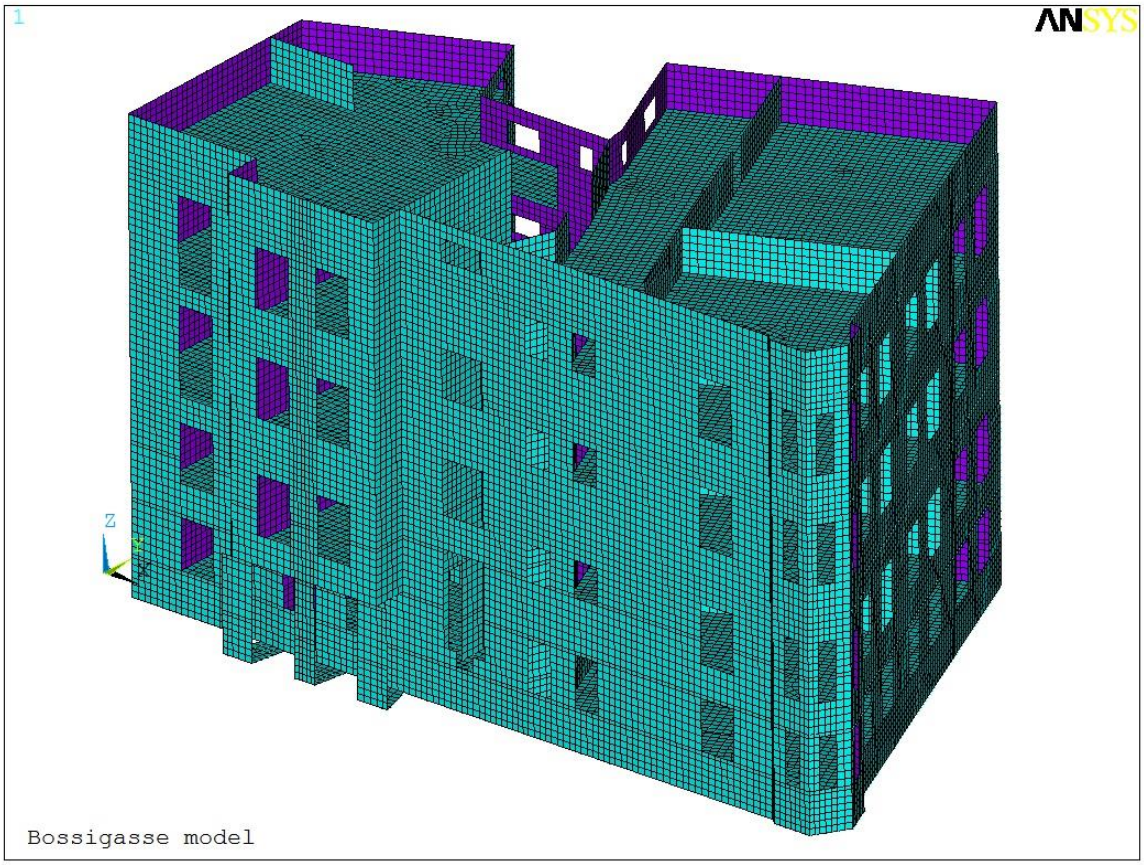

Fig (2). Finite Element Model

24.2 *Assessment of the structural capacity: the nonlinear static analysis*

Nonlinear analyses were carried out on both the initial and the update FE models of the tested structure in order to estimate the non-linear behavior of the structure excited by a progressively increasing force applied along one horizontal direction. The irregularity in plane of the building imposed an arbitrary choice of two perpendicular horizontal directions in the model. The first direction has been chosen according to the mode shape of the first estimated natural frequency, while the second one is the orthogonal one to the first direction.

In a nonlinear static analysis the definition of the horizontal static load distribution is the first step to handle [Fajfar, 2000]: each load path provides different information about the resistance of the structure. The use of two different load paths is recommended in the Eurocode 8 [EN 1998-1, 2005]: the uniform one and the one related to the vibration mode with the higher participation mass. In [Fajfar, 2000] the application of two load distributions is recommended, but no indication about the distributions to apply is provided. The uniform load distribution enhances the request of the lower floors with respect to the upper ones and the shear resistance with respect to the bending moment. The uniform distribution is well defined in the structure with mass equally distributed along the height of the building. The unimodal load distribution recommended in

Eurocode 8 [EN 1998-1, 2005] increases the target displacement with respect to the uniform distribution.

The analysed building has an irregular mass distribution along its height, so the unimodal load pattern has been chosen to emphasize the possible different drifts of the floors. In this study the structural asymmetry in plan was neglected, even if some scholars have already dealt with this issue ([Fajfar, 2002], [Penelis, 2002]). The reason of that choice is the presence of elastic diaphragms in the FEM modelling the wooden slabs: these elements complicate the structural analysis. Furthermore, the torsional effects are here neglected because the case study proposed is only a benchmark used to define a procedure to estimate the fragility functions enhanced by field testing data. In this application the effects of both the higher modes and the variation of the vibration modes with the progressive damage have been also neglected in this nonlinear static analysis. This could cause overestimation of the capacity of the building to resist to seismic excitation: the assumption has been made here because of the knowledge of the building real conditions estimated by the field testing. In fact in this case the use of an adaptive nonlinear static analysis does not improve extremely the seismic vulnerability assessment of the building with respect to the use of a conventional non-linear static analysis. Therefore a conventional nonlinear static analysis with a fixed load distribution was carried out. This kind of analysis is based on the assumption to use a static force instead of a dynamic one. Finally the force was applied to the model at the height of each floor distributed along one side of the building, as shown by red arrows in the Figure 3.

By progressive increase of the horizontal static force the capacity of the structure was estimated.

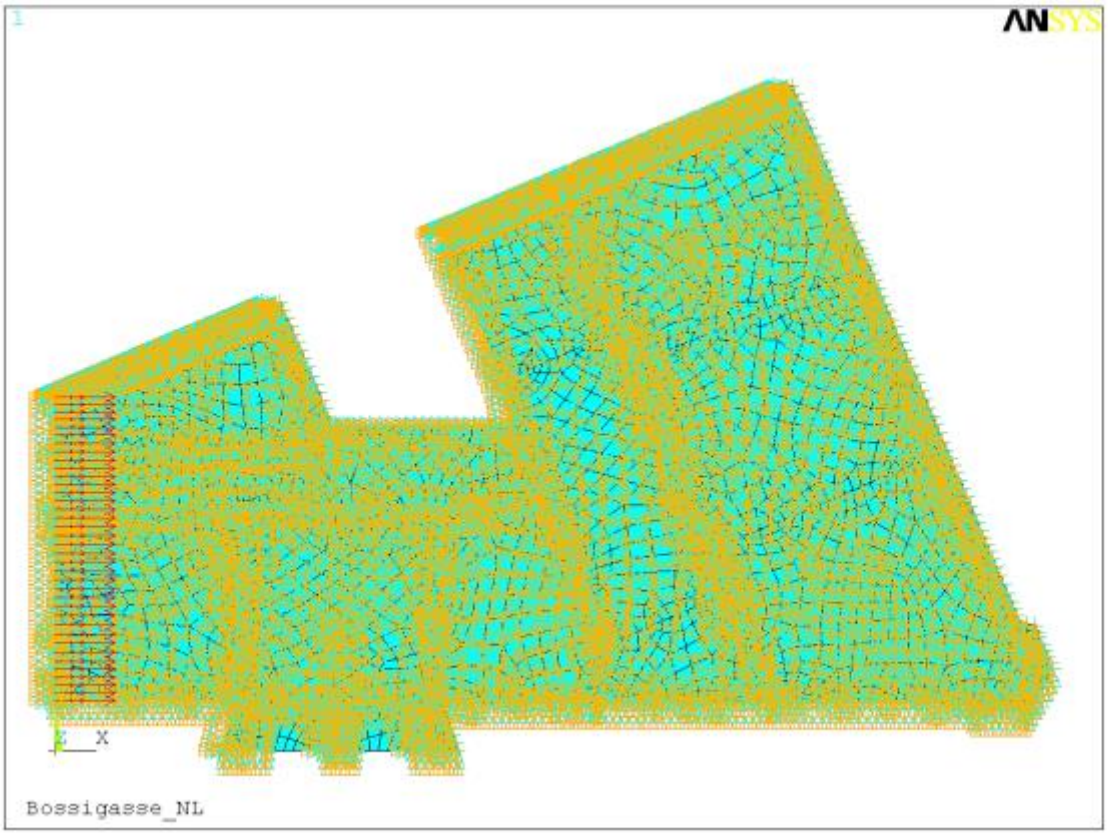

Fig (3). Linear force distribution at one floor of the building in x direction

The design of seismic resistant structure or the simple seismic vulnerability assessment of the structure resistance is defined by means of the damage rather than strength [Ellingwood, 2001]. In order to evaluate the seismic risk of a region, the vulnerability has to be assessed through a reliability analysis that requires the definition of limit states. The limit states are defined as function of a damage index.

The European standards [EN 1998-3, 2005] define for the masonry structures three different global Limit States (LS):

- Near Collapse (NC),
- Significant Damage (SD),
- Damage Limitation (DL).

In a non-linear static analysis these LS are estimated respect to the displacement capacity of the structure.

The NC LS is defined from the Ultimate Displacement Capacity (UDC) of the structure, e.g. the displacement at which the total lateral shear base is dropped below 80% of lateral load resisting elements. The SD LS is the structural state at which the displacement at the roof control point is equal to the 3/4 of the UDC. Finally, the DL LS is related to the reaching of the plastic deformation of a part of the structure. It is calculated as the yield point of the elastic-perfectly plastic SDoF reduced model. The yield force of the idealised SDoF system is one where the plastic mechanism is reached, but respect to the other construction materials, the masonry has a large post-yield deformation and it cannot be really to approximate with the elastic-perfectly plastic behaviour. No useful indication is given about the method to calculate the maximum displacement for the idealized SDoF system in a masonry structure considering that the maximum displacement of the SDoF system correspond to the plastic mechanism deformation. For that reason this maximum displacement was taken equal to the displacement measured at the top of the structure when it reaches the peak lateral resistance. In that way the yield force of the SDoF is related to the peak lateral force through the reduction factor that defines the displacement-base shear force of the SDoF system from the displacement (at the top of the structure)-lateral resistance force of the whole structure. The yield displacement of the SDoF can be calculated applying the principle of equal energy to the elastic-perfectly plastic behaviour and the pushover curve of the SDoF system.

The LS defined in the European standards for the global assessment of existing masonry structures are different from the ones defined in the American standards ([ASCE 31, 2003], [ASCE 41, 2006]) and the ones proposed in HAZUS [HAZUS HM 2.1]. That generates difficulty and misunderstandings in the structural fragility estimation of the structures in Europe. On the other hand, in HAZUS the same LS are used to define the structural condition respect to different natural hazards and obtain the risk maps respect to all the natural catastrophes.

In the calculation proposed hereafter the LS used for the fragility estimation are the ones defined in the Eurocode 8 part 3, because only the seismic risk estimation is the direct purpose of this project.

The capacity curves resulting from the non-linear static analysis define the maximum equivalent lateral force that can be applied to the structure up to its collapse. These curves are used in the normal practice and also in this study to estimate the pushover curves. The pushover curve indicates the capacity of an equivalent Single Degree of Freedom in which the (Multi-Degree of Freedom) model of the structure is transformed. In this transformation the displacements of the capacity curve are normalized to get equal to one the displacement of control node. In this study the method proposed in European standards [EN 1998-1, 2004] for such transformation is used.

The lateral forces $\bar{F}_i$ are normalized to get the following equation

$$m_i \Phi_i = \bar{F}_i,$$

Where Φ_i are the displacements at each floor normalized in the way that the displacement at control node Φ_n is equal to one and m_i are the mass of each floor. The mass of the equivalent SDoF oscillator is calculated by

$$m^* = \sum m_i \Phi_i = \bar{F}_i.$$

The force applied to the equivalent SDoF system and the displacement obtained are estimated by the following equations:

$$F^* = \frac{F_b}{\Gamma}$$

$$d^* = \frac{d_n}{\Gamma}$$

Where Γ is the transformation factor obtained by the equation

$$\Gamma = \frac{m^*}{\sum m_i \Phi_i^2} = \frac{\sum \bar{F}_i}{\sum \frac{\bar{F}_i^2}{m_i}}.$$

The yielding displacement is defined by

$$d_y^* = 2\left(d_m^* - \frac{E_m^*}{F_y^*}\right)$$

Where E_m^* is the total energy dissipated by the structure up to the collapse and F_y^* is the force that produce yielding in the SDoF system. Finally the period of the equivalent SDoF system is defined by the equation

$$T^* = 2\pi\sqrt{\frac{m^* d_y^*}{F_y^*}}.$$

The method proposed here for the fragility function estimation is based on this equivalent SDoF system of which the pushover curve defines the nonlinear elasto-plastic behavior. These kind of methods for the fragility estimation based on the capacity of SDoF system equivalent to structure are called hybrid.

The Figure 4 shows the force-displacement curve (pushover curve) of the equivalent SDOF oscillator in the two directions. In order to show the changes in the estimated fragility function due to the use the updated FEM instead of the initial one and therefore the use of field testing data, the Figure 4 shows the capacity curves for both the FEMs. Finally the Figure 4 shows the LSs in terms of displacement of the equivalent SDoF system as defined in the Eurocode 8 part 3 [EN 1998-1, 1995]: they are the threshold value of the displacement of which exceeding define the fragility of the structure.

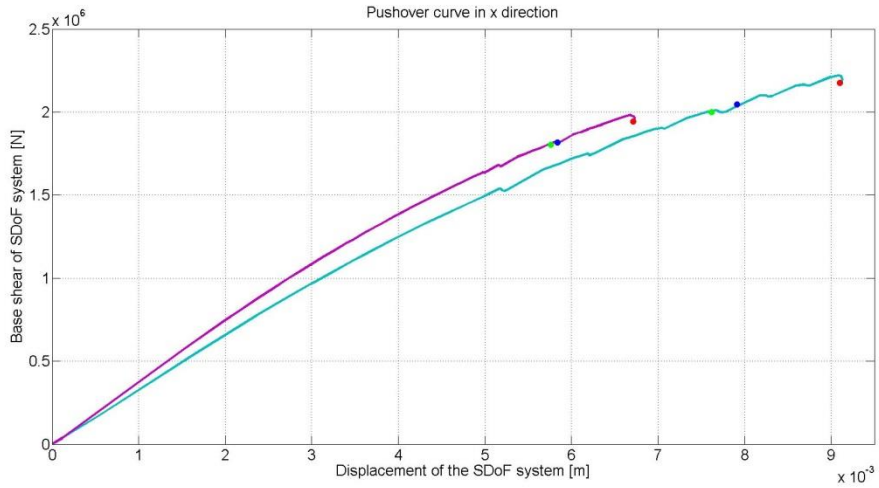

a

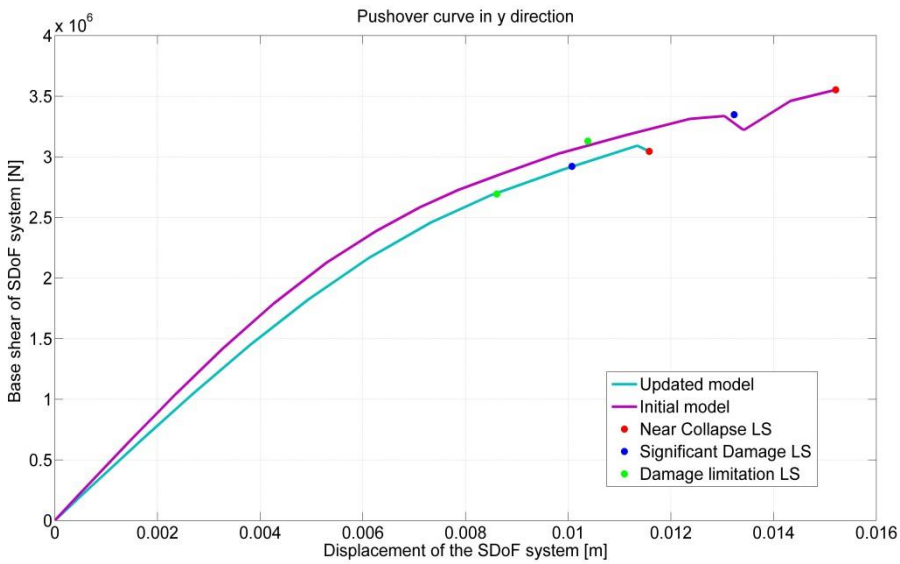

Fig (4). Pushover curves of the SDoF system equivalent to the model of the structure excited both in (a) x direction and (b) y direction. Both the pushover curve of the SDoF system obtained from the initial FEM and the updated one are shown.

24.3 *Ground Motion Hazard Level Selection*

The fragility estimation of structures is strictly related to the seismic intensity considered in the calculation, as afore said. Therefore the selection of the seismic load is a challenge to estimate the fragility of the structure. The intensity, measured as PGA (or PGD) is only one feature necessary to describe the seismic excitation. The seismogenetic mechanism and the type of soil are the features necessary to identify or define the seismic load effectively. The European standards for the construction in seismic area [EN 1998-1, 2004] indicate them as characteristics to select real accelograms or generate artificial ones. Further these standards [EN 1998-1, 2004] identify the reference PGA of the area where the structure is located amplified by the importance factor of the structure and the ground type factor as the features to scale a set of recorded accelerograms for a

nonlinear time-history analysis. Therefore it is possible to summarize that the European standards indicate the PGA as feature to use to scale the recorded accelerograms. In order to carry out an incremental dynamic analysis the choice of feature to scale recorded accelerograms is not univocal. The spectral response acceleration at the fundamental period of the structure (Sa(T1)) is the earthquake intensity measure more commonly used to scale accelerograms to carry out an Incremental Dynamic Analysis(IDA). Sometimes the PGV and seldom the spectral response displacement at the fundamental period of the structure are used as scaling factors for the set of accelerograms to use for an IDA ([Ellingwood, 2001], [Iervolino, 2008]). In literature complex and vectorial intensity measures have been also proposed. Some studies the spectral acceleration at the fundamental period of the structure is the most simple intensity measure of the ones effective in case the damage measure is the maximum interstorey drift ratio [Iervolino 2008]. The spectral response acceleration at the fundamental period of the structure (Sa(T1)) is this intensity measure used hereafter to scale the set of natural accelograms selected to carry out a IDA of the equivalent SDoF model of the structure.

The procedure applied to carry out an IDA of the reduced structural model is described step by step in this and in the following section. Its first step is the selection of adequate set of real accelerograms. The building analyzed as case study is located in Vienna, so seismic records in the "Second European Strong-Motion Database" have been selected. The parameters set in the database to select appropriate seismic records are the type of soil and the seismogenetic mechanism, according to EC8-1 [EN 1998-1, 2004]. Vienna is generally a pull apart basin, with the most common types of rupture mechanism to be strike-slip and sometimes thrust faults and according to the soil classification of the EC8-1 [EN 1998-1, 2004] its ground type is B. Near-field characteristics of the earthquake were neglected in the selection of the seismic records: sources of faulting of most recent seismic events felt in Vienna are far away from the city. The European earthquake records matching these selection criteria are 30. Half of them were randomly selected to carry out the IDA. Both the record in the x direction and y direction are available in the database and both were used in the IDA, because the same records cannot be used to carry out nonlinear time-history analysis in the two orthogonal direction of the structure, as prescribed in the EC8 [EN 1998-1, 2004].

Table (3). Selected natural aceelerograms used in the fragility estimation

Date- time	Country	Earthquake	Recording station	PGA [m/s^2]	PGV [cm/s]	PGD [cm]	Total duration [s]
1983-08-06 15:43:53	Gr	Off coast of Magion Oros penisula	Ierissos – Police station	0.26	1.34	0.16	22.33
1983-08-26 12:52:09	Gr	Ierissos	Ierissos – Police station	1.63	7.56	0.59	24.47
1983-10-30 07:12:28	TU	Panisler	Horasan-Meteoroloji Mudurlugu	1.37	8.36	1.11	32.87
1990-05-05 07:21:17	It	Potenza	Brienza	0.96	6.72	0.66	46.97
1990-12-16 15:45:51	AR	Javakheti	Bogdanovka (GE)	0.53	2.21	0.27	35.19

1990-12-16 15:45:51	AR	Javakheti	Bavra (AR)	1.28	4.98	0.69	40.51
1992-03-13 17:18:40	TU	Erzincan	Erzincan-Meteorologij Mudurlu	5.31	84.57	18.90	29.84
1992-03-15 16:16:16	TU	Pulumur	Erzincan-Meteorologij Mudurlu	0.34	3.68	0.38	37.76
1994-11-29 14:30:30	GR	Off coast of Levkas island	Vasiliki-Town Hall	1.00	5.56	0.55	28.37
1996-07-15 00:13:30	FR	Epagny	Genf-Marziano (SW)	0.08	0.30	0.02	29.03
1996-07-15 00:13:30	FR	Epagny	Yverdon-Jordils (SW)	0.04	0.12	0.01	25.26
1998-06-04 21:36:54	IC	Mt. Hengill	Kaldarholt (IC)	0.40	1.28	0.08	27.19
1998-06-04 21:36:54	IC	Mt. Hengill	Hella	0.15	0.60	0.05	46.99
1999-08-17 00:01:40	TU	Izmit	Gebze-Arcelik	2.08	22.73	14.82	131.55
1999-08-17 00:01:40	TU	Izmit	Goymuk-Devlet Hastanesi	1.30	9.85	1.34	32.14
1999-08-17 00:01:40	TU	Izmit	Istanbul-Bayindirlik ve Iskan	0.57	6.92	5.83	168.77
1999-08-17 00:01:40	TU	Izmit	Bursa-Sivil-Savunma Mudurluga	0.54	8.52	4.41	170.76
1999-08-17 00:01:40	TU	Izmit	Istanbul-Mecidiyekoy	0.64	4.22	2.32	144.27
1999-08-17 00:01:40	TU	Izmit	Yesilkoy-Havaalani	0.87	14.61	7.15	126.60
1999-08-17 00:01:40	TU	Izmit	Cekmece-kucuk	1.71	9.28	2.46	164.04
1999-08-17 00:01:40	TU	Izmit	Botas-Gas Terminal	0.97	10.70	2.82	116.72
1999-08-17 00:01:40	TU	Izmit	Tekirdag-Bayindirlik Mudurlug	0.33	3.57	1.03	71.91
1999-08-17 00:01:40	TU	Izmit	Balikesir-Bayindirlik ve Iska	0.17	4.24	3.50	154.38
1999-08-17 00:01:40	TU	Izmit	Usak-Meteorologji Mudurlugu	0.14	3.17	2.55	159.90
1999-08-17 00:01:40	TU	Izmit	Manisa-Bayindirlik Mudurluku	0.12	2.80	1.80	193.27
1999-08-17 00:01:40	TU	Izmit	Denizli-Bayindirlik ve Iskan	0.11	4.38	3.93	125.99
1999-08-17 00:01:40	TU	Izmit	Tosya-Meteoroloji Mudurlugu	0.11	3.84	2.84	162.50
2000-06-17 15:40:41	IC	South Iceland	Kaldarholt	7.76	39.50	6.34	79.98

2000-06-17 15:40:41	IC	South Iceland	Hella	4.58	46.64	8.46	92.99
2000-06-17 15:40:41	IC	South Iceland	Solheimar	3.90	10.91	2.97	76.99

The second step of the procedure is the calculation of the response acceleration spectrum of each earthquake record. This spectrum was scaled respect to the spectral response acceleration at the fundamental period of the structure (Sa(T1)) and then the earthquake signal corresponding to each scaled response spectrum is calculated. In such way a set of scaled signals is obtained for each natural earthquake accelerograms selected.

The pushover curves indicate the nonlinear elasto-plastic behavior of the equivalent SDoF system in which the FEM is transformed, so the fundamental frequency or period used in the scaling of earthquake records is the one of the SDoF system, as said in the previous section. The fundamental periods/frequencies of the SDoF oscillators equivalent to structural model excited in x and y directions are different, as well the ones estimated for the SDoF system equivalent to the initial FE model and the one equivalent to the updated FE model. For those reasons the set of selected earthquake records scaled respect to the response acceleration of the fundamental period of one equivalent SDoF oscillator (Sa(T1)) is different to the set scaled respect to another equivalent SDoF system. The Figure 5 shows the response acceleration spectra for each SDoF system used in the following step of the proposed method for the seismic vulnerability assessment. The grey line on the figures indicates the vibration period of the corresponding SDoF. The vibration periods of these equivalent oscillators are similar, so the different scale of acceleration response spectra is not clear in this figure.

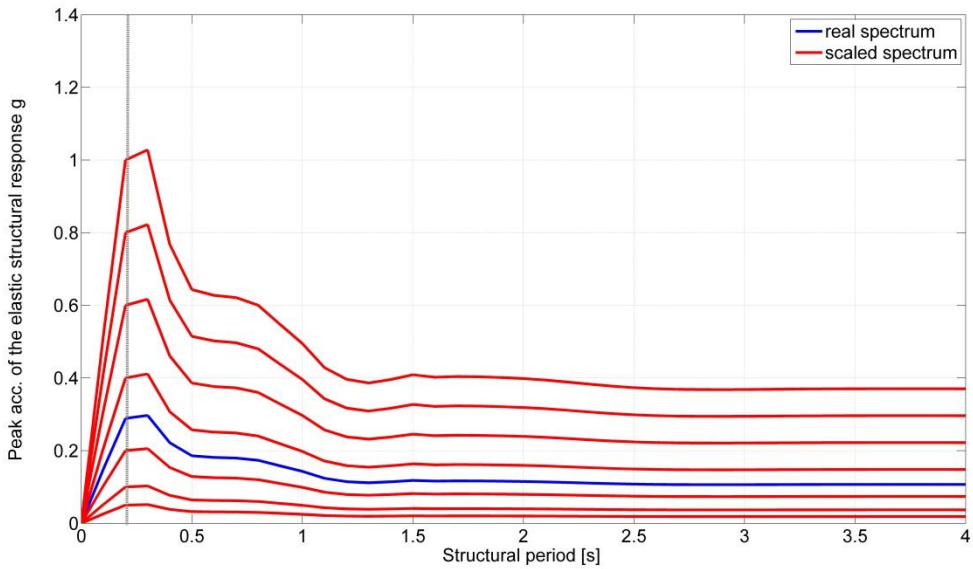

a

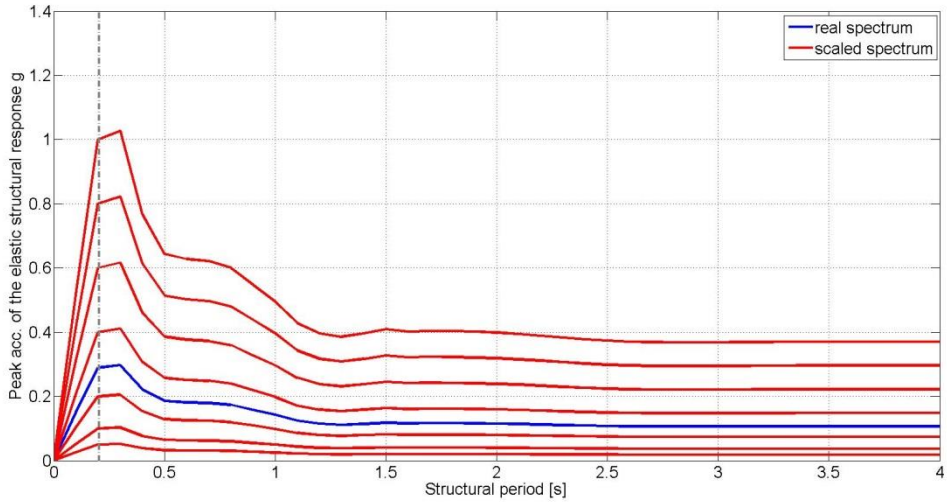
real spectrum
scaled spectrum
Peak acc. of the elastic structural response g
Structural period [s]

b

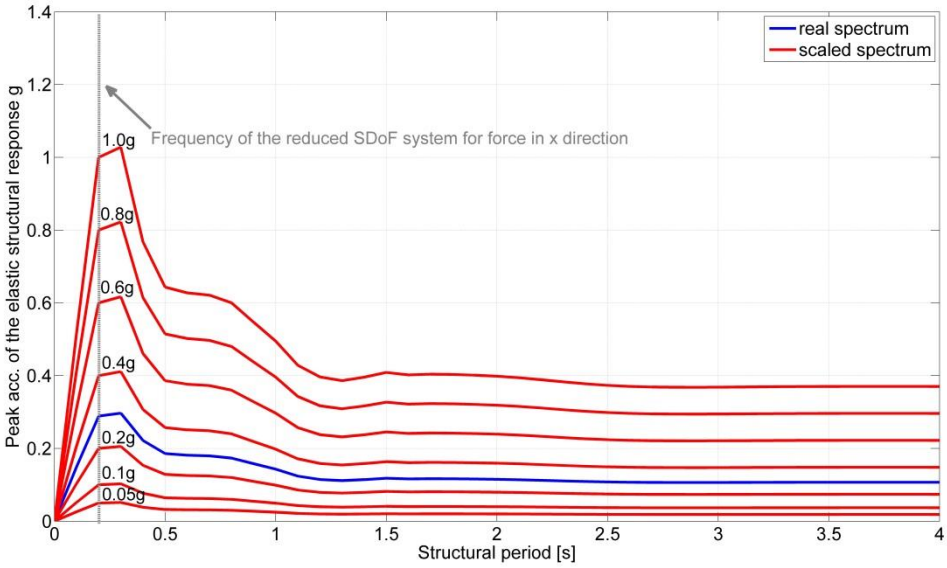
real spectrum
scaled spectrum
Frequency of the reduced SDoF system for force in x direction
1.0g
0.8g
0.6g
0.4g
0.2g
0.1g
0.05g
Peak acc. of the elastic structural response g
Structural period [s]

c

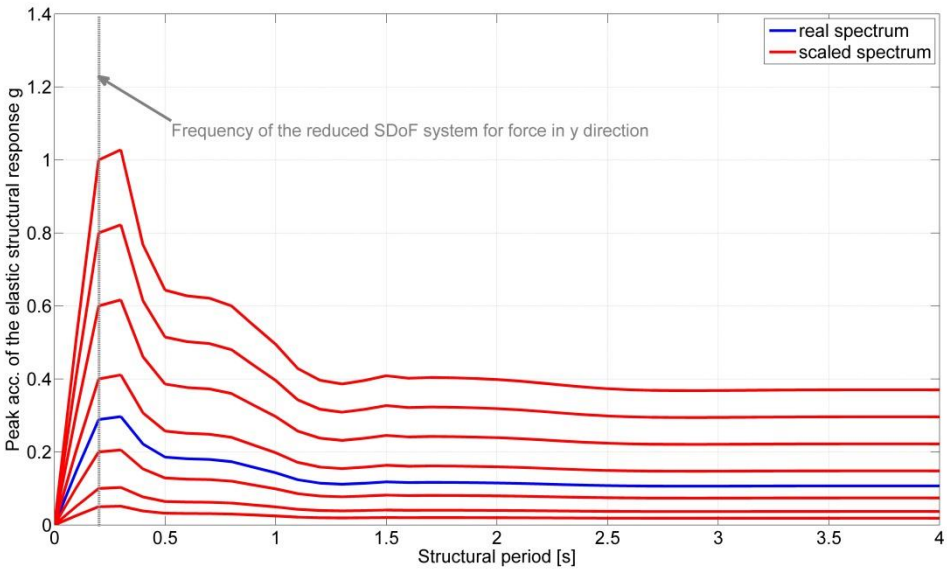
real spectrum
scaled spectrum
Frequency of the reduced SDoF system for force in y direction
Peak acc. of the elastic structural response g
Structural period [s]

d

Fig (5). Response acceleration spectrum of one of the 15 earthquake natural records selected to carry out the Incremental Dynamic Analysis. (a)SDoF system equivalent to the initial model excited in x direction; (b) SDoF system equivalent to the initial model excited in y direction; (c) SDoF system equivalent to the updated model excited in x direction; (d) SDoF system equivalent to the updated model excited in y direction.

24.4 ***Nonlinear dynamic analysis***

A pushover curve describes the nonlinear behavior of the SDoF system equivalent to the structural model analyzed and excited in a given direction. For this reason the pushover curves for the SDoF systems equivalent to both the initial and the update model excited both in x and y direction are used hereafter to define the elasto-plastic behavior of the correspond SDoF system in a set of nonlinear dynamic analyses. The probabilistic scenario was defined selecting 15 natural earthquake accelerograms with features similar to the ones of possible earthquakes occurring in the area where the analyzed structure is located. The intensity of each of these accelerograms was scaled with an incremental value of the response acceleration at the fundamental period of the structure (Sa(T1)) in the range of [0.05g,1] ([0.05, 0.1, 0.2, 0.4, 0.6, 0.8, 1g]). In this way a probabilistic scenario with set of earthquake signals characterized by an incremental value of intensity was defined for each equivalent SDoF system of which the pushover curve was calculated. For each SDoF system the nonlinear time-history analyses carried out applying the set of scaled accelerograms define the seismic vulnerability of its corresponding model of the structure with progressive increase of the seismic intensity (IDA). In order to carry out the nonlinear time-history analyses of a SDoF system its pushover curve are doubled: in this way the nonlinear behavior of SDoF oscillator excited in the two opposite direction is described. The Figure 6 is the doubled pushover curve for SDoF equivalent to the updated structural model excited in x direction. The black line is a curve obtained from a regression analysis of that curve, so it is an analytical description of the nonlinear elasto-plastic behavior of that SDoF oscillator that can be used in the motion integration of the dynamic analyses. A polynomial regression of the fourth degree is applied to define the analytical description of the nonlinear elasto-plastic behavior of each SDoFs system used in this study. This polynomial degree better approximate also the doubled pushover curve of the SDOF system equivalent to the initial structural model excited in y direction (see Figure 7) that is the most complicate to pushover curve defined in this case study to analytically approximate.

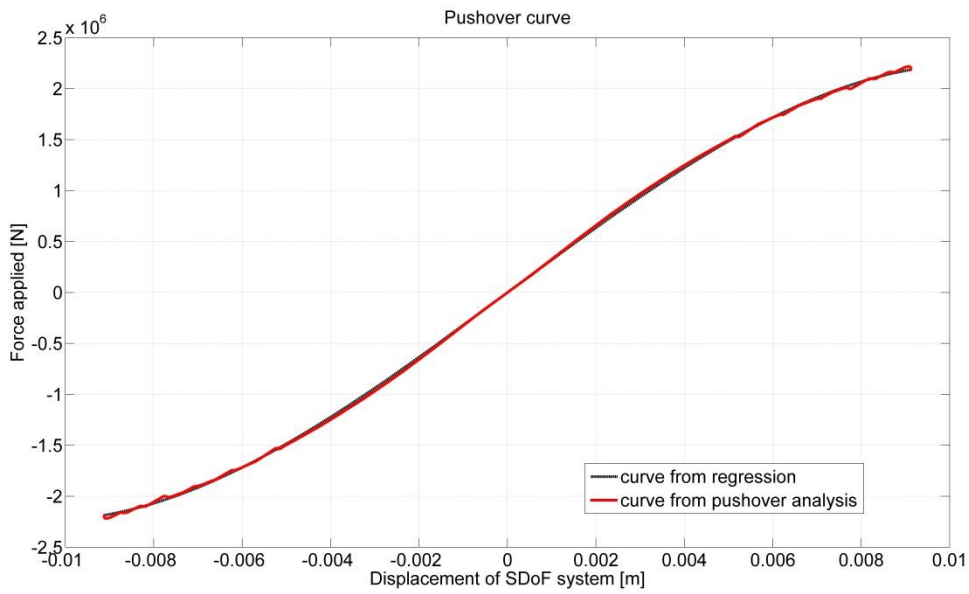

Fig (6). Double pushover curve of the oscillator equivalent to the to the updated structural model excited in x direction.

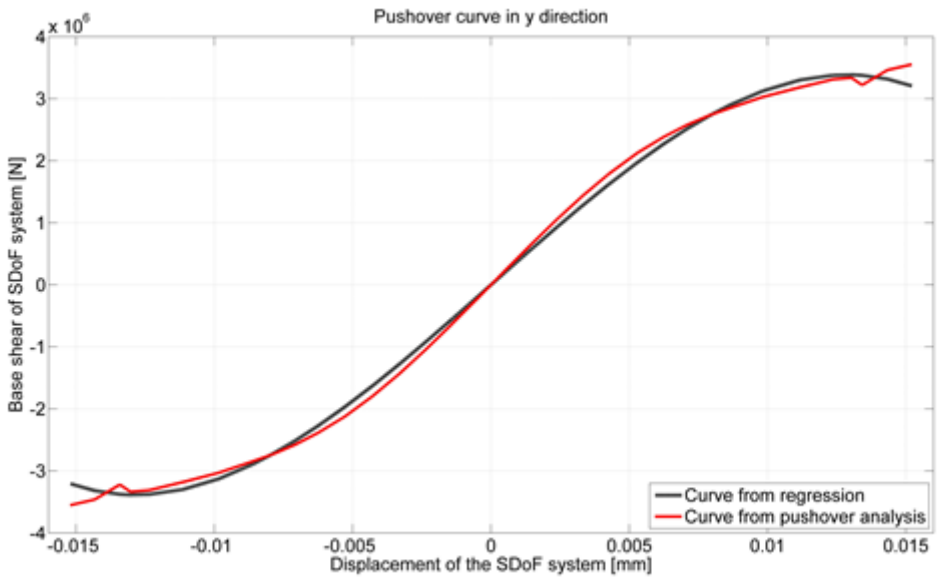

Fig (7). Doubled pushover curve of the SDoF system equivalent to the initial model of the structure excited in y direction.

In this study the pushover curve is used to define the nonlinear elesto-plastic behavior of the equivalent SDoF system instead of simplified analytical models, like elasto-perfectely plastic model, Bouc-Wen model or Takeda model, etc. to reduce the number of approximation done to estimate the fragility function. The behavior of the SDoF system in plastic range for unloading is considered linear taking into account a cycle-test carried out on a single wall of another URM building located in Vienna and built at the same time of the analyzed one. A cycle of this test is showed in Figure 8. The damping ratio of equivalent SDoF systems is taken equal to 5% during all the dynamic analyses. In fact the stiffness of each SDoF oscillator changes depending of the pushover curve, so also its natural frequency and damping coefficient change.

The graphical results of the IDA carried out for the SDoF oscillators equivalent to the initial and updated structural model are showed in Figure 9. In the figure the dotted colored lines indicate the LS defined in the nonlinear static analysis. In the IDA the Engineering Demand Parameter is the maximum displacement of the equivalent SDoF system and the Intensity Measure is response acceleration at the frequency of the SDoF system.

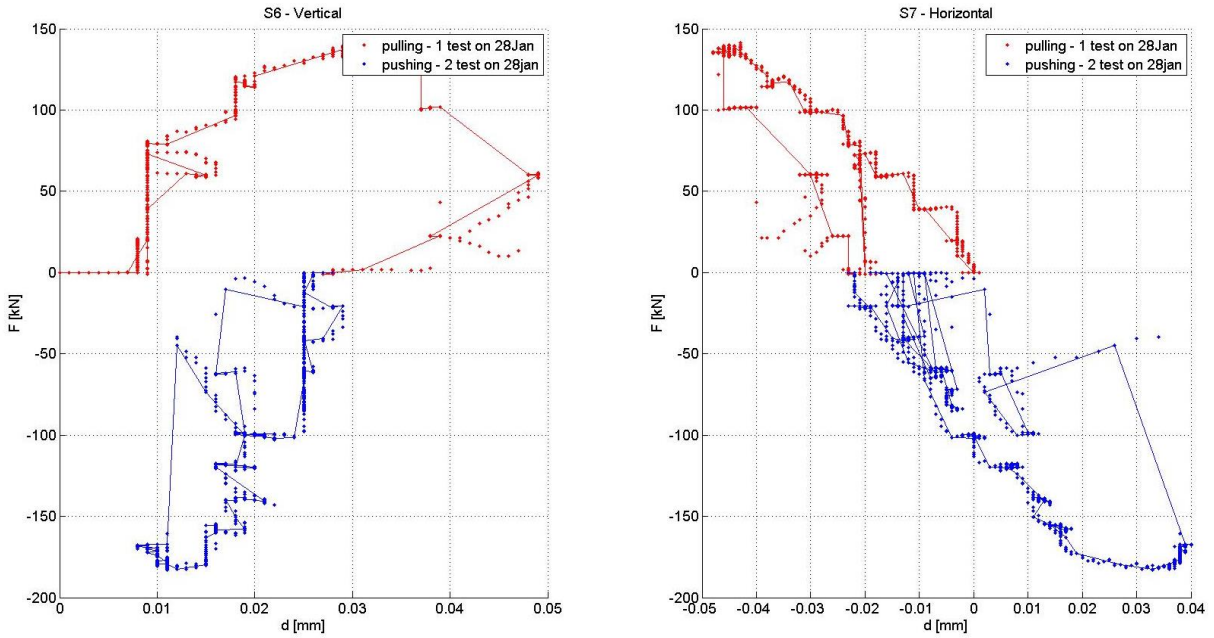

Fig (8). Measurement of a cycle-test carried out on a single wall of another URM building located in Vienna and built at the same time of the analyzed one.

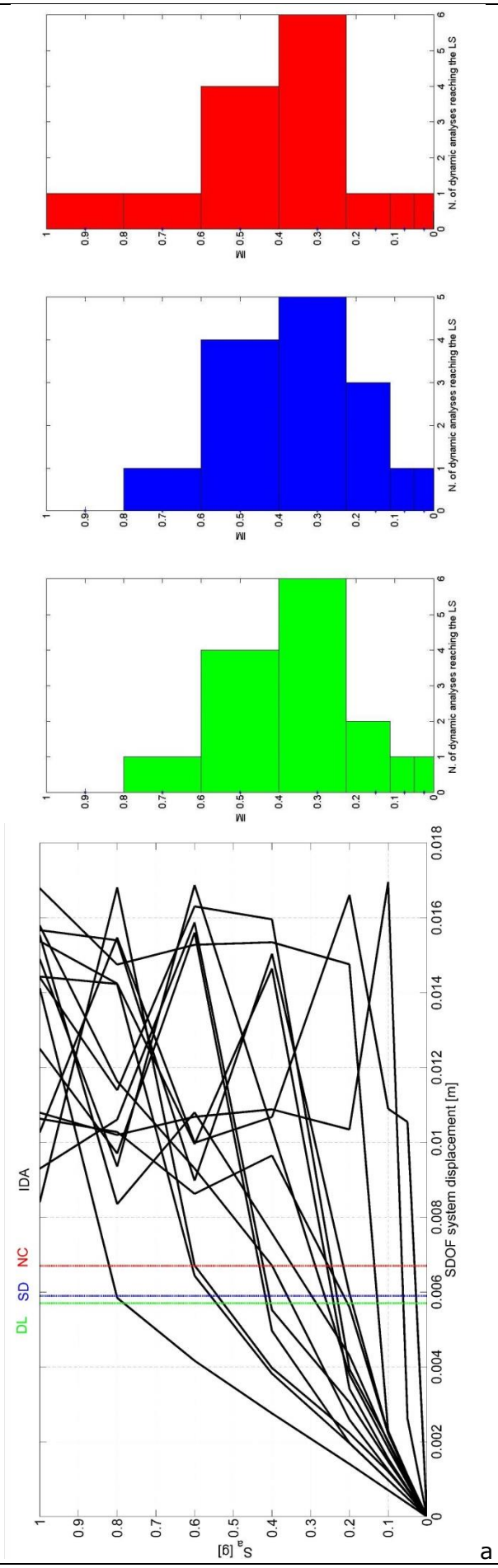
DL
SD
NC
IDA
S_a [g]
SDOF system displacement [m]
IM
N. of dynamic analyses reaching the LS

a

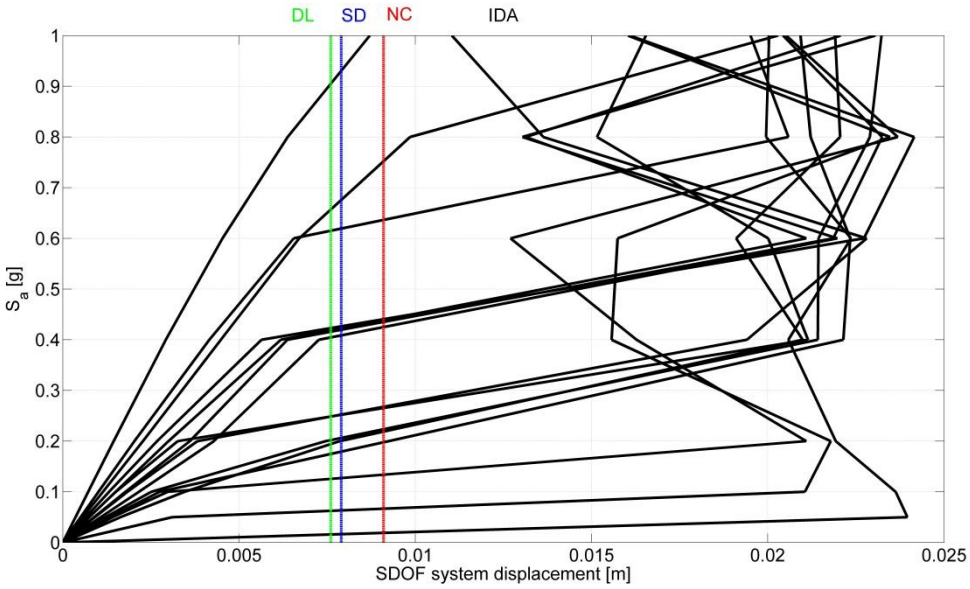
DL
SD
NC
IDA
S_a [g]
SDOF system displacement [m]

b

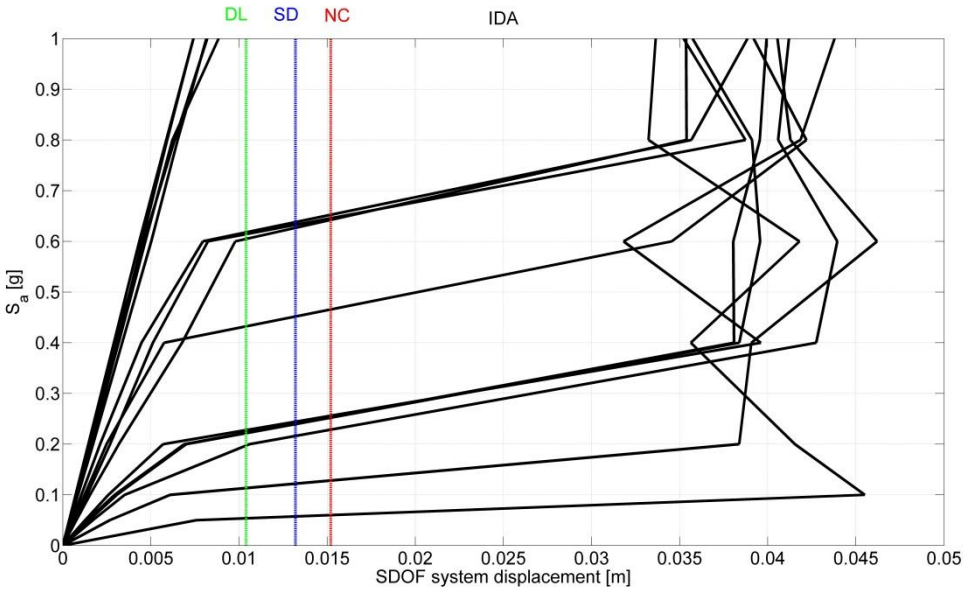
DL
SD
NC
IDA
S_a [g]
SDOF system displacement [m]

c

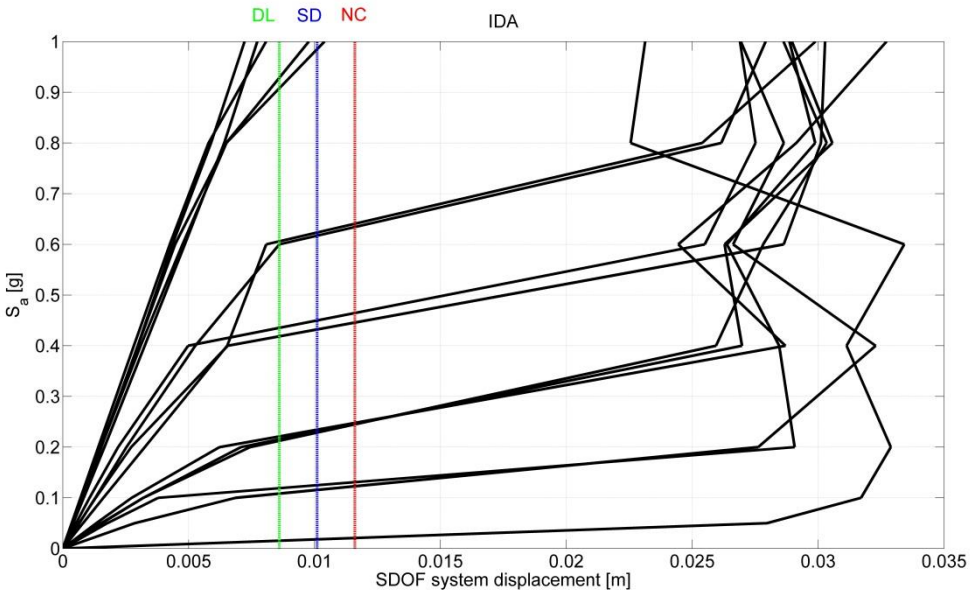

d

Fig (9). IDA. EPM is the peak displacement of the equivalent SDoF oscillator and the IM is the acceleration spectral response at the linear frequency of the SDoF system. (a)SDoF system equivalent to the initial model excited in x direction; (b) SDoF system equivalent to the initial model excited in y direction; (c) SDoF system equivalent to the updated model excited in x direction; (d) SDoF system equivalent to the updated model excited in y direction.

24.5 *Fragility function estimation and curve fitting*

From the result of the IDA it is possible to estimate the probability of the structure to reach a LS as function of an IM of the earthquake. The reaching of a LS is defined as Failure (F), so the fragility of the structure is calculated by the equation:

$$P_f = \int_{IM} P[F|IM] f(IM) d(im),$$

where the failure of the structure is conditioned by the intensity of the occurred earthquake (P[F|IM]). The term f(IM) is the result of a probabilistic seismic hazard analysis or PSHA as defined in [Cornell, 1968].

The Figure 10.a shows also the discrete distribution of the failure values (F) for each IM level. Using this discrete description of the conditional probability it is possible to calculate the discrete cumulative one. The points in the Figure 10 indicate the cumulative probability of the simple oscillator equivalent to the updated structural model excited in x direction to reach the different LSs.
The probability distribution of reaching the EPM threshold of a LS for increasing values of the IM of the seismic intensity can be approximate by a lognormal distribution, as shown in the histograms of the Figure 9.a. Therefore the equation that describes this probability distribution is

$$P(F|IM = x) = \Phi\left(\frac{\ln\left(\frac{x}{\vartheta}\right)}{\beta}\right),$$

where x is the level of IM, θ is the normal mean, β is the standard deviation of ln(IM) and Φ() indicates the distribution function. The estimation of the values of θ and β is necessary to calculate the analytical fragility of the structure. Furthermore this estimation has to be based on a limited number of values observed in the IDA, so a classic approach for the estimation of parameters from a data characterized by a probability distribution is

applied: the maximum likelihood method. The maximum likelihood method to estimate the characteristic statistical parameters of the progressive probability of reaching the EPM threshold value of a LS is an unescapable choice due to the truncated value of the IDA. In this study the values of the IM (S_a [g]) are scaled up to 1g, but higher values of the IM are necessary to get the total probability of exceeding of the threshold value of EPM for all LSs. This would increase the computational cost without an corresponding increase of the quality of the analysis [Baker, 2014].
The Probability Density Function (PDF) (φ) of the normal distribution describing the exceeding of the EPM threshold value of a LS for a given value of earthquake intensity IM_i is

$$Likelihood = \varphi\left(\frac{\ln(IM_i/\vartheta)}{\beta}\right).$$

It is possible to calculate the probability of failure as far the maximum value of IM at which the intensity of seismic load is scaled (IM_{max})

$$Likelihood = \varphi\left(\frac{\ln(IM_{max}/\vartheta)}{\beta}\right),$$

but at that value the cumulative failure probability related to a LS could be lower than one. Therefore the failure probability related to a LS can be calculated also for value of the $IM<IM_{max}$, as the complementary of the failure probability for IM_{max}:

$$Likelihood = 1 - \varphi\left(\frac{\ln(IM_{max}/\vartheta)}{\beta}\right).$$

Taking into account that the earthquake accelerograms can be assumed to be independent one from the other and the total number of different earthquakes accelerograms used in the analysis is n and the number of accelerograms that cause exceeding of the EPM threshold value is m, the likelihood of structural reaching of a LS using the set of those n accelerograms is

$$Likelihood = \left(\prod_{i=1}^{m} \phi\left(\frac{\ln(IM_i/\vartheta)}{\beta}\right)\right)\left(1 - \phi\left(\frac{\ln(IM_{max}/\vartheta)}{\beta}\right)\right)^{n-m}.$$

The estimation of the parameters θ and β is simplified by the use of the logarithm of the likelihood equation. Therefore the parameters could be estimated by solving the following optimization problem (Baker, 2014):

Find $(\hat{\theta}, \hat{\beta})$

that

$$max\left(\sum_{i=1}^{m} ln\phi\left(\frac{\ln(IM_i/\vartheta)}{\beta}\right)\right) + (n-m)\left(1 - \phi\left(\frac{\ln(IM_{max}/\vartheta)}{\beta}\right)\right) .$$

The fitting curves for the simple oscillator equivalent to the updated structural model in case the excitation in x direction are showed in Figure 10.

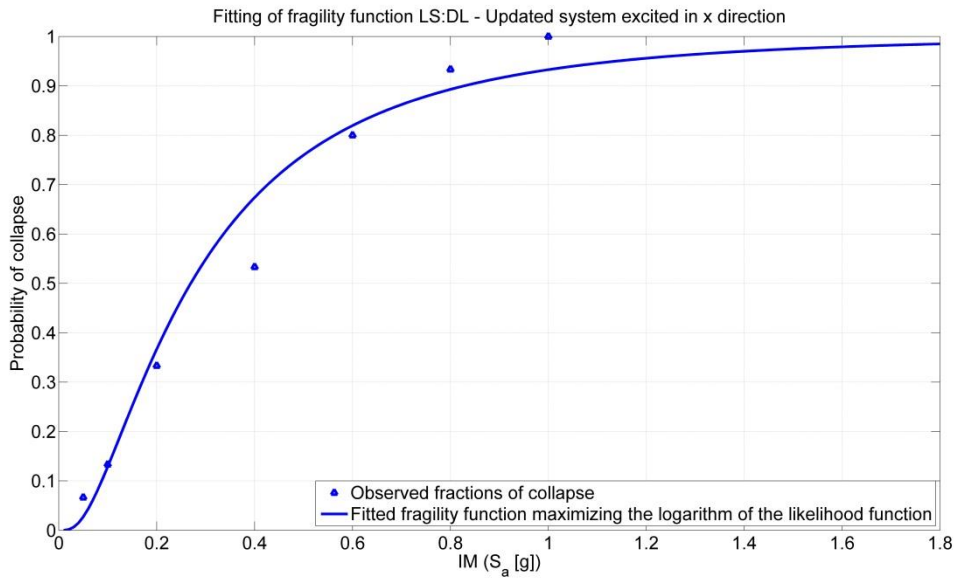
Fitting of fragility function LS:DL - Updated system excited in x direction
Probability of collapse
IM (S_a [g])
Observed fractions of collapse
Fitted fragility function maximizing the logarithm of the likelihood function

a

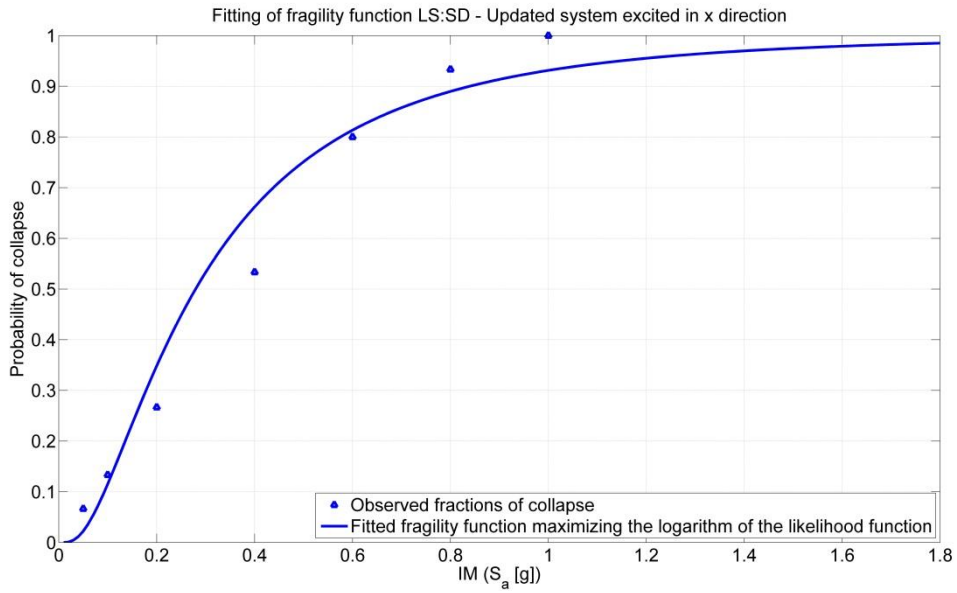
Fitting of fragility function LS:SD - Updated system excited in x direction
Probability of collapse
IM (S_a [g])
Observed fractions of collapse
Fitted fragility function maximizing the logarithm of the likelihood function

b

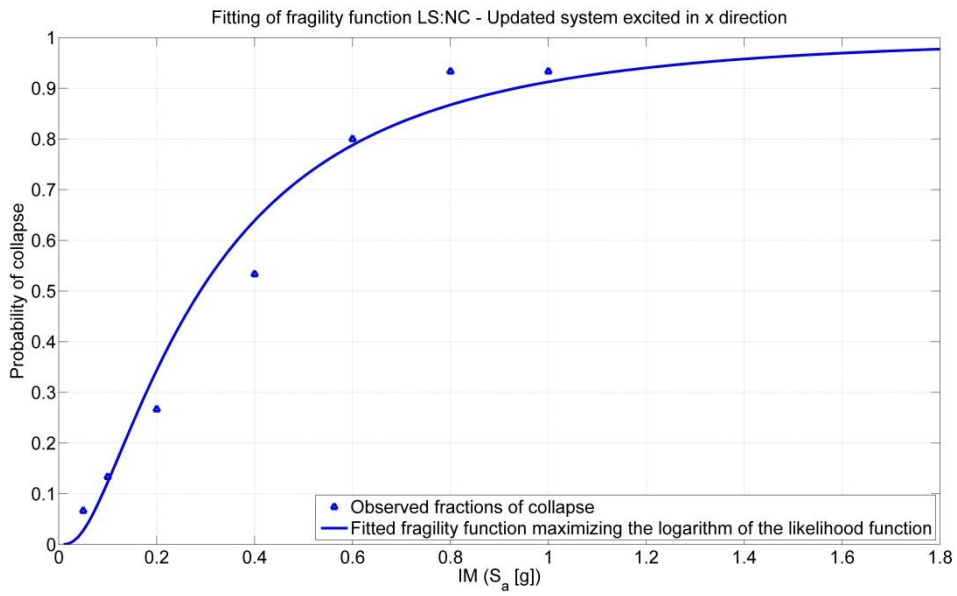

c

Fig (10). Fragility functions of the SDoF oscillator equivalent to updated structural model in case the excitation in x direction. a: LS: Damage Limitation; b: LS: Severe Damage; c: LS: Near Collapse. The dots are the observed fractions of failure (F), i.e. the discrete definition of the Failure for the progressive increase of the Intensity Measure of seismic excitation. The continuous line is the fitted fragility function based on the observed fractions of Failure.

24.6 *Analysis of the fragility functions*

The fragility functions of the simple oscillator equivalent to both the initial and the updated structural model in case of excitation both in x and y direction of the URM building analyzed are shown in Figure 12. From this figure it is clear that for moderate intensity of quakes the vulnerability of the structure is underestimate in direction x and overestimate in direction y in case the initial model is used. For low earthquake intensity (S_a <0.2g) the vulnerability of the structure is overestimated in direction y in case the initial model is used. The updated model does not improve the vulnerability assessment in x direction in case seismic events of low intensity occur.

Comparing the fragility functions (Figure 10) and the pushover curves (Figure 4) it is clear that the underestimation of the vulnerability in x direction and its overestimation in y direction for moderate seismic load in case the structural model is not improved by field testing data is a result due to the changes of the structural capacity due to the use of field testing data. For low intensity of seismic load the change in the structural capacity assessment due to the model updating does not produce shift of the seismic vulnerability assessment.

It is possible to conclude that the use of the field testing data to improved the numerical/analytical model of the structure produces a better understanding of the influence of uncertainty of the seismic load in the structural vulnerability assessment.

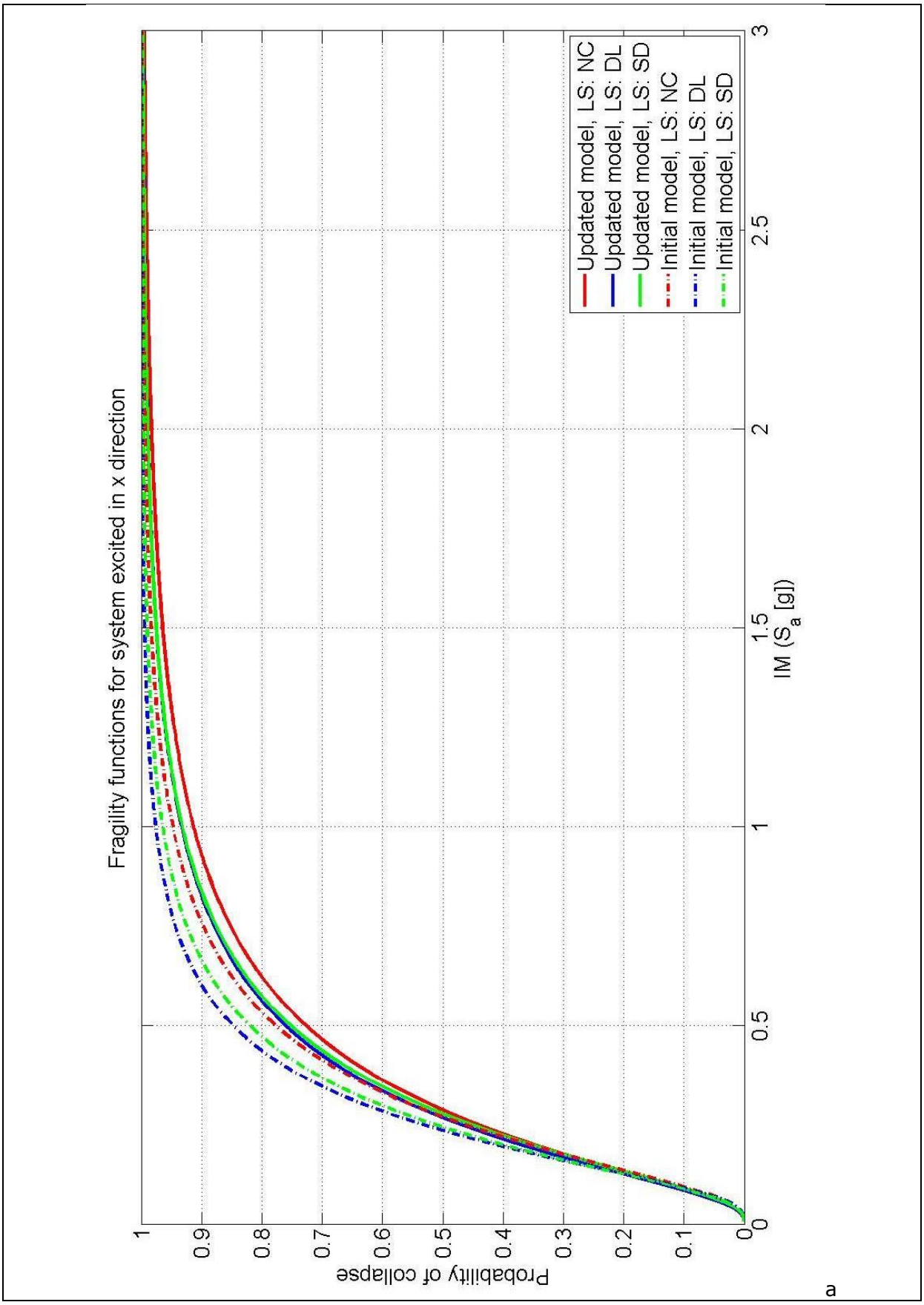
Fragility functions for system excited in x direction
Probability of collapse
IM (S_a [g])
0
0.1
0.2
0.3
0.4
0.5
0.6
0.7
0.8
0.9
1
0.5
1
1.5
2
2.5
3
Updated model, LS: NC
Updated model, LS: DL
Updated model, LS: SD
Initial model, LS: NC
Initial model, LS: DL
Initial model, LS: SD

a

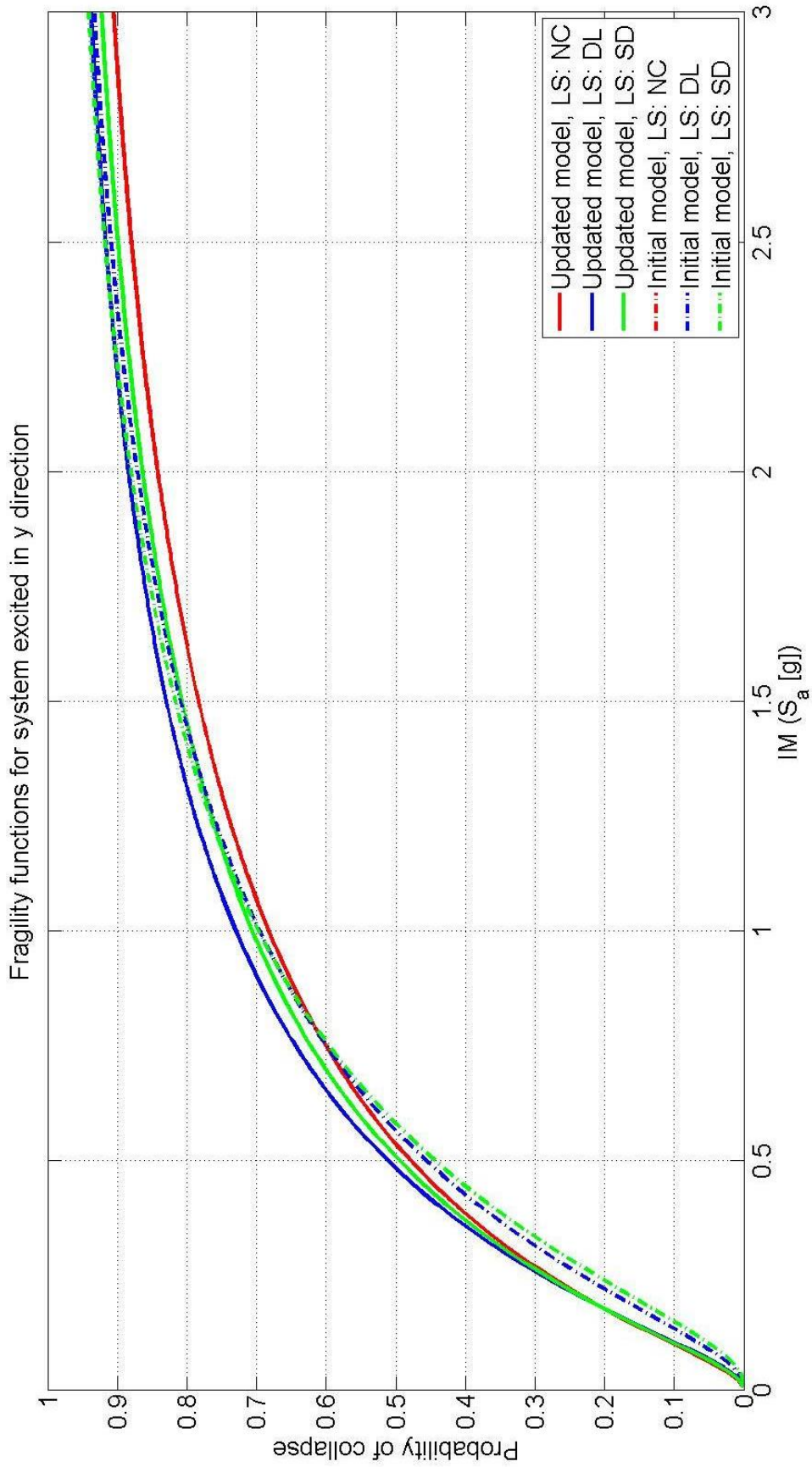

b

Fig (11). Fragility functions of the structure excited in (a) x direction and (b) y direction.

Table (4). Estimate parameters of the lognormal distribution

$\hat{\beta}$		DL	SD	NC
X direction	Initial model	1.32	1.18	1.73
	Updated model	0.76	0.88	0.91
Y direction	Initial model	1.11	1.05	1.05
	Updated model	1.19	1.24	1.31
$\hat{\theta}$		DL	SD	NC
X direction	Initial model	0.54	0.79	2.18
	Updated model	0.27	0.25	0.29
Y direction	Initial model	0.57	0.58	0.58
	Updated model	0.48	0.51	0.54

25. Conclusion and remarks

The design of seismic resistant structure or the simple seismic evaluation of the structure resistance is defined by means of the damage rather than strength [Ellingwood, 2001]. In order to evaluate the seismic risk of a region, the vulnerability has to be assessed through a reliability analysis that requires the definition of limit states. The limit states are defined as function of a damage index. The inter-storey drift is the mostly used damage index. This index is easy to measure or estimate, but it does not give information about the dissipation of the energy during the earthquake, and the remaining capacity of the structure. That is the reason why other damage indices have been defined in literature. In order to perform a reliability analysis the uncertainty related to the damage assessment has to be estimated. The occurrence of a seismic event characterized by a given level of intensity (seismic hazard) is also affected by uncertainty, so it is described as occurrence annual probability. The conditioned probability of structural damage (expressed as LS) respect to the occurrence probability of seismic event characterized by a particular intensity level is calculated by means of a full stochastic reliability analysis. This probability expressed in terms of cumulative probability is called fragility function [Ellingwood, 2001]. It is important to emphasize that the damage index indicate the global damage condition of the whole structure, so the fragility is related the condition of the whole structure [Ellingwood, 2001]. In some case limit states for local damage have been defined and fragility related to them is derived [Rota, 2010].

A point of interest is the evaluation of the uncertainty in the structural seismic assessment for a specific seismic load intensity level. The uncertainty can be both stochastic and epistemic. These two different kinds of uncertainty are seldom distinguished in studies of seismic vulnerability, especially when the seismic vulnerability is estimated through fully empirical methods or partially empirical ones. The uncertainty of the structural seismic assessment is produced by different factors: the uncertainty in knowledge and the variability of same parameters of the materials, construction details

and geometry. The European standards define different knowledge levels to take into account the uncertainty of some factors in the structural seismic assessment. These knowledge levels, as their name indicates, indicate the level of missing knowledge of the structure, so they define the epistemic uncertainty [Tondelli, 2012]. Actually the knowledge levels include implicitly both the epistemic and stochastic uncertainties. In the seismic assessment of the whole structure the knowledge level produce a reduction of the material strength even if it includes the uncertainty related to not only the materials, but also the construction details and the global structural model [Tondelli, 2012].

The dynamic tests on the whole structure are not explicitly included in the tests necessary to have a Knowledge Level 3. On the other hand the objective of the field testing is the increase of the structural knowledge to reduce the global uncertainty in the structural seismic assessment. All the non-destructive tests that can be carried out on existing structure improve the structural knowledge reducing the uncertainty of the seismic assessment in the linear range: no additional information is produced by field tests about the non-linear range of the structural behaviour. The structural model updated by using the information derived from field tests, including tests on the materials, describes well the linear elastic behaviour of the structure, while the uncertainty affects the structural nonlinear behaviour described by the model.

In case no specific tests on the materials characteristics of a structure are carried out, but only field dynamic tests that give information about the global elastic behaviour of the structure, the Knowledge Level 2, as defined in the European standards [EN 1998, 2005], should be chosen for the seismic assessment of the structure. The Knowledge Level 3 proves for tests on the materials to be done. On the other hand, the in-situ tests defined in the European standards are not distinctly defined.

The method proposed for the seismic vulnerability assessment of URM building is based on the deterministic assessment of the structural capacity because the improvement of the analytical/numerical model of the structure by field testing data. This method could be defined as semi-probabilistic: the capacity is estimated in deterministic way, while the demand in probabilistic way.

It is possible to conclude that field testing data reduce the stochastic uncertainty in the structural capacity assessment, but they do not reduce the epistemic uncertainty. Therefore the structural capacity assessment should be estimated using a possibilistic approach.

Finally the proposed method is simple and easy to apply also by the practitioners. Its computational cost is limited due to the use of SDoF equivalent oscillator to carry out the probabilistic assessment of the seismic vulnerability.

26. Reference list

[HazUS] http://www.fema.gov/hazus

[GEM] http://www.globalquakemodel.org/

[SAMCo F08a, 2006] SAMCo Final Report 2006, F08a Guideline for the assessment of existing structures, 2006.

[SAMCo, F08b, 2006] SAMCo Final Report 2006 F08b Guideline for structural health monitoring, 2006.

[LESSLOSS R02/2007, 2007] Flesch R et al. European manual for in-situ assessment of important existing structures, LESSLOSS Report 2007/02. IUSS Press, 2007

[EN 1998-3, 2005] EN 1998-3 (2005). Eurocode 8: Design of structures for earthquake resistance – Part 3: assessment and retrofitting of buildings.

[EN 1996-1-1, 2006] EN 1996-1-1 (2006). Eurocode 6: Design of masonry structures – part 1-1: general rules for reinforced and unreinforced masonry structures.

[Zimmermann, 2012] Zimmermann T and Strauss A. Masonry and earthquakes: material properties, experimental testing and design approaches. In: Moustafa A. (ed) Earthquake-resistant structures - design, assessment and rehabilitation. Chapter 7. Intech, 2012.

[Furtmüller, 2011] Furtmüller T and Adam C. Numerische Modellierung des nichtlinearen Verhaltens von Mauerwerksscheiben in Gründerzeithäusern unter Normalkraft und Schub. In: Erdbeben in Wiener Becken. Beurteilung, Gefährdung, Standortrisiko. VCE Holding GmbH, Vienna, Austria, 2011.

[Morga, 2013] Morga M, Flesch R, Rusnov B, Seismic performance evaluation of existing unreinforced masonry structures, Proocedings of VEESD 2013, Vienna, Austria 28-30 August 2013, paper n. 412.
[EN 1998-1, 2004] EN 1998-1 (2004). Eurocode 8: Design of structures for earthquake resistance – Part 1: General rules, seismic actions and rules for buildings

[ASCE 31, 2003] ASCE/SEI 31-03, (2003), Seismic evaluation of existing buildings.

[ASCE 41, 2006] ASCE/SEI 41-06, (2006), Seismic rehabilitation of existing buildings.

[Iervolino, 2008] Iervolino I, Manfredi G. A revie of ground motion record selection strategies for dynamic structural anlysis. In: Birsi O, Wagg J, Modern testing techniques of mechanical and structural systems. CISM Couses and Lectures 502, Springer, 2008.

[Cornell, 1968] Cornell CA. Engineering seismic risk analysis. Bullettin of the Seismilogical Society of America, (1968), 58:1583-1606.

[Baker, 2014] Baker JW .Efficient analytical fragility function fitting using dynamic structural analysis. Earthquake Spectra, (2014), in press.

[Ellingwood, 2001] Ellingwood BR. Earthquake risk assessment of building structures, Reliability engineering and system safety, (2001) 74: 251-262.

[Rota, 2010] Rota M, Penna A and Magenes G .A methodology for deriving analytical fragility curves for masonry buildings based on stochastic nonlinear analysis. Engineering structures, (2010) 32: 1312-1323.

[Tondelli, 2012] Tondelli M, Rota M, Penna A and Magenes G. Evaluation of uncertainties in the seismic assessment of existing masonry buildings. Journal of earthquake engineering, (2012) 16: 36-64.